SCHOOL OF ENGINEERING
Department of Power and Propulsion

EngD THESIS

Academic Year 2003-2007

Marco Mucino

CCGT Performance Simulation and Diagnostics for Operations Optimisation and Risk Management

Supervisors: Professor Pericles Pilidis
Dr. Y.G. Li
Dr. Lance Moir

5th October 2007

This thesis is submitted in partial fulfilment of the requirements for the degree of Doctor in Engineering

Abstract

This thesis presents a techno-economic performance simulation and diagnostics computational system for the operations optimisation and risk management of a CCGT power station. The project objective was to provide a technological solution to a business problem originated at the Manx Electricity Authority (MEA).

The CCGT performance simulation program was created from the integration of existing and new performance simulation codes of the main components of a CCGT power station using Visual Basic for Applications (VBA) in Excel ®. The specifications of the real gas turbine (GT) engines at MEA demanded the modification of Turbomatch, a GT performance simulation code developed at Cranfield University. The new capabilities were successfully validated against previous work in the public domain. In the case of the steam cycle, the model for a double pressure once-through steam generator (OTSG) was produced. A novel approach using theoretical thermo-hydraulic models for heat exchangers and empiric correlations delivered positive results. Steamomatch, another code developed at the university, was used for the steam turbine performance simulation. An economic module based on the practitioners' definition for spark spread was developed. The economic module makes use of the technical results, which are permanently accessible through the user interface of the system. The assessment of an existing gas turbine engine performance diagnostics system, Pythia, was made. The study tested the capabilities of the program under different ambient and operating conditions, signal noise levels and sensor faults. A set of guidelines aimed to increase the success rate of the diagnostic under the data and sensor restricted scenario presented by at MEA was generated.

Once the development phase was concluded, technical and economic studies on the particular generation schedule for a cold day of winter 2007 were conducted. Variable ambient and operating conditions for each of the 48 time block forming the schedule were considered. The results showed error values below the 2% band for key technical parameters such as fuel flow, thermal efficiency and power output. On the economic side, the study quantified the loss making operation strategy of the plant during the off-peak market period of the day. But it also demonstrated the profit made during the peak hours lead to an overall positive cash flow for the day.

A number of optimisation strategies to increase the profitability of the plant were proposed highlighting the economic benefit of them. These scenarios were based on the technical performance simulation of the plant under these specific conditions, increasing the reliability of the study. Finally, a number of risk management strategies aimed to protect the operations of a power generator from the main technical and economic risk variables were outlined.

It was concluded that the use of techno-economic advanced tools such as eCCGT and Pythia can positively affect the way an operator manages a power generation asset through the implementation of virtually proven optimisation and risk management strategies.

Acknowledgements

I would like to take this opportunity to thank and express my sincere gratitude to Professor Pericles Pilidis for his guidance and support during the difficult and not so difficult times. I would also like to thank Dr. Li for his helpful advice and Mr. Mike Newby for the motivating discussions. I express my sincere gratitude to Dr. Lance Moir for his invaluable support.

I would like to thank my parents for teaching me the value of knowledge and the sense of rightness, it is because of them who I am. My gratitude is for my beloved wife who shared with me this long journey, for her love and support. I can not thank enough to my sisters who have always been there for me. Last but not least, my best regards to all my dearest friends at home and those I found at Cranfield.

The financial support from the National Council on Science and Technology of Mexico (CONACYT) is greatly appreciated.

To my parents

Table of Contents

List of Figures

List of Tables

Chapter 1 General Introduction

1.1 Background

The Manx Electricity Authority (MEA) is a public company responsible for the secure supply of electricity and gas to the Isle of Man [1]. The company undertook a massive expansion in its operations during the period between 1999 and 2004 in response to the Isle of Man Department of Trade and Industry's strategic objectives for the island economy at that time [2]. These objectives were: to end dependency on heavy fuel oil and determine the means to develop a natural gas infrastructure; to reduce the unacceptably high price of electricity on the Island, and to prepare the MEA for unprecedented demand growth [3].

The MEA board decided to invest in a number of projects to prepare the company for the challenges to come. This project included a state-of-the-art CCGT plant to increase the installed capacity on the island and complement the imports coming from the UK power market through the Interconnection cable. Additionally, a dedicated port in the Scotland to Ireland gas pipe was planned.

The Combined Cycle Gas Turbine (CCGT) generation plant was considered as a long-term solution to the electricity supply, dependency in heavy fuel oil and environmental concerns. Figure 1-1 show the chronogram of the main events during the 1998 to 2004 period. The design of the plant started in 2001 just after the Interconnector cable began its operations and a series of business opportunities emerged with the NETA agreement at the UK markets, projecting the CCGT plant as the critical leverage to capitalize on the cable.

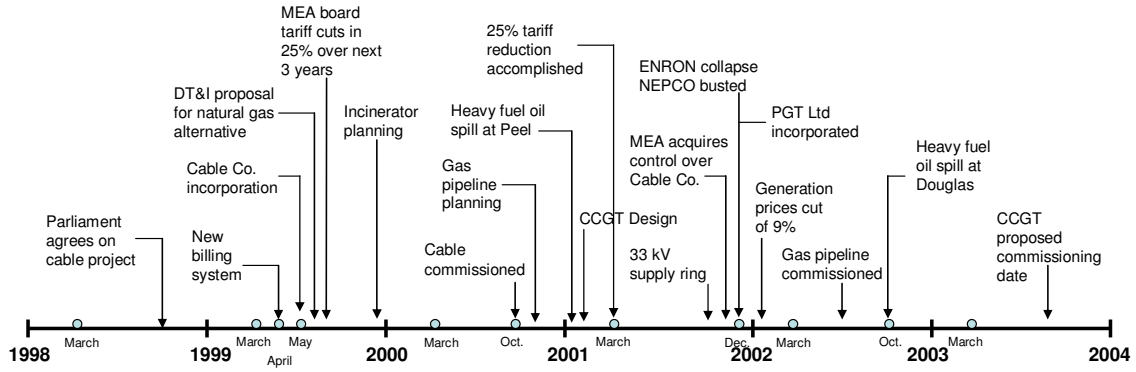

Figure 1-1 Chronogram of events (1992-2004)

The plant's production surplus would have been sold to an Enron subsidiary through a bilateral long term contract, fixing the company future revenue and more importantly hedging the operation of the plant from the highly volatile power and gas markets. Unfortunately, Enron collapse brought the dissolution of the contract.

As a result, MEA directors took the decision to trade in the power exchange and bear the full price volatility rather than incur in big penalties and image deterioration

resulting from undelivered power production to holders of future and forward contracts. A double edge sword combining the unprecedented prices of the energy commodities brought financial difficulties to the company.

1.2 Problem statement

The disruption in the original MEA's business strategy brought up extra pressure on the plant's operations as the company lacks the economies of scale needed to compete in the UK power market. The limited knowledge and expertise on CCGT technology made any immediate reduction in operating costs unviable. The reliability and availability figures were slowly building up as happens during the infancy of any power plant. Finally, the surge in world energy prices experienced during these recent years, particularly on the natural gas, reduced the operating margins of the company.

1.3 Thesis statement

The proposed solution to the problem identified in previous section is stated in the following thesis:

> *The development of Combined Cycle Gas Turbine performance simulation and diagnostics techno-economic tool would allow the company to assess and forecast the short and long term operating cash flows of the plant that in turn would facilitate the optimisation of the plant operations, create a robust trading strategy, protect the company from market volatility and, ultimately, increase the profitability of the business. In addition, the tool could support the development of the human resources within the company.*

The development of the CCGT technological tool will make possible to estimate the technical performance of the plant from the particular generation schedule set by the operator taking into account the effect of the ambient conditions (temperature, pressure and humidity). The system will allow the operator to simulate the performance of the main components of the power plant: gas turbine engine, steam generator and steam turbine under complex operating conditions such as component degradation or to quantify the impact of the emission abatement system of the gas turbine engines on the overall performance of the plant. Additionally, the tool can be used to simulate the performance of the plant under different operating regimes: gas turbine + single pressure system, gas turbine only, gas turbine + 2 double pressure system, etc.

The technical capabilities of the program can be integrated into a user friendly system where the operator of the plant would effortless introduce the different conditions for their simulation, and obtain the data ready for its analysis. The pertinent economic techniques should be implemented in the system to provide a complete overview of the plant. The system could be used to create and to evaluate innovative strategies to optimise the economic performance of the plant. Ultimately, the appropriate business strategies to protect the company from the highly volatile energy markets could be developed and virtually proved before implemented.

1.3.1 Objectives

The main objectives of the project and author's final contributions to knowledge were:

1. Develop and implement the required performance simulation capabilities in Turbomatch for the successful modelling of the gas turbine engine.
2. Adapt the thermodynamic gas turbine engine model to field data from MEA.
3. Create a performance simulation model for the steam generator.
4. Test the existing gas turbine engine performance diagnostics system under real operating conditions.
5. Integration and validation of a combined cycle modelling program from the individual gas turbine engine, steam generator and steam turbine models.
6. Develop a flexible and user friend environment for the implementation of the CCGT performance simulation tool.
7. Implement an economic module for the profitability assessment of the plant.
8. Propose and evaluate a number of operations optimisation strategies using the CCGT performance simulation program
9. Define a series of risk management strategies for the operations of the power plant.
10. Transfer the technological tools developed during the project to MEA Operations and Maintenance (O&M) department.

1.4 Thesis structure

The structure of this thesis was designed to highlight the contribution in three areas of the CCGT technology research field: *Plant Modelling*, *Plant Diagnostics* and *Plant Management*. Each of the sections contains one or more chapters where the main objectives of the thesis were developed. The diversity of topics covered in each of the chapters made it unviable to consolidate a single literature review, methodology or discussion sections for the whole thesis. Instead, each of the chapters features a concentrated revision of the particular theoretical or practical concepts used and presents the appropriate results and discussion. Integrated conclusions and recommendations for the project are given.

SECTION I

PLANT MODELLING

Chapter 2 Gas Turbine Engine Performance Simulation

2.1 Introduction

The following chapter presents the development of the thermodynamic model of a gas turbine engine similar to General Electric's LM2500+ found at Pulrose power plant, Manx Electricity Authority (MEA), Isle of Man.

Since the gas turbine (GT) performance determines the available energy for steam production and sets the boiler and steam turbine operating conditions, and consequently their performance, an acceptable accuracy of the model over the operational range of the power plant is needed. The model has to reproduce the performance of the engine under different ambient (temperature, pressure and humidity) and operating (power settings, degradation, fuel type) conditions. The accuracy of the model has general implications on the whole Combined Cycle (CC) power plant performance as the GT thermal efficiency accounts for up to 40% points of the overall plant thermal efficiency.

The LM2500+ engine operated at Pulrose plant is a versatile aeroderivative engine that can be found in the maritime, defence, oil and gas, and power generation industries. MEA's engine is the latest version of the LM2500+ with a two-stage power turbine, water injection for emission abatement, duel fuel operation (natural gas and diesel oil) and 30.5 MW nominal power output [4].

Table 2.1 Turbomatch capabilities

What do we need?	What do we have?	Status
Design point simulation	Design point simulation	OK
Off design simulation	Off design simulation	OK
Degradation	Degradation	OK
Engine modelling	Engine modelling	OK
Multifuel capability	Kerosene, Natural Gas (fixed composition)	Limited
Engine model adaptation		Missing
Effect of ambient humidity		Missing
Water/steam injection at the combustion chamber		Missing
Effect of the working fluid on the engine components characteristics		Missing

In order to produce an accurate thermodynamic model of the engine, advanced GT performance simulation software is required. Although a wide range of commercial and academic (GateCycle [5], Thermoflow [6], EtaPro [7], Gasturb [8]) computational programs are available, the nature of the collaborative project between Cranfield University and Manx Electricity Authority favoured the use and development of Turbomatch [9]. Turbomatch is an in-house program developed at Cranfield University

with a series of capabilities that allow the user to simulate design and off design performance of engine and to build several engines' configuration and operating cycles. However, the characteristics of MEA's engines demanded the improvement of some existing functional capabilities of Turbomatch. The results of a gap analysis on Turbomatch's capabilities are shown in Table 2.1.

A review on the particular research field of each of the limited or missing capabilities listed above is found in section 2.3. The theoretical background needed to implement such capabilities and the computational methods are described in sections 2.4 and 2.5, respectively. The engine model design and adaptation is found in section 2.6 and 2.7 where an account of the assumptions and considerations is made. Finally, a thoroughly analysis of the engine performance under different ambient and operating conditions is made, and the results are shown section 2.8.

2.2 Nomenclature

$\dot{m}$	Mass flow
$\dot{Q}$	Heat flow
$\dot{W}$	Work
C	Specific heat
CC	Combined Cycle
CCGT	Combined Cycles Gas Turbine
CEA	Chemical Equilibrium with Applications
CV	Calorific Value
DLE	Dry Low Emissions
DP	Design Point
ECV	Equivalent Calorific Value
EGT	Exhaust Gas Temperature
FAR	Fuel-to-air ratio
GT	Gas Turbine
h	enthalpy
HHV	High Heating Value
HPT	High Pressure Turbine
HPTN	High Pressure Turbine Nozzle
HRSG	Heat Recovery Steam Generator
HSPT	High Speed Power Turbine
IGV	Inlet Guide Vanes
INJT	Injected water/steam temperature
INJW	Injected water/steam mass flow
INJWAR	Injected water/steam water-to-air ratio
INJX	Injected water/steam quality (0=liquid, 1=vapour)
ke	Kinetic energy, Kerosene
KFUEL	Fuel type identifier
LHV	Low Heating Value
LMTD	Mean Logarithmic Temperature Difference
M	Molecular weight
m	Mass

MEA	Manx Electricity Authority
MW	Mega Watts
N	Number of moles
NGV	Nozzle Guide Vane
OD	Off-design Point
P	Pressure
pe	Potential energy
R	Gas constant
s	Entropy
SM	Surge Margin
STIG	STeam Injected Gas turbine
T	Temperature
TET	Turbine Entry Temperature
TMF	Turbine Mid-Frame
V	Velocity
VSV	Variable Stator Vanes
W	Mass flow
WAA	Air mass flow at station A
WAF	Fuel mass flow at station A
WAR	Water-to-air ratio
WAW	Water mass flow at station A
WFR	Water-to-fuel ratio
X	Water quality
y	Molar fraction

Greek letters

ω	Specific humidity
ϕ	Relative humidity, entropy function
Φ	Equivalence ratio
η	Efficiency
θ	Total energy
γ	Specific heat ratio
σ	Error threshold

Subscripts

2	Compressor inlet
25	9^{th}-stage compressor bleed off
3	Compressor discharge
4	HPT inlet
48	HSPT inlet
5	Exhaust nozzle
a	Air
A	Station A
B	Station B
BS	Isentropic conditions of station B
cc	Combustion chamber
f	Fuel
g	Gases

i	Index, inlet
m	Mixture
o	Outlet
p	Pressure
v	Volume, vapour
w	Water

2.3 Literature review

2.3.1 Effects of ambient humidity on the gas turbine engine performance

The effect of the ambient humidity on gas turbine performance is more prominent at high temperatures and relative humidity conditions becoming an issue of geography and meteorology for most industrial engines. However, it is not always the case for an aero/aviation engine that can be operated, during the same military mission or commercial flight, in contrasting ambient conditions – from the humid coasts to dry desserts –. Early research in gas turbine performance simulation identified the need for the estimation of properties for different working medium resulting in the development of mathematical method to compute the effect of air humidity and fuel composition [10]. From an operator's point of view, the use of correction factors is a more straight forward way to know the effect of humidity in the engine performance [11]. Walsh and Fletcher [12] only give a qualitative description of the effects of water on the engine performance that could be used for preliminary assessments.

Current publications entirely devoted to the ambient humidity and its effects on performance are scarce. An assessment of moisture condensation effect on engine performance test is one of the limited examples [13]. Instead, the topic is found as part of a large study on advanced wet or evaporative cycles [14, 15]. These results show temperature is the main parameter responsible for the variation in power output decreasing at a rate of approximately 8% per 10°C for a fixed relative humidity. Whereas the effect of humidity, when saturated air is considered (100% relative humidity) only comes visible at higher ambient temperatures with 2% decrease in power output at 40°C.

On the other hand, Mathioudakis [16] conducted an interesting analysis of the effect ambient humidity has on the engine performance diagnostics accuracy concluding that if humidity is not taken into account, uncertainty bands in measured quantities may be too broad reducing the discriminative ability for diagnostics. It is obvious no recent publication is entire devoted to evaluate the effect of the ambient humidity on the engine performance. Instead, it has reached a status of "commodity" capability (i.e. a "given" characteristic) in every gas turbine performance program destined for the analysis of more complex phenomenon or concepts.

As mentioned before, the introduction of water-spray cooling techniques for power augmentation at the cold section of the engine has turned the attention back to the effects of water on the engine performance; an exhaustive review is found in [17]. Cycles such as water-spray inlet chilling (or fogging) and evaporative compressor

cooling (or spray intercooling) cycles have been successfully implemented [18, 19, 20] and discussed by many authors [21, 22, 23, 24].

To model the evaporative cooling cycles referred above, the initial value of the ambient humidity must be measured and considered into the thermodynamic calculations. The relative humidity sets a limit to the amount of water that can be injected before air becomes saturated and can not hold more water in gaseous state, hence, small water droplets start to condensate. The fact air can become over-saturated after the injection of water is not a limitation to the cycle. However, it demands more complex mathematical models – water droplet formation and two-phase flow aerodynamics – for its simulation [24]. In practice, the over-saturation of air is not desirable as it brings several engine component degradation issues [25]. The high rate of adoption of the technology had push some engine manufacturers to fund research projects in the sensor and control systems, specially designed for the conditions of excess humidity in the compressor [26]. The study of cooling or evaporative cycles is out of the scope of this project.

2.3.2 Effects of water/steam injection at the combustion chamber on the gas turbine engine performance

The injection of water or steam into the combustor chamber of the gas turbine engines was a recurrent research topic in the 1970s as a mean of reducing the atmospheric emissions of NOx. The main objective of the water injection at the combustor is to reduce the temperature of the combustion flame. The NOx formation occurs at high temperatures when the nitrogen found in the excess air is attracted to the molecular oxygen formed at high temperatures. Fundamental research on water injection at the combustion chamber to reduce NOx emissions [27, 28, 29] identified the water-to-fuel ratio as the main parameter affecting the amount of reduction of NOx emissions. Although relevant, the analysis of the engine emissions levels is out of the scope of this thesis work.

The main effects of the water injection on the engine performance are: a) a boost in power output caused by the increase in mass flow at the turbine and specific heat of the gases and the following raise in compressor pressure ratio, and b) a drop in thermal efficiency originated by a surge in fuel consumption [12, 30]. The change in efficiency using steam is less than when using water, as more energy is required for the later to evaporate.

Up to the mid-1990s the use of water and steam injection to reduce the emissions was common practice as exemplified by several publications from operators and manufacturers [31, 32, 33]. Though, the introduction of alternative technologies for emissions abatement, particularly the development the Dry Low Emissions (DLE) combustor technology had an impact on its market share [34, 35]. Kreitmeien [30] made a techno-economic analysis of the water injection and early DLE technologies reporting that for the same level of NOx emissions the water injected engine experienced a drop of thermal efficiency of 4% (and 11% power augmentation) while the DLE maintained the same levels of thermal efficiency and power output. Since the DLE technology emerged, the research work on this field is scarce and its application in industry limited.

Later research on the field was done by Mathioudakis [36, 37] who conducted an analytical study of the cycle reaching the same conclusions presented by early investigations: the water-to-fuel ratio is the parameter affecting the level of NOx emissions, power augmentation and thermal efficiency. He also suggests that the engine model has to provide for the change in the compressor operational point by means of variable geometry or non-dimensional scaling factors to have a more accurate estimation of the power deviation. Cardu and Baica [38] discuss the benefits to design a gas turbine engine with an equivalence ratio of 1 (stoichiometric mixture) and to use the injection of water to reduce the combustion flame temperature to nominal, safe levels. A reduction in turbine entry temperature, smaller compressor and even further reduced NOx emissions are claimed to be the main advantages of the proposed cycle.

The injection of steam, instead of liquid water, increases the power output and, contrary to what happens when water is injected, thermal efficiency of the cycle increases. This cycle is often referred as the STIG (Steam injected gas turbine) or Chen (after his inventor) cycle. During the1970s the steam injected gas turbine cycle as a mean to increase power output and thermal efficiency was being investigated and developed [39, 40, 41]. The technology remains in use as it provides a very cost effective way to increase power output without major modifications to power [42, 43] and process plants [44]. The present work does not consider the implementation of the Chen or STIG cycle.

2.3.3 Estimation of thermodynamic properties of different working fluids for gas turbine performance simulation

The accurate gas turbine engine performance simulation requires the estimation of the thermodynamic properties of different working fluids, namely, air and the products of combustion (with different equivalence ratios). There are different methods to calculate properties of the working fluid in a gas turbine engine performance simulation program: a) using ready-made polynomials; b) to implement specialized software on combustion kinetics; c) use of property tables; and d) use the concept of an ideal mixture of gases.

The use of ready-made polynomials is the least flexible solution to calculate properties of air or combustion products. Clearly, if the fuel composition is modified, the polynomial has to change. McMillan [9] implemented a set of ready-made polynomials from JANAF into Turbomatch that calculate the properties for dry air and the combustion products of Kerosene as a function of temperature and fuel-to-air (*FAR*) ratio. Walsh and Fletcher [12] also provide a set of polynomials with the same characteristics. Although an additional equation to calculate the properties of natural gas (with a fixed chemical composition) as a function of the same Kerosene combustion gases properties polynomials is also provided.

The property table method was implemented by GasTurb [8], a commercially available GT performance software. The use of tables reduces the computational time, but its accuracy depends on the density of data stored in the tables. And, similarly to the ready-made polynomials, when the composition of fuel is changed, a whole new set of tables for every fuel-to-air ratio have to be created.

A publicly available user-friendly code named Chemical Equilibrium with Applications (CEA) developed at NASA using the McBride and Gordon [45] polynomials was found. The program facilitates the characterisation of the fuel and air (dry or humid) mixture and provides a more complete set of results including dissociation effects. The software requires constant input from the user to characterise the reactants to different operating conditions of the engine. The results of the program would have to be compiled in property tables, with the advantages and limitations before mentioned. An alternative solution is the actual integration of CEA (or any other specialized combustion kinetics software) into the main performance simulation program. In the opinion of author the accuracy of the results would exceed the needs of the performance program for most cases, but it will make possible the estimation of emissions (NOx, CO_2, CO, etc), a desirable capability in these days when environmental impact of thermal engines is a concern. The disadvantages are the complexity of the integration process and an increase in convergence time of the performance program.

Finally, the thermodynamic concept of an ideal mixture of gases is widely used in the gas turbine engine performance simulation field [37, 10, 46]. Guha [47] proposes a set of simplified equations derived using the ideal mixture concept for the calculation of thermodynamic properties of combustion gases as a function of dry air. Its final mathematical expressions, introduces several factors that reduce the visibility and clarity of the process. More importantly, the factors do not take into account moist air.

The ideal mixture of gases method requires two main milestones: a) the characterisation of the mixture; and b) the calculation of properties for each component in the mixture. The characterisation of air (dry or moist) poses no difficulty as it has a constant composition over a wide range of ambient conditions [48]. On the other hand, the composition of the combustion products depends on whether a complete or incomplete process is assumed. A simple mass balance between reactants and products is done when a complete combustion is chosen [49]. On the other hand, very complex combustion kinetics analyses are required to model an incomplete combustion and to include the dissociation effects [50, 51]. There are many sets of polynomials for the calculation of properties of the common elements in air and combustion products [12, 52, 53, 54].

McBride and Gordon [45] developed a set of polynomials to calculate the thermodynamic properties of a large number of elements over a compound range (200-800 K and 800-2000 K). Some calculations showed a deviation of 8% at the boundary between the two ranges. Since temperatures experienced inside gas turbine engines are close to this boundary there would be an inherent error in the calculations. Bucker and Wagner [55] present a set of polynomials specifically designed to calculate the properties of moist air and combustion products and be used in gas turbine engine performance calculations. Each polynomial is defined over the range of 200-2000 K eliminating the inaccuracies presented by other models. Additionally, a simplified model to account for the dissociation effects, that become prominent after 1200 K, is included. The dissociation model was developed using CEA code to generate dissociation rate factors used in the calculations.

2.4 Theoretical method

2.4.1 Thermodynamic properties of different working fluids

As mentioned before, to implement the concept of the thermodynamic ideal mixture of gases, two main milestones had to be met: the characterisation of the mixture and the calculation of thermodynamic properties of every one of the mixture components. Section 2.4.1.1 gives the theoretical background behind the actual concept of an ideal mixture of gases, while Sections 2.4.1.2 and 2.4.1.3 cover the first milestone, the characterisation of the mixture, for air (dry and moist) and combustion products, respectively.

As for the polynomials used in the calculation of properties of the mixture components, the decision to use those in [55] was made. Their model would provide Turbomatch with the same capabilities than the more advanced CEA program without the need of building exhaustive tables or increase its dependency on an external program.

2.4.1.1 Thermodynamic properties of an ideal mixture of gases

The gases that comprise a mixture are often at high temperature and low pressure relative to the critical-point values of individual gases. In such cases the gas mixture and its components can be treated as ideal gases with negligible error [48]. In addition, properties like h, u, C_v and C_p of an ideal gas depend on the temperature only and are independent of the pressure or volume of the ideal-gas mixture.

There are two different types of properties: extensive and intensive. The extensive properties of a mixture are the sum of all contributions made by every component. For example, the total mass or moles of a mixture is the sum of the masses or moles of the individual components. On the other hand, intensive properties – such as h, u, s per unit mass or per unit mole – are approximated by a weighted average of the properties of the components. The weighting factor is either the mass fraction or mole fraction of each component y_i, calculated by dividing the component mass or number of moles over the mixture total mass or moles. For example,

$$h_m = \sum_{i=1}^{k} y_i h_i \qquad \text{or} \qquad C_{p,m} = \sum_{i=1}^{k} y_i C_{p,i} \tag{2-1}$$

where h_m and $C_{p,m}$ are the enthalpy and specific heat at constant pressure of the mixture, respectively. Since the mass of a substance can be expressed in terms of moles N and molecular weight M as $m = NM$, the average molecular weight of the mixture M_m can be expressed as

$$M_m = \frac{m_m}{N_m} = \frac{\sum N_i M_i}{N_m} = \sum_{i=1}^{k} y_i M_i \tag{2-2}$$

It is clear that to calculate the properties of the mixture, the identification of every component and their concentration is required. The following two sections explain how

to characterise air (dry and moist) and the combustion products for different hydrocarbon based fuels.

2.4.1.2 Characterisation of dry and moist air

Air is found in the atmosphere as a mix of different elements including water vapour. Air containing no water vapour is called dry air. The concentration of the other elements in air such as N_2, O_2, Ar, Ne show no variation under different conditions, therefore, the atmospheric air can be thought as the mixture of dry air and water vapour. Table 2.2 presents the volumetric percentage of air elements:

Table 2.2 Dry air elements

Element	Volumetric percentage
Nitrogen	78.08%
Oxygen	20.95%
Argon	0.1%
Neon	0.002%
Carbon dioxide	0.03%

The water vapour in the air can be considered an ideal gas without compromising in accuracy. In other words, the water vapour enthalpy is a function of temperature only, *h= h (T)*. Ji X, Lu X and Yan J [56] carried out an assessment of three different methods to calculate the properties of saturated and unsaturated moist air: ideal, mixing ideal and real. They conclude the ideal model can be safely used for low pressures up to 10 bar and temperatures above 280 K, and for high pressures (over 10 bar) only for temperatures over 360 K. The operational range of the method coincides with the conditions inside the compressor of an engine. We approximate the enthalpy of water vapour to the enthalpy of saturated vapour for a particular temperature as,

$$\begin{matrix} h_v(T > 280K, low\ P) \\ h_v(T > 360K, high\ P) \end{matrix} = h_g(T) \qquad 2\text{-}3$$

The amount of water vapour in air can be specified as an absolute or relative number. The absolute ω value represents the amount of vapour per unit of mass of dry air (m_a), or,

$$\omega = \frac{m_v}{m_a} \qquad 2\text{-}4$$

There is a limit of water vapour the air can hold before any additional moisture starts to condensate. This limit is a function of water saturation pressure (P_g) at a particular temperature. The relative humidity is defined as the ratio of actual vapour mass (m_v) to the maximum amount of vapour air can hold the same temperature,

$$\phi = \frac{m_v}{m_g} \qquad 2\text{-}5$$

Using the ideal gas general equation $PV = mRT$ and combining equations 2-4 and 2-5 , the two quantities can be expressed as a function of the other,

$$\phi = \frac{\omega P}{(0.622 + \omega) P_g} \quad \text{and} \quad \omega = \frac{0.622 \cdot \phi P_g}{P - \phi P_g} \qquad 2\text{-}6$$

where P is the total pressure of air, and P_g is the water vapour saturation pressure at a particular temperature.

In most practical applications, the amount of dry air remains constant while the water vapours fraction changes. For gas turbine engine performance programs, such as Turbomatch, moist air can be modelled using a factor called the water-to-air ratio *WAR* that corresponds to the absolute humidity ω.

2.4.1.3 Characterisation of combustion products

To calculate the thermodynamic properties of combustion products the characterisation of such mixture is needed. The final composition of the combustion products can only be obtained when applying the mass balance to every particular element in the reaction. That is, the total mass of an element in the products has to be equal to the total mass of the same element in the reactants.

The combustion process can be complete or incomplete. The complete combustion is defined as the process in which all fuel is consumed in the presence of an oxidiser to produce CO_2, H_2O, N_2 and SO_2. It is an incomplete combustion when unburned fuel and components such as C, H_2, CO, OH or NO_3 and NO_2 are present. The dissociation effect can be understood as the rearrangement of chemical elements to produce components with a lower enthalpy of formation than more complex products. During a combustion process the large amount of energy released by the fuel is used to form chemical elements such as CO_2, H_2O, N_2 and SO_2. After the bulk of the combustion products are formed, the levels of energy in the mixture decrease making it difficult to maintain the same rate of formation for complex molecules. Therefore, more simple compounds such as CO, OH, NO_x start forming. However, the reversibility nature of these reactions initiates a large number of chemical reactions before reaching a thermodynamic balance.

For most combustion processes, elements of air, excluding the O_2, and injected water are considered to be inert elements [48, 49], in other words, they do not take part in the reaction and maintain the same chemical composition and mass throughout the process. The minimum amount of air for the complete oxidation of a fuel is called stoichiometric or theoretical air. Any additional air present during the combustion process is called excess air. Theoretically, the excess air will not react during the combustion hence it will be found as part of the products unchanged.

The amount of fuel can be expressed in a dimensionless number called the Fuel-to-Air ratio (*FAR*). The ratio of the actual *FAR* to the stoichiometric *FAR* is called the equivalence ratio Φ. The percentage excess air in a reaction can be expressed in terms of equivalence ratio as,

$$excess\ air(\%) = \frac{100}{\Phi} - 100 \qquad 2\text{-}7$$

In most gas turbine engine applications, the combustion processes are designed to take place in excess air (100% to 250%) to maintain the flame temperature below the mechanical limits of the materials used and to induce a more complete combustion. As a consequence, the composition and properties of the combustion products are closer to those of air than to pure combustion products.

For hydrocarbon-based fuels, assuming a complete combustion with no dissociation, there is a general formula to estimate the stoichiometric moles number of air (oxidizer) and the main combustion products [49].

$$\overbrace{C_u H_v O_w N_x S_y}^{Fuel\ composition} + (u + \frac{v}{4} - \frac{w}{2} + y)(O_2 + 3.76\,N_2) + \overbrace{zH_2O}^{injected\ water} \longrightarrow$$
$$uCO_2 + \frac{v}{2}H_2O + ySO_2 + \left[3.76\left(u + \frac{v}{4} - \frac{w}{2} + y\right) + \frac{x}{2}\right]N_2 + \overbrace{zH_2O}^{injected\ water} \qquad 2\text{-}8$$

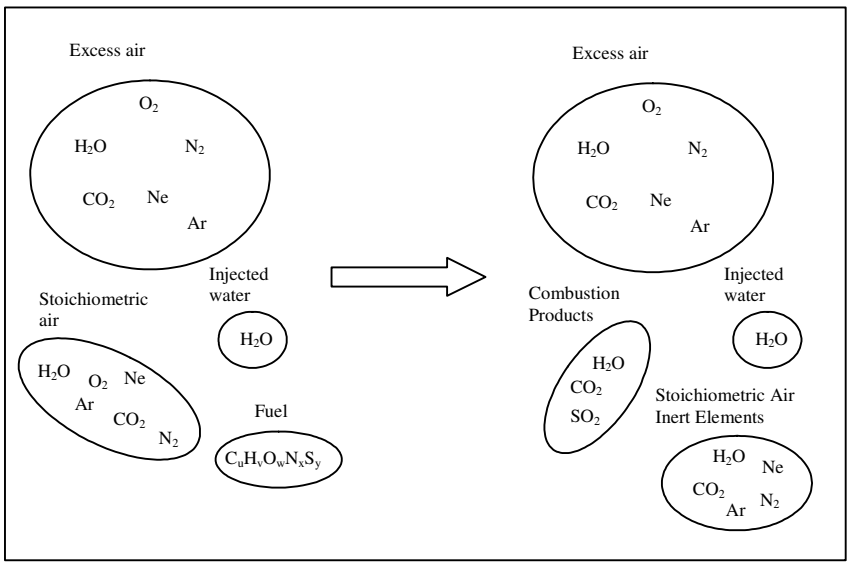

Figure 2-1 Graphical representation of the mass balance in a combustion reaction

Equation 2-8 can only be used when the chemical composition of the fuel is exact. Any fractional or decimal representation of any fuel is indication of an average of the different types of the same fuel. For example, natural gas chemical composition varies according to geological and geographical characteristics of the reservoir. Therefore, a chromatography analysis of a natural gas sample must be performed before attempting

to apply a theoretical model to determine the composition of its combustion products, even if the combustion is considered to be complete. Figure 2-1 depicts the mass conservation principle for a complete combustion process with excess air and water injection.

2.4.2 Injection of water/steam in the combustion chamber of a gas turbine engine

The main objective of the water injection at the combustor is to reduce the temperature of the combustion flame and/or increase power output. The combustion chamber is defined as the system and volume of control (see Figure 2-2). This thermodynamic analysis is considered for steady state conditions only. The chamber is an open system with three inlet and two outlet mass streams, where $\dot{m}_a$ is the main air flow coming from the compressor, $\dot{m}_f$ is the fuel flow, $\dot{m}_w$ is the water/steam flow and $\dot{m}_g$ is the combustion products. Using the mass conservation law we can state that

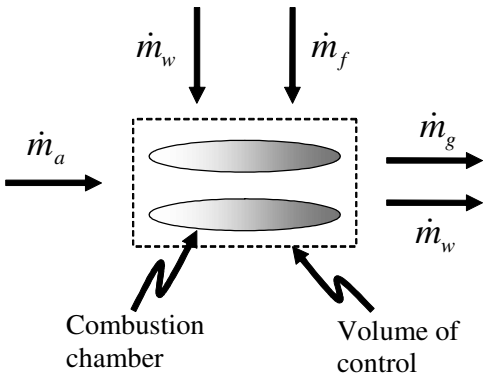

Figure 2-2 Combustion chamber thermodynamic system

$$\dot{m}_a + \dot{m}_f + \dot{m}_w = \dot{m}_g + \dot{m}_w \qquad 2\text{-}9$$

Equation 2-9 shows that the mass flow of the combustion products is the sum air and fuel mass flows, the oxidation of the fuel changes the actual chemical composition of the elements involved during the process. Section 2.4.1.3 gives a more detailed analysis on the composition of the combustion products.

Since the system under study is defined as an adiabatic steady-flow combustion process, the volume boundaries are expected to be insulated preventing any heat losses or inputs from the surroundings, $\dot{Q}_{in} = \dot{Q}_{out} \cong 0$. No work is being done by or to the system, $\dot{W}_{in} = \dot{W}_{out} = 0$, and potential energy is assumed to be negligible, $pe \cong 0$. Recombining the mass and energy balance equations and rearranging,

$$\dot{m}_a\theta_a + \dot{m}_f\theta_f + \dot{m}_w\theta_{w,i} = \dot{m}_g\theta_g + \dot{m}_w\theta_{w,o} \qquad 2\text{-}10$$

where $\theta = (h + ke)$ is the total energy of the fluid. The kinetic energy is expressed as $ke = V^2/2$, with V as the velocity of the fluid. On the other hand, the enthalpy h represents the state and chemical energies of the element $h = h_{state} + h_{chemical}$. It is also assumed that the inlet velocities of fuel and injected water are negligible in comparison to their enthalpies, therefore $\theta = h$ for the inlet conditions. Finally, it is considered the state energy of the fuel is insignificant compared to the chemical energy.

$$\dot{m}_a \theta_a + \dot{m}_f h_f + \dot{m}_w h_{w,i} = \dot{m}_g \theta_g + \dot{m}_w \theta_{w,o} \qquad 2\text{-}11$$

It is important to remember that any thermodynamic analysis looks only after the initial and final energy states of the system and disregards any intermediate step. Hence, it assumes a combustion process as a chemical reaction where fuel is oxidized by air and a large quantity of energy is released [48]. In the case of an adiabatic and complete combustion process, the heat generated is absorbed by the newly created, non-reactive products and inert elements like N_2, H_2O, Ar, etc. raising the final energy state of the mixture.

In theory, the outlet temperature of the combustion products is the adiabatic flame temperature, mainly, a function of the amount of air present during the combustion process. In reality, a temperature close to the adiabatic temperature is reached at the primary combustion zone to be later reduced by the cooling flows before leaving the chamber $T_{g,o}$.

For a given combustor outlet temperature $T_{g,o}$, equation 2-11 can be solved to calculate the fuel flow needed to bring the final mixture to the desired temperature. Substituting the fuel enthalpy h_f for the low heating value[1] (LHV) of the fuel and adding the combustor efficiency factor to account for any losses we have,

$$\dot{m}_f = \frac{(\dot{m}_g \theta_g - \dot{m}_a \theta_a) + \dot{m}_w (\theta_{w,o} - h_{w,i})}{LHV \cdot \eta_{cc}} \qquad 2\text{-}12$$

The amount of energy absorbed by the water depends on the phase (liquid or vapour) the water is injected. Figure 2-3 shows the water liquid/vapour diagram for any given operating pressure. Where T_B is the combustor outlet total temperature, and T_A and T_C are the temperatures at which water is injected for a liquid or vapour phase respectively. From the diagram, it is clear that a larger amount of energy is required to bring the water from point A to point B than from point C to point B. For example, if P=30 bars, T_B=1500°C, T_A= 40°C and T_C=500°C, the energy absorbed by the water for either case

[1] The enthalpy of combustion is also known as the heating value of a fuel when it represents the heat released when fuel is completely burned and the products are returned to the state of the reactants. In other words, the heating value is the absolute value of enthalpy of combustion of the fuel. The heating value depends on the phase of the H_2O in the products. It is called higher heating value (HHV) when H_2O is in liquid state, and it is called low heating value (LHV) when the H_2O in the products is in vapour form. Therefore the difference between the HHV and LHV is the enthalpy of vaporisation of water at the specified pressure.

would be $\Delta\theta_{w,L}$= 5745 kJ/Kg or $\Delta\theta_{w,V}$= 2456 kJ/Kg. For this particular case, injecting the water in liquid phase will demand 2.4 times more energy than doing it in vapour phase.

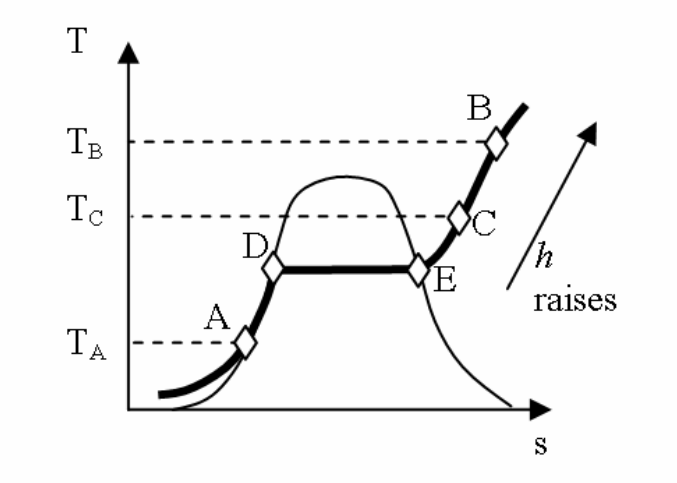

Figure 2-3 Water T-s diagram

Some useful observations on the effect the implementation of the wet combustion cycle has on the engine overall performance can be drawn from equation 2-12. If the combustor outlet total temperature is set to a specific value, the fuel consumption of the engine is proportional to the water mass flow injected. As a consequence, the engine thermal efficiency will decrease. On the other hand, if the fuel flow remains constant, the outlet total temperature of the combustion products will be inversely proportional to the water flow. On the positive side, the additional mass flow with a different specific heat of the working fluid will be expanded at the turbine(s) offsetting the negative effect of the injection of water or steam at the combustor chamber. A more detailed explanation is found in the results section 2.8.3.

2.4.3 Working fluid correction

This section describes the impact different working fluids i.e. dry air, moist air, combustion products have on the engine components performance.

In advanced engine performance calculations the usage of component characteristics or maps is common practice. These maps are built using non-dimensional parameters to facilitate its use with any particular engine. The maps are scaled up or down depending on the required operating parameters of the engine under study.

The non-dimensional parameters used in the construction of the maps are derived from the aerothermodynamic relationships between pressures, temperatures, speed, mass flows, isentropic efficiencies, etc. where the working fluid properties play an important role. For example, the speed of sound at a particular temperature will be determined by the properties of the working fluid, being more specific, by the square root of the ratio of specific heats (γ) and the constant of proportionality of the fluid, R.

As almost every component map is built using dry air properties, an error will be found when attempting to calculate the performance of a component using a working fluid different to dry air (moist air or combustion products). To eliminate this source of error, a correction of the full non-dimensional quantities outlined in [12] was followed in this work:

a) Load map in terms of referred parameters group for dry air.
b) Multiply referred speed (*N*) by square root or ratios of dry γ and *R* to prevailing values.

$$CNC = \frac{N}{\sqrt{T}} \cdot \frac{\sqrt{\gamma_{dry} \cdot R_{dry}}}{\sqrt{\gamma_x \cdot R_x}} \qquad 2\text{-}13$$

c) Look up referred map with the adjusted referred speed and beta.
d) Multiply each group output from the map by the ratios of prevailing γ and R to the dry datum with appropriate exponents.

$$CNC = \frac{N}{\sqrt{T}} \cdot \frac{\sqrt{\gamma_x \cdot R_x}}{\sqrt{\gamma_{dry} \cdot R_{dry}}} \quad \text{and} \quad NDMF = \frac{W\sqrt{T}}{P} \cdot \frac{\sqrt{R_{dry}}}{\sqrt{\gamma_{dry}}} \cdot \frac{\sqrt{\gamma_x}}{\sqrt{R_x}} \qquad 2\text{-}14$$

2.5 Computational tool

2.5.1 Turbomatch

Turbomatch is a powerful gas turbine engine performance simulation program, its ability to model any particular engine configuration originates on its modular structure. A master subroutine controls the entire process, from the pre-processing to the generation of the output files, calling several internal subroutines and functions in between. An input file with the engine configuration and data is produced by the user.

The pre-processing stages involve the identification of the input file name and path and to load the data from the input file into predefined arrays and variables. It is at this stage that the calculation units, operating mode (design or off-design), geometry (variable or fixed) and fuel type are defined. Any of these options are defined using a two letter codeword. In the case of the fuel type the original version had only KE for kerosene. Further modifications to the code were necessary to increase the number of options to 5 including kerosene (KE), diesel (DI), two types of natural gas "M" and "T" with different composition (GM and GT) and hydrogen (HY).

The configuration of the engine is set in the input file using predefined 6 letter codewords for each of the engine components i.e. NOZDIV for divergent nozzle, BURNER for combustion chamber, among many others. Every component (or brick) will be assigned two station numbers, inlet and outlet, and two corresponding arrays that store the more important variables to be transfer to and from the brick. These variables are managed in arrays called station vectors that include values for 8 parameters: Fuel-to-air ratio (FAR), Total temperature, Total pressure, Static temperature, Static pressure,

Velocity, Area and Mass Flow. The implementation of the humidity effects and the wet combustion required to increase the number of station variables to 10: water-to-air ratio (WAR) and the water quality (X) were included.

Every component will receive from the previous brick a vector with the inlet conditions (except for the case of the INTAKE). Inside the component the necessary calculations based on the appropriate aero-thermodynamic theoretical tools are carried out. For the implementation of water/steam injection into the BURNER brick involved the modification of the thermodynamic energy balance.

All computations inside the brick or component demand auxiliary or support subroutines and functions. For example, in the case of the compressor and turbine, the use of maps or component characteristics required a specialized subroutine to search and extract data from the multidimensional tables containing these maps. Another set of subroutines and functions, used almost by every brick in the program, calculate the thermodynamic properties and gas constant R of the working fluid. The original subroutines and functions could only calculate the properties of dry air or the combustion products of Kerosene. New subroutines and functions able to calculate the properties of dry air, moist air and combustion products from different fuels were put in place as described by the next sections.

The program can perform two types of analysis: design point (nominal or warrantee point) and off-design (part load) point conditions. The results of the analyses are printed on the output text file. The file contains a detailed description of the main parameters of each component and a table with the values of all the station vectors.

The following subsections provide details on the improvements done to Turbomatch to provide the program with new functional capabilities listed in the introduction of this chapter, and for which, the previous theoretical background was presented. Inside the newly created *WorkingFluidProperties* module, the following new subroutines are found: HUMIDITY, WTP, TRM, AIRTAB, WFSCAL, GASCONST and BURNER. A brief explanation of the changes done to the input and output files and general remarks is found in sections 2.5.9, 2.5.10 and 2.5.11.

2.5.2 HUMIDITY

HUMIDITY is a new subroutine responsible for calculate the water content in ambient air. The subroutine is called by the INTAKE brick where the ambient pressure and temperature values are also known. The relative humidity is an input data provided by user, consequently, a new INTAKE brick data variable has been created. The subroutine follows the theoretical method presented in section 2.4.1.2 to calculate the absolute humidity ω or the amount of water in the air by mass.

As mentioned in section 2.4.1.2, the moisture in air is usually considered to be an additional component to dry air. The new *TRM* subroutine (section 2.5.3) was designed to calculate the properties of air using *WAR* to account for the humidity effects. The subroutine arguments are:

HUMIDITY (P, T, RELHUM, WAR, X)

where *P* is the pressure, *T* is temperature, *RELHUM* is the relative humidity, *WAR* is the water-to-air ratio, and *X* is the water quality. The quality is included only for the sake of future modifications to Turbomatch that can evaluate the properties air with a mixture of liquid and vapour water.

2.5.3 TRM

TRM is a function that calculates the thermodynamic properties (enthalpy, calorific heat and entropy) for the working fluid. The original version delivered results for dry air and combustion products from Kerosene using single polynomials for each property (enthalpy, specific heat and entropy). The polynomials are a function of temperature and *FAR*, using a value of zero (0) for the later when properties of dry air are needed. Since temperature *T* was the only dependent variable in the expression, it was clear that the polynomials were designed under the ideal gas mixture assumption.

The new TRM delivers the thermodynamic properties of dry air, moist air and the products of combustion for different fuels. The subroutine is based on the concept of the ideal gases mixture introduced in section 2.4.1. The subroutine follows a sequential process to identify the composition of the mixture and to calculate the molar fraction of each component as described in next section.

The fuel type is chosen using a two letter codeword part of the input file (see section 2.5.9.5 for a detailed description). A first concept of the TRM function considered the possibility of allowing the user to choose from an existing fuel type set or to define a new type of hydro-carbon based fuel, unfortunately, the rigid structure and format of Turbomatch's input file made difficult its implementation. The version, at the time of writing, has a fixed number of fuel types: Kerosene (KE), Diesel (DI), Natural gas Type "M" (GM), Natural gas Type "T" (GT) and Hydrogen (HY). Further modifications to Turbomatch's internal code would be necessary if new fuel types were added.

Since the number of fuel types and their chemical composition remained fixed, the characterisation of their combustion products was done outside Turbomatch to reduce the algorithm computation time. A dedicated Excel® spreadsheet was created to carry out these calculations. Assuming a complete combustion, equation 2-8 was used to derive the molar stoichiometric fractions for the combustion products and the stoichiometric *FAR*. In the case of the natural gas blends, the mass balance analysis was carried out for each of the species before deriving the properties of the mixture through a weighted average. Finally, the results were transferred to Turbomatch as global arrays accessible to all subroutines and functions.

2.5.3.1 Code

The new functional requirements of TRM demanded a flexible logic able to carry out the calculations for all types of working fluid using the same structure and data. The need for calculating the properties of different working fluids either at the cold (compressor) or hot (turbine) sections of the engine, to account for the water/steam

injection at the combustion chamber and include the atmospheric humidity effects pushed for the modification of the existing arguments. The new arguments of the function are,

TRM (FAR, T, ID, WAR, X, P)

*w*here *FAR* is the fuel to air ratio, *T* is the temperature, *ID* is the identification number for the particular property i.e. 1= calorific heat, 2=enthalpy and 3=entropy, *WAR* is water-to-air ratio (by mass), *X* is the water quality and *P* is pressure.

Note that pressure *P* was only included as an argument of the function to build the required infrastructure for future modifications to Turbomatch, and NOT as a working variable in the subroutine. The aforementioned improvements, out of the scope of this project, could comprise the injection of water or vapour at the intake or compressor of the engine that requires the pressure *P* to access the water properties polynomials (or commonly presented in tables). Having the pressure *P* in the argument would facilitate the upgrading of TRM with a more advanced subroutine that includes the effect of real gases.

Figure 2-4 shows the diagram flow for the latest version of TRM. It can be divided in three steps: a) COMBPROD: the estimation of the molar fraction of each component of the working fluid, b) GASCALC: the calculation of the properties of each individual component for a particular temperature, and c) the computation of the mixture properties.

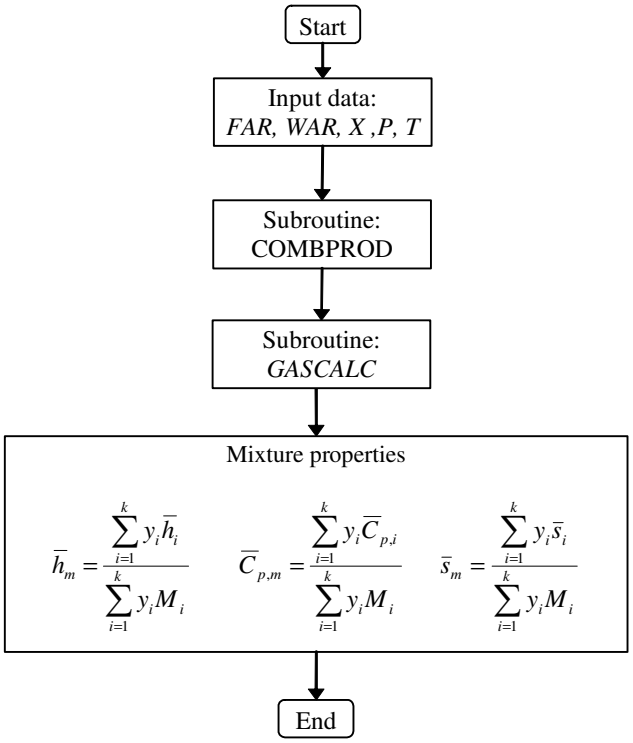

Figure 2-4 TRM function diagram flow

COMBPROD

The main objective of the subroutine is the calculation of the molar fractions for all mixture components. A global vector *y* is created to store the results obtained. The arguments of the subroutine are:

COMBPROD (FAR, WAR, X, P)

Figure 2-5 shows the diagram flow for COMPROD subroutine. The main logic behind this subroutine is sequential upgrading steps of the working fluid molar fraction result vector *y*. The process begins with a general step to change WAR from a mass basis to a molar basis WAR_{molar}.

The results vector *y* takes the values of dry air volumetric percentages assuming the working fluid is indeed dry air. Then, a first conditional evaluates if the fluid under analysis contains water vapour through $WAR_{molar} > 0$. A positive answer will equate the molar concentration of water in the result vector y_{water} to WAR_{molar}. When negative, the process continues to the next upgrade phase.

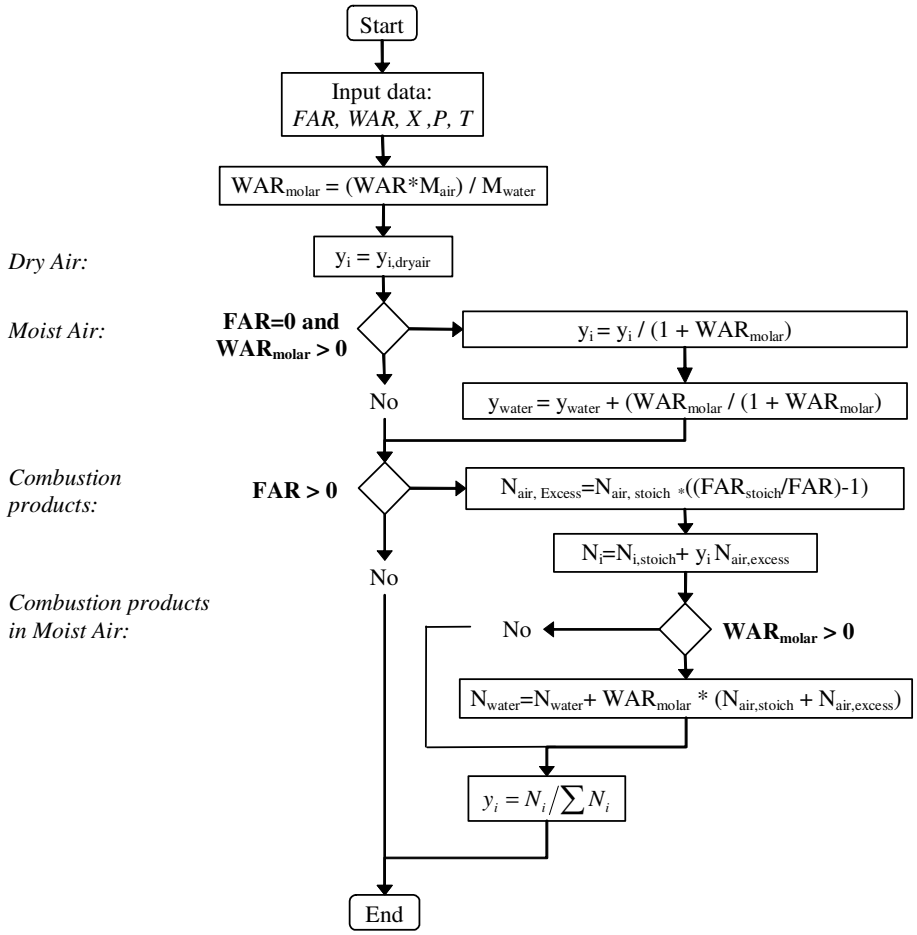

Figure 2-5 COMBPROD subroutine chart flow

A second conditional will evaluate if $FAR > 0$, if positive the working fluid is treated as a mixture of products of combustion, when negative the process continues to the end of subroutine with y unchanged. In the positive case, the estimation of the moles for each component in the mixture is done and results are stored in vector N. Next, the moles of excess air, $N_{air,excess}$, are calculated from equation 2-7. Subsequently, the moles for each component of excess air are computed as the product of the current working fluid molar fraction vector y and the number of moles of excess air, $N_{air,excess}$. To know the total number of moles of each component in the final mixture, the sum of the stoichiometric moles of the combustion products, $N_{i,stoich}$, and moles of each component from the excess of air $N_{air,excess}$ is done.

Up to this point, the code has calculated the number of moles for each component of the products of combustion and stored them in the vector N. An additional step designed to account for the injection of water effect on at the combustion chamber is included. In this case, the conditional evaluates if $WAR_{molar} > 0$. When negative the code continues to the calculation of y. When positive, the number of moles of water injected at the combustor is estimated with the product of WAR_{molar} and the total number moles of air admitted into the combustor ($N_{air,stoich}$+$N_{air,excess}$). The final number of water moles in the mixture is estimated with sum of the moles of water injected and the moles of water in the combustion products.

Finally, the estimation of the molar fraction for each component of the final mixture y_i is done dividing the number of moles for each component N_i by the total number of moles in the mixture $\sum N_i$. This result vector will be used by TRM once the properties for the individual component are calculated in subroutine GASCALC.

GASCALC
The GASCALC subroutine carries out the calculation of the thermodynamic properties for the individual components of the mixture using the polynomials developed by [55]. Assuming the mixture is an ideal gas, temperature T is the only independent variable used.

2.5.3.2 Validation

Before the implementation of the new TRM into Turbomatch, a validation exercise was made. The comparison between the new TRM and the polynomials used by Walsh and Fletcher [12] and the CEA [45] program is found next.

Walsh and Fletcher
The comparison on the properties of dry air is shown in Figure 2-6. The results present a maximum error of around 0.08% at very low temperatures. This means the assumption made that dry air behaves as an ideal gas across the range 200K<T<2000K is valid, or at least, that is the same consideration made by Walsh and Fletcher to construct their correlations. The method used of treating dry air as a mixture of ideal gases was justified by these results.

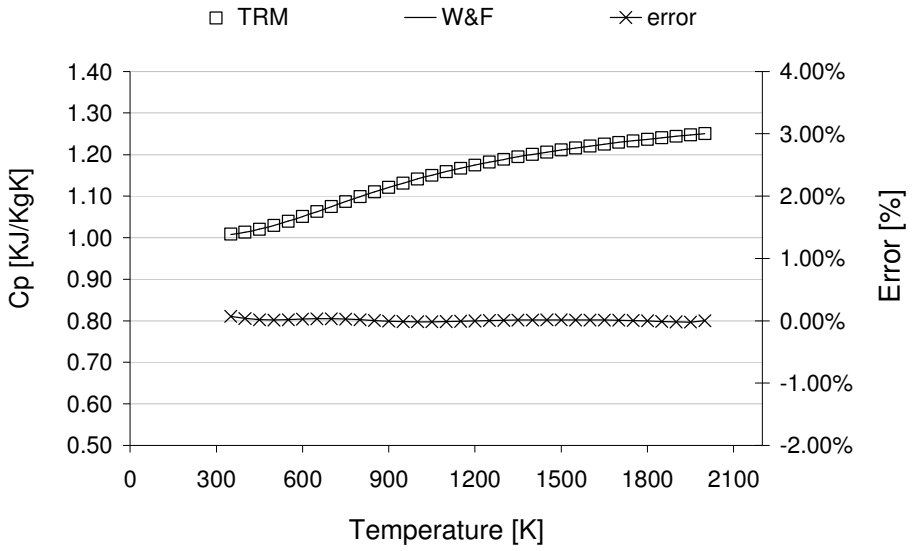

Figure 2-6 Specific calorific heat for dry air

The results for combustion products of Kerosene are found in Figure 2-7. To create this graph an arbitrary value of FAR=0.02 was chosen and the analysis was done over the 350K<T<2000K range. In this case, the lower limit of the range was defined knowing it is very unlikely that the properties of the exhaust gases for temperatures below 350 K will ever be needed. The results are encouraging since the maximum absolute error is about 0.60% for temperatures close to the lower limit, at which, the exhaust gases of a gas turbine engine never reach. On the high end of the range, the function produces an acceptable error of 0.30%.

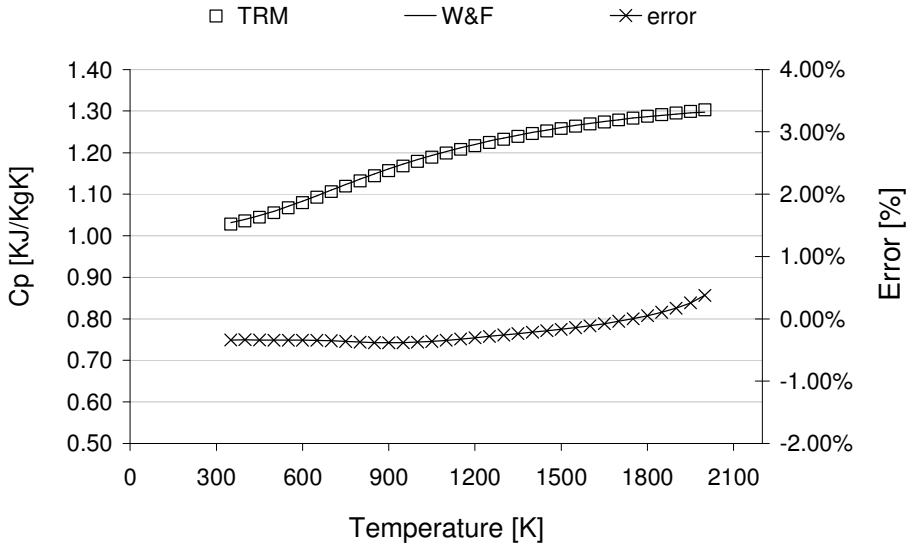

Figure 2-7 Specific calorific heat for kerosene combustion products @ FAR=0.02

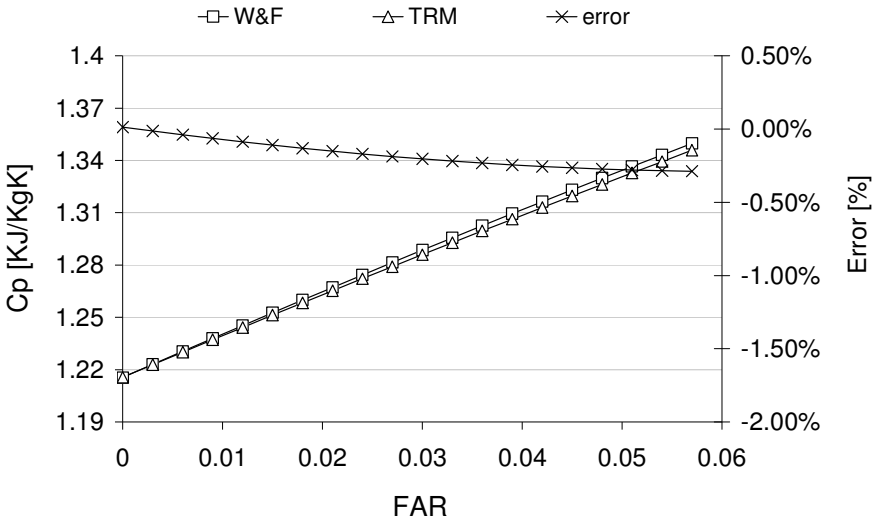

Figure 2-8 Specific calorific heat for kerosene combustion products @ T_4=1545 K

In order to assess the ability of TRM to deliver the accurate results for a wide range of FAR, a final analysis was done. The temperature was fixed to an arbitrary value 1545 K while FAR was varied in the range of 0<FAR<0.07, results are presented in Figure 2-8. The maximum absolute error is around 0.30% at *FAR* values close to the stoichiometric *FAR* for kerosene of 0.68.

Chemical Equilibrium with Applications (CEA)

A second comparison against NASA's CEA program was made. The analysis was done using the same value of FAR=0.02, the temperature range of 350K<T<2000K and assuming a complete combustion process (see Figure 2-9). The fitness between the two curves has an error within a band of ± 0.6%. The oscillation of CEA's results after 1000 K, explicitly shown by the error curve, is caused by the program's iterative solver looking to balance out the system when no disassociation is considered.

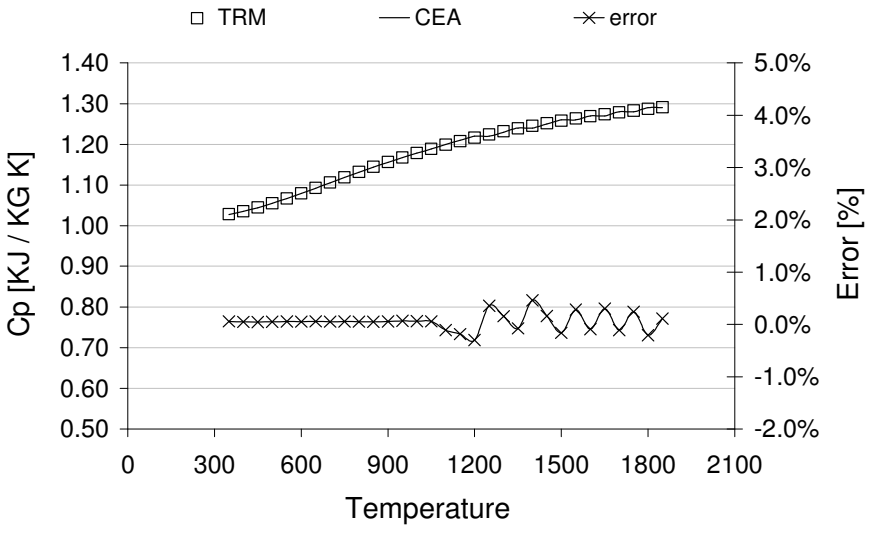

Figure 2-9 Specific calorific heat for kerosene combustion products @ FAR=0.02

2.5.4 AIRTAB

AIRTAB subroutine searches the solution domain of TRM for the temperature at which the working fluid presents an exact value of calorific heat, enthalpy or entropy for the given particular FAR and WAR values. The non-linearity attribute of the governing equations to estimate the performance of the gas turbine engine demands an iterative approach to obtain a solution.

The original AIRTAB subroutine used explicit polynomials and a simple iterative algorithm to solve the system. The polynomials were derived from the expression found at the old TRM hence it could only solve cases in which dry air or the combustion products of kerosene were defined as working fluids. The iterative algorithm evaluated the error between the n_{th} and n_{th}-1 solutions until reaching a predefined minimum absolute error. This subroutine became obsolete once the new TRM function was developed.

The new AIRTAB subroutine uses the TRM function and an original iterative algorithm developed by the author to find the corresponding temperature. The use of TRM function offered certainty to find a solution within a proven temperature domain for any particular type of working fluid.

The most important part of this subroutine is the iterative algorithm. One of the algorithms considered was the linear approximation, extremely simple but with the disadvantage of compromising accuracy for processing time. Another option was the gradient based algorithm. In comparison to other simpler options, this algorithm performs at its best when solving complicated response surfaces. On the other hand it demands a more elaborate code than others. It relies on the magnitude of a predefined error and the percentage increment to achieve good accuracy levels. It disadvantage is that it can spend many iterations going from one side of the maximum to the other because the error margin is to big to reach the maximum point. At the end, an original algorithm that follows an intuitive non-linear approximation based in multiples of 10 was created by the author.

This new algorithm delivers fast solutions without compromising in accuracy. In fact, it reports a reduction in number of iterations of around 50% in comparison to the original iterative algorithm. One of the main features of the algorithm is that the accuracy level depends on the internal parameters of the algorithm rather than a fixed error. To limit the solution domain, the algorithm requires a starting point and the right magnitude of the initial steps. Note the algorithm has been only tested for one-dimensional systems and no warrantee is made on its performance to find a solution over 2D or 3D solution domains.

2.5.4.1 Code

The use of TRM as part of AIRTAB subroutine meant the same input data, excluding temperature, was needed. The subroutine arguments are the following:

AIRTAB (ID, FAR, WAR, X, P)

where *ID* is the identification number of the known property (1=specific heat, 2= enthalpy, 3=entropy), the *FAR* is the fuel to air ratio, *WAR* is the water to air ration, *X* is the water quality and *P* is the pressure. The addition of *P* is to build the required infrastructure for future modifications to the subroutine.

A section of the subroutine's code containing the iterative algorithm is found below. In this case, the target value is stored in the variable PROP while T returns the solution (temperature) of the system. A temporary variable TT is also defined. The algorithm is built using two nested loops – ILOOP and IILOOP – that will manage the magnitude of the steps and the value of the increment, respectively. The counter M and the factor (1000/10*M) define the magnitude of the step. For M=0, the step magnitude will be in the order of the thousand units (1000) whilst M=6 will signify steps of only one-thousand of a unit (0.001). The second loop IILOOP defines the value of the increment by multiplying the value of the counter N times the step magnitude. For example, if M=0 and N=2 the total increment is 2000.

```
        TT=0
        T=0
ILOOP:      DO M=0,6
IILOOP:             DO N=1,9
                        TT = T+N*(1000/10**M)
                        IF (PROP < TRM(FAR,TT,ID,WAR,X,P)) EXIT
IILOOP
                    END DO
                T=T+(N-1)*(1000/10**M)
                END DO
```

The temporary variable TT will take the value of 1000 for the first iteration. TRM will evaluate the property of the working fluid at 1000 K and will report the solution to be compared against the target value PROP. If PROP is less than TRM's result, the code will exit IILOOP. Otherwise, it will set the value of N=2 and evaluate TRM at 2000 K.

Every time the code exits IILOOP the final solution variable T will sum up a new value equal to the final step magnitude times the increment value of N-1. The code will return to ILOOP to set M=1 to make the magnitude of the step of a hundred units (100) only. The process repeats itself until M=6 and T stores the final solution to the system.

2.5.5 GASCONST

The function calculates the gas constant *R* of the working fluid. The original subroutine could only calculate the gas constant for dry air and combustion products of kerosene as a function of FAR, taking a value of zero when dry air properties were needed.

The new version of GASCONST obtains the gas constant for any particular gas dividing the universal gas constant by the molecular weight of the working fluid. Equation 2-2 is used to calculate the molecular weight of the working fluid. The molar fraction *y* is estimated using the COMBPROD subroutine while the molecular weight of the

components of the mixture is retrieved from the data block *BLOCKDATA_WORKINGFLUID.F90*. The arguments of the subroutine are:

GASCONST (FAR, WAR, X, P)

where *FAR* is the fuel to air ratio, *WAR* is the water to air ratio, *X* is the water quality and *P* is the mixture pressure. Again, the pressure *P* is included for the sake of future modifications to Turbomatch only.

2.5.6 BURNER

The new functional requirements for Turbomatch demanded the ability to calculate the performance of an engine operating with the injection of water or steam at the combustor. The following section describes the modifications made to the BURNER subroutine.

The implementation of the wet combustion cycle brought a series of changes to different sections: the component brick data, the energy balance equation, the implementation of a new iterative process and the calculation of the correct fuel and air mass flows, among other secondary actions needed to make the whole subroutine work. Additionally, a new subroutine dedicated to estimate the properties of water at different conditions was developed.

2.5.6.1 Code

The first step was to define three new brick data variables in the subroutine: the water flow (*INJW*), water temperature (*INJT*) and water quality (*INJX*). The injected non-dimensional water content in air *INJWAR* is calculated dividing *INJW* by W_A, the mass flow at the combustor inlet that represents the sum of air and water vapour, when humidity is considered. *INJWAR* becomes a water-to-working fluid ratio rather water-to-air ratio.

In the case the user wants to provide the water flow as the non-dimensional water-to-working fluid ratio, the *INJW* should be input as a negative value. The program will equate INJWAR= –INJW and calculate *INJW* as the product of *INJWAR* times the inlet total mass flow W_A.

The water quality variable *INJX* can only take values of one (1) for liquid or zero (0) for steam. Whenever water is injected as steam, *INJX*=0, the temperature *INJT* must be above the steam saturation temperature at the particular pressure. If the later is not true, *INJT* takes the value of the saturation temperature to avoid any conflict.

The energy balance is calculated using equation 2-12 divided by $\dot{m}_a$ (or W_A) to obtain a non-dimensional expression using the terms of *FAR* and *WAR*:

$$FAR = \frac{\left(\theta_g - \theta_a\right) + INJWAR\left(\theta_{w,o} - h_{w,i}\right)}{\left(LHV\right)\cdot\eta_{cc}} \qquad 2\text{-}15$$

where *LHV* is determined by the global variable *KFUEL* (section 2.5.9.5), the properties of water – $\theta_{w,o}$ and $h_{w,i}$ – are calculated using subroutine WTP (section 2.5.7), and the properties of air θ_a and combustion products θ_g using TRM (section 2.5.3). The fact θ_g is a function of *FAR* demands the use of an iterative routine to solve the system. The initial value of FAR to evaluate θ_g is zero (0), that is, the combustion products are considered to be air. The result obtained is reintroduced into the expression until there is no significant error between the solution and the value used to calculate θ_g. After some tests, it was found five is the number of iterations before the system reaches the equilibrium. Once FAR is calculated, still inside the iterative routine, the fuel flow is obtained using $\dot{m}_f = FAR \times \dot{m}_a$.

After the solution is found all different parameters are referred back to air. If the correction is not made, the properties of the combustion products will be overestimated. Below, an extract from the subroutine code used for this purpose is found.

```
WAA=WA/(1+FAR_A+WAR_A)
WAW=WA*WAR_A/(1+FAR_A+WAR_A)
WAF=WA*FAR_A/(1+FAR_A+WAR_A)

WB=WAA+WAW+WAF+INJW+ṁ_f
FAR_B=(WAF+ṁ_f)/WAA
WAR_B=(WAW+INJW)/WAA
```

The air (*WAA*), water (*WAW*) and fuel[2] (*WAF*) mass flows fractions in W_A are calculated using the non-dimensional quantities of *FAR* and *WAR* at inlet. Once the different flows in W_A are known, the outlet total mass flow W_B can be calculated by adding the injected water (*INJW*) and fuel ($\dot{m}_f$) flows to W_A. The outlet fuel-to-air ratio FAR_B is the sum of *WAF* and $\dot{m}_f$ divided by *WAA*. In the case of the water-to-air ratio WAR_B, the addition of *INJW* to *WAW* becomes relevant as humidity or an injection of water before the combustor must be considered in the final mixture.

2.5.7 WTP

WTP is a new function that calculates the properties of water. It contains a number of polynomials that can deliver properties for water in different states, liquid and vapour, at different pressure levels. It is used by BURNER to compute the enthalpy difference of water during the energy balance workings. The function arguments are:

WTP(T, P, X)

where *T* is temperature, *P* is pressure and *X* is state or identification number (0=saturated water, 1=superheated steam, 2=saturated steam). The function was specifically designed to facilitate the calculation of the wet combustion cycle and to

[2] Included for the sake of future modifications to Turbomatch that would allow unburned hydrocarbons as part of the working fluid to be simulated.

prevent ill scenarios to be calculated by Turbomatch. In the case water is injected in a superheated steam quality *X=1*, the temperature *T* must be above the saturation temperature at pressure *P*. To avoid any critical failure in Turbomatch caused by ill defined values, the WTP function estimates the saturation temperature T_{sat} and compares it against temperature *T*. If $T_{sat} > T$ then *T* takes the value of T_{sat}, otherwise the program continues the calculation of the enthalpy.

2.5.8 WFSCAL (Scaling factor calculation)

WFSCAL is a new subroutine that generates the scaling factors used to correct the characteristics or maps of different engine components. There was no mechanism in Turbomatch to account for the effect of changes in the working fluid characteristics on the performance of individual engine components, particularly compressors and turbines. Turbomatch's maps were created using the properties of dry air only. Section 2.4.3 presents a brief explanation on the subject and outlines the procedure followed. The arguments of the subroutine are:

WFSCAL(FAR ,WAR ,X ,T ,P , INSCNC, OUTSWAC, OUTSCNC)

where *FAR* is fuel-to-air ratio, *WAR* water-to-air ratio, *X* is the water quality, *T* is temperature and *P* is the pressure, required to calculate the properties of the working fluid. On the other hand, *INSCNC* is the rotational speed scaling factor to enter the maps, while *OUTSWAC* and *OUTSCNC* are the non-dimensional mass flow and speed exit factor respectively. The subroutine is included at the first sections of the COMPRE and TURBIN bricks where they fed the information on the working fluid into the subroutine. The scaling factors are used before and after the calculations using the maps.

2.5.9 General aspects

2.5.9.1 Units

Turbomatch uses a particular set of units throughout all internal calculations. The unit flags for imperial (IM) and international (SI) only define the right conversion factor to be applied when loading data from the input file and before printing the results on the output file. Therefore, any modification to the internal workings has to use the internal units (see Table 2.3).

Table 2.3 Turbomatch units

Pressure	atm	Atmospheres
Length	ft	Feet
Energy	CHU	Calories

All quantities generated by the new TRM and GASCONST subroutines had to be converted using a factor of 4.187 KJ/Kg = 1 CHU/lb. Similarly, the calorific values for the fuels (*LHV*) were converted to CHU/lb.

2.5.9.2 Station vector dimension

The original dimension of the station vectors in Turbomatch was eight (8). It has been mentioned these station vectors contain the relevant thermodynamic information of the different components. There is one vector for the inlet and another for the outlet. The inlet vector receives the information from the previous component's outlet vector. The outlet vector is filled with the results of the internal calculations, and sometime with values from the inlet vector.

The development of the new capabilities into required the expansion of the vector dimension to carry extra information. Two new quantities were defined: *WAR* water-to-air ratio and *X* water quality. Hence, the dimension of the station vectors was brought to ten (10) as shown in Table 2.4.

Table 2.4 Station vector (array) description

ID	Description	Nomenclature
1	Fuel-to-air ratio	FAR
2	Mass flow	W
3	Static pressure	PS
4	Total pressure	P
5	Static temperature	TS
6	Total temperature	T
7	Velocity	V
8	Area	A
9	Water-to-air ratio	WAR
10	Water quality	X

2.5.9.3 Water-to-air (WAR) ratio station variable

The water-to-air ratio *WAR* station variable was implemented to account for the additional water mass present in the working fluid. Before the combustion chamber, *WAR* represents the moisture in air, calculated by subroutine HUMIDITY inside the INTAKE brick.

Past the combustion chamber engine stations, *WAR* represents the additional water content in the main flow of combustion products. It is important to mention that even though water is a big contributor to the combustion products themselves, *WAR* only concern is the amount of water externally added to the main stream.

2.5.9.4 Water quality (X) station variable

The water quality station variable *X* was introduced to represent the percentage of water vapour from the total water mass flow contained in the working fluid. The quality variable is complemented by the water-to-air ratio *WAR* that defines the total amount of water per unit of dry air. When $WAR \neq 0$ the quality variable can take values from $0 \leq X$

≤ 1. For X=0 no water has yet evaporated, conversely, $X=1$ means all water is in vapour state. All other values in between represent a liquid-vapour mixture commonly used in the Rankine cycle calculations.

In the near future, Turbomatch could be modified to simulate the injection of water at the intake of the engine or at any stage in the compressor. The phenomenon would involve the evaporation of water causing a cooling effect on the main stream. However, if the amount of water injected is beyond the maximum value air can hold as vapour, the water will remain liquid or even condensate. This mixture will then be represented by a fraction value for *X*.

In the meantime, the variable needs to be managed correctly to show the appropriate values, 0 or 1. Fortunately, the simulation of the humidity effects and the injection of water at the combustor only produce values of X=1. Moist air is by definition a mixture of dry air and water vapour (X=1), while all the water injected at the combustor will evaporate to reach a superheated state (X=1).

At the start of any performance case calculation, the initial value of X is zero. It is only if WAR at the INTAKE brick is different to zero that X takes a value of 1. The station vector is passed on to the next brick keeping the same quality throughout the engine. At the combustor, where the injection of even more water is expected, a conditional evaluates the scenario. If WAR at the inlet of the combustor and the INJWAR are zero, then the outlet WAR and X are zero. Otherwise the inlet WAR and X vector variables will be passed on to the outlet station. It is obvious that if water is injected at the combustor WAR≠0 and X=1.

2.5.9.5 Fuel selection

The selection of fuel is done by the use of a two letter codeword. The codeword is found in the same line where the design or off-design performance case mode (*DP* or *OD*), imperial or metric units (*IM* or *SI*), constant or variable geometry (*CT* or *VA*) and printing options (*FP* or *SP*) are defined. For the purpose of this explanation, the line is called the “flag line”. As mentioned before, Turbomatch original version could calculate the performance of an engine burning Kerosene. The two letter codeword for this single option was *KE*. Therefore, any implementation of an expanded list of fuel types would require a new set of codewords.

These codewords are defined inside the main subroutine as part of a large codebreaker string. A subroutine compares the two letters found in the flag line against the codebreaker string and stores the position at which the codeword is found. Once the position is found, the program returns to the main subroutine and enters a SELECT CASE unit. In this SELECT CASE different global or local variables take a specific value that reflects the chosen flag. In the case of the fuel type, the global variable KFUEL is used.

Table 2.5 Fuel types with codeword

KFUEL	Fuel	Codeword
1	Kerosene	KE
2	Diesel	DI
3	Hydrogen	HY
4	Natural gas type M	GM
5	Natural gas type T	GT

The final codebreaker string is DPODIMSIKEDIHYGMGTCTVAFPSPNPXP. The new string includes the new two letter codewords for the predefined list of fuels: kerosene (*KE*), diesel (*DI*), hydrogen (*HY*), natural gas type M (GM) and natural gas type T (*GT*). Once the SELECT CASE unit is entered, *KFUEL* will take values from 1 to 5 depending on the codeword used. Such value is of great importance since it is used to enter data blocks containing the information of the chosen fuel during the calculation of the working fluid properties and the combustion energy balance. The arrays have a shape of (5, 10) with the row indicating the type of fuel (*KFUEL*) in the order listed in Table 2.5 and the 10 columns storing the data described Table 2.6.

Table 2.6 Gas properties data – array structure

Column position	Element	Description
1	N_2	Stoichiometric moles of each component of the combustion products (N_i)
2	O_2	
3	Ar	
4	Ne	
5	H_2O	
6	CO_2	
7	CO	
8	SO_2	
9	Fuel-to-air ratio	Stoichiometric FAR (FAR_{stoich})
10	Air	Stoichiometric moles of air ($N_{air,stoich}$)

Additionally, the Low Heating Value (LHV) for each fuel is stored in another array of shape (1,5) and accessed with the *KFUEL* variable. Other vectors with the composition of dry air in a volumetric percentage (equal to molar fraction for ideal gases), molecular weight and gas constant *R* for the components of combustion products were also defined. The dimension of these arrays is (1,8) and maintain the same order of the first eight elements of Table 2.6.

All the above data is found in the files named *COMMON_WORKINGFLUID.FI* and *BLOCKDATA_WORKINGFLUID.F90*. More types of fuel can be added by modifying the size of the arrays and making the pertinent changes in the master subroutine.

2.5.9.6 Isentropic process calculations

An error in the estimation of real and isentropic conditions inside various components occurred after the new TRM, AIRTAB and GASCONST subroutines were implemented. The miscalculations were traced back to the incorrect use of an expression in the original Turbomatch. The obvious mistake in the definition of equations 2-16 is the incosistency of units.

$$\phi_{BS} = R \cdot \left(\phi_A + \ln\left(\frac{P_{BS}}{P_A} \right) \right) \qquad \text{or} \qquad \phi_{BS} = \phi_A + \ln\left(\frac{P_{BS}}{P_A} \right) \tag{2-16}$$

This error was present throughout the program in subroutines like COMPRE, TURBIN, MIXFUL, NOZDIV, AFROMV, VFROMA, INTAKE, NOZCON, among others. Another ill defined equation 2-17 was found in subroutines MIXFUL and NOZDIV.

$$T_2 = T_1 \cdot e^{4\left(\frac{\phi_2 - \phi_1}{R} \right)} \tag{2-17}$$

where the factor four (4) is the inverse of an approximation of C_p to 0.25, in units CHU/lb K. The correct expression should not include the gas constant R.
I

2.5.10 Input file

The input file is the only interface between Turbomatch and the user. Turbomatch has a number of dedicated subroutines and functions specifically programmed to process the data found in the input file. The data must follow a predetermine format and nomenclature, or else, the program will crash. The insertion of an additional line of data will require the modification of the master program and other internal subroutines. More importantly, all other past programmes using Turbomatch as a core engine i.e. Pythia [57] could become obsolete.

Consequently, the implementation of new capabilities into Turbomatch was achieved with minor changes to the input file (see Figure 2-10). The number of fuel types was increased to five (5) using two letter codeword system (section 2.5.9.5). Additional brick data variables were added to different bricks or components. One brick data variable to allocate the relative humidity value to the INTAKE brick was defined. In the case of the BURNER, the injection of water/steam demanded the definition of three new brick data variables.

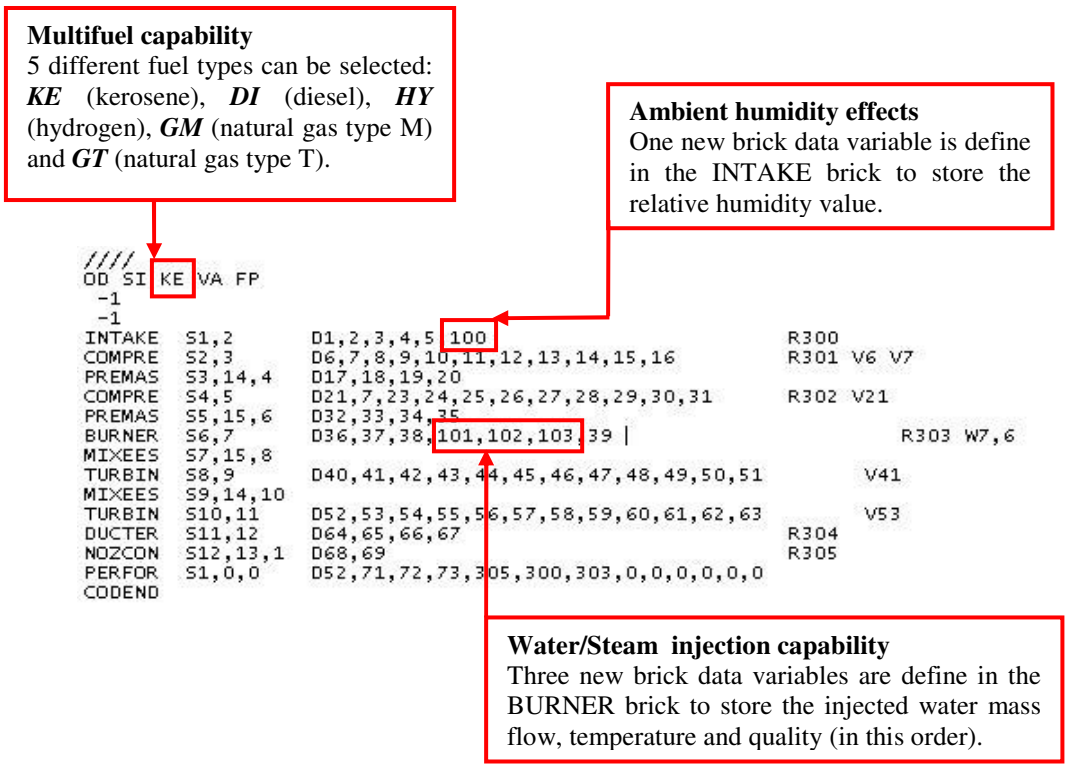

Figure 2-10 Turbomatch input file (extract)

2.5.11 Output file

All modifications done to Turbomatch generated new relevant information that needed to be included it the output file, specially that involving the injection of water or steam at the combustor and the simulation of moist air.

The Turbomatch output file is a text file generated by the program with the results of design or off-design performance cases. The output file contains, apart from the results, the whole input file reprinted at the beginning of the file. Thereafter, detailed print out of the parameters of each of the engine model component, given and calculated, is found.

Few modifications were done to the component report section to include the new parameters for two components: INTAKE and BURNER (see Figure 2-11). For the INTAKE, the relative humidity, an input value, is included in the print out. As for the BURNER, the injected water mass flow is found along side the fuel flow.

Once the component report is finished, the value for all the station variables is produced in a form of a Table. Figure 2-12 displays the arrangement. The major changes in this section are the inclusion of the new *WAR* and *X* station vector variables.

Ambient humidity effects
The used value of relative humidity is reported in the INTAKE brick component section.

```
***** AMBIENT AND INLET PARAMETERS *****
Alt. =      0.0       I.S.A. Dev. =     0.250       PDev. =     0.000
Mach No. =   0.00      Etar = 1.0000         Momentum Drag =       0.00
Rel.Humidity = 70.00

***** COMPRESSOR  1 PARAMETERS *****
PRSF =  0.35801E+00     ETASF =  0.10133E+01     WASF =  0.85857E+00
DGPRSF =  0.10000E+01     DGETASF =  0.10000E+01     DGWASF =  0.10000E+01
Z = 0.75000             PR =   3.300             ETA = 0.85000
PCN =   1.0000          CN = 1.00000             COMWK =  0.12169E+08
STATOR ANGLE =   0.00

***** COMPRESSOR  2 PARAMETERS *****
PRSF =  0.98775E+00     ETASF =  0.10375E+01     WASF =  0.28321E+00
DGPRSF =  0.10000E+01     DGETASF =  0.10000E+01     DGWASF =  0.10000E+01
Z = 0.65000             PR =   6.500             ETA = 0.85000
PCN =   1.0000          CN = 1.00000             COMWK =  0.27943E+08
STATOR ANGLE =   0.00

***** COMBUSTION CHAMBER PARAMETERS *****
ETASF =  0.99000E+00  DGETASF =  0.10000E+01
ETA = 0.99000           DLP = 0.8580       WFB =   1.9154       WWB = 0.83825
```

Water injection capability
The injected water/steam mass flow value is reported in the BURNER brick component section.

Figure 2-11 Turbomatch output file (extract 1)

```
***** CONVERGENT NOZZLE  1 PARAMETERS *****
NCOSF =  0.10000E+01  DGNCOCF =  0.10000E+01
Area =  0.5612          Exit Velocity =  321.37  Gross Thrust =  24799.50
Nozzle Coeff. =  0.97489E+00


Scale Factor on above Mass Flows, Areas, Thrusts & Powers =     1.0000


Station   F.A.R.   W.A.R.    X   Mass Flow   Pstatic    Ptotal Tstatic  Ttotal     Vel     Area
    1   0.00000  0.00757  1.000    76.783   1.00000   1.00000  288.40  288.40     0.0  ******
    2   0.00000  0.00757  1.000    76.783    ******   1.00000  ******  288.40  ******  ******
    3   0.00000  0.00757  1.000    76.783    ******   3.28694  ******  428.68  ******  ******
    4   0.00000  0.00757  1.000    69.099    ******   3.28694  ******  428.68  ******  ******
    5   0.00000  0.00757  1.000    69.099    ******  18.46950  ******  742.96  ******  ******
    6   0.00000  0.00757  1.000    67.717    ******  18.46950  ******  742.96  ******  ******
    7   0.02430  0.01865  1.000    70.095    ******  17.70400  ****** 1551.37  ******  ******
    8   0.02381  0.01843  1.000    71.477    ******  17.70400  ****** 1537.30  ******  ******
    9   0.02381  0.01843  1.000    71.477    ******   4.48115  ****** 1159.02  ******  ******
   10   0.02143  0.01734  1.000    79.155    ******   4.48115  ****** 1095.27  ******  ******
   11   0.02143  0.01734  1.000    79.155    ******   1.32130  ******  839.35  ******  ******
   12   0.02143  0.01734  1.000    79.155    ******   1.32130  ******  839.35  ******  ******
   13   0.02143  0.01734  1.000    79.155   1.00000   1.24202  794.36  839.35   321.4  0.5612
   14   0.00000  0.00757  1.000     7.678    ******   3.22120  ******  428.68  ******  ******
   15   0.00000  0.00757  1.000     1.382    ******  17.54603  ******  742.96  ******  ******

  Shaft Power =  24000000.00
   Net Thrust =     24799.50
 Equiv. Power =  25598996.00
    Fuel Flow =    1.6330
       S.F.C. =  68.0412
     E.S.F.C. =  63.7912
Sp. Sh. Power =    312568.22
Sp. Eq. Power =    333393.03
Sh. Th. Effy. =    0.3408
```

WAR and X
The new WAR and X station vector variables are included in the results

Figure 2-12 Turbomatch output file (extract 2)

2.6 GT Engine Modelling

The LM2500 is an aeroderivative engine widely used in the power generation, oil & gas, maritime industries. The first version of the engine, introduced in 1961, was fitted with 16-stage compressor and a 6-stage power turbine. In 1996, an improved model (LM2500+) came to market. The engine has a 17-stage compressor – with a variable stator vane system – and a 2-stage high speed power turbine. It features the latest nozzle coating and cooling technologies that permits higher operating temperatures. The engine is rated at 29.98 MW with a thermal efficiency close to 39-40% [4].

The success of a performance simulation entirely depends on the thermodynamic engine model designed. Two different types of components are identified: the main and secondary components. The main components such as compressor, burner, turbine and exhaust nozzles define to the overall engine performance. While the secondary components bleed flow, cooling systems, variable geometry systems, among others account for the final percentile points in accuracy.

2.6.1 Intake

The intake model had to handle a wide range of ambient conditions (temperature, pressure, altitude and relative humidity). Additionally, MEA's engines are fitted with a filtering system aimed to reduce the ingestion of particles that can damage the integrity of the engine components and its performance. Such filtering system generates a pressure drop on the main stream and traps water vapour particles reducing the inlet mass flow relative humidity. While the pressure drop is considered in the model, the reduction in relative humidity is not.

A heat exchanger outside the engine enclosure, part of the Power turbine NGV cooling system, demand a secondary inlet air stream. This secondary air stream is extracted from inside the engine enclosure and vented into the atmosphere after used, and it is not physically connected to the main air stream. Therefore it was decided to use two INTAKE bricks instead of a combination of an INTAKE and a PREMAS bricks to split the main stream. The chosen configuration facilitated the design point performance adaptation (see section 2.7.2) and reduced any negative impact at off-design conditions.

2.6.2 Compressor and bleeds

The engine has a 17-stage axial compressor with a nominal pressure ratio of 23:1. It has a Variable Stator Vane (*VSV*) system fitted from stage 0 (*IGV*) to 7^{th} stage. Two sets of temperature and pressure sensors are fitted at the 9^{th} stage bleed flow and 16^{th} stage (compressor discharge). The rotational speed of the shaft and the *VSV* actuator position in percentage are also available. There are two methods to model the compressor: single or multiple component bricks, each with its own advantages and shortcomings.

The single component brick method consists in the definition of one COMPRE brick with a pressure ratio of 23:1 and the adaptation of its isentropic efficiency value to deliver the right compressor discharge temperature and pressure. The advantages of

such approach are: simplicity of design and less stringent data requirements. However, to favour this option would have signified loosing any chance to model the variable geometry system (*VSV*) and bleed flows. Additionally, as the model was also planned to be used in the diagnostics analysis of the engine, a single compressor brick would have reduced the diagnostics observability of the first 9 stages of the compressor that are more likely to present degradation (fouling) issues.

The multiple COMPRE bricks method facilitates the modelling of different bleed flows and VSV systems, and improves observability by increasing the number of simulated performance data sets. To represent any flow bleed from the compressor, the single brick has to be modelled into multiple sections. The air flow is extracted from the end of each section using a PREMAS brick. Each compressor section is adapted by matching simulated to real performance data. The only disadvantage of the method is the amount of real data needed to adapt each section. Hence, the final number of sections is determined by the number and location of the bleeds flows and is limited the available real data sets.

The LM2500+ has 3 main bleed flows at the 9^{th}, 13^{th} and 16^{th} (compressor discharge) stages and two sets of data (pressure and temperature) from the 9^{th} and 16^{th} stage flows.

- The 9^{th} stage bleed system comprises two different piping circuits: the turbine mid frame (*TMF*) and the power turbine piping systems. Both circuits are designed to supply the low temperature and relatively low pressure air flow to their respective cooling devices. To model these air extractions, the compressor model had to be split in two sections. The first section would model the performance from the IGV (stage 0) up to the 9^{th} stage, while the second would provide information about the last stages (9^{th} to 16^{th} stage). By doing so, temperature and pressure data from the air bleed are needed. Fortunately, the original sensor arrangement provides measurements from this particular bleed flow. As a result, the compressor model was split in two sections that allow the representation of the 9^{th} stage bleed flow.

  It is important to mention that the pressure reading at the 9^{th} stage is almost two times the pressure level experienced at the vicinity of the Power Turbine and *TMF*. The considerable pressure difference has a positive consequence as it warrantees the flow can be reinserted into the main gas path without any resistance. In the case of the Power Turbine nozzle guide vane's (*NGV)* cooling system, the pressure drop is significant as the flow has to leave the engine enclosure, enter the heat exchanger and return to the engine. In the case of *TMF* cooling flow, the pressure drop is irrelevant since it follows a short and direct path to the *TMF* structure. On the negative side, extracting flows with pressure and temperature values above the normal conditions of the destination increase the energy losses at the compressor.

  To reduce these energy losses, the bleed flow needed to be extracted upstream in the compressor where the right pressure and temperatures could be found. Unfortunately, this design is unrealisable. As mentioned in the compressor section, the engine is fitted with a *VSV* system for the first 7 stages where any

extraction of flow is impossible. Additionally, a few more inches, in the axial direction, are reserved to bolt down the support of the *VSV* torque shaft, shifting any bleed to its actual position.

- The 13th stage bleed flow is used for cooling applications at the high pressure turbine (see section 2.6.4). If we had followed the same modelling logic than with the 9th stage bleed flows, the second section of the compressor model would have had to be split in two. However, the lack of pressure and temperature measurements at the 13th stage prevented it. The performance adaptation of the second and third sections would have been impossible, unless big assumptions – decreasing the model reliability – were to be made. Any diagnostics attempt would not have a baseline to compare against making the analysis meaningless. Therefore, it was decided the 13th stage bleed would be modelled as an extraction from the 9th stage using a PREMAS brick.

- Finally, the 16th stage (compressor discharge) parasitic or bleed flows are used for the following applications: high pressure turbine first nozzle cooling, high pressure turbine rotor cooling, bearing thrust balancing, sump isolation, among others. The fact the 13th stage bleed flow was already shifted to the end of the compressor and it is aimed for the same high pressure nozzles cooling systems, there is no need to include an additional extraction from the compressor discharge. On the other hand, Turbomatch is unable to effectively simulate any of the rotor, bearing thrust, sump isolation and sealing applications, hence, no further bleed flows were modelled.

The *VSV* system modifies the incidence angles of the air to ensure the engine's operability while increasing the surge margin, and maintains fairly constant exhaust conditions that directly affects the production of steam downstream the GT engine. The decision to split the compressor in two bricks makes the simulation of the VSV system possible, though, a small error is induced since the first compressor brick simulate the performance of the first 9 stages while the VSV only covers from 0 (IGV) to 7th stages. To model the VSV in Turbomatch, the variable geometry option in the "flag line" must be chosen.

Turbomatch considers the initial angle at design point equal to zero, from where a positive or negative value is used in off-design performance cases. An iterative process to find an approximate schedule is described in section 2.7.3.2.

2.6.3 Burner

The engines at MEA's Pulrose power plant feature an annular combustor fitted with a dual-fuel injection system (gas and fuel oil) and the injection of water or stream for emissions abatement. The BURNER brick is able to model such particularities thanks to the modifications done to Turbomatch (see section 2.5.6). The combustion efficiency and pressure drop are also modelled.

2.6.4 High pressure turbine

The high pressure turbine (*HPT*)) drives the compressor by extracting energy from the high temperature and pressure gas flow leaving the combustion chamber. The *HPT* consists of the: *HPT* rotor, 1st stage nozzle (*HPTN1*), 2nd stage nozzle (*HPTN2*) and turbine mid frame (*TMF*).

The two sets of nozzles (*HPTN1* and *HPTN2*) direct the hot gas from the combustor onto the blades at the optimum angle and velocity. Complex cooling systems are built into the *HPT* nozzles and rotor to increase part life cycle and reliability. Impingement, convection and film cooling circuits within each individual *HPTN1* vane are supplied with high pressure cooling air directly from the compressor discharge chamber. Similarly, the *HPTN2* receives the cooling air flow from the 13th stage bleed piping through air tubes on the nozzle support.

The turbine mid frame (*TMF*) supports the aft end of the *HPT* rotor and the forward end of the power turbine rotor. The 1st stage power turbine nozzles are also attached to the *TMF*. A circumferential array of struts, in direct contact with the main gas path is used to anchor all different components. To avoid any structural damage, an air flow extracted from the compressor 9th stage is injected into the strut through holes in the turbine casing.

To model the high pressure turbine required the combination of various bricks. One TURBIN brick calculates the thermodynamic exit conditions of the gas, the MIXXES brick complements the representation of *HPT* nozzle cooling system and a HETHOT-HETCOL compound brick models the effect of the *TMF* (and its cooling system) on the gas path. Finally a MIXEES brick is used to reinsert the bleed flow back into the main stream.

- A single TURBIN brick is responsible for the simulation of thermodynamic expansion of the working fluid. The rotational speed of the turbine shaft is equated to that of the compressor to model the physical coupling between them. The isentropic efficiency magnitude of the turbine is derived from field data through an iterative process (see section 2.7.2.4). Pressure and temperature measurements from the power turbine inlet are used in the absence of any sensor at the HPT inlet or outlet.

  Wilcock, Young and Horlock [58] propose there is a negative effect of the nozzle cooling film on the overall engine efficiency. The cooling film creates an additional boundary layer at the nozzle surface reducing the free flow area. As a result, the isentropic efficiency of the turbine is affected. Since it is not possible to isolate the effect of the cooling film any approximation of the turbine's isentropic efficiency will intrinsically include the detrimental effect cause by it.

- To complement the representation of the HPT nozzles cooling system a single MIXXES brick was employed. The brick reinserts the cooling flow extracted from the compressor discharge bleed flow (the representation of the real 13th and 16th stage bleed flows) before the TURBIN brick. The main impact is not to reduce the temperature of the main stream but to allow the cooling flow to return

to the gas path and to be expanded inside the TURBIN brick. It has been explained an increase of 1-2% in the turbine mass flow, like those experienced when water or steam is injected into the combustor, can bring notable repercussions on the overall engine performance.

In reality, the cooling flows are reinserted at various points inside the high pressure turbine stages. The first stage of the turbine only expands the cooling flow reinserted at the HPTN1, while the second stage expands the sum of the HPTN1 and the HPTN2 cooling flows. Ideally, the turbine should have to be divided in two sections following the same logic than with the compressor but the lack of pressure and temperature readings to adapt the two bricks prevented it. Therefore, the only feasible option was to reinsert the cooling flow before the TURBIN brick aware of the small error induced by this approach.

- Two modelling methods were pre-evaluated: the heat exchanger (HETCOL-HETHOT) method or the DUCTER-AFTERBURNER method.

The DUCTER-AFTERBURNER method was the more simple but unrealistic of the two. The DUCTER would account for the pressure drop while the AFTERBURNER, used in the intercooler mode, would deal with the reduction in temperature. An analysis of the code of the AFTERBURNER revealed that it only calculates the heat loss as a function of a "negative fuel flow". This parameter is multiplied by the calorific value of the fuel to obtain the loss of energy in the gas flow. These calculations have no connection with the concept of the heat transfer between two flows, hence the method was discarded.

The heat exchanger method makes use of two separate but interlinked bricks: HETHOT and HETCOL. The bricks simulate the actual heat transfer between cold and hot streams using the Mean Logarithmic Temperature Difference (*LMTD*) definition. The outlet conditions of the cold and hot stream can be calculated using a user-defined value for the heat exchanger effectiveness. Although such effectiveness varies as a function of the temperature and mass of the two flows, its calculation involves complex mathematical models and specific geometric dimensions and flow characteristics outside of the scope of this modelling exercise.

Henceforth, it was decided to use a HETCOL-HETHOT compound brick to model the effect of the TMF on the engine performance. It was assumed the TMF generated a drop in pressure and temperature caused by the partial blockage of the main gas path and the heat exchange between the gas and the cooling air flows, respectively.

- The TMF-strut cooling-system bleed air is reinserted into the main stream after the HETCOL-HETHOT compound brick. In reality, the air flows inside the engine rotor before being readmitted.

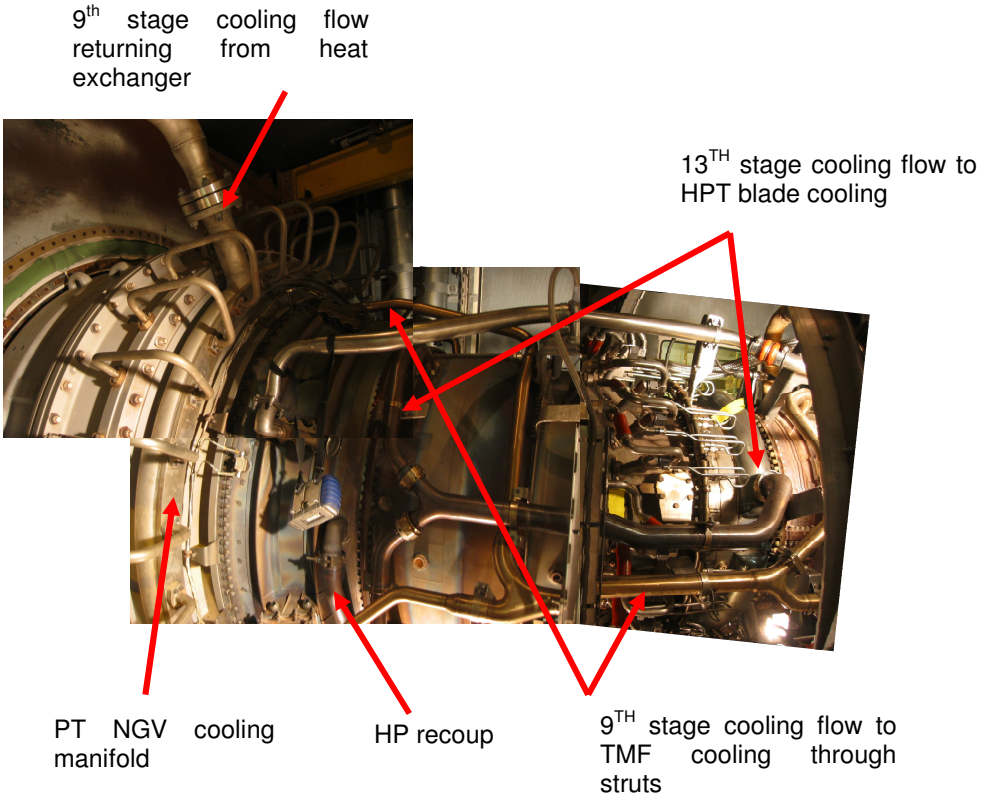

Figure 2-13 Engine cooling system piping (Courtesy MEA)

2.6.5 Power turbine

The power turbine is a free-turbine aerodynamically coupled to the gas-generator. MEA's engines are fitted with the two-stage high speed power turbine (HSPT) type considered to be a more industrial than aeroderivative.

The power turbine nozzles redirect the exhaust gases of the gas generator against the rotor blades. The stage 1 nozzles are connected to, and considered part of the turbine mid frame. These nozzles are cooled down using air bled from the compressor 9th stage further cooled at an external heat exchanger. The bleed air enters a manifold that supplies the cooling flow to each of the nozzles.

The HSPT performance is approximated using a TURBIN brick to simulate the expansion of the gas, a compound brick HETHOT-HETCOL to represent the 1st stage nozzle cooling system and a MIXEES brick to reinsert the cooling flow back into the main stream.

- The TURBIN brick simulate the thermodynamic conditions of the gas after the expansion. The TURBIN brick is used in its Free Power Turbine mode that means no work is extracted by any compressor, instead, a specific power demand or the exhaust pressure is defined by the user.

- The HETCOL-HETHOT compound brick is used to model the nozzle guide vanes cooling system. The cooling air enters a manifold that distributes the flow

to all vanes. Only a small portion of this air is released through the trailing edge, instead, the air flows across the vane and towards the engine rotor. This cooling system can be considered as a cross-flow single-pass heat exchanger, where a temperature and pressure drop on the hot and cold streams is expected.

- A MIXEES brick is used to reinsert the cooling flow before the TURBIN brick. The decision is based on the same reasoning behind the high pressure turbine cooling flows modelling.

2.6.6 Exhaust

Gas turbine engines specifically designed to work inside a combined cycle must maintain a minimum exhaust pressure over the engine's operating range. The gases will flow through arrays of tubes, inside which water flows, attaining pressure losses until they are expanded into the atmosphere. The total pressure drop across the steam generator is called the back pressure. A NOZZLE brick was used to model the exhaust conditions of the gas turbine.

2.6.7 Final Engine model

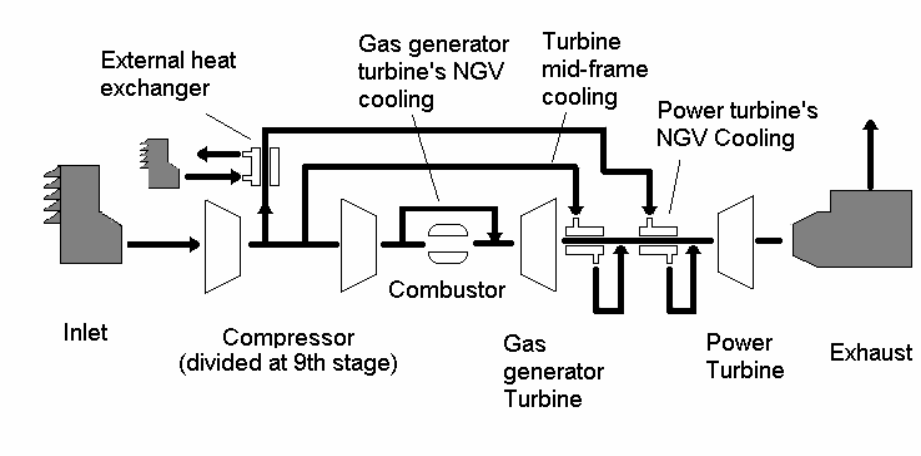

Figure 2-14 Final engine model configuration

The final engine model configuration is shown in Figure 2-14. As mentioned in section 2.6.1, two different inlet bricks were included to differentiate from the core inlet mass flow and the secondary inlet mass flow used to cool down the bleed off from the compressor 9th stage at a heat exchanger. The two sections of the compressor are easily identified along with the three bleed off flows. The TMF and power turbine's NGV cooling system arrangements, sections 2.6.4 and 2.6.5 respectively, are positioned one after the other.

2.7 LM2500+ Engine Model Adaptation

The objective of the performance adaptation process is to modify the fundamental parameters (isentropic efficiency, mass flow, TET, fuel flow, etc) of the main

components of the engine model and other elements to approximate the performance simulation results to field or OEM data reports. Some techniques introduced [59, 60] use complex numerical methods to approximate the fundamental parameters for design and off-design point with high accuracy but rely on a good first approximation of the engine model. More importantly, the off-design method can not handle VSV scheduling effects that are fundamental in the operation of several engines used in CCGT power plants as it allows to maintain exhaust temperatures within a narrow range from the design point conditions.

Two phases of the engine model's adaptation are presented: design point and off-design point adaptation. In the case of the design point adaptation method, a generic and manual approach that allows the adaptation of the model performance simulation at any operating reference point (or design point condition) using the power output as the main control variable (or handle) is offered. It can be used to construct the model from the start or to modify an existing model following the generic adaptation process depicted in Figure 2-15.

The off-design adaptation process comprises of only two steps: surge margin modification and VSV scheduling. Although there are other off-design adaptation methods as mentioned earlier, the process followed made use of the existing Turbomatch capabilities. And as it will be shown later, the process captures the effect of the VSV scheduling on the engine performance.

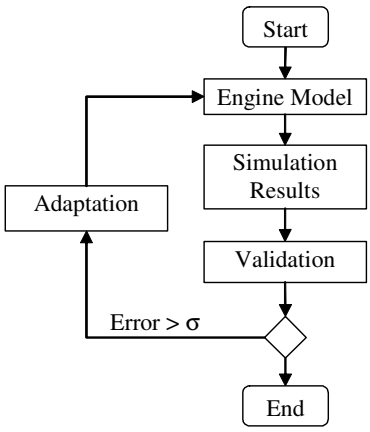

Figure 2-15 Adaptation process flow diagram

2.7.1 Field data

The limited amount of field data at steady state conditions from MEA engines made it difficult to adapt the engine models at exactly the engine manufacturer warrantee point. A series of points taken at steady state conditions were recorded from GT6 and GT7 engines. Since all points were recorded during the same day there is no comparative effect from the engine health condition variable. The points were taken at various power ouput conditions: 15, 18, 20, 22, 25 & 27 MW with the corresponding ambient conditions for each case.

These data points were obtained before the latest improvements of the data mining techniques and instrumentation at MEA Pulrose power station were fully functional; hence, they present inaccuracies and missing important parameters such as fuel flow and exhaust mass flow.

2.7.2 Design point performance adaptation

2.7.2.1 Step 1: Inlet

The first step involves the right initialisation of the air conditions at the engine's inlet plenum. The four main parameters are: inlet plenum temperature, inlet plenum pressure, relative humidity and inlet mass flow. Simple atmospheric measurements will provide the values of temperature, pressure and humidity that can be corrected in the case any intake system is present. The following are the assumptions made during the model adaptation:

- Always use the temperature measurement at the engine inlet plenum coming from the control system.
- The filters do not absorb any water vapour hence there is no change in atmospheric relative humidity.
- The pressure drop across the filters (in mm of H_2O) has to be subtracted from the atmospheric pressure as there is no inlet plenum pressure measurement.

An initial value for the inlet mass flow is guessed. This variable can be used to fine tune the fuel flow and overall thermal efficiency, but it also affects the turbines' exit pressure and temperature. Since the fuel flow is calculated using the fuel-to-air ratio at the combustor, higher inlet mass flows will bring an increase in fuel flow, hence, a drop in overall thermal efficiency for a fixed power output. The energy drop across each turbine depends on the properties of the working fluid and mass flow. Therefore, if the inlet mass flow is reduced, the gases will suffer a higher pressure and temperature drop at the turbines (and vice versa).

2.7.2.2 Step 2: Compressor

Once the compressor inlet conditions are known, the adaptation of the compressor parameters follows. The first COMPRE brick pressure ratio is obtained by dividing the real pressure at 9th stage by the air pressure after the intake filters, $PR_1=P_{25}/P_2$. Similarly, the second COMPRE brick pressure ratio is estimated dividing the compressor discharge pressure by the pressure reading at 9th stage, $PR_2=P_3/P_{25}$.

The isentropic efficiency of both compressor sections is initialised with values within an 84% to 88% range. To adapt the compressor discharge temperature T_3 and the temperature at the 9th stage T_{25} the isentropic efficiencies are modified until the error between simulated and real reaches a small value.

2.7.2.3 Step 3: Combustor

The combustor entry temperature and pressure are T_3 and P_3. suggest there is a small pressure drop ΔP across the combustor that makes $P_4=P_3-\Delta P$ [61]. A first guess of the combustor exit temperature (T_4) is done. The temperature will be changed if the model does not converge at the exhaust nozzle, meaning there is not enough energy in the gas to generate the required power output, or if the different temperatures down stream the engine do not match.

In the case of MEA's LM2500+ engine, the water injection mass flow (or water-to-air ratio) and temperature are defined at the combustor. A common value of WAR=0.011 for wet-air conditions is used.

2.7.2.4 Step 4: HPT and HSPT

The inlet and outlet conditions at the power turbine are given by sensors T_{48} and P_{48} and T_{10} (or EGT), respectively. To complement the data, it is also assumed the back pressure of the power turbine to be close to 1.02 atm, a common value used in combined cycle applications.

In the case of the power turbine, it is important to add the consumption of the auxiliary systems to the main power requirement. Up to 260 kW are thought to be consumed by the secondary or auxiliary equipment.

The isentropic efficiency value for both the high pressure and power turbines is initialised to values between 85-90%. The exit temperatures and pressures for each turbine will depend on the isentropic efficiency and the amount of energy demanded by the compressor or engine load, for the HPT and HSPT, respectively. After the first iterations, small increments in the isentropic efficiency can be made to increase the exhaust pressure with no great effect on the exit temperatures, and vice versa.

2.7.2.5 Step 5: Heat exchangers

The effectiveness of the heat exchanger has no great effect on the overall performance but it can be used to fine tune T_{48}; common values from 75% to 85% are used. The pressure drop across the heat transfer take small values from 0% to 1% during first iterations to assure convergence.

2.7.2.6 Step 6: Cooling flows

The magnitude of the cooling mass flows bled from the compressor can take initial values from 0% to 4%. The bleed flows have a big effect on the inlet and outlet turbine temperatures and the overall performance of the engine.

The bleed flows are modified to adapt the expected values at T_{48} and EGT. Without the cooling flows, the temperatures at the hot section of the engine could not be easily adapted because they would be solely related to the energy drop across the turbine and gas-generator turbine inlet temperature (*TET*).

Since the fuel flow is calculated using the fuel-to-air ratio (*FAR*), the extraction of cooling air from the compressor will decrease the flow entering the combustor reducing the fuel flow and increasing the overall thermal efficiency. Hence, the bleed air flows are used in the fine tuning of the engine performance, especially to modify the fuel flow consumption.

2.7.2.7 Final design point performance validation

The design point or warrantee point of the LM2500+ is defined by General Electric at 27.96 MW, 60% relative humidity, 15°C ambient temperature, 1 atm of ambient pressure, and, no injection of water at the combustor. During the commissioning period of the engine and after any major overhaul, a performance test is made to certify that the engine is achieving the expected performance. When any deviation from the ambient conditions is present, correction factors on the thermal efficiency (or heat rate) and power output are used. Additional corrections are made to account for the degradation of the engine.

One point from the data, closest to the warrantee point, was chosen to adapt each engine model. Table 2.7 shows the results of the design point adaptation GT7 27MW.

Table 2.7 Design point adaptation results for GT7 engine models

Measurement	Label	GT7 @27 MW
Plenum temperature	**T2**	0.00%
Plenum pressure	**P2**	0.00%
Power		0.00%
Thermal efficiency	η_{th}	-
Fuel	***f***	-
Exhaust mass flow	***m***	-0.11%
Water injection flow	***w***	0.27%
9^{th} stage bleed pressure	**P25**	-0.11%
Compressor pressure	**P3**	-0.03%
Compressor temperature	**T3**	-0.02%
Gas-generator turbine entry temperature	**T4**	-
PT-Inlet pressure	**P48**	1.30%
PT-Inlet temperature	**T48**	-0.57%
Exhaust pressure	**P5**	-
Exhaust temperature	**T5**	0.48%

The accuracy of the models performance adaptation is acceptable for both engines. The deviation from field data is less than 0.5% for most of the parameters with some exceptions showing values in the range of 0.8% to 1.3%. However, at the time of writing, there are still some concerns about the accuracy of the exhaust mass flow reported by the station control system. Clearly, any change in exhaust mass flow target value will directly affect the fuel flow and thermal efficiency parameters as well as the turbines' performance. Unfortunately, the lack of a reliable fuel flow measurement prevented the fine tuning of the exhaust mass flow and thermal efficiency.

2.7.3 Off design performance adaptation

Once the model has been adapted for design point it is important to assess its accuracy at off-design conditions. To keep the length of this thesis to a reasonable size, the results presented in the following sections correspond to the GT7 model only.

The ambient conditions were set to different values from the design point adaptation conditions to have a valid comparative exercise. The conditions used were: 15° temperature, 1 atm pressure, 60% relative humidity and 0.011 water-to-air ratio. Several cases at different power settings in the range of [36MW, 10MW] at uneven steps were simulated.

2.7.3.1 Step 1: Surge margin modification

According to Saravanamuttoo [61] the design operating point of most engines is located at the peak of the compressor characteristic and close to the surge margin. The margin of operation is small with respect of surge but it allows the compressor to accommodate changes in mass flow without choking. Consequently, a surge margin (*SM*) value of 0.9 was chosen for the original (design point) model. Unfortunately, the first simulations at off-design conditions produced unsatisfactory results.

Figure 2-16 shows the running line of the first section of the compressor (refer to section 2.6.2 for modelling). The model presented convergence problems from medium (23MW) to low power settings (10MW). But more importantly, it showed large discrepancies with the various field data points, bearing in mind ambient conditions have no effect on the non-dimensional running line path.

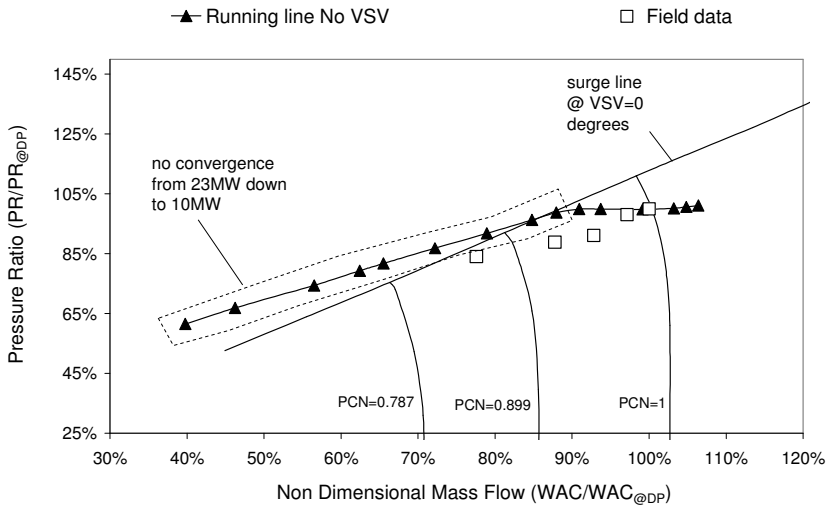

Figure 2-16 Running line front section compressor with surge margin = 0.9

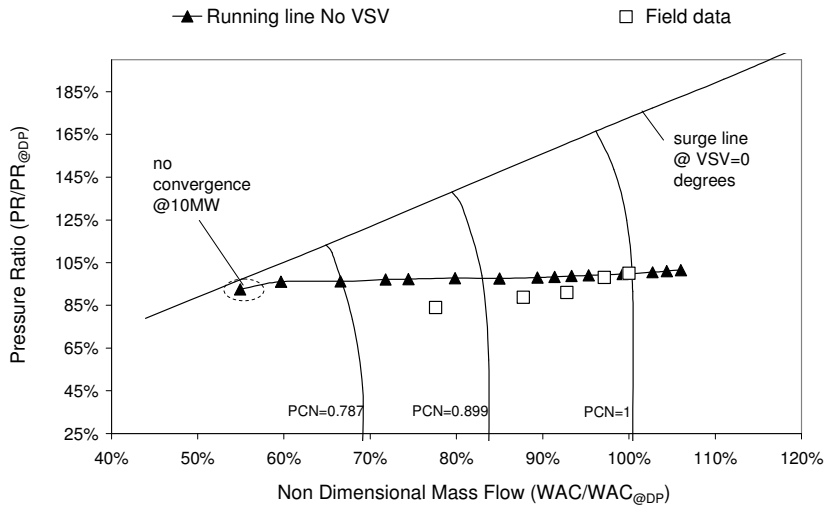

Figure 2-17 Running line front-section compressor with surge margin = 0.6

In fact, the running line follows a horizontal trajectory that accentuate the surge problems of the first stages of a single compressor or high pressure compressor in a multiple spool engine at part loads and low speeds as mentioned in [12]. The surge margin was modified to a value of 0.6 at which 14 out of 15 cases achieved convergence as illustrated in Figure 2-17. Again, the running line follows a near-to-horizontal trajectory until it reaches the surge line missing out all field data points.

The modification of the surge margin value improved the convergence of the model at low power settings but it also affect the performance of the engine. Hence, a more detailed analysis of few important parameters for the bottoming cycle and overall engine performance such as T_5 and W_5.

Figure 2-18 shows the results for the exhaust gases temperature (T_5) for two cases with surge margin values 0.9 and 0.6. Both curves present a similar parabolic behaviour that has the same explanation regardless of the values reported. The operation of the engine at low power settings is translated into low pressure ratios and component efficiencies that reduce the cycle overall thermal efficiency, therefore, the exhaust gases temperature and/or pressure increase as the engine wastes more energy. As the operating pressure ratio and component efficiencies increase the thermal efficiency will increase, consequently T_5 will decrease until reaching a minimum. This section characterises for a high rate of change in thermal efficiency, therefore, pushing T_5 down at a faster rate. After reaching the maximum thermal efficiency point, the cycle enters into diminishing returns at high pressure ratios as the amount of work consumed by the compressor is more than the power generated by the turbines. For SM=0.9, the exhaust temperature goes from 102% at DP at high power settings to a minimum of 99.6% DP just above design point (@28MW) before increasing once more until the model fails to converge. In the case of SM=0.6, the results follow the same trend over a wider convergence range where the minimum 98.1% DP takes place @21MW.

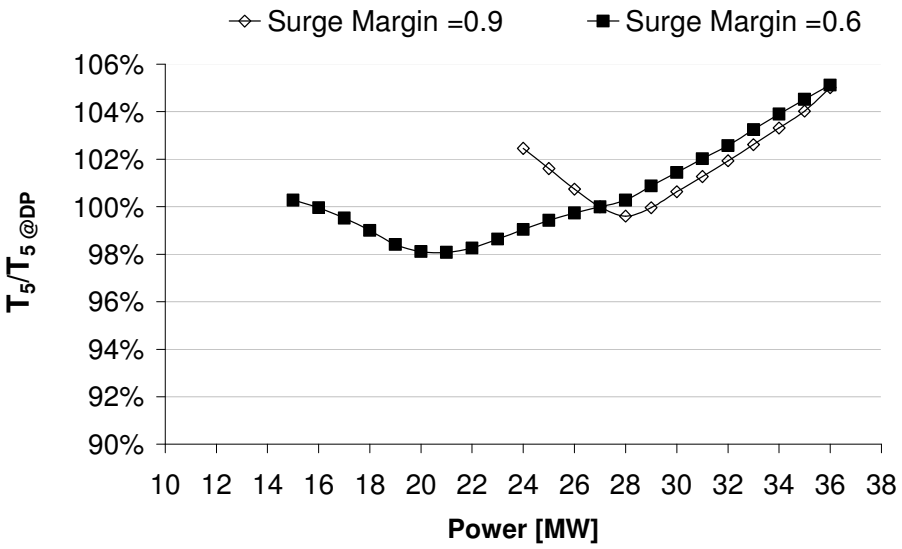

Figure 2-18 Total exhaust temperature (T_5)

The exhaust mass flow (W_5) results are presented in Figure 2-19. The disparity between cases from 36MW to 27MW is nearly zero after which some gap starts to appear. On the last point of convergence for case SM=0.9, that is at 24MW, only a difference between cases of 2% DP is found.

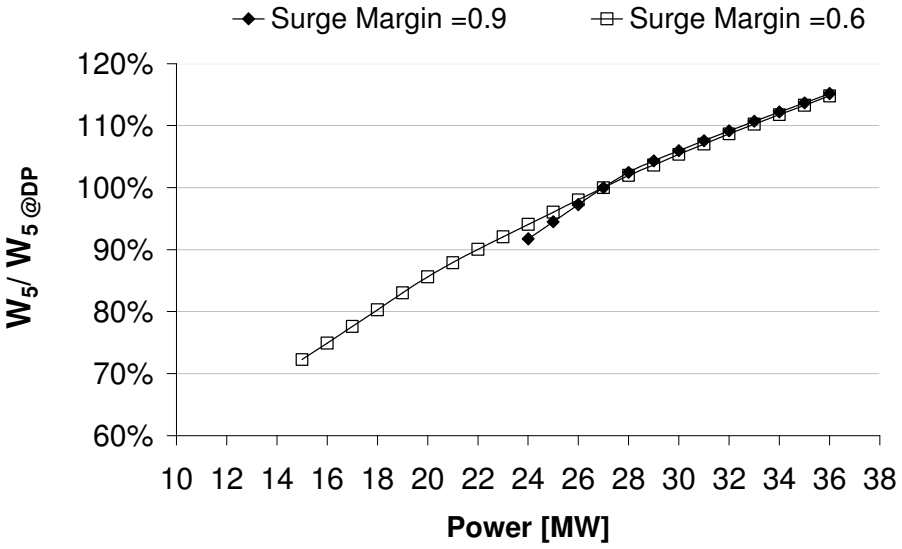

Figure 2-19 Exhaust mass flow (W_5)

The interest in the exhaust conditions is based on the dominant role the gas turbine engine plays inside a combined cycle gas turbine (CCGT) power plant. The accuracy in the performance simulation of the bottoming cycle (steam or Rankine cycle), including the heat recovery steam generator, depends on the performance simulation output from the gas turbine engine. An engine used in CCGT applications is designed to maintain a

fairly constant exhaust temperature across the operating power range of the engine to ensure the steam production conditions are met.

Table 2.8 Off design adaptation results with surge margin = 0.9

Case	Label	30	29	27	25
Plenum temperature	**T2**	0.00%	-0.01%	0.00%	0.00%
Plenum pressure	**P2**	0.06%	0.00%	0.00%	0.00%
Power	**Power**	0.00%	0.00%	0.00%	0.00%
Thermal efficiency	***eta***	–	–	-	-
Fuel	***fuel***	-	-	-	-
Exhaust mass flow	***mass***	1.17%	0.93%	-0.26%	-2.79%
Water injection flow	***water***	0.91%	0.97%	0.43%	0.28%
9th stage bleed pressure	**P25**	-4.43%	-4.00%	-0.11%	2.06%
Compressor pressure	**P3**	-0.56%	-0.16%	-0.21%	-2.97%
Compressor temperature	**T3**	0.71%	0.45%	0.11%	0.55%
Gas-generator turbine entry temperature	**T4**	-	-	-	-
PT-Inlet pressure	**P48**	0.20%	0.89%	0.88%	-0.16%
PT-Inlet temperature	**T48**	-0.20%	0.62%	-0.46%	3.50%
Exhaust pressure	**P5**	-	-	-	-
Exhaust temperature	**T5**	1.45%	2.40%	0.61%	5.31%

Table 2.9 Off design adaptation results with surge margin = 0.6

Case	Label	30	29	27	25	20	18	15
Plenum temperature	**T2**	0.0%	0.0%	0.0%	0.0%	0.0%	0.0%	0.0%
Plenum pressure	**P2**	0.1%	0.0%	0.0%	0.0%	0.0%	0.0%	0.0%
Power	**Power**	0.0%	0.0%	0.0%	0.0%	0.0%	0.0%	0.0%
Thermal efficiency	η_{th}	–	–	–	–	–	–	–
Fuel	***fuel***	–	–	–	–	–	–	–
Exhaust mass flow	***mass***	0.8%	0.6%	-0.2%	-1.3%	-8.4%	-7.1%	-6.3%
Water injection flow	***water***	0.9%	1.0%	0.4%	0.3%	0.3%	0.5%	0.3%
9th stage bleed pressure	**P25**	-4.0%	-3.6%	-0.1%	1.4%	7.4%	10.1%	15.9%
Compressor pressure	**P3**	-0.7%	-0.4%	-0.2%	-1.7%	-5.4%	-7.5%	-12.3%
Compressor temperature	**T3**	0.9%	0.6%	0.1%	-0.1%	-0.5%	-0.8%	-1.1%
Gas-generator turbine entry temperature	**T4**	–	–	–	–	–	–	–
PT-Inlet pressure	**P48**	0.0%	0.8%	0.9%	0.4%	0.0%	-0.1%	-1.3%
PT-Inlet temperature	**T48**	0.2%	1.0%	-0.5%	1.7%	3.0%	4.3%	5.7%
Exhaust pressure	**P5**	–	–	–	–	–	–	–
Exhaust temperature	**T5**	1.9%	2.9%	0.6%	3.2%	4.4%	6.5%	7.7%

The limited convergence of SM=0.9 case and available field data points reduced the range of the validation to only points close to design point (see Table 2.8). Large errors are found in P_{25} and P_3 with values up to 2% and 3%, respectively, only 2MW below

the design point. An underestimation in P_{25} of -4.4% @ 31MW is also found. On the other hand, a large overestimation of T_5 is found @25MW explained by the U-shape trend shown in Figure 2-18.

Table 2.9 shows the results for the SM=0.6 case where, similar to the results shown before for case SM=0.9, T_3 and T_{48} present the best fit with less than 1.3% across the whole power range while P_{25} and P_3 show the worst fit with errors up to 15.9% for the first and 12.3% for the later. Referring back to the running line analysis, Figure 2-16 and Figure 2-17 depict the deviation of the simulated running lines from the trend observed in the field data.

The results shown in Table 2.8 and Table 2.9 suggested further steps in the adaptation process should focus in modifying the operating running line of the compressor front section. This modification will reduce the error on P_{25} and P_3, and will potentially eliminate the parabolic trend of the exhaust temperature T_5.

2.7.3.2 Step 2: VSV scheduling

The previous section stressed the need to optimise the compressor running line of the first section of the compressor. One of the solutions to adapt an engine model at off-design conditions is the introduction of variable geometry. Another is variable blow off valves although it is a wasteful practice. From a practical point of view, the decision to use VSV is based on the fact the actual LM2500+ engine is fitted with this system.

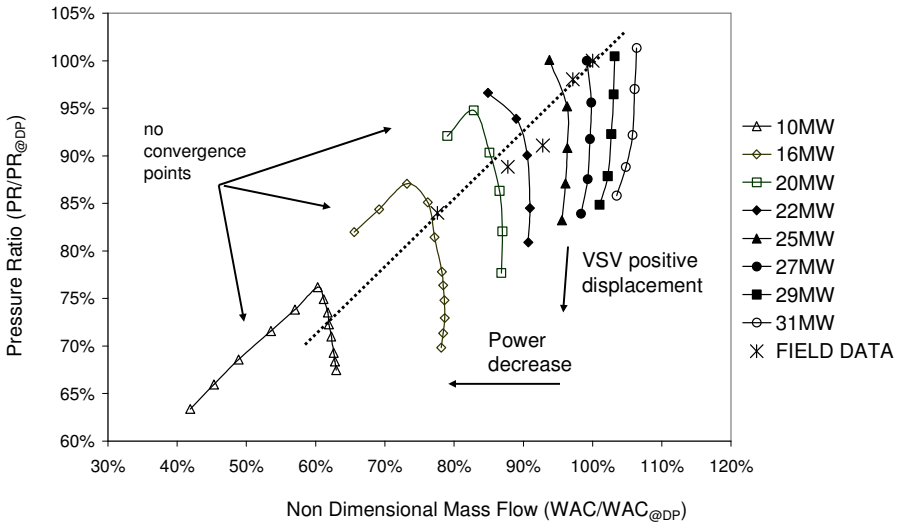

Figure 2-20 Effect of variable geometry on the front stages of the compressor with SM=0.9

To build an optimal VSV schedule, it is important to know the effect the angle variation has on the compressor operating point. Figure 2-20 and Figure 2-21 show the results of a sensitivity analysis using values for the VSV displacement in the range of [0°, 8°] for the high and medium power settings and [0°, 20°] for the low operating points. The convergence issues in the model with SM=0.9 can be easily recognized in Figure 2-20

for the low power settings (10, 16, 20 and 22 MW) and small VSV positive displacements. On the other hand, the SM=0.6 case shows only one point of no convergence at 10MW and 0° displacement.

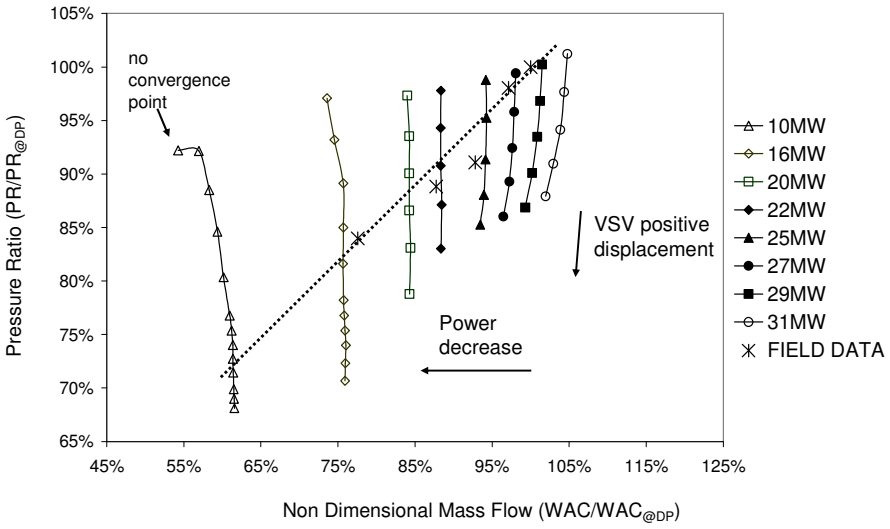

Figure 2-21 Effect of variable geometry on the front stages of the compressor with SM=0.6

A dotted line has been sketched to connect the scattered field data points. The line indicates the proposed path of the new compressor running line after the VSV scheduling is completed. The proposed running line was drawn, in both cases, over three points with very similar ambient conditions and water injection flows that presented a more complete set of measurements. The other two points had some deficiencies in accuracy, particularly in the fuel and exhaust mass flows.

An iterative process to match simulated with proposed running line produced the VSV schedule shown in Figure 2-22 that can be used indistinctive of the chosen surge margin value. The VSV schedule is constructed by three different regions, two linear and one non-linear. A linear region goes from DP at 27MW to 15MW. The second, non-linear, is found at the end from 15MW to 10MW. Finally, a third linear region with negative displacements was used for power settings above design point.

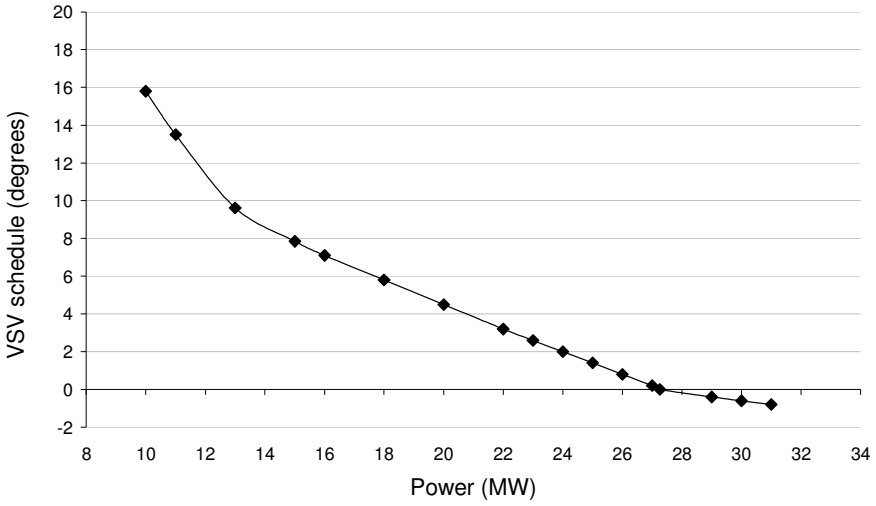

Figure 2-22 VSV scheduling

Once the VSV schedule was defined, new simulations using the same ambient conditions and WAR values from *Step 1* (see previous section) were carried out to create new improved running lines for the two cases of SM=0.6 and 0.9. For the sake of brevity only the results for SM=0.9 are shown next. Figure 2-23 and Figure 2-24 depicts the compressor characteristic for the front and rear sections of the compressor with the original running line (no variable geometry) and the new running line using the VSV schedule for case SM=0.9.

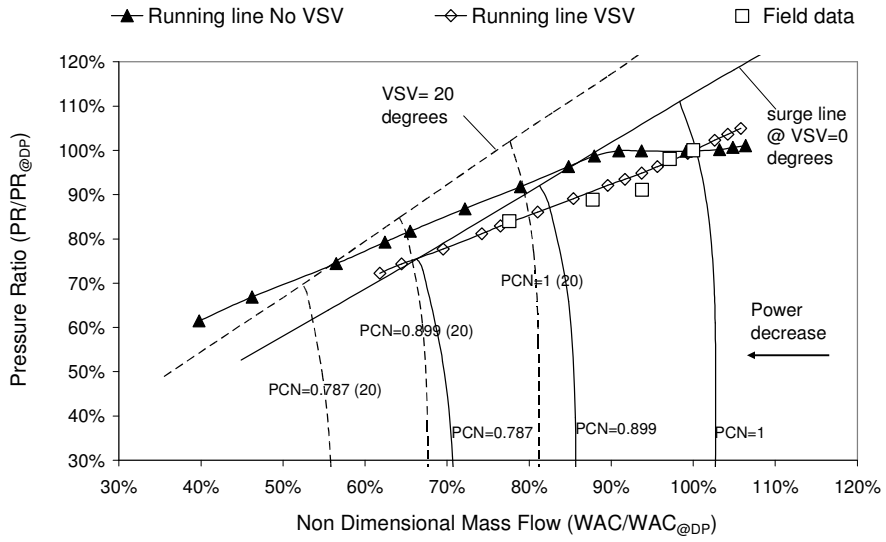

Figure 2-23 Running lines with and without VSV scheduling for SM=0.9

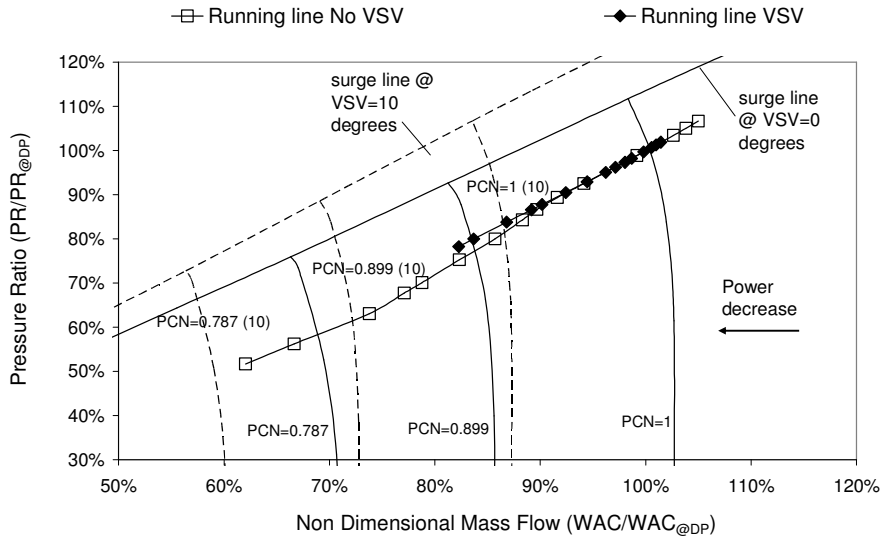

Figure 2-24 Running lines with and without VSV scheduling for SM=0.9

The new running line for the front stages crosses the scattered field data points and deviates from the horizontal path of the original running lines. The primary effect is the reduction in pressure ratio for power levels below the design point, and an increase for those above.

With the reduction in pressure ratio the air mass flow (mainly affected by the change in density) and the rotational speed increase to maintain the same levels of power. In the case of the rear stages (see Figure 2-24) the increase in mass flow seems to not have a major effect. It is important to remember that the air bleed off at the end of the front section of the compressor, reduces the chances of the rear stages of choking.

As a follow up of the analysis done on the exhaust conditions in the previous section the new simulation results for T_5 and W_5 are commented next. Figure 2-25 shows the new profile for exhaust temperature with a reduction of 6% DP @10MW and an increase of 2% DP @31MW. The main achievement of the implementation of the variable geometry was to produce a more linear exhaust temperature curve closer to the real engine performance. In the case of the exhaust mass flow, there is virtually no difference between cases SM=0.9 and 0.6. Figure 2-26 shows a reduction of 20% DP @10MW and a small increase for power levels above design point.

After a thoroughly comparison of all performance parameters results from cases SM=0.9 and 0.6 it was concluded there is not any significant variation between SM values. Therefore, a value of SM=0.9 was chosen for the final model. The decision is supported by the fact most engine designers favour design operating points close to the surge margin [61].

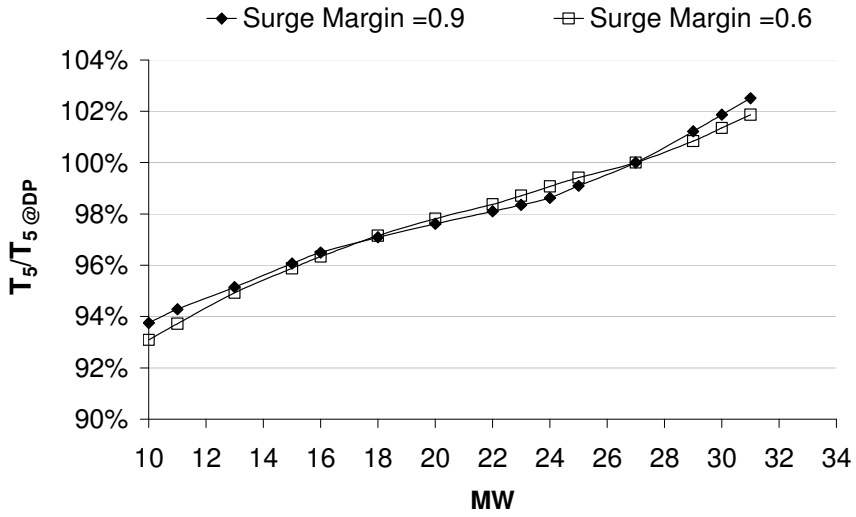

Figure 2-25 Exhaust temperature (T_5)

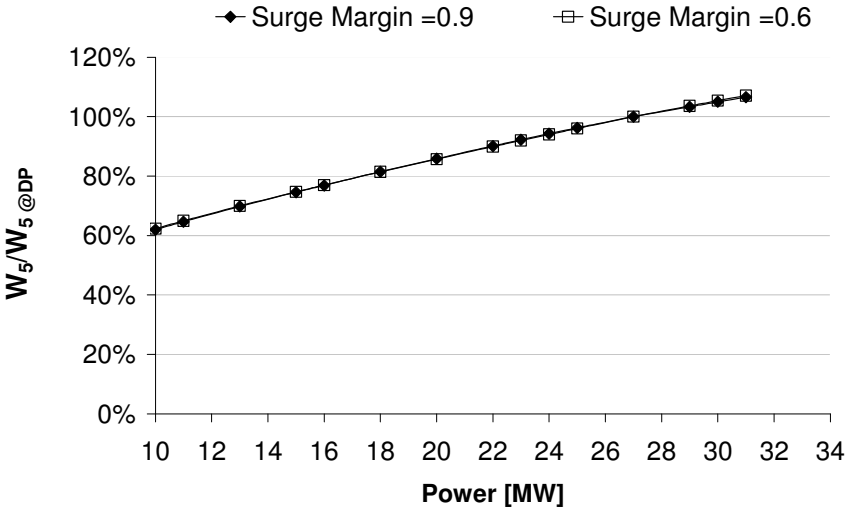

Figure 2-26 Exhaust mass flow (W_5)

2.7.3.3 Final off-design performance validation

The final results of the off-design performance validation for GT7 using a SM=0.9 are presented in the table below. The VSV scheduling improved the model accuracy for pressures and temperatures in the cold section of the engine. P_{25} and P_3, before a major concern, reduced their inaccuracies in a few orders of magnitude. Results from the original model (see Table 2.7) showed an error in P_{25} of 2.06% @ 25MW, which has been reduced to 1.8%. But more importantly, satisfactory error levels were maintained below 3.3% even at low power settings. On the other hand P_3, the error @ 25MW went from 2.9% to only -0.5%, reaching only 6.5% @ 15MW.

The compressor discharge temperature, T_3, show exceptional results with errors below 0.6% for all points, which are comparable with the results from the validation in *Step* 1.

The reason is that the overall pressure ratio of the compressor remain almost the same, hence, the raise in temperature associated with this pressure change is exactly the same.

Table 2.10 Off-design adaptation results with VSV scheduling and SM=0.9

Case	Label	30 MW	29 MW	27 MW	25 MW	20 MW	18 MW	15 MW
Plenum temperature	**T2**	0.0%	0.0%	0.0%	0.0%	0.0%	0.0%	0.0%
Plenum pressure	**P2**	0.0%	0.0%	0.0%	0.0%	0.0%	0.0%	0.0%
Power	**Power**	0.0%	0.0%	0.0%	0.0%	0.0%	0.0%	0.0%
Thermal efficiency	***eta***	-	-	-	-	-	-	-
Fuel	***fuel***	-	-	-	-	-	-	-
Exhaust mass flow	***mass***	0.8%	0.6%	0.0%	-0.7%	-7.7%	-5.7%	-3.2%
Water injection flow	***water***	0.9%	1.1%	0.4%	0.2%	0.3%	0.5%	0.3%
9^{th} stage bleed pressure	**P25**	-1.7%	-1.6%	-0.7%	-1.8%	-2.3%	-3.3%	-3.3%
Compressor pressure	**P3**	-1.2%	-0.7%	0.0%	-0.5%	-3.1%	-4.2%	-6.5%
Compressor temperature	**T3**	0.6%	0.4%	0.1%	0.0%	0.3%	0.1%	0.0%
Gas-generator turbine entry temperature	**T4**	-	-	-	-	-	-	-
PT-Inlet pressure	**P48**	0.1%	0.7%	1.0%	0.7%	0.3%	0.4%	-0.1%
PT-Inlet temperature	**T48**	0.2%	1.1%	-0.7%	0.9%	2.1%	2.5%	1.6%
Exhaust pressure	**P5**	-	-	-	-	-	-	-
Exhaust temperature	**T5**	1.9%	2.9%	0.3%	2.3%	3.4%	4.3%	3.1%

The hot section of the engine presents quite encouraging results for both temperatures and pressures. P_{48} show remarkable results with error values within 1% across the whole power range. In the case of temperatures, T_{48} presents the largest errors @18 and 20MW with 2.1 and 2.5%, and a great improvement from the original model @ 25MW reducing the error from 3.5% (refer to Table 2.8) to 0.9%. The results for T_5 are satisfactory showing the largest error @18 and 20 MW with 3.4% and 4.3% respectively.

The exhaust mass flow, W_5, shows exceptional results for most of the points with error values below 1% and only 3.2% @15MW. However, the accuracy of the model suffers greatly @18 and 20MW with error values of -7.7% and -5.7%. Next section presents the final results for off-design operating conditions using the new capabilities developed.

2.8 LM2500+ Performance Simulation

In this section the results of the performance simulation for different ambient and operating conditions is presented. A special attention is given to the parameters to be used in the integration of the gas turbine engine model into the combined cycle program

and the economic analysis. These variables are: exhaust temperature and mass flow, fuel flow and engine thermal efficiency. In some cases extra parameters are included to help explaining a particular behaviour.

The exhaust conditions will be used in the calculation of the performance of the steam generator. The temperature of the exhaust gases is very important as it will determine the maximum temperature of the steam produced. Whereas the exhaust mass flow will influence the mass flow of steam generated.

The fuel flow is fundamental for the calculation of its consumption over a period of time that can be a day, a week or months. Knowing the fuel flow consumption some risk management strategies can be analysed. In the case of the overall thermal efficiency, this parameter is actively used in the calculation of the operating margin of the plant, also refer to as the spark spread of the plant.

The results here presented are limited to the new capabilities implemented into Turbomatch described throughout this chapter. These capabilities are: ambient humidity effects, multifuel and the injection of water/steam at the combustor. The simulations were carried out using the power output as a handle (fixed).

2.8.1 Humidity effects

The Isle of Man is a particularly humid land situated in the Irish Sea with relative humidity values around 90% throughout the year. A sensitivity analysis on different performance parameters as a function of relative humidity at different ambient temperatures is found next. All results in this section are given in percentage variation of the humid to dry conditions.

The effect of humidity in the engine performance is directly linked to the change in working fluid properties. Moist air is a mixture of water vapour and dry air (see section 2.4.1.2) that present a small change in molecular weight and specific heat (or enthalpy) relative to dry air. The change in properties modifies the full non-dimensional parameters in the gas turbine engine components' characteristic causing the compressor to shift its operating point to accommodate the change in mass flow. Figure 2-27 and Figure 2-28 present the effect of humidity for the compressor discharge conditions, T_3 and P_3, respectively. These results are in line with the effects described in [12] for fixed power output or thrust without water injection at the combustor.

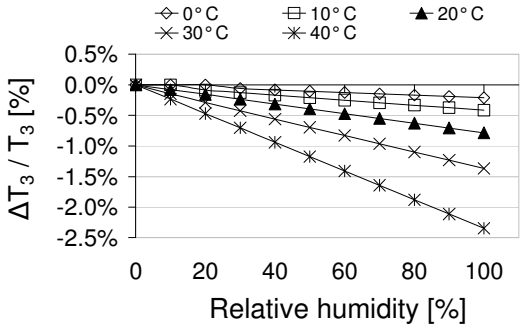

Figure 2-27 Compressor discharge temperature (T_3)

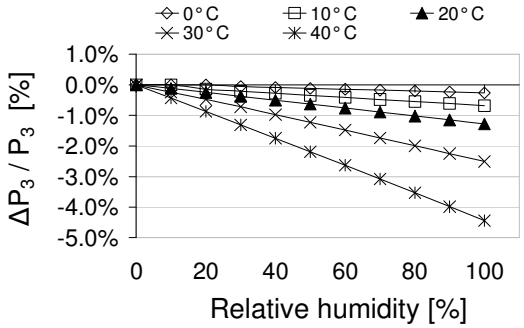

Figure 2-28 Compressor discharge pressure (P_3)

By introducing the effects of ambient humidity into the engine performance simulation a more accurate estimate of the fuel flow and thermal efficiency can be obtained. Figure 2-29 and Figure 2-30 show the results for both parameters. As expected the effect of humidity is greater at high temperatures and relative humidity values above 60%. However, even at normal ambient temperature conditions the effect is not negligible from an economic point of view. The increase in fuel flow at 10°C and 60% relative humidity is around 0.25%, increasing to 0.3% for 100% relative humidity. If we assume a £10m fuel bill a year, the 0.25% represents £25,000 variation. These figures turn even more dramatic if we consider the case of an engine operating in very hot and humid conditions (rainforest, coast, off-shore platform) with temperature values near 40°C and relative humidity of 90%.

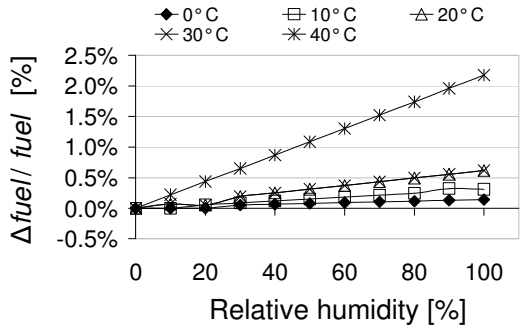

Figure 2-29 Fuel flow (*f*)

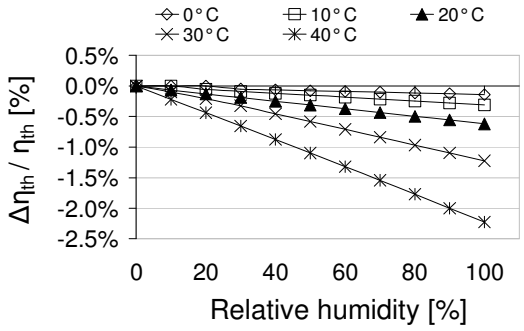

Figure 2-30 Thermal efficiency (η_{th})

In the case of the parameters to be used in the performance simulation of the steam generator, Figure 2-31 and Figure 2-32 present the results for the exhaust temperature and mass flow, respectively. The order of magnitude of the effect of humidity on T_5 is far too small in comparison with the fuel flow, T_3 or P_3. A similar situation in presented by W5 with a small decrease of 0.2% for ambient temperature of 30°C. Therefore, a marginal variation in steam production and conditions is expected.

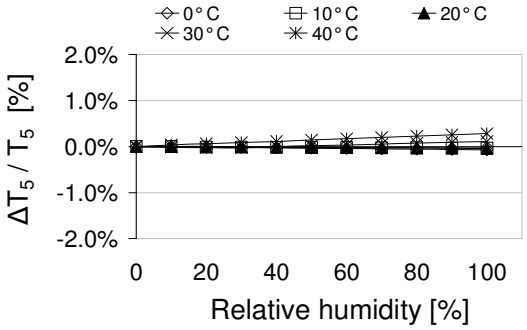

Figure 2-31 Exhaust temperature (T_5)

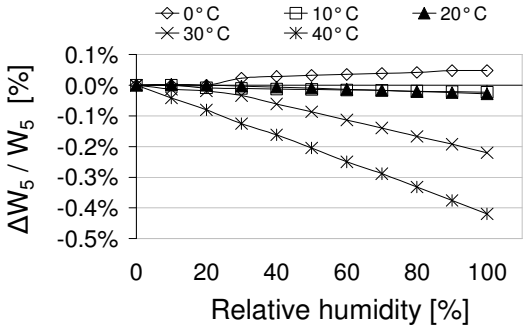

Figure 2-32 Exhaust mass flow (W_5)

2.8.2 Influence of fuel type on engine performance

As mentioned at the beginning of this chapter, the characteristics of MEA LM2500+ engines required the implementation of a multifuel capability that could simulate the performance of the engine using different fuels. This section presents the effect of using different fuels (GT, KE, DI and HY, refer to section 2.5.9.5) on the engine performance, particularly on exhaust conditions and main economic parameters (fuel flow and thermal efficiency). The reference performance DP was obtained using Natural Gas Type "M" as fuel. A similar study [62] on the same topic using analytical expressions referred to methane and using T_3 as handle was found in the public domain with similar conclusions to those presented here.

To carry out a sensible comparison analysis between type of fuel that could deliver valuable information few assumptions and considerations were done. First, the model had to be run in design point mode as Turbomatch is unable to change the type of fuel under off-design mode conditions what could accommodate a change in operating point to produce the expected performance. Second, the power output remained as handle (fixed) to produce useful results from an operator's point of view. Last, TET was optimised to obtain exhaust pressure values equal to the reference performance, hence, keeping the thermal efficiency fairly constant (see Figure 2-33 and Figure 2-34).

The modification of TET is a more realistic approach as it only involves changing the limit of operation of T_{48} in the engine control system. An alternative was to modify the inlet mass flow. It would have meant to re-scale the compressor and turbine characteristics (maps) as the program was being used in the design point mode, thus making it a completely different engine for every fuel-type case.

When the inlet mass flow is fixed, the change in fuel consumption is function of turbine entry temperature (T_4), the fuel calorific value and the properties of the products of combustion. There is a specific amount of any fuel that will introduce enough energy into the system (combustor) to produce flue gases at a particular T_4. Nevertheless, these flue gases do not contain the same amount of energy for all types of fuel.

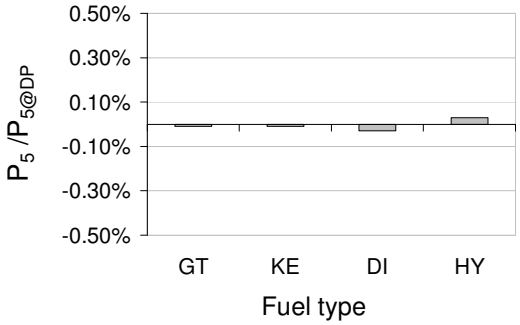

Figure 2-33 Exhaust pressure (P_5)

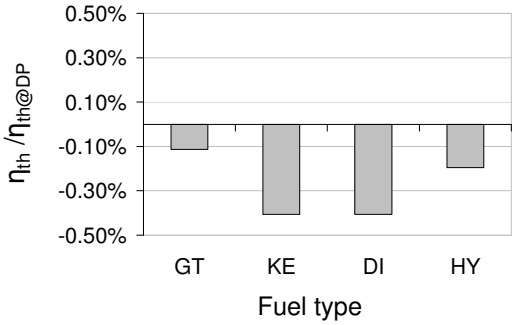

Figure 2-34 Thermal efficiency (η_{th})

The chemical composition of the fuel determines its calorific value and the properties of the products of its combustion. It is common knowledge that the chemical composition – consequently the low heating value – of natural gas changes from one extraction site to the other. It is the volumetric percentage of propane and methane (the two more abundant components in natural gas) that determines the final calorific value of the fuel.

From another perspective, the more atoms of carbon in the fuel the higher the quantity of carbon dioxide (CO_2) in the products of combustion, while the more atoms of hydrogen the more water vapour will be present. Since the specific heat of water vapour is considerably higher than CO_2, a hydrogen rich fuel will generate more power than a carbon rich fuel for the same mass of flue gases when fuel flow is assumed to be relatively small to the inlet air mass flow.

Figure 2-35 presents the difference in TET between the fuel-switch performance and the reference performance for all cases. The first observation made on GT case is that a small reduction in TET of approximately -2.5°C will reduce fuel consumption in nearly 4.5%. It can be explained from the fact GT calorific value is around 4.7% higher than GT, or, that GT is a more methane-rich gas mixture that will produce more water vapour when burned.

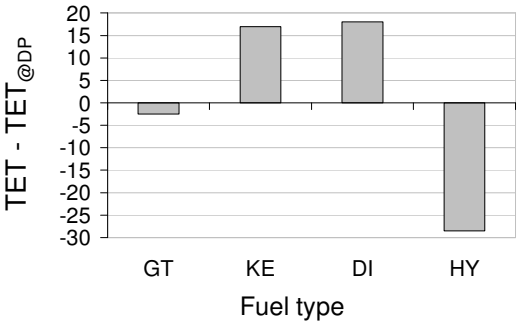

Figure 2-35 Turbine entry temperature (T_4)

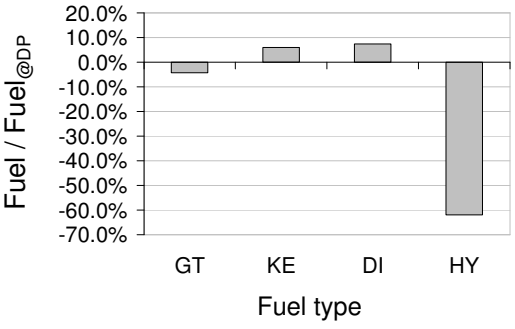

Figure 2-36 Fuel flow (*f*)

In the case of KE and DI, it is interesting to see that a change in TET of 17°C and 18°C, which correspond for 1.1% of the reference value, can bring a surge in fuel flow of 6.0% and 7.4%, respectively (see Figure 2-36). In fact, Kerosene and Diesel fuels have similar caloric value but it is lower than any type of natural gas. Finally, the dramatic

reduction of hydrogen flow in 62% and the nearly 30°C T_4 difference is strongly linked to the fact hydrogen has 163% more energy than natural gas and only water vapour is produced when burned.

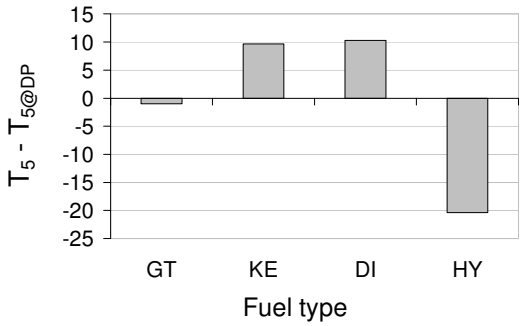

Figure 2-37 Exhaust temperature (T_5)

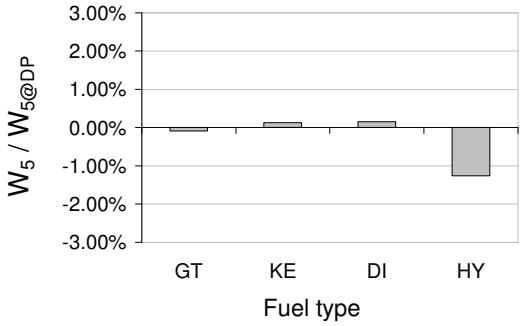

Figure 2-38 Exhaust mass flow (W_5)

The change in exhaust temperature, T_5, should be close to the change in TET since there is not any deviation in pressure across the engine, but, it is a few degrees below. The reason is that the entropy change at every expansion in the turbines is different for the combustion products of each fuel.

From a more practical perspective, Figure 2-37 shows a deviation of around 10°C for KE and DI cases, only a 1.3% increase with respect of natural gas type "M", which could affect the live steam temperature or its mass flow if the temperature control limit were exceeded. Finally, Figure 2-38 presents no change in exhaust mass flow that is in line with the assumptions and considerations made. The small change in HY case is the result of the fuel flow change itself. Therefore, the change in fuel type will not have a major impact on the steam production.

2.8.3 Water injection at the combustion chamber

The last case analysed is the effect of the water (and steam) injection at the combustion chamber. The main objective of the water injection at the burner is to reduce the temperature of the combustion flame. A complete explanation of the thermodynamic principles behind this concept is found in section 2.4.2.

An analysis of the effect in the injection of water and steam in the combustion chamber using TET as a handle (fixed) is found next. No variable geometry effects were included in the simulations. The results are presented as a percentage change on the performance versus the water-to-fuel ratio (*WFR*).

The injection of water (or steam) into the burner affects the energetic balance of the system. If the outlet temperature of the combustor (*TET* or T_4) is fixed, the final mixture of combustion products plus water (or steam) has to leave the combustor at that particular temperature. The injected water mass flow will demand extra energy to reach the outlet conditions (*TET*). This energy will come from additional fuel flow burned. The amount of fuel depends on the phase in which water is injected: liquid (water) or vapour (steam).

Figure 2-39 shows the change in fuel flow as a function of water-to-fuel ratio. It can be observed that if water is injected in its liquid state, the fuel flow increases almost two times that when steam is injected. The important message is that water will absorb energy in excess of the latent heat of evaporation at that particular pressure level while steam only needs a fraction of that to reach the superheated point at the defined TET.

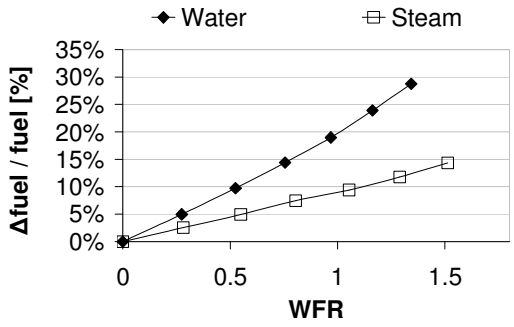

Figure 2-39 Fuel flow (*f*)

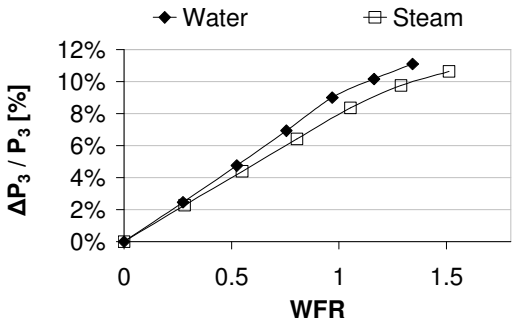

Figure 2-40 Compressor discharge pressure (P_3)

The compressor operating point is also affected by the injection of water. Figure 2-40 shows the deviation in P_3 as a function of *WFR*. For a fixed TET, the compressor has to increase its pressure ratio to accommodate for the additional mass flow entering the turbine thus speeding up the gas generator [37]. As a result, the surge margin of the compressor will be reduced as the running line is pushed up and to the right [12]. Finally, the increased pressure ratio brings a higher T_3 that has a positive effect on the fuel flow, but not enough to offset the energy requirements of water.

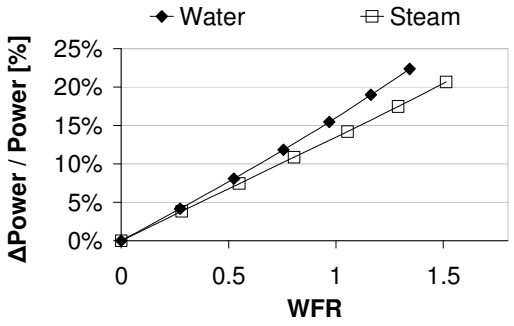

Figure 2-41 Shaft power output

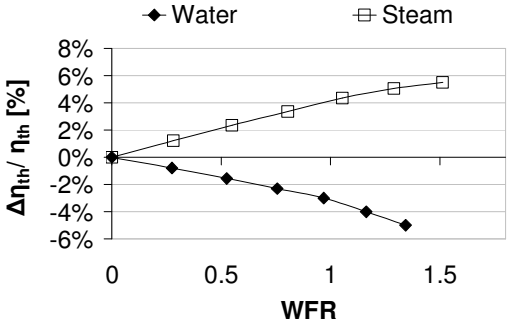

Figure 2-42 Thermal efficiency (η_{th})

The power output increases with the injection of either water or steam (see Figure 2-41). The increase of the mass flow at the turbines has a positive effect on the power generated. The result does not depend on the state in which water is injected, since the combustion products final mixture is increased in the same amount. However, it is the actual thermodynamic properties of the working fluid being expanded that gives water a slightly advantage over steam. The additional energy required to evaporate water at the combustor is still contained in the flue gases at the moment of the expansion, thus, a marginal increase in power output with respect to the injection of steam is obtained.

Mathioudakis [35] reports an increase of approximately 15% for a WFR = 1, exactly the same result obtained in the simulation results presented here.

In the case of the thermal efficiency, contrary to what is observed with the power output, there is a significant difference between the injection of water or steam. Figure 2-42 shows a substantial reduction in thermal efficiency when water is injected compared to the positive trend experienced with steam. It is the fuel flow consumption that dominates the overall engine performance. In the case of water, the power output boost can not offset the surge in heat input (fuel consumption) hence the thermal efficiency falls. On the other hand, a smaller energy demand when steam is injected has a positive effect on the thermal efficiency.

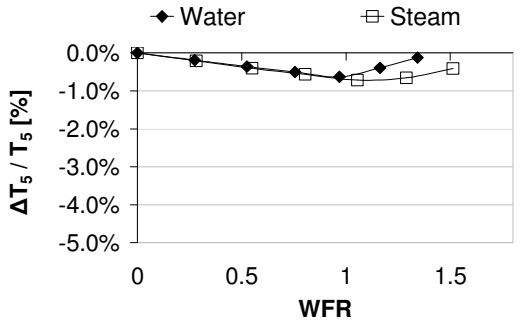

Figure 2-43 Exhaust temperature (T_5)

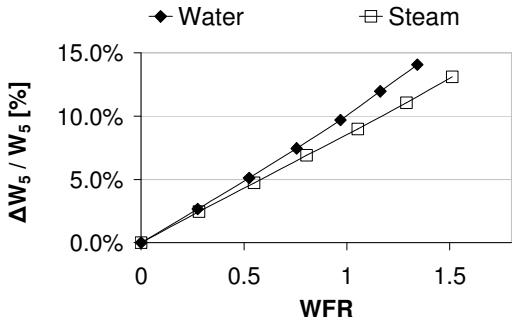

Figure 2-44 Exhaust mass flow (W_5)

Finally, a brief analysis of the exhaust conditions focused on the expected performance of the bottoming cycle is carried out. Figure 2-43 shows a small negative deviation in the exhaust temperature for water and steam that will have a minor effect on the steam production at the heat exchanger. On the other hand, the increase in exhaust mass flow shown in Figure 2-44 would boost the steam production for water and steam alike. In the case of water, these results could alleviate the negative effect on the gas turbine engine overall thermal efficiency by increasing the combined cycle efficiency.

2.9 Summary

This chapter presented the development a performance simulation model for a gas turbine engine similar to the LM2500+. The specifications of the MEA's LM2500+ engines demanded the improvement of some of the Turbomatch capabilities. A review on previous work in the field for each of the modifications was done. The theoretical method used in the development of the algorithms for each of the improved capabilities is found in section 2.4.

A detailed description of the modifications done to the Turbomatch code and structure to implement the new capabilities is found in section 2.5.

An improved Turbomatch model of the LM2500+ engine was generated. A two-section compressor model was used to simulate the bleed off air flows for cooling purposes. The model includes an external heat exchanger used to cool down the bleed off air flow coming from the 9th stage of the compressor. Other main components are considered.

The adaptation of the thermodynamic model of the gas turbine engine was made for design and off-design operating conditions (see section 2.7). The design point adaptation results are very positive; most of the parameters show error values below 1%. On the case of the off-design adaptation, the design-point-adapted model presented big discrepancies between the simulated and real data, but more importantly, it failed to converge at medium power settings (25-15 MW). The implementation of a VSV schedule as a function of the power settings solved the convergence problems and improved the adaptation results.

A detailed analysis on the sensitivity of the gas turbine engine performance to different ambient and operating conditions was conducted. The analysis main objective was to assess the new capabilities developed in section 2.8, that is, humidity effects, different fuels and water injection at the combustor.

Chapter 3 Heat Recovery Steam Generator performance simulation

3.1 Introduction

The expansion of the use of the Combined Cycle Gas Turbine (CCGT) thermal cycle in the late 1950s sparked the development of the heat recovery steam generators (HRSG) market for power generation applications. Only after the operating temperatures inside the gas turbine engine (GT) increased substantially that the implementation of a bottoming Rankine cycle proved economically and practically viable.

The modelling of the HRSG performance as part of any thermal plant used for power generation or to supply industrial process heat is of great importance. The accurate performance simulation of any power plant can provide extra information to the operations team that otherwise would involve labour intensive, long field experiments or data collection programmes. The simulation results can be used to develop adequate unit and plant operation optimisation analysis to increase the productivity of the assets. In addition, the extended knowledge of the unit's performance can be extremely useful when a condition based maintenance (CBM) strategy is pursued.

This chapter presents a theoretical-practical approach to the performance simulation modelling of a dual pressure Once-Through type Heat Recovery Steam Generator (OTSG). A detailed analysis of the heat transfer phenomenon is carried out to estimate the total energy transfer and pressure drop across the boiler (see sections 3.4.1 and 3.4.3). The effect of fouling in the boiler performance is also considered.

A computational program developed following the actual control logic of the OTSG is presented in section 3.6. The proposed approach simplifies the numerical solution of the problem and reduces the convergence time. Empiric correlations, developed from field data, are used to set the temperature and pressure initial boundary conditions. Finally, results of the simulation are shown in section 3.7.

3.2 Nomenclature

$\dot{m}$	Mass flow
$\dot{q}$ or $\dot{Q}$	Heat flow
A	Heat transfer area
A_f	Fin surface area
A_p	Tube (outside) primary heat transfer surface area
A_{FF}	Tube internal free flow area, $A_{FF}=\pi d_i^2/4$
C	Martinelli Factor
CBM	Condition Based Maintenance
C*	Heat capacity rate ratio $C^*=C_{min}/C_{max}$
CC	Combined cycle
CCGT	Combined Cycle Gas Turbine
CF	Cleanliness factor
CHP	Combined Heat and Power

Cp	Specific heat capacity at constant pressure
d_i	Internal tube diameter
d_o	External tube diameter
d_e	Fin tip diameter
f	Bhatti-Shah friction factor
g	Gravity force
GT	Gas turbine engine
G_{Tot}	Total mass velocity of liquid plus vapour
H	Vertical position
h or $\overline{h}$	Heat transfer coefficient (U)
Hg	Hagen number
HP	High pressure
HRSG	Heat Recovery Steam Generator
HX	Heat Exchanger
IST	Innovative Steam Technologies
ke	Kinetic energy
K	Thermal conductivity
L	Tube circuit length
L_1	Tube length between headers
L_2	Core length for flow normal to the tube bank
L_3	Height of the header
L_p	Tube length for pressure drop, $L_p = L_1 + \zeta_{h,i} + \zeta_{h,o}$
LP	Low pressure
M	Liquid molecular weight
MEA	Manx Electricity Authority
N_f	Fin density, $N_f = 1 / p_f$
N_r	Number of tubes in the flow direction
N_t	Total number of tubes, $Nt = L_1L_2/X_{long}X_{transv}$
NTU	Number of transfer units
Nu	Nusselt number
OTSG	Once Through Steam Generator
pe	Potential energy
P	Pressure
p*	Cooper's reduced pressure $p^*=p/p_c$
p_f	Fin pitch
pH	Acidity factor
Pr	Prandtl number
R	Thermal resistance
Re	Reynolds number
R_f	HP to LP mass flow ratio, $R_f = \dot{m}_{hp} / \dot{m}_{lp}$
s	Entropy
ST	Steam turbine
T	Temperature
u	Velocity
U	Overall heat transfer coefficient
x	Vapour quality
X_{long}	Tube bank longitudinal pitch

X_{transv}	Tube bank transverse pitch
X_{tt}	Martinelli parameter
X_{diag}	Tube bank diagonal pitch

Greek letters

α, β, γ	Constants
δ	Annular liquid film thickness
ζ	Fin thickness
$\zeta_{h,i}$	Header inlet thickness
$\zeta_{h,o}$	Header outlet thickness
ε	Effectiveness
η_0	Extended surface factor
η_f	Fins efficiency
θ	Enthalpy
θ_{dry}	Dry angle
μ	Dynamic viscosity
ρ	Density
φ	Vapour void fraction

Subscripts

b	Bare tube outside surface
c	Cold side, Cooper's critical pressure
cb	Convective boiling
conv	Convective (resistance)
corr	Correlation
exh	Exhaust gases
f	Fouling materials (resistance)
G or g	Exhaust gases
h	Hot side
hp	High pressure
i	Inlet
L	liquid
lp	Low pressure
max	Maximum
min	Minimum
nb	Nucleate boiling
o	Outlet
s	Gas side surface
stk	Stack
t	Tube side
t,f	Surface heat transfer coefficient for the liquid phase inside the evaporator
t,g	Surface heat transfer coefficient for the vapour phase inside the evaporator
th	Thermal
tot	Total area of outer surface
tp	Two phase
w	Water/steam, wall (resistance)

3.3 Literature review

The concept of the once-through or one-pass heat exchangers has been implemented in the power generation industry for many years [63]. The structural robustness of this type of boilers permits the generation of steam at extreme pressure conditions. This is the case with the fossil-fuel fired once-through boilers for high sub and supercritical water pressure conditions used in traditional steam power plants [64-66]. The nuclear power generation industry has also adopted this type of heat exchangers with particularities such as helical tubing designs [67, 68], and/or the use of helium or sodium to heat up the water [69-72]. However, the use of Once-Through type Heat Recovery Steam Generators (OTSG) for Combined Cycle Gas Turbine (CCGT) power plants applications is relatively new, with some designs including supplemental firing systems that allow the production of steam when the gas turbine is not available [73]. Manufacturers of this type of boiler for the power generation industry include Innovative Steam Technologies [74], Babcok & Wilcox [75], Rockwell Int, [72].

Research on performance simulation of once-through heat recovery steam generators for CCGT power plants or Combined Heat and Power (CHP) is not abundant, although publications devoted to the analysis of the thermo-hydraulic performance of OTSGs are more frequent.

Dechamps [63] presents the characterisation of the performance of an OTSG as part of a combined cycle power plant and discusses the operational behaviour of the OTSG. An economic analysis on the advantages of implementing an OTSG with supplemental firing system for small CCGT plants applications was presented in [73]. A dynamic performance model of a dual pressure OTSG for use in CCGT power plant is presented in [76]. Chan et.al. [77] describes a validated simulation model for a CCGT power plant using external performance simulation models of the main components including the OTSG.

In the case of the thermo-hydraulic performance analysis of once-through heat exchangers, the studies usually include detailed description of the mathematical models used, developed or corrected as well as brief introduction of the computational programme used. Although this type of research dates back to 1950s, it was the development of computers what made the analysis of more complex models possible [64, 70].

A complete analysis of the steady-state performance simulation of a Babcok and Wilcox once-through steam generator (SG) is described in [75]. The model estimates the local thermo-hydraulic conditions of tubes and tube supports represented as a porous media with distributed resistance to flow and heat transfer. Lausterer [78] reports positive results from the development of a non-linear model of an OTSG of Benson type using efficient numerical methods for its solution.

Bruens [67] undertakes an exhaustive study of different types of OTSG using non-linear physical and mathematical models, including heat transfer and frictional pressure loss correlations for helically-coiled heat exchangers and steam generators. Leithner [65]

carries out a similar analysis using a practical approach for the definition of the temperature and pressure boundary conditions. A description of secondary equipment i.e. pumps is also found. Later research conducted by Dumont [79] presents a mathematical model for a single pressure OTSG. The study includes a comparison of the performance obtained with an OTSG and a common tube-drum type HRSG.

Other publications including analysis in similar detail to those described earlier, but featuring molten sodium-water systems, are found in [71, 80, 81].

In some cases, the development of the performance simulation models was intended for its posterior application to performance-based control systems. Early research by Sanathanan [70] includes a study of the dynamic modelling of a large OTSG for nuclear applications using non-linear, partial differential equations and the selection of the optimal control logic taking into account variable time delay responses. Katayama [82] presents an approach to the design of optimal servo-type controller for a supercritical once-through steam generator under variable pressure operation. The system includes a non-linear performance simulation model of the boiler for the dynamic control of the unit. Jarkovsky [66] describes the implementation of a dynamic performance simulation model as part of a control system for an OTSG with supplemental firing sub-system.

Few publications describe the effect of fouling on the boiler performance. Johnson [83] describes the reduction of steam generation rate in nuclear OTSGs due to increased flow resistance in the nucleate boiling region. Chemical cleaning is suggested to be more effective than pure hydraulic methods. Innovative Steam Technologies [74] gives some indications on the causes of fouling suggesting stringent control of water purity as the most important preventive measure. Cleaning procedures are found inside the customer's operation manual.

It is a common practice to include additional correction factors calculated from experimental data to account for the deviations presented by the empiric correlations available in the literature. The majority of these modifications are done to the two-phase flow models developed during the 1930s to 1940s. Inaccuracies in the estimation of a two-phase heat transfer coefficient have been reported and correction factors proposed [84, 85]. In some cases, even models used for single-phase, laminar or turbulent, flows need some modifications as shown in [79].

The complexity of the thermo-hydraulic physical phenomenon inside an OTSG and the inaccuracy presented by the common empiric correlations used has motivated the research of highly specialised heat transfer, vibration instability, volume forces mechanisms. A theoretical and experimental study to investigate the dynamics of two-phase flows with special reference to density wave oscillations is found in [86]. A study of flow instability for the two-phase region using five different estimation methods (Martinelli-Nelson, Kozeki, Thom, Chisholm and Baroczy) is described in [87].

Glebov [88] presented an analysis of the temperature oscillations and variable thermal stresses depending on the structural and operational parameters influenced by the nucleate boiling phenomenon. Fan [89] reports the results from analysis of the critical

heat flux phenomenon in annular flows inside vertical upward round tubes showing large deviations between empiric correlations and experimental data.

3.4 Theoretical method

In a Once-Through type Heat Recovery Steam Generator (OTSG), water flows in sequence from the economizer, to the evaporator, to the superheater, in one single pass, inside the same tubing. The advantages of such an arrangement are the simplicity of design, the reduction in size and secondary equipment, and high overall effectiveness. However, it demands high purity water to reduce the mineral deposits inside its tubes.

The OTSG simplified design and construction originates complex thermo and hydro dynamics inside the tubing where water changes from a liquid state to a two-phase substance before reaching a complete superheated gaseous state at the unit's exit. All this process takes place without certain knowledge of the physical location of the economizer, evaporator and superheater sections, thus the transfer area of each section is difficult to approximate. Consequently, the analytical modelling of the heat transfer processes occurring inside an OTSG becomes more complicated than with a tube-drum type HRSG where the heat exchange surfaces are well defined easing the calculation of the overall heat transfer coefficient.

This section provides a detailed description of the theoretical method used to estimate the steady-state performance of a dual pressure OTSG. The thermodynamic analysis of the energetic balance inside the OTSG is described and illustrated with help of a T-Q diagram in sections 3.4.1 and 3.4.2, respectively. The mathematical models used for the estimation of the heat transfer coefficient and frictional pressure losses are found in sections 3.4.6 and 3.4.7.

3.4.1 Energy balance

The analysis of the heat transfer mechanisms inside any type of heat exchanger involves the appropriate definition of the thermodynamic systems and volumes of control. The characteristics of the boundaries will define the type of interaction the system has with its surroundings i.e. heat transfer or work generation/consumption.

A first approach is to consider the complete heat exchanger (OTSG) as the thermodynamic system and volume of control. The boundaries of the volume are the OTSG walls through which three fluid streams cross the boundaries of the volume without mixing: gas turbine exhaust gases mass flow, $\dot{m}_g$, and two water flows, $\dot{m}_{hp}$ and $\dot{m}_{lp}$, for high and low pressure systems, respectively (see Figure 3-1a).

Assuming a steady-state operation of the heat exchanger, negligible kinetic and potential energy changes ($ke \cong 0$, $pe \cong 0$), no work interactions ($\dot{W} = 0$) for each fluid stream and no heat loss to the surrounding medium ($\dot{Q} = 0$), recombining mass and energy balance equations, and rearranging,

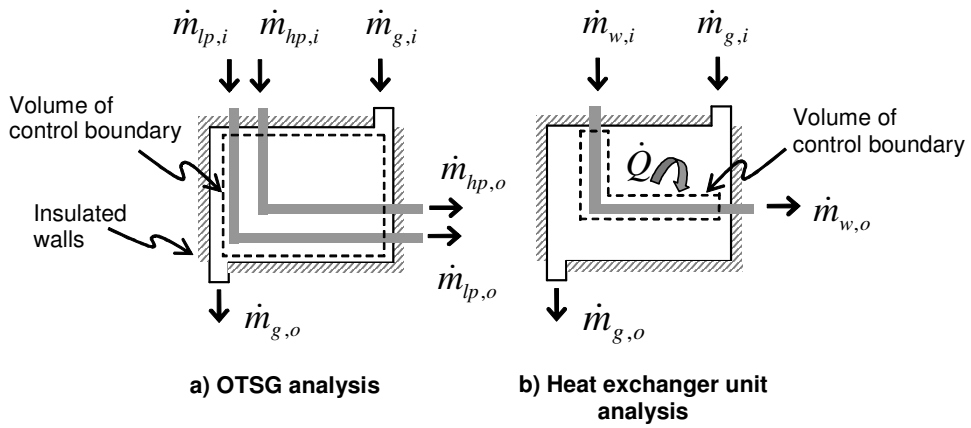

Figure 3-1 Definition of the thermodynamic systems for a once-through steam generator

$$\dot{m}_{hp}\left(\theta_{hp,o}-\theta_{hp,i}\right)+\dot{m}_{lp}\left(\theta_{lp,o}-\theta_{lp.i}\right)=-\dot{m}_{g}\left(\theta_{g,o}-\theta_{g,i}\right) \qquad 3\text{-}1$$

To effectively know the actual conditions of the fluid streams at exit of the OTSG, an analysis of the energy balance at the different sections of the heat exchanger is required. A new volume of control is defined as the fluid stream, either inside or outside the tubes, that is, the water or the exhaust gases. Figure 3-1b illustrates the concept.

In case b, the volume boundaries are not insulated, therefore it is subject to a non adiabatic, steady state process. A heat flow from hot side (exhaust gases) to the cold side (water/steam) will be present and $\dot{Q}$ is not equal to zero. Assuming changes in kinetic and potential energies to be negligible ($ke \cong 0$, $pe \cong 0$) and no work interactions ($\dot{W}=0$) for each fluid stream, and applying the energy and mass balance concepts,

$$\dot{Q}=\dot{m}_{w}\left(\theta_{w,o}-\theta_{w,i}\right)=-\dot{m}_{g}\left(\theta_{g,o}-\theta_{g,i}\right) \qquad 3\text{-}2$$

Equation 3-2 can be used to determine the energy balance between water and exhaust gases at every heat exchanger unit: *economizer*, *evaporator* and *superheater,* when no heat losses are considered.

The Newton's Cooling Law establishes a direct proportionality between the heat flow transfer rate and the temperature difference of cold and hot streams. The constant of proportionality is defined by the product of the heat transfer surface, *A*, and the heat transfer coefficient, *U*. The equation can be expressed as:

$$\dot{Q}=UA\left(\Delta T\right) \qquad 3\text{-}3$$

It can be implied that the actual energy transfer from the exhaust gases to water expressed in equation 3-2 must be equal to the heat transfer calculated from equation 3-3 leading to,

$$\begin{aligned}\dot{Q} &= \dot{m}_w\left(\theta_{w,o} - \theta_{w,i}\right) \\ &= -\dot{m}_g\left(\theta_{g,o} - \theta_{g,i}\right) \\ &= UA\left(\Delta T\right)\end{aligned} \qquad 3\text{-}4$$

3.4.2 T-Q diagram

A common tool used in the analysis and design of HRSG is the T-Q diagram that describes the thermodynamic processes followed by the exhaust gases and water in terms of energy transferred and temperature. Figure 3-2 depicts the T-Q diagram (and detail) of a double pressure heat recovery steam generator where a counter-flow single-pass heat transfer process between fumes and water is considered. The vertical dotted lines indicate the end and beginning of a heat transfer unit (superheater, evaporator and economizer) on both HP and LP water circuits.

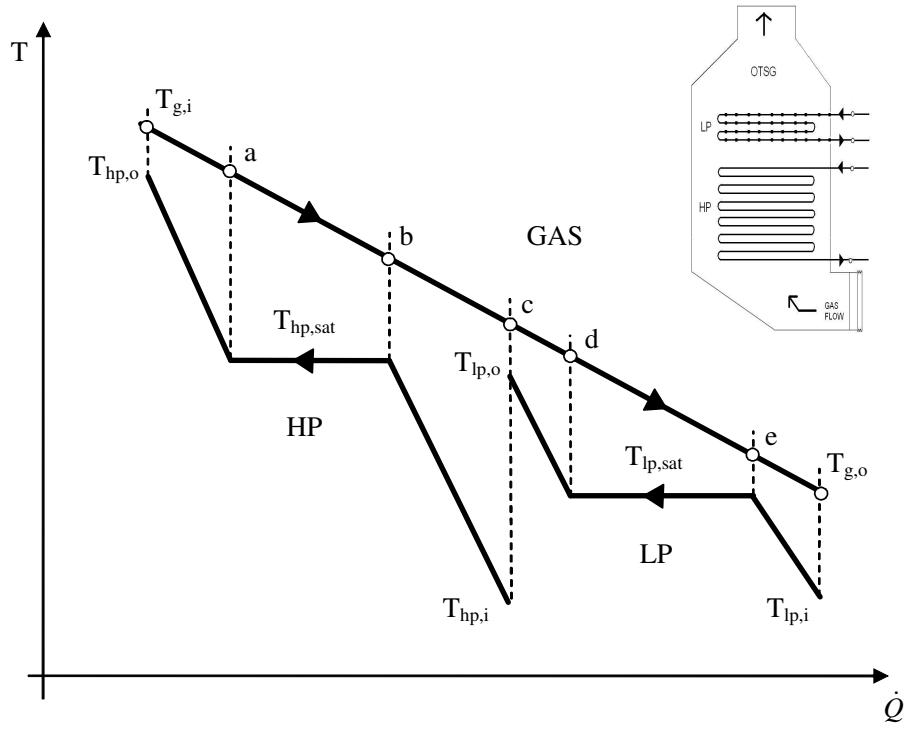

Figure 3-2 T-Q diagram of a duel pressure once-through steam generator

The energy balance between exhaust gases and water as expressed in equation 3-2 takes place at every heat transfer unit for the HP and LP circuits. The exhaust gases mass flow experience a drop in total enthalpy – indicated as a drop in temperature (and pressure) – equal to the energy required by the water mass flow to increase its temperature from one point on the thermodynamic process to the next. For example, at the inlet of the boiler, the exhaust gases go from the initial temperature conditions ($T_{g,i}$) to a lower temperature at point *a* (T_a) while the HP water increases its temperature from the saturated conditions ($T_{hp,sat}$) to the live steam exit conditions ($T_{hp,o}$) set by the control system.

It is worth notice that the exhaust gases mass flow is usually 7 to 10 times larger than the amount of water inside the tubes. Therefore, a larger temperature change on the water side than on the fumes side is expected at the superheater and economizer sections. In the case of the evaporator sections, only the exhaust gases exhibit a drop in temperature since the water maintain a constant temperature value throughout the process.

In practice, the actual energy transferred from exhaust gases to water depends on the physical dimensions of the heat exchanger and the thermo-hydraulic conditions of the two streams. Since the steam exit temperature is set by the control system, any deficiency in the heat transfer process will produce a reduction in steam mass flow.

Next section provides a brief description of one of the common methods used to calculate the performance of a heat exchanger to solve equation 3-3.

3.4.3 Heat transfer

Two of the most common methods for the calculation of the heat exchanger performance are: the Logarithmic mean temperature difference (LMTD) and the Effectiveness-NTU (ε -NTU) methods.

The LMTD approach is used when the inlet and outlet conditions of the fluids are known and design parameters such as the heat flow, surface area or overall heat transfer coefficient may be determined. The LMTD is more often used in sizing or design problems. When any of the outlet conditions is unknown, the analysis involves an iterative approach for which the ε -NTU method is better suited.

The effectiveness-NTU method is more appropriate for rating or evaluation problems. The geometrical characteristics of the OTSG are known making the heat transfer surface area value readily available. The initial conditions, set by the boiler and steam turbine control systems, will determine the inlet conditions and will provide some information on the expected performance.

3.4.3.1 ε -NTU method

In the ε-NTU method, the heat exchanger effectiveness is defined as the ratio between the actual heat transfer rate, $\dot{Q}_{actual}$, and the maximum thermodynamically permissible heat transfer, $\dot{Q}_{\max}$,

$$\varepsilon = \frac{\dot{Q}_{actual}}{\dot{Q}_{\max}} \qquad 3\text{-}5$$

where $\dot{Q}_{actual}$ is found from the energy balance either on the cold or hot stream (equation 3-2). The maximum heat transfer will occur in a heat exchanger of infinite area if a fluid undergoes a temperature change equal to the maximum temperature difference

available $T_{\max} = T_{h,i} - T_{c,i}$. The direction of the heat flow will depend on the fluid presenting the smaller capacity rate, C_{min}. Therefore,

$$Q_{\max} = C_{\min} \Delta T_{\max} = C_{\min} \left(T_{h,i} - T_{c,i} \right) \quad 3\text{-}6$$

The heat exchanger effectiveness, ε, is a non dimensional parameter dependent, in most of cases, on the number of transfer units, *NTU*, the heat capacity rate ratio *C** equals C_{min}/C_{max}, and the flow arrangement for a direct transfer type heat exchanger.

$$\varepsilon = \theta\left(NTU, C^*, flow.arragement\right) \quad 3\text{-}7$$

where the functional relationship θ is dependent on the flow arrangement. For a horizontal counter flow heat exchanger [90], the effectiveness is describe as

$$\varepsilon = \frac{1 - e^{\left[-NTU\left(1-C^*\right)\right]}}{1 - C^* e^{\left[-NTU\left(1-C^*\right)\right]}} \quad 3\text{-}8$$

With

$$NTU = \frac{UA}{C_{\min}} = \frac{1}{C_{\min}} \int_A U dA \quad 3\text{-}9$$

if *U* is not a constant or changes with area type, the definition of the second equality applies. *NTU* may also be interpreted as the relative magnitude of the heat transfer rate compared to the rate of enthalpy change of the smaller heat capacity rate fluid. The overall thermal conductance is the product of the overall heat transfer coefficient, *U* or $\overline{h}$, and the overall heat transfer surface area, *A*. It can also be described as inverse of the overall thermal resistance between two fluid streams $UA = 1/R_{th}$. Next section describes the common technique used for the estimation of the overall thermal conductance.

3.4.4 Overall thermal conductance (UA)

The overall thermal conductance is approximated using the concept of thermal circuits derived from direct analogy to the electric circuits. In the thermal circuits the heat flows through a set of thermal resistances arranged in series or parallel. In pure conduction scenarios, every layer of material in a compounded wall is represented by a thermal resistance. In the case of a heat exchanger, the 'layers' are not only conductive but convective. A thermal circuit for the heat exchanger analysed includes the thermal resistance of convection of the fluids, R_h and R_c, the conductive resistance of the wall, R_w, and the conductive resistance of the fouling materials on the transfer surface, $R_{h,f}$ and $R_{c,f}$. The thermal circuit has the 5 resistances arranged in series as expressed in equation 3-10.

$$UA = \left(R_h + R_{h,f} + R_w + R_{c,f} + R_c\right)^{-1} \quad 3\text{-}10$$

- The conductive thermal resistance is derived from the integration of the Fourier Law of conduction for a tube over the thickness of the tube wall and fin. Equation 3-11 presents the compound thermal resistance for a tube with enhanced areas (fins) where k_w and k_f are the thermal conductivity of the material for the tube and fin, respectively.

$$R_w = \frac{\ln\left(\frac{d_o}{d_i}\right)}{2\pi K_w L_1 N_t} + \frac{\ln\left(\frac{d_e}{d_o}\right)}{2\pi K_f \delta N_f L_1 N_t} \quad 3\text{-}11$$

- The convective thermal resistance is a function of the heat transfer surface area (A) and the average heat transfer coefficient ($\bar{h}$ or U). The use of enhanced areas in the construction of any heat exchanger has a diminishing effect on the convective thermal resistance measured in terms of a comparison between the same HX with and without enhanced surfaces. The extended surface factor or overall surface efficiency, η_0, is expressed as

$$\eta_o = 1 - \left(1 - \eta_f\right)\frac{A_f}{A_o} \quad 3\text{-}12$$

where η_f is the fin efficiency, A_f is the fin area and A_0 is the smooth tube HX surface area. Hence, the general expression for the convective thermal resistance using the extended surface is

$$R = \frac{1}{(\eta_0 \bar{h} A)} \quad 3\text{-}13$$

121. The fouling thermal resistance is difficult to measure or model due to its transient nature. Instead, the fouling resistance can be computed by coupling the heat transfer coefficient of a clean condition into a relationship proposed by Somerscale [91] termed the cleanliness factor (*CF)* relationship,

$$R_f = \frac{\left(1 - CF\right)R_{conv}}{CF} \quad 3\text{-}14$$

The fouling effects on the pressure drop analysis are more evident inside the water tubes. Sediments on the internal wall of the tubes reduce the cross sectional area augmenting the mass velocities ($\dot{m}$/area), which in turn, increase the Reynolds number and the friction factor. To account for the fouling effects a reduction in the internal free flow area is considered

$$A_{FF,f} = CF \cdot A_{FF} \quad 3\text{-}15$$

The following two sections provide a detailed explanation of the derivation of the heat transfer surface and heat transfer coefficient required for the calculation of the convective thermal resistance for each of the heat exchanger units (economizer, evaporator and superheater).

3.4.5 Heat transfer area (A)

The estimation of the convective heat transfer area for the fumes (exhaust gases) side and water side is presented in this subsection. The heat transfer area for the water side is the internal area of the entire tube bank, A_i. While, the fumes side area is the sum of the fin total area (A_f) and the primary external total area, A_p, as expressed in equations 3-16 to 3-19.

Fin total area:

$$A_f = \left[\frac{2\pi\left(d_e^{\,2} - d_o^{\,2}\right)}{4} + \pi d_e \zeta \right] N_f L_1 N_t \qquad 3\text{-}16$$

Primary total tube-bank area:

$$A_p = \pi d_o \left(L_1 - \zeta N_f L_1\right) N_t + 2\left(L_2 L_3 - \frac{\pi d_o^2}{4} N_t \right) \qquad 3\text{-}17$$

External tube-bank total area:

$$A_o = A_f + A_p \qquad 3\text{-}18$$

Internal tube-bank total area:

$$A_i = \pi d_i N_t L_1 \qquad 3\text{-}19$$

In some cases, the estimation of the heat transfer coefficient is a function of the actual heat transfer area. The empiric correlations for the calculation of the convective heat transfer coefficient on the fumes (gases) side (refer to section 3.4.6.3) are function of the actual geometrical parameters of the heat exchanger such as tube arrangement, fin total area, and primary total tube area.

3.4.6 Heat transfer coefficient (U or h)

The heat transfer coefficient is a measure of the effect of the thermal boundary layer on the heat transfer between a flow and a surface. The formation of the thermal boundary layer depends on the existence of a temperature difference between the free flow and the surface area. The thermal boundary layer grows in the direction of the flow as a function of the velocity and thermophysical properties of the fluid and the geometry of the surface. The heat transfer coefficient for a particular geometry can be estimated from the Nusselt number expressed in terms of the Reynolds and Prandtl dimensionless parameters of the fluid. The following sections present the empiric correlations used to estimate the Nusselt number for the different conditions found in the heat exchanger.

3.4.6.1 Tube-side: Economizer and Super-heater

The fluid inside the economizer and superheater virtual sections is a single-phase fluid in the tubes based on the thermodynamic and operating conditions. Gnielinski [92] recommend the following equation which applies to transition, turbulent and hydro-dynamically developed flow in circular or non-circular duct computing the economizer heat transfer coefficient:

$$Nu_t = \frac{\left(f/2\right)\left(\mathrm{Re}_t - 1000\right)\mathrm{Pr}_t}{1 + 12.7 * \sqrt{\left(f/2\right)}\left(\mathrm{Pr}^{2/3} - 1\right)} \qquad 3\text{-}20$$

The range of application of equation 3-20 is $0.5 \le \mathrm{Pr} \le 2000$ and $3000 \le \mathrm{Re}_t \le 5x10^6$. For laminar flow, the Sieder and Tate [93] correlation can be use

$$Nu_t = 1.86\left[\frac{\mathrm{Re}_t\,\mathrm{Pr}_t\,d_i}{L_1}\right]^{1/3} \qquad 3\text{-}21$$

$$\mathrm{Pr}_t = \frac{\mu_t Cp}{K_t} \qquad 3\text{-}22$$

And the heat transfer coefficient h_t is determined as follows;

$$h_t = \frac{Nu_t K_t}{d_i} \qquad 3\text{-}23$$

3.4.6.2 Tube-side: Evaporator

The general equation for the local flow boiling heat transfer coefficient h_{tp} for evaporation in a horizontal plain tube in the Kattan-Thome-Favrat [94] method for an internal tube diameter of d_i is:

$$h_{tp} = \frac{d_i \theta_{dry} h_{t,g} + d_i\left(2\pi - \theta_{dry}\right)h_{t,f}}{2\pi d_i} \qquad 3\text{-}24$$

where the heat transfer coefficient on the liquid and vapour surfaces are $h_{t,f}$ and $h_{t,g}$, respectively. To simplify the calculations it is assumed a vapour phase angle (θ_{dry}) equals to zero. Hence h_{tp} is equal to $h_{t,f}$, which is obtained from an asymptotic expression that combines the nucleate boiling h_{nb} and convective boiling h_{cb} contributions using an exponent of 3 as:

$$h_{t,f} = \left(h_{nb}^3 + h_{cb}^3\right)^{1/3} \qquad 3\text{-}25$$

We use the dimensionally reduced pressure p^* correlation of Cooper [95] to determine h_{nb}:

$$h_{nb} = 55 p^{*0.12} \left(-\log_{10} p^*\right)^{-0.55} M^{-0.5} \dot{q}^{0.67} \qquad 3\text{-}26$$

On the other hand, characterizing the proposed annular flow as a film flow rather than a tubular flow, the convective boiling heat transfer coefficient h_{cb} is calculated with:

$$h_{cb} = 0.0133 \left[\frac{4\,\dot{m}(1-x)\,\delta}{(1-\varphi)\mu_L}\right]^{0.69} \left[\frac{Cp_L \mu_L}{k_L}\right]^{0.4} \frac{k_L}{\delta} \qquad 3\text{-}27$$

Assuming tubular flow on the dry perimeter of the tube at the mass velocity of the vapour, $\dot{m}x$, the vapour-phase heat transfer coefficient $h_{t,g}$ is obtained with the Dittus-Boelter [96] turbulent flow heat transfer correlation:

$$h_{t,g} = 0.023 \left[\frac{\dot{m} x d_i}{\varphi \mu_G}\right]^{0.8} \left[\frac{Cp_G \mu_G}{k_G}\right]^{0.4} \frac{k_G}{d_i} \qquad 3\text{-}28$$

The vapour void fraction φ is predicted using the drift flux void fraction model of Rouhani-Axelsson for vertical tubes that was modified by Steiner [97] for horizontal tubes.

$$\varphi = \frac{x}{\rho_G}\left\{\left[1 + 0.12(1-x)\right]\left(\frac{x}{\rho_G} + \frac{1-x}{\rho_L}\right) + \frac{1.18}{\dot{m}}\left[\frac{g\sigma(\rho_L - \rho_G)}{\rho_L^2}\right]^{1/4}(1-x)\right\}^{-1} \qquad 3\text{-}29$$

3.4.6.3 Fumes Side

The analysis of the fumes side contemplates convection as the main heat transport mechanism since radiation levels are negligible. The heat transfer coefficient for the fumes side is highly dependant on the physical arrangement of the tube bank. Figure 3-3 shows the arrangement of the OTSG under analysis. The hydrodynamic boundary layer separation from the tube surface creates turbulent flow regions that reduce the free flow area and increase the fluid's Reynolds number. Equation 3-30 presents an empirical correlation to estimate the Nusselt number in cross flow over pipes from the geometric parameters of the heat exchanger and fluid conditions and properties. Values for parameters "C", "m", "n" and "l" are given in Table 3.1.

$$Nu_s = C\,\mathrm{Re}_s^m \left(\frac{A_f + A_p}{A_p}\right)^n \mathrm{Pr}_s^l \qquad 3\text{-}30$$

Table 3.1 Coefficient for Nusselt correlation

	C	m	n	l
Inline arrangement	0.22	0.6	-0.15	0.333
Staggered arrangement	0.38	0.6	-0.15	0.333

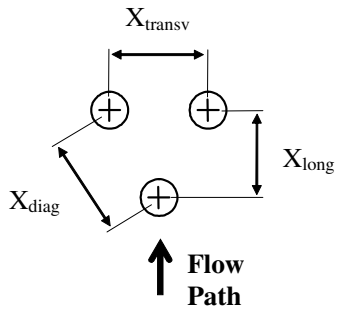

Figure 3-3 Triangular arrangement of a dual pressure once-through steam generator

3.4.7 Pressure drop (∆P)

The pressure drop experienced by a flow in direct contact with a surface is dependent on the friction forces created inside the hydrodynamic boundary layer. The friction factor is a function of the velocity distribution of the flow created by surface and volume forces (viscosity effects between molecules) and geometry of the surface. If the velocity of the flow is forced to zero, a pressure drop equal to the initial kinetic energy of the fluid would be experienced. The next sections present different empiric correlations used to estimate the pressure drop in the water or exhaust gases for particular fluid and geometric conditions.

3.4.7.1 Tube-Side: Economizer and Superheater

The pressure drop is computed from the equation 3-31, given below.

$$\Delta P = \frac{f_t \rho u^2}{2g} \frac{L_p}{d_i} \qquad 3\text{-}31$$

with the friction factor $f_t = \frac{64}{\mathrm{Re}_t}$ for laminar flow and $f_t = \frac{0.3164}{\sqrt[4]{\mathrm{Re}_t}}$ for turbulent flow.

3.4.7.2 Tube-Side: Evaporator

Hence, the two phase pressure drop for flows inside tubes is the sum of three contributions: the static pressure drop ΔP_{static}, the momentum pressure drop ΔP_{mom} and the frictional pressure drop ΔP_{frict} as;

$$\Delta P_{total} = \Delta P_{static} + \Delta P_{mom} + \Delta P_{frict} \qquad 3\text{-}32$$

For a horizontal tube, there is no change in static head i.e. $H=0$ so $\Delta P_{static} = 0$. The momentum pressure drop reflects the change in kinetic energy of the flow and is for the present case given as;

$$\Delta P_{mom} = G_{tot}^2 \left\{ \left[\frac{(1-x)^2}{\rho_L (1-\varphi)} + \frac{x^2}{\rho_G \varphi} \right]_{out} - \left[\frac{(1-x)^2}{\rho_L (1-\varphi)} + \frac{x^2}{\rho_G \varphi} \right]_{in} \right\} \qquad 3\text{-}33$$

The frictional pressure drop in two phase flows is typically predicted using separated flow models. The first of these analyses was performed by Lockhart and Martinelli [98] and then followed by many others. The basic equations for the separated flow model are not dependent on the particular flow configuration adopted. It is assumed that the velocities of each phase are constant, in any given cross section, within the zone occupied by the phase.

The method of Lockhart and Martinelli is the original method that predicted the two phase frictional pressure drop based on a two phase multiplier for the liquid-phase, or the vapour- phase respectively, as;

$$\Delta P_{frict} = 4\Phi_{Ltt}^2 f_L \left(\frac{L_p}{d_i} \right) G_{tot}^2 (1-x)^2 \left(\frac{1}{2\rho_L} \right)$$

$$\Delta P_{frict} = 4\Phi_{Gtt}^2 f_G \left(\frac{L_p}{d_i} \right) G_{tot}^2 x^2 \left(\frac{1}{2\rho_G} \right) \qquad 3\text{-}34$$

with $f = \frac{0.079}{\mathrm{Re}_t^{0.25}}$ and $\mathrm{Re}_t = \frac{G_{tot} d_i}{\mu}$ used to calculate the frictions factors of the liquid f_L and the vapour f_G with their respective physical properties. Their corresponding two phase multipliers are;

$$\Phi_{Ltt}^2 = 1 + \frac{C}{X_{tt}} + \frac{1}{X_{tt}^2}, \text{ for } \mathrm{Re}_L > 4000$$

$$\Phi_{Gtt}^2 = 1 + CX_{tt} + X_{tt}^2, \text{ for } \mathrm{Re}_L < 4000 \qquad 3\text{-}35$$

where X_{tt} is the Martinelli parameter for both phases in the turbulent regions defined in equation 3-36 using the C values presented in Table 3.2.

$$X_{tt} = \left(\frac{1-x}{x} \right)^{0.9} \left(\frac{\rho_G}{\rho_L} \right)^{0.5} \left(\frac{\mu_L}{\mu_G} \right)^{0.1} \qquad 3\text{-}36$$

Table 3.2 Martinelli factor

Liquid	Gas	C
Turbulent	Turbulent	20
Laminar	Turbulent	12
Turbulent	Laminar	10
Laminar	Laminar	5

3.4.7.3 Fumes side

Shah [99] suggests the use of correlations for flow normal to inline and staggered plain tube bundles developed by Gaddis and Gnielinski [100] and recast in terms of the Hagen number per tube row by Martin [101]. The main expression is:

$$Hg = Hg_{lam} + Hg_{turb,i}\left[1-\exp\left(1-\frac{\mathrm{Re}_s+1000}{2000}\right)\right] \qquad 3\text{-}37$$

The pressure drop for flow normal to the tube bundle is then computed from:

$$\Delta p = \frac{\mu_s^2}{\rho_s g}\frac{N_r}{d_o^2}Hg \qquad 3\text{-}38$$

3.4.8 Thermophysical properties

The thermophysical properties needed for the thermodynamic and heat transfer mathematical models were obtained using McBride [102] computer program and Deschamps [103] functions. Other quantities used were taken from standard look up tables available from books on the subjects.

3.5 Practical method

The objective of this section is to complement the theoretical method with relevant practical information regarding the operation and control of a once-through heat recovery steam generator. The start-up operation of a double pressure OTSG and the effect of the steam and gas turbine engines operation on the boiler performance are briefly covered. The description of the empiric correlations created from field data to set the temperature and pressure initial boundary conditions to the simulation problem is found.

3.5.1 Start-up operation

During the start-up of the boiler, the feedwater mass flow is estimated using the energy balance equations across the OTSG. The amount of water being admitted into the boiler tubing depends on the effective and safe initial conditions for the operation of the steam

turbine, the actual performance readings from the gas turbine engine, and, the empiric correlations embedded in the OTSG control system itself.

Once full steam production is achieved and steady state conditions are met, temperature is set as the control variable. The feedwater mass flow is reduced if the temperature falls from the set point, or viceversa.

To reduce the thermal shock factor, steam production should start as soon as the exhaust gases temperature exiting the OTSG, $T_{g,o}$, has reached the minimum permissible temperature. The LP system should not be operated until the HP system reaches the operational set point. The reason for this starting sequence is that sufficient HP feedwater flow is required to protect the lower pressure circuits from higher temperatures that would be produced at low HP flows. The tube material properties vary with the vertical position of the tube within the OTSG.

3.5.2 Steam turbine set points

The sliding pressure and the throttling valve methods are commonly used in the control of the steam cycle. The sliding pressure method determines a variation in operating pressure for loads below nominal that will ensure a high quality steam to maximize Rankine efficiency and to eliminate the risk of condensation at the LP turbine exit stages. These pressure relationships are usually a non-linear function of the steam turbine operating conditions. The throttling method controls the position of the main valves to satisfy the thermodynamic conditions at the inlet of the steam turbine. The model developed use the sliding pressure following the actual control system of the plant.

In addition to the operating pressure level, the temperature of the superheated steam must be defined to avoid any mechanical failure on any of the components in the steam path. The control also looks to achieve optimum steam qualities at the exit of the LP section of steam turbine to extend the life of the parts.

3.5.3 Gas turbine performance parameters

The gas turbine performance parameters used to control an OTSG are the exhaust gases temperature – measured at the OTSG plenum, $T_{g,i}$, also identified as T_{exh} – and mass flow, $\dot{m}_g$. These two parameters allow to reduce the number of unknowns in the energy balance analysis (equation 3-42) after calculating the specific heat of the exhaust gases, Cp_g, or the enthalpy values, θ_g.

Since the exhaust gases temperature, T_{exh}, is proportional to the gas turbine engine power settings and ambient conditions, it is commonly used as independent variable in a number of empiric correlations and control set points that estimate variables such as steam turbine operating pressure, stack temperature, LP feedwater flow, etc.

3.5.4 Empirical correlations

The empiric correlations embedded in the control system of the OTSG are set to constrain the operating variables to a predetermined performance. The correlations provided by the manufacturer are only valid at the boiler's nominal operation. Hence, a correction factor or a new set of empiric correlations are needed when simulating the performance out of the design point. The following are the mathematical relationships used by the control system of the OTSG.

3.5.4.1 Steam cycle operating pressures

The estimation of the operating pressure of the steam cycle is made using the equation presented below. The empiric correlation is function of the exhaust gases temperature only. Unfortunately, the limited amount of data prevented the development of a more complete formula using the exhaust gases mass flow. A fixed ratio between HP and LP pressures was used.

$$P_{hp} = \alpha \cdot T_{exh}^2 + \beta \cdot T_{exh} + \gamma \qquad 3\text{-}39$$

3.5.4.2 LP feedwater mass flow

The low pressure system feedwater mass flow is a guess of the expected LP steam mass flow production as operational issues prevent the admission of LP feedwater into the boiler until the HP steam conditions are reached. The mathematical expression that approximates the LP feedwater mass flow as a function of the exhaust gases temperature is of the type,

$$R_f = \alpha \cdot T_{exh}^2 + \beta \cdot T_{exh} + \gamma \qquad 3\text{-}40$$

3.5.4.3 Stack temperature

The temperature of the exhaust gases at the boiler exit, or stack temperature $T_{g,o} = T_{stk}$, must be maintained above the water and acid dew point (approx 100ºC). The condensation of water on the cold tubes at the top of the boiler or within the exhaust flues is highly undesirable as the exhaust gases will contain acidic gases, due to the product of combustion and fuel chemical composition. These acidic gases, such as sulphur dioxide and nitrous oxide, will form corrosive acids on contact with water which will attack the boiler tubes and exhaust flues. If allowed to persist, this process will attack the tubes and fins within a short time reducing the operating life of the plant. The following is the mathematical relationship for the stack temperature as a function of the exhaust gases at the OTSG plenum for full load operation,

$$T_{stk,corr} = \alpha * T_{exh} + \beta \qquad 3\text{-}41$$

3.5.5 Fouling

The deposition of particles on both sides of a heat exchanger tubing increases the thermal resistance therefore reduces the overall HX effectiveness, and increases the pressure drop. The mineral particles in the water tend to deposit on the tube's inner surface, while particles found in the gas turbine engine exhaust gases, mainly soot, sticks to the tube's external surface and fins. The amount of soot produced is largely determined by the type of fuel being used. Some of the consequences of fouling are listed as follows,

- Increases maintenance costs resulting from cleaning, chemical additives, or trouble shooting.
- Results in loss of production due reduced capacity as fouling develops and longer shutdowns associated with cleaning.
- Increased gas turbine exhaust back pressure and water system pressure drop.

High purity water should be used at all times to reduce fouling (particles deposition inside the tubes) and acid droplets formation on the tubes at top of the OTSG. Both pH and conductivity must be continuously controlled and monitored to confirm that the water quality is always within the specification [74].

3.6 Computational tool

The OTSG software was programmed to facilitate a) the interconnectivity with other external programs part of a thermal cycle analysis platform, b) internal coherence, and c) the efficient use of the computational resources. Figure 3-4a presents the computational flow chart of a double pressure OTSG system. The main considerations behind this proposition are: the use of the empirical correlations to set the limits to the solution domain and to subordinate the LP circuit to the HP results.

The process begins with the calculations of R_f, $T_{hp,o}$, $P_{lp,o}$, $P_{hp,o}$ and $T_{stk,corr}$ values using the empirical correlations described earlier. $T_{lp,o}$ is guessed and $\dot{m}_{hp}$ and $\dot{m}_{lp}$ are computed using equation 3-42.

$$\dot{m}_{hp} = \frac{\dot{m}_g * Cp_g * \left(T_{g,i} - T_{g,o}\right) - \dot{m}_{lp}\left(\theta_{lp,o} - \theta_{lp,i}\right)}{\left(\theta_{hp,o} - \theta_{hp,i}\right)} \qquad 3\text{-}42$$

Figure 3-4b shows the calculations inside every HX unit (i.e. superheater, evaporator and economizer). A first guess of the number of tubes, $N_{t,HXunit}$, that defines the heat transfer area is made. The energy required to produce water/steam at specific conditions is computed using the water thermodynamic polynomials (refer to section 3.4.8) and equation 3-3. If a considerable error between the two quantities is found, a new $N_{t,HXunit}$ is guessed until convergence is achieved. The pressure drop at the unit is estimated and stored, assuming the pressure conditions at the subsequent HX units remain unchanged.

Once all three high pressure circuit HX units' internal iterations converge the HP-loop condition must be satisfied. If the sum of the calculated number of tubes for each section

is not equal to the known total number of tubes for the HP circuit, the $T_{lp,o}$ is modified until convergence is achieved.

At this point, an energy balance for the entire OTSG at the conditions defined using the empiric correlations for R_f, the steam turbine operating conditions and $T_{lp,o}$ guess has been reached. However, only the high pressure HX circuit has complied with the equality proposed in equation 3-2. It is necessary to conduct the heat transfer calculations using equation 3-3 for the low pressure HX units.

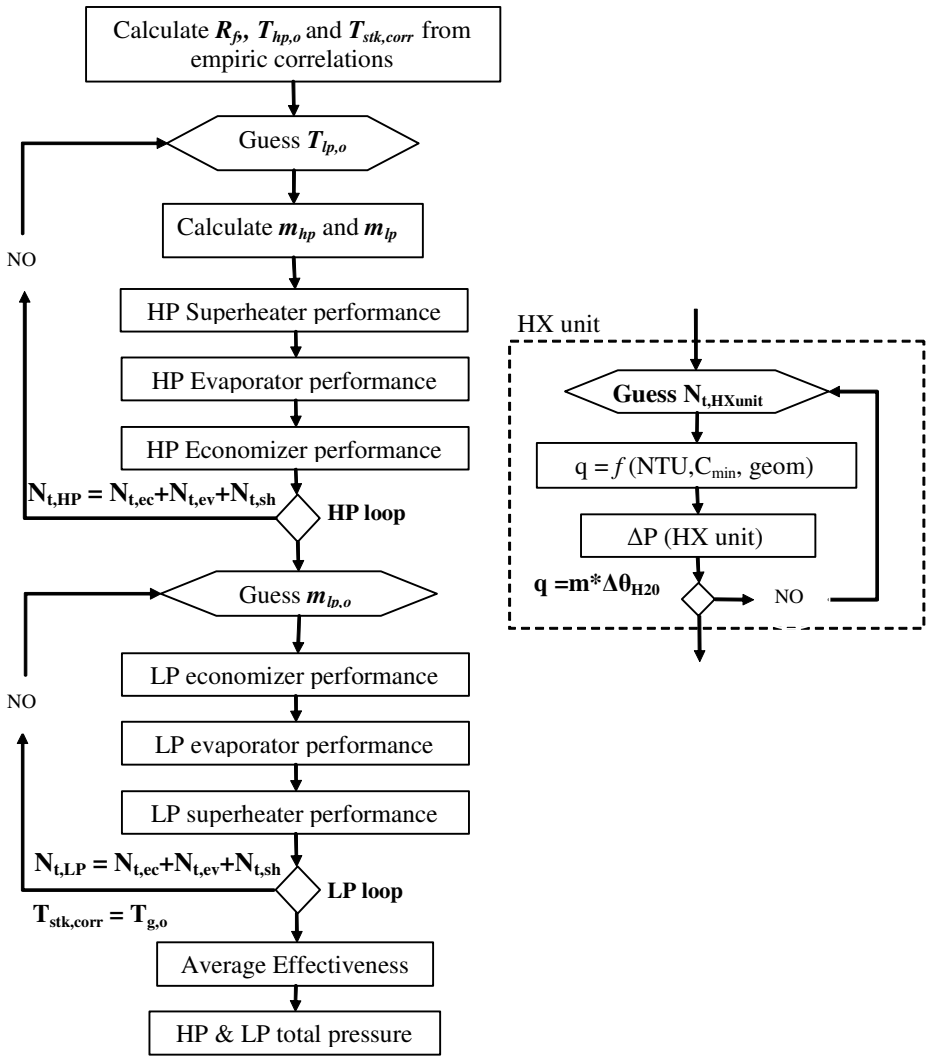

Figure 3-4 Computational flow chart of a) Dual pressure once-through type steam generator and b)HX unit

Any modification to the LP conditions inside the LP-loop would alter the energy balance for the entire OTSG forcing the program to return to the HP-loop increasing the

processing time and inaccuracies. To prevent such scenario, $\dot{m}_{hp}$ and $T_{lp,o}$ are kept fixed while the LP mass flow, $\dot{m}_{lp}$, is modified preserving the energy balance throughout the boiler. In other words, the LP circuit operating conditions is subordinate to the HP circuit conditions.

When the LP-HX units have been solved, a double condition must be satisfied. The sum of number of tubes for each HX unit has to be equal to the known LP total number of tubes, and the calculated stack temperature, $T_{g,o}$, shall not differ from the $T_{stk,corr}$. If the conditions are not satisfied, a new value for the LP mass flow is guessed until convergence is achieved.

This approach is close to the actual operation of the boiler described in section 3.5.1 where the LP circuit adapts to the operating conditions of the HP circuit after the later has reached the set point defined by the control system i.e. live steam temperature and pressure. Finally, the overall OTSG effectiveness and the HP and LP circuits total pressure drop are calculated.

3.6.1 Log book

This section provides the main characteristics the different versions of the OTSG performance simulation software described in the previous section. Additionally, a detailed description of some issues raised during the development and recommendations for future improvements of the program is found.

Versions

- Original version
  - Calculates single and double pressure cases
  - Uses an ascending iterative process with very small increments.
  - Convergence time of approximately 60 min.
  - Thermophysical properties are called as external input file.
  - Stand alone program, no connectivity achieved!
  - Well defined subroutines
  - Long output file.
  - Moderate accuracy consequence of limited data

- OTSG 1.1
  - New in-house iterative algorithm was implemented.
  - Convergence time reduced to a maximum of 10 seconds.
  - Modifications to the solving algorithms caused accuracy variations. The accuracy values outside the design point remain unchanged however it presented large errors near to design point operation.
  - The single pressure system stopped working.

- OTSG 1.2
  - Connectivity achieved. The program was modified to work as a Dynamic Link Library (DLL) subroutine inside an integration system

- The code was modified to actively deal with a persistent error caused by unrealistic input conditions.
- Output file eliminated.

3.7 OTSG performance simulation

3.7.1 Field data

The data used to derive the empiric correlations and to adapt the performance simulation model was limited, only recorded during the OTSG were operating in a double pressure mode. Few data points at exhaust temperatures, T_{exh}, around 780K and 735K were obtained during a performance test on the plant and used for the development of the software. The sets of data contain parameters extracted directly from the boiler control system and values simulated as a result of the energy balance calculations carried out for the performance test.

3.7.2 Design point performance

The results for the design point performance simulation are presented in Table 3.3. Only values for the double pressure operating mode are reported since no information for the single pressure operating mode was available. A maximum error of 0.5% on the HP and LP mass flows was obtained while other parameters show even smaller deviations from field values. Such small errors were expected as all empiric correlations (see section 3.5.4) and other correction factors, applied to some of the heat transfer coefficient mathematical models, were first adapted to design point operating conditions. Rather than focusing on the accuracy of the results, these values represent the positive response from the method employed.

Table 3.3 OTSG design point adaptation

		Double pressure
Parameter	Units	Error
T_{stk}	K	0.00%
T_{lp}	K	0.11%
T_{hp}	K	0.00%
$\dot{m}_{lp}$	Kg/s	-0.50%
$\dot{m}_{hp}$	Kg/s	-0.51%

3.7.3 Double pressure off-design performance

The results are presented as a function of the exhaust gases temperature following the decision to use the exhaust gases temperature T_{exh} as independent variable for the development of the empiric correlations.

Figure 3-5 shows the deviation in percentage of the simulated to the field data. In general, the simulation error tends to increase as the operating point of the boiler leaves the design point conditions. Errors of 1% in the computed HP and LP steam mass flow

rates are found that suggests the R_f correlation needs to be constructed from a larger amount of data. These results coincided with the overestimation of the LP live steam temperature T_{lp} in about 5%. Last, the computed and real OTSG stack temperatures agree (about 0.15% difference).

It is important to mention that no allowance for any deviation in ambient and operating conditions from design point is made. The exhaust temperature values from some of the data points were close to each other even though the power output from the gas turbine supplying the flue gases presented more dissimilar values. It was learned from Chapter 2 (Gas turbine performance diagnostics) results that deviations in ambient and operating conditions can affect the accuracy of gas turbine engine performance simulation that is directly linked to the boiler performance.

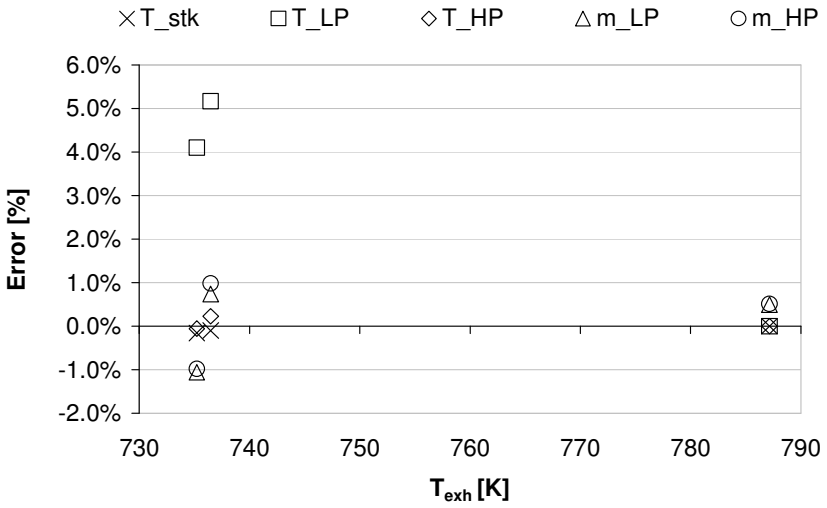

Figure 3-5 Double-pressure off-design performance simulation

On the positive side, the simulation provided fresh information that is not ready available from the control system, for example, the effectiveness of the different sections of the boiler. Figure 3-6 and Figure 3-7 reports effectiveness values for the HP and LP pressure circuits respectively.

The results show higher effectiveness values for the evaporator sections on both HP and LP circuits, followed by the superheater and the least being the economizer. There are two reasons for the high effectiveness at the evaporator: the lack of an approach point and the constant water temperature over the section at which the heat transfers takes place.

> First, the approach point set in common HRSGs is designed to avoid the beginning of the water evaporation in the economizer tubing section. The disadvantage of the approach point is the reduction in heat transfer effectiveness at the evaporator since the same heat transfer surface has to take the water to its evaporation point and complete the process until reaching the vapour saturation point before steam can flow towards the superheater. Therefore, the absence of

the separation drums in OTSG increases the effectiveness of the evaporator, and the boiler in general, as water is heated and evaporated inside the same tube. From a structural and practical perspective, the evaporation of water inside a same tube occurring in an OTSG brings about vibration and mechanical problems on the tube-banks leading to failure.

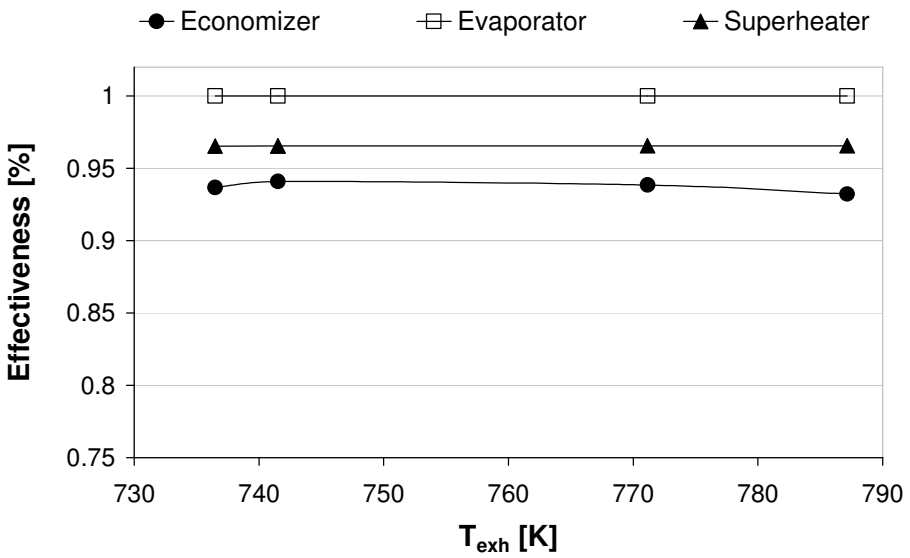

Figure 3-6 Effectiveness of the high pressure HX units

Secondly, the fact the heat transfer phenomenon inside the evaporator occurs at a constant temperature, as opposed to the increasing temperature conditions in the superheater and economizer, has a beneficial effect captured by any of the methods used to solve equation 3-3.

On the other hand, the effectiveness of the superheater is higher than the economizer because the heat transfer requirements from the superheater are less than those from the economizer. The energy needed to superheat saturated steam is far less than the energy need to bring water from near ambient conditions to the evaporation temperature. Additionally, the higher temperatures experienced at the superheater section facilitates the heat transfer between the exhaust gases and the steam.

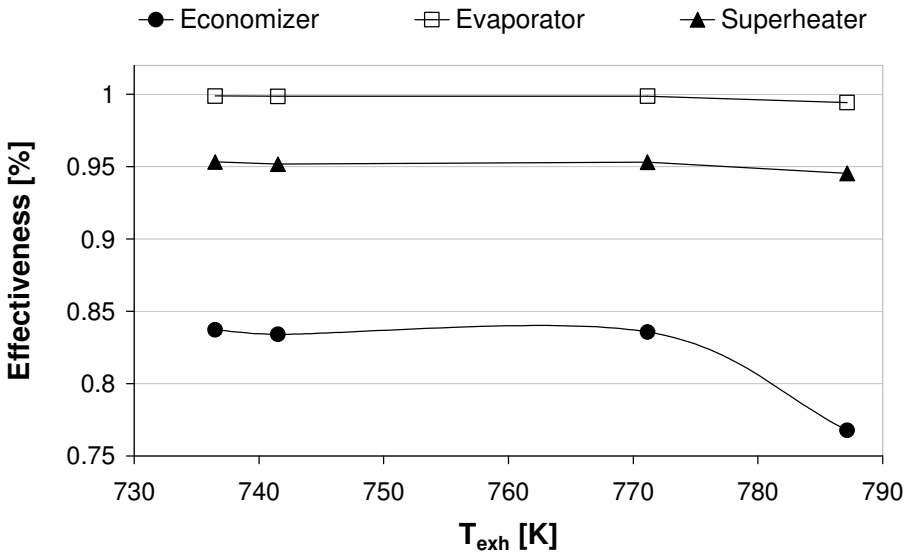

Figure 3-7 Effectiveness of the low pressure HX units

3.7.4 Single pressure off-design performance

As mentioned before, the data used during the development of the simulation model did not include performance values recorded during the operation of the boiler in the single pressure operating mode. Hence, there was not benchmark to compare the results of the simulation against. Instead, it was decided that a direct comparison with the double pressure mode simulation results could be prove more useful.

Figure 3-8 and Figure 3-9 show a comparison of the OTSG overall effectiveness and HP steam mass flow production between the single and double pressure operating modes. It can be observed the single pressure mode delivers an average of 9% more steam mass flow than the double pressure system as there is not LP steam production. In contrast, the overall effectiveness decreases an average of 3.81% result of the boiler's inability to extract the energy at lower temperatures.

The fact that for a lower exhaust gases temperature correspond a lower set of steam turbine's operating pressures explains why the effectiveness raises as the temperature decreases. It is evident the whole CCGT thermal efficiency will decrease when the OTSG is used in the single pressure operating mode.

From a practical point of view, the operation of the boiler on the single pressure mode, even if the effectiveness of the unit is reduced, prepares the OTSG two switch to the double pressure operating mode faster, hence, pushing up the steam cycle power output and OTSG effectiveness. MEA's has adopted such strategy to increase the power plant overall thermal efficiency in the recent months. Unfortunately, the part load and ramping operation regime tends to reduce the life of the tube banks increasing the probabilities of mechanical failure.

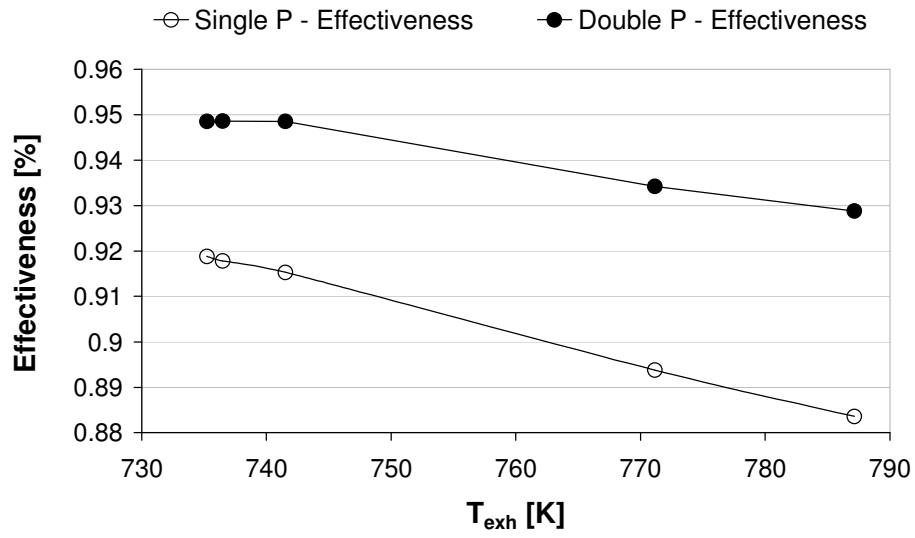

Figure 3-8 Overall effectiveness for single and double pressure operating modes

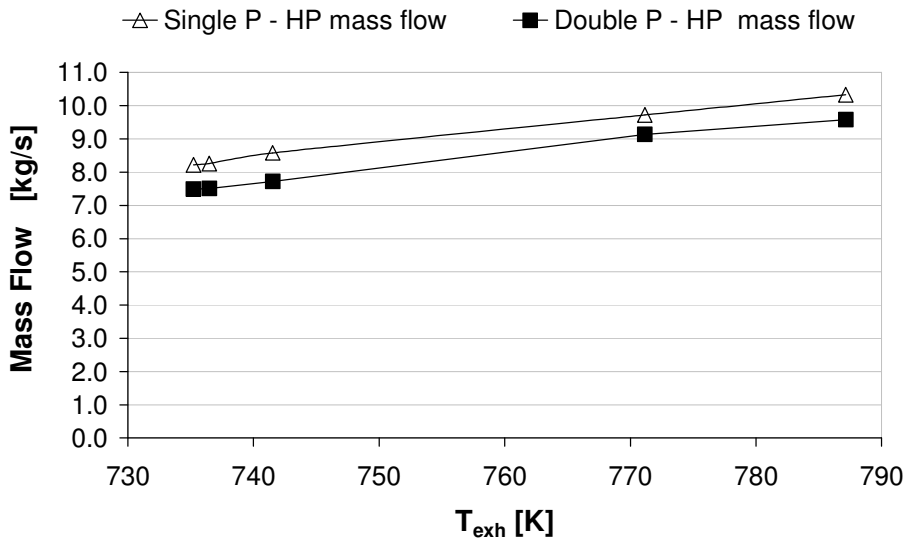

Figure 3-9 HP steam mass flows for single and double pressure operating modes

3.7.5 Pressure drop

The pressure drop across the gas and water streams operating on a double pressure mode are shown in Figure 3-10 and Figure 3-11. The pressure drop values obtained for the exhaust gas side agrees with the common figure of 20 mbars used by the engine manufacturers during the design phase of an industrial gas turbine engine for CC applications. The higher the back pressure seen by the GT, the smaller the expansion ratio at the gas generator and power turbines, thus the less power produced. A small pressure drop across the OTSG would then maximize the thermal efficiency of the

entire plant. It is important to remember, pressure drop depends on the HRSG geometry (physical dimensions and design) and the design fluid velocity.

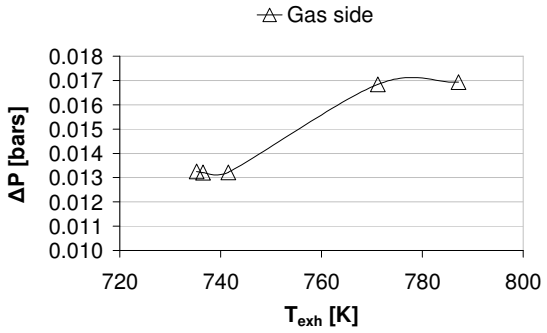

Figure 3-10 Gas side pressure drop in double pressure operating mode

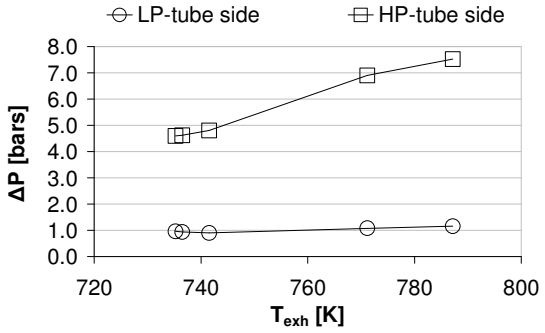

Figure 3-11 Water side pressure drop in double pressure operating mode

The pressure drop results for the HP and LP circuits are not as positive as the gas side figures. A maximum pressure drop of 7.5 bars and 1.0 bar in the HP and LP circuits, close to nominal operating conditions, was computed. These results fall short from the expected double digit pressure drop values observed in the field. A revision of the mathematical method and/or its implementation in the program needs to be done. Nevertheless, these results provide some qualitative information to compare the pressure drop inside the different sections on the gas and tube sides.

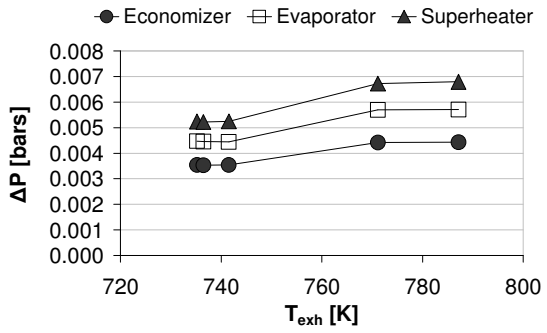

Figure 3-12 Gas side pressure drop at the HX units

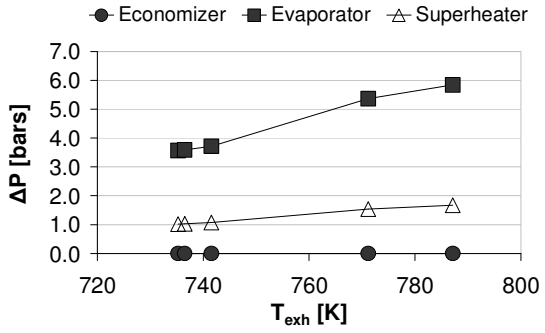

Figure 3-13 HP water side pressure drop at the HX units

Figure 3-12 and Figure 3-13 present detailed pressure drop results for the gas side and HP water side, respectively. The largest pressure drop at the fumes side occurs at the superheater, followed by the evaporator and the economizer. The high temperatures and velocities of the flue gases at the superheater section of the OTSG contribute to find high Reynolds numbers that translate into higher friction losses.

On the other hand, the largest HP tube side pressure drop occurs at the evaporator, followed by the superheater and the economizer. The evaporation of water inside the evaporation region not only increases the heat transfer coefficient but the frictional losses. Complex thermal and hydraulic mechanisms such as nucleation and boiling are found across the tubes before water is completely evaporated. As it is known, the

process increases the entropy levels of the water what brings an increase in volume forces (interaction between molecules). Consequently, a highly turbulent flow is expected in his section and confirmed with high Reynolds and Prandtl numbers calculations. This all translates into larger frictional losses that invariably lead to higher pressure losses.

The superheater presents the larger pressure losses after the evaporator. Even though there is not any phase change taking place inside the tubing, the flow is highly turbulent result of the energy gained in the economizer and evaporator. On the other hand, the water entering the economizer can be considered to be a laminar flow that is not subject to high temperatures, therefore it must be the section presenting lower pressure drop values.

3.7.6 Performance degradation

The performance degradation case was carried out assuming a cleanliness factor of 100% for the gas side and 95% for the tube side. Figure 3-14 shows the negative effect of fouling on the HP and LP steam production and OTSG overall effectiveness. To compensate for the production and performance losses, the GT and ST will have to operate outside the optimum conditions increasing the frequency of scheduled maintenance windows, adding extra pressure to the O&M budget of the operator.

Figure 3-15 presents the pressure drop analysis results. An increase in pressure drop of 6% to 8% for the HP circuit and 2% for the LP circuit at different operating conditions is found. The proposed reduction in free flow area inside the tubes, A_{FF}, to model the fouling negative effects of particle deposition seems to deliver positive results. However a more exhaustive analysis of this relationship should be conducted to have a definitive statement.

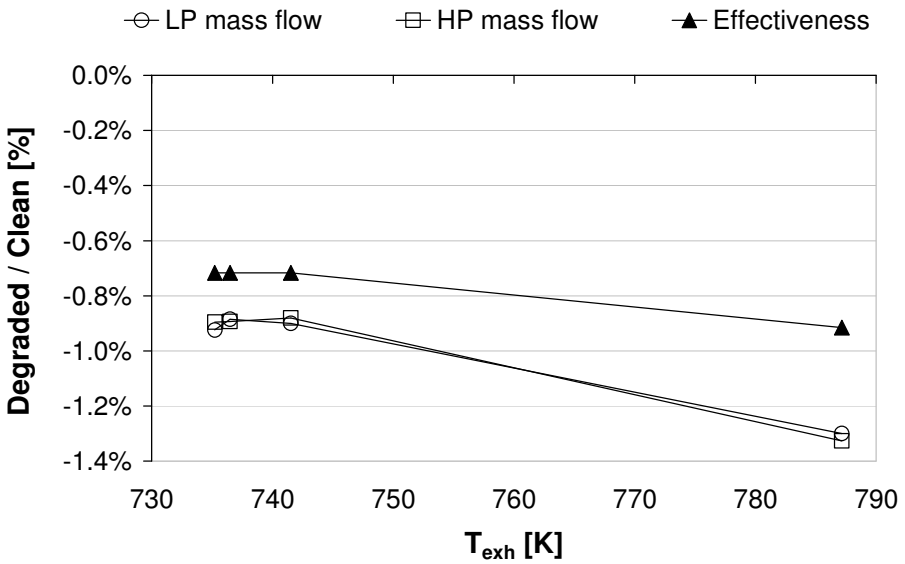

Figure 3-14 Effectiveness deviation between degraded and clean conditions

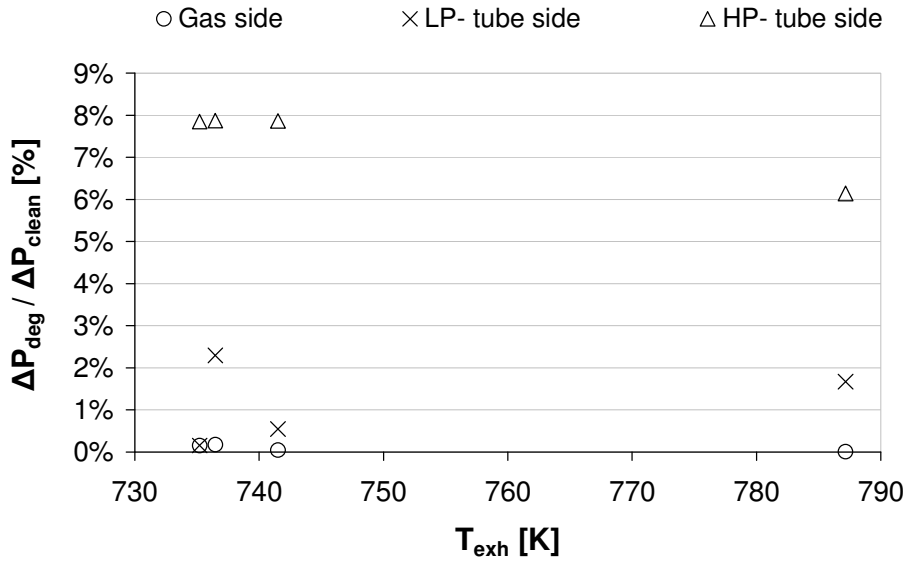

Figure 3-15 Pressure drop deviation between degraded and clean conditions

3.8 Summary

The chapter introduced a theoretical-practical approach to OTSG performance simulations. The review of previous work in the field showed a small number of publications devoted to the performance simulation of once through steam generators for power generation in combined cycle applications. References to actual once through boiler manufacturers were included.

A description of the thermodynamic and heat transfer fundamentals required for the performance simulation was considered. Detailed mathematical models used for the estimation of the heat transfer coefficient, heat transfer surface and pressure drop at the fumes and water sides were provided. Relevant information on the operation of a double pressure OTSG was considered for the construction of the thermodynamic model of the boiler. A set of empiric correlations derived from field data were included to reduce the number of unknowns and improve convergence time.

A computational program was developed following an innovative process where the low pressure circuit subordinates to the high pressure performance.

The results showed the mathematical models used are appropriate but areas of opportunity for improvement exist in the estimation of the pressure drop. To increase accuracy of the simulation, more robust correlations produced from larger set of data points is required. The correction for ambient and operating conditions was identified as a desirable capability of the program.

Chapter 4 Combined Cycle Performance Simulation

4.1 Introduction

The volatility in the energy markets has pushed the power industry to look for even more efficient and cheaper ways of producing electricity. The introduction of advanced, technology based systems can deliver the competitive advantage the companies need. From the operator's point of view, the ability to simulate the performance of a power station under different ambient and operating conditions can deliver valuable information that can be used to design the appropriate Operations & Maintenance (O&M) strategy [105].

Combined Cycle Gas Turbine (CCGT) power plants are rather valuable assets for companies, providing flexibility to the operations along with high performance. CCGT power stations can react to market changes more effectively, seizing an opportunity or preventing a loss. The development of value added systems for such technology is a reasonable strategy to follow.

This chapter presents the development of a computational tool for the performance simulation of a CCGT power station. The system integrates the programs of the GT and OTSG described in Chapter 2 and Chapter 3, respectively, and the Steamomatch code developed by [106].

A brief literature review on the development of CCGT performance simulation programs is found in section 4.3. Similarly, section 4.4 presents a concise account of the theoretical background of the CCGT technology.

The integration was made using the Visual Basic for Applications compiler inside Microsoft Excel ® as described in section 4.5.1. The system can successfully simulate all operating modes of a power plant with similar specifications to MEA's Pulrose Plant.

The effect of different ambient and operating parameters on the combined cycle performance is presented in section 4.6. Finally, the simulation of the power plant performance for 48 time blocks of a cold day of winter 2007 focusing on the main cycle's performance parameters is reported in section 4.7.

4.2 Nomenclature

O&M	Operations and Maintenance
CCGT	Combined Cycle Gas Turbine
CC	Combined Cycle
OTSG	Once Through Steam Generator
MEA	Manx Electricity Authority
HRSG	Heat Recovery Steam Generator
EGT	Exhaust Gases Temperature
GT	Gas turbine engine

HP	High Pressure
ST	Steam Turbine
VBA	Visual Basic for Applications
I/O	Input and Output
DLL	Dynamic Link Library
LP	Low Pressure
ISA	International Standards Association
INJW	Water injection flow
WAR	Water to Air ratio
W	Mass Flow
T	Temperature
P	Pressure
HPT	High Pressure Turbine
NETA	New Electricity Trading Agreement
NOx	Nitrogen Oxides
s	Entropy
ETA	Thermal Efficiency
PUMPMW	Water pumps power consumption
DCS	Data Collection System
TET	Turbine Entry Temperature

Greek letters

η	Efficiency
Δ	Increment

Subindixes

5	Exhaust nozzle
3	Compressor discharge
48	Power turbine inlet
amb	Ambient
plenum	Gas turbine engine inlet plenum

4.3 Literature review

The development of computational tools for the technical and economic analysis of existing or conceptual CCGT power plants seems to be a frequent topic in power generation academic and commercial research areas during the last 25 years. Clearly, the complexity and precision of the programs has increased over the years side by side with the development in the personal computers' hardware and software. Today, the programs such as Gatecycle [5], ThermoFlow [6], EtaPro [7], among other are in the leading edge of the power cycles' modelling market.

On the other hand, a great number of academic papers describing the efforts made in the integration of specialized or flexible programs for the theoretical analysis of the emerging technologies and concepts are found [107-113].

In some cases, a group of academic, operators and manufactures work into joint projects to develop or improve these programs. The projects usually involve complex integration

of different platforms. These programs are oriented for economic analysis of preliminary and existing power plants using the proprietary thermodynamic models from the manufacturers [114-118].

The majority of these platforms allow the user to carry out design and off-design point performance evaluations of the power plant taking into account different ambient and operating conditions.

4.4 Theoretical background

4.4.1 Combined cycle thermal cycle

The motive behind the development of the combined cycle power plant is the need to find a more effective way to utilise the chemical-thermal energy of fuels to generate electricity. The simple thermodynamic cycles such as Rankine, Brayton, Diesel cycles can only achieve a limited thermal efficiency before releasing large amounts of energy to the atmosphere as a cycle by-product. The thermal efficiency of a cycle increases every time the waste fluid temperature and pressure is the closest to ambient conditions when released. In other words, the more energy the cycle can extract from the working fluid (air, steam or combustion gases) the more efficient it is.

The thermodynamic concept of the combined cycles aims for the reutilisation of a high energy content waste fluid by a second cycle before the final atmospheric release [119]. The cycle operating at the higher temperatures is called the topping cycle while the cycle reutilising the energy flux is the bottoming cycle.. In order to implement the combined cycle into a real power plant an effective way to transfer the energy between cycles is required. The solution adopted by the industry involves the construction of large heat transfer units called heat recovery steam generators (HRSG).

The Combined Cycle Gas Turbine (CCGT) power plant uses the Brayton cycle as the topping cycle while the Ranking cycle acts as the bottoming cycle. The reliability of the steam cycle coupled with the flexibility of the gas turbine makes the CCGT a very attractive medium to base load power plant. The specifications for a gas turbine to be used in a combined cycle are different to those for an engine operating in a simple open cycle. If the exhaust gas temperature (EGT) of a gas turbine is too low the HRSG will not be able to generate the high quality steam flow required by the steam turbine to deliver the expected power output. A compromise between the gas turbine thermal efficiency and EGT must be made.

4.4.2 Additional firing

Only when the steam generator is fitted with an additional firing kit, the steam cycle can gain some independency. Additional firing systems are installed inside the HRSG to maintain the production when the GT is not operational [120].

4.4.3 Reheaters

In order to increase the thermal efficiency of the Rankine cycle (either in a simple or combined cycle) steam can be reheated in the boiler or HRSG to be safely expanded again. However, this process can not go on indefinitely as the steam will reach a point of diminishing returns.

4.4.4 Pressure systems

As mentioned before, the objective of the combined cycle is to increase the thermal efficiency of a power plant through the reutilisation of the Brayton cycle's waste exhaust gases by a bottoming Rankine cycle. The more efficient the heat transfer from the exhaust gases to the water/steam process is, the higher the overall efficiency of the combined cycle. To achieve this goal dual and triple pressure systems are used.

The systems are based on the fact that the limited energy contained in the exhaust gases will only be able to generate a limited amount of high pressure steam. Once the exhaust gases leave the HP heat exchange units the remaining energy in the gases would be wasted. To prevent it, additional pressure systems are fitted to the HRSG. The energy required to generate medium or low pressure steam at a particular temperature is less but still within the energetic levels of the pre-used exhaust gases. In the design of a HRSG multiple pressure, the heat exchange units of the different pressures are partially intertwined to achieve better results. The operation of these multiple pressure systems demands long start up times and constant supervision when operating at part loads [121].

4.5 Computational tool

The development of the combined cycle performance simulation platform eCCGT is described in this section. The conceptual and functional characteristics of the system and the actual algorithm and main subroutines are presented. Additionally, a brief description of the Data Collection System (DCS) developed in collaboration with MEA for the extraction of field data is made.

4.5.1 eCCGT

The main objective of the system was to integrate the existing programs of the gas turbine, steam generator and steam turbine into a coherent and user friendly environment to allow the performance simulation of the plant and individual components. Some of the interconnectivity features of the system and subroutines were built based on previous work by Sae-Lim [122]. A brief description of assumptions and considerations made during the integration of the cycle and the development of the main functional characteristics of the system are presented next.

4.5.1.1 Cycle integration

- The specifications of MEA's CCGT Pulrose Plant are: two dual-fuel (natural gas and fuel oil) LM2500+ gas turbine engines, GT6 and GT7, with water injection at the

combustor for emissions abatement delivering 31MW when operated at full load; two double-pressure once-through type heat recovery steam generators, OTSG6 and OTSG7, individually producing 9.8 kg/s and 2.2 kg/s of steam at high and low pressure respectively when operated at full load; and, one double-pressure steam turbine, ST8, without reheat generating an additional 23 MW at nominal operating conditions.

The nature of the collaborative project between Cranfield University and MEA favoured the use of Turbomatch [9] for the simulation of the gas turbine engine performance. The new capabilities implemented into the program ensure the reliability of the simulated values. Two separate models have been adapted for design and off-design operating conditions to capture the different health conditions of the two engines.

A program to simulate the performance of the OTSG for single and double-pressure operating conditions has been developed by the author (see Chapter 3). The program introduces a theoretical-practical approach that combines theoretical thermo-hydraulic models with empiric correlations and the actual control sequence of the boiler. The approach simplifies the internal calculations and reduces the convergence time. A model of the OTSG using the geometrical and operating characteristics of the boilers at MEA was created.

In the case of the steam turbine, Steamomatch a program developed by Zwebek [106] was used. The program is based on the steam turbine performance estimation and optimisation techniques developed by Cotton [123], which makes use of correction curves and the Stodola number for the off-design performance calculations. A detailed description of the program is out of the scope of this project.

As for the condenser, a provision for the user to provide the water exit temperature and condenser operating pressure was made. The implementation of a separate thermo-hydraulic model of the condenser could produce more accurate results of the operating pressure and condensate temperature as a function of load factor and ambient temperature.

- Note the back-pressure feedback-loop between gas turbine and steam generator has not been modelled. A more accurate modelling would reinsert the gas-side pressure drop value calculated at the steam generator model back into the gas turbine model. An iterative process would then be carried out until the difference between back-pressure values used in the gas turbine model and the calculated by the steam generator model were small.

4.5.1.2 Cycle losses

The cycle losses have been partly considered using fixed values for the gas and steam turbine secondary equipment's power consumption. Other losses from the auxiliary equipment of the condenser, water pumps, on-site consumption were not included. Consequently, the simulation will overestimate the total power output of the plant compared to real values.

For the gas turbine, the parasitic power consumption is added to the main power demand before the performance simulation is carried out. The auxiliary equipment is supplied by the GT's generator affecting the off-design operating point of the engine, and eventually, the performance. The magnitude of the losses was extracted from a performance test guide suggesting a value of 260 kW for an engine similar to the LM2500+ operating at full load and standard ambient conditions.

In the case of the steam turbine, a list of the secondary equipment with their respective power consumption at full load and standard ambient conditions was included in the equipment's specifications. The total consumption is calculated around 150 kW. In this case, the auxiliary equipment consumption has not any effect on the performance of the turbine, therefore, it is subtracted at the end of the simulation.

The future implementation of empiric correlations to calculate the losses as a function of load factor and ambient conditions would increase the accuracy of the simulation.

4.5.1.3 Functional characteristics

- An unlimited number of cases with particular ambient and operating conditions can be simulated. The conditions are manually introduced on the main screen before selecting the cases to be analysed.

  The effect of the ambient temperature, pressure and relative humidity conditions on the plant performance can be easily assessed and the main technical and economic parameters used for the optimisation of the O&M strategies. Day-to-day or seasonal analyses can be performed to forecast the fuel consumption of the plant and/or to define the position of the plant in the market.

  The system facilitates the simulation of all operating modes available from a typical CCGT power station. A plant with similar specifications to those of MEA's Pulrose plant can be operated in 15 possible modes as listed in Table 4.1; where 1P and 2P means the operation of the OTSG model in a single or double-pressure mode, respectively. A set of rules to differentiate between operating modes was implemented, though, in some cases, it is the actual convergence range of the one of the models that defines the final operating mode.

Table 4.1 CCGT operating modes

No	Operating mode	No	Operating mode
1	GT6	9	GT6 +2P & GT7
2	GT6 + 1P	10	GT6 & GT7 +1P
3	GT6 +2P	11	GT6 & GT7 +2P
4	GT7	12	GT6 + 1P & GT + 1P
5	GT7 +1P	13	GT6 + 1P & GT7 + 2P
6	GT7 +2P	14	GT6 + 2P & GT7 + 1P
7	GT6 & GT7	15	GT6 + 2P & GT7 + 2P
8	GT6 +1P & GT7		

- The system offers the possibility to modify some parameters of the gas and steam cycles models to simulate more specific operating conditions. The user can alter the default values through a graphical interface accessed from the main screen of the system.

In the case of the gas cycle, the ability to simulate the performance of a physically deteriorated engine and the option to switch on & off the water injection at the combustor were identified as crucial features of the system.

> The use of a gas turbine engine diagnostics system (see Chapter 5) can provide the actual deterioration values for each of the engine components that will increase the accuracy of performance simulation. More importantly, the operator will have additional information to evaluate any short or long term operation and maintenance strategies. From an economic point of view, a more accurate estimation of the fuel consumption and production costs can be done.
>
> The current version of the system maintains constant deterioration values for all cases. The future implementation of time dependant deterioration curves could offer a more realistic scenario when simulating the performance of the plant over larger periods.
>
> In the same way, the ability to simulate the performance of the plant with and without water injection at the combustor can provide additional information to the operator. As described in Chapter 2, the injection of water into the combustion chamber reduces the thermal efficiency of the engine. In times of reduced operating margins, the operator can evaluate the effect of switching off the emission abatement system to increase the overall thermal efficiency of the plant.

In the case of the steam cycle, the operating conditions of the condenser and the isentropic efficiency values for the steam turbine sections and pumps are available for modification.

> As mentioned earlier, the decision to not include a separate model of the condenser in the cycle simulations demanded a provision in the system to define the condensate exit temperature and the condenser operating pressure. The benefit of this approach is ability to quantify the effect any deviations in these two parameters have on the plant performance. Ultimately, a cost-benefit analysis on the operation strategy of the condenser could be conducted.
>
> The ability to modify the values of the isentropic efficiency of the steam turbine sections and pumps could increase the accuracy of the simulation through the optimisation of the parameters, or, if desired, take into account the effects of the ongoing physical deterioration of the engine.

4.5.1.4 Code

As mentioned earlier, one of the main two requirements for the system was to integrate the main components programs into a robust platform for the simulation of the combined cycle performance. The platform needed to be able to handle the programs wrote in FORTRAN and facilitate the development of a graphical interface (see section 4.5.1.5). Different options were considered including the use of FORTRAN and MATLAB. Ultimately, Microsoft Excel® Visual Basic for Applications (VBA) compiler was chosen for the development of the system.

The GT, OTSG and ST programs where compiled in FORTRAN as Dynamic Link Libraries (DLLs) and declared as internal subroutines inside the VBA program. Excel® allowed the development of a more advanced and efficient user interface in combination with spreadsheets, eliminating the need for pre- and post- processing of data. Additionally, the selection of VBA proved more convenient to all parties since MEA personnel have experience developing their own proprietary VBA-based programs, therefore, could opt to modify the interface to fit their own requirements.

The program follows a modularised structure that enables a quick reorganisation of the code and facilitates the future modification of one or more modules maintaining the integrity of the program. The *Control* module contains the master subroutine of the same name that defines the code's main flow. Figure 4-1 depicts the algorithm of the Control subroutine.

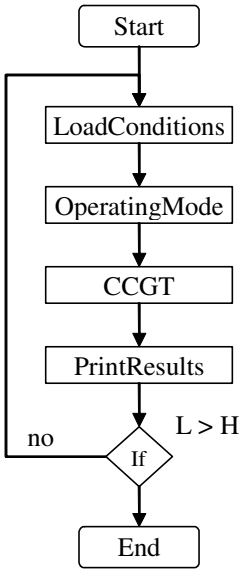

Figure 4-1 Control subroutine flow chart

The subroutine receives the values of *L* and *H* as arguments, denoting the Low and High row numbers of to the cases selected by the user. The subroutine then calls the second level subroutines: *Loadconditions, OperatingMode, CCGT* and *PrintResults*. An internal loop makes the subroutine to repeat itself until the ongoing row number is equal to the high end of the range, that is, *R* equals *H*. In every loop, the row number, *R*, is

passed onto the second level subroutines as a pointer needed for the input & output operations.

The following sections briefly describe the two more important subroutines: *OperatingMode* and *CCGT*. Additionally, the *InputPrint* and *PrintIndividual* modules that contain most of the input and output subroutines (I/O) are covered.

4.5.1.4.1 OperatingMode

The *OperatingMode* subroutine, located inside the module of the same name, was designed to identify the right operating mode of the plant from the user inputs. Table 4.1 lists the 15 operating modes in which a CCGT power station similar to MEA's Pulrose plant can be operated. A set of rules differentiate between operating modes, though, in some cases, it is the actual convergence range of the thermodynamic models that determine the final mode. The subroutine arguments are:

OperatingMode (CONFIG, MW6, MW7, MW6ST8, MW7ST8)

where *CONFIG* is the computed operating mode, *MW6* is the power output required from GT6, *MW7* is the power output required from GT7 and *MW6ST8* & *MW7ST8* are the power output produced by the steam turbine from the steam flow generated at the OTSG6 and OTSG7, respectively.

By having a stand-alone subroutine for the definition of the operating mode the implementation of an optimisation subroutine, based in either an iterative search or advanced numeric techniques such as genetic algorithms, could be achieved without much trouble.

4.5.1.4.2 CCGT

The CCGT subroutine executes the main components (GT, OTSG and ST) according to the chosen operating mode. It also estimates the overall thermal efficiency of the plant and prints the results for the individual components (see section 4.5.1.4.4). The arguments of the subroutine are:

CCGT *(CONFIG, R, AMBT, INP, RHUM, MWGT6, MWGT7, MWST8, FUELGT6, ETHGT6, FUELGT7, ETHGT7, ETHCCGT)*

where *CONFIG* is the chosen operating mode, *R* is the ongoing case row. With the ambient conditions: temperature (*AMBT*), plenum pressure (*INP*) and relative humidity (*RHUM*); the gas turbines power output requirements (*MWGT6* and *MWGT7*); the recalculated total power output from the steam turbine (*MWST8)*; the fuel consumption of each gas turbine (*FUELGT6* and *FUELGT7*), and the thermal efficiency of the GT and CCGT (*ETHGT6*, *ETHGT7* and *ETHCCGT*).

The main components DLLs are called using a shell-subroutine that deals with the input and output operations and other calculations. A brief description of these subroutines is found next.

TM

The *TM* subroutine, found inside the Turbomatch module, contains 5 other subroutines in addition to the main *Turbomatch* subroutine declared from a DLL compiled in FORTRAN. Figure 4-2 shows the computational flow chart of the subroutine. The arguments of *TM* are:

TM (ID, AMBT, INP, RHUM, MW, INJW, INJT, INJX, FUEL, ETHGT, EXHP, EXHT, EXHM, COMPOUTP, COMPOUTT, PTINP, PTINT)

where *ID* is the identification number of the engine model. The usual ambient conditions (*AMBT, INP, RHUM*) and the power output requirements (*MW*) are input to the subroutine. A long list of output variables are produced: water injection conditions (*INJT, INJW, INJX),* fuel (*FUEL*), exhaust conditions (*EXHT, EXHM, EXHM*), compressor discharge pressure and temperature (*COMPOUTP* and *COMPOUTT*), and, power turbine inlet conditions (*PTINT* and *PTINP*).

- *LoadDegradation* and *LoadWaterInjection* call the values of the component degradation and the water injection conditions defined by the user through the graphical interface of the system (see section 4.5.1.5).

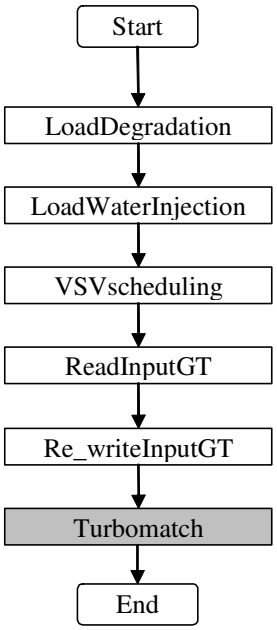

Figure 4-2 TM subroutine flow chart

- *VSVscheduling* calculates the angular displacement of the variable stator vanes system of the front section of the compressor. The value is interpolated from a predefined table using the power output requirements (*MW*). The table is found in a *hidden* spreadsheet called VSV.

- *ReadInputGT* reads the Turbomatch input file of the chosen engine excluding the off-design conditions, and stores the results inside a character vector for later use.

- *Re_writeInputGT* rewrites the contents of the vector created in the previous subroutine before writing the off-design conditions of the ongoing case.

- *Turbomatch* is the DLL subroutine declared inside the module. It carries out all the thermodynamic calculations of the gas cycle taking into consideration the ambient and operating conditions defined by user and imported into *TM* subroutine. The results of the performance simulation are offered as arguments of the *Turbomatch* subroutine to be later passed onto *CCGT* subroutine.

BOILER

Boiler, located inside the OTSG module, is the shell-subroutine created to encapsulate the simulation of the steam generator performance. Two more secondary subroutines: *LoadCondenser* and *PLevels* are called before executing the OTSG program using a DLL (see Figure 4-3). The arguments of the Boiler subroutine are:

BOILER (P, AMBT, MWGT, RMG, TEXH, TSTK, RMS_HP, RMS_LP, P_LP, P_HP, T_LP, T_HP, DPG_HP, P_IN)

where *P* defines the single (1) or double pressure (2) operating mode. The input variables are: ambient temperature (*AMBT*), gas turbine power output (*MWGT*), exhaust gases mass flow (*RMG*) and exhaust gases temperature (*TEXH*). Other variables such as the operating pressures (*P_LP* and *P_HP*) and the condenser operating pressure (*P_IN*) are calculated by the secondary subroutines. While the output variables are: stack temperature (*TSTK*), LP steam mass flow (*RMS_LP*), HP steam mass flow (*RMS_HP*), LP steam temperature (*T_LP*), HP steam temperature (*T_HP*) and pressure drop on the tube side for the HP circuit (*DPG_HP*).

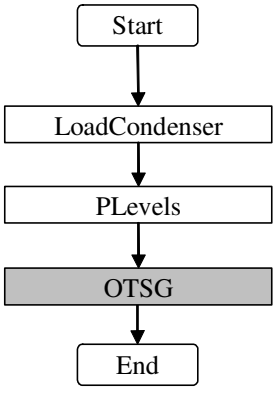

Figure 4-3 Boiler subroutine flow chart

- *LoadCondenser* subroutine retrieves the values of the condenser operating conditions defined by the user through the graphical interface of the system. (see section 4.5.1.5)

- *PLevels* estimates the operating pressure of the steam generator from an empiric correlation using the gas turbine exhaust temperature as independent variable. During the implementation of this correlation, the main OTSG subroutine presented convergence problems when the ambient temperature was increase beyond 5°C.

For a constant power output, the increase in ambient temperature produces a rise in the gas turbine exhaust gases temperature and reduces the mass flow. Under these circumstances, the correlation failed to provide a reliable set of operating pressures, which caused the OTSG program to crash. The solution was to modify the FORTRAN code to include a special exit strategy that allows the modifications of the pressure levels inside the code until convergence is achieved.

ST

The steam turbine calculations are carried inside *ST* subroutine found in the Steam Turbine module. The *SteamTurbinework* DLL is executed after the *LoadEfficiencies* secondary subroutine retrieves the values of the isentropic efficiency for the turbine sections and pumps (see Figure 4-4). The arguments of the *ST* subroutine are:

ST (P, AMBT, TSTK, RMS_HP, RMS_LP, P_HP, P_LP, T_HP, T_LP, P_IN, dummy, WST, dummy, H18, X18, T19, P19, H19, X19, HPWST, H20, X20, T21, PC, dummy, X21, LPWSTG, HPWPMP, LPWPMP)

where *P* defines the single (1) or double pressure (2) operating mode. The input variables are: ambient temperature (*AMBT*), stack temperature (*TSTK*), LP steam mass flow, temperature and pressure (*RMS_LP, T_LP, P_LP*), HP steam mass flow, temperature and pressure (*RMS_HP, T_HP, P_HP*), condenser operating pressure *(P_IN or PC*).

The results of the simulation are: steam turbine power output (*WST*), steam conditions at steam turbine HP inlet (*H18, X18*), steam conditions at steam turbine HP outlet (*T19, P19, H19, X19*), steam conditions at steam turbine LP inlet (*H20, X20*), steam conditions at steam turbine LP outlet (*H21, X21*). Finally, HP and LP steam sections power output (*HPWST* and *LPWST*) and the HP and LP pump power consumption (*HPWPMP* and *LPWPMP*). Three unused variables are referred here as *dummy* variables.

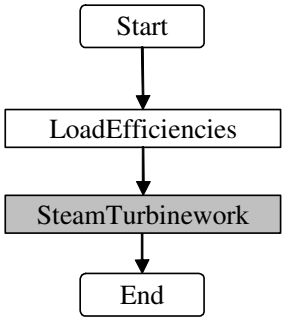

Figure 4-4 ST subroutine flow chart

4.5.1.4.3 InputPrint module

The *InputPrint* module contains several of the input and output (I/O) subroutines used in the system. Grouping these subroutines together in one single module increases the system's flexibility and transparency. Any future modification to the graphical interface can be made without disturbing the internal workings of the system. The subroutines contained inside the module are:

- *LoadConditions* subroutine loads the ambient and operating conditions defined by the user. The subroutine reads the values from a specific row number, *R*. A correction of the values to ensure the homogeneity of units across the system is made: Ambient temperature (*AMBT*) is converted from absolute °C to ISA deviation by subtracting 15 ° from the input value. The ambient pressure (*INP*) is converted from bars to atmospheres (Turbomatch's operating units). And all power output requirements (*MWGT6, MWGT7, MW6ST8, MW7ST8*) are converted from MW to Watts.

- *PrintResults* subroutine print the performance simulation results for each case on the specific row number, *R*. The results for both gas turbine engines are included: power output (*MWGT6* and *MWGT7*), thermal efficiency (*ETHGT6* and *ETHGT7*) and fuel consumption (*FUELGT6* and *FUELGT7*). The steam turbine power output and thermal efficiency are also found (*MWST8* and *ETHST8*). Finally, the plant's overall thermal efficiency is printed (*ETHCCGT*). All power values are converted back from Watts to MegaWatts.

- *LoadDegradation*, *LoadWaterInjection*, *LoadEfficiencies* and *LoadCondenser* subroutines included in section 4.5.1.4.2 are found in this module.

4.5.1.4.4 PrintIndividual module

The *PrintIndividual* module contains the subroutines responsible for printing the performance simulation results for the main five components (GT6, GT7, OTSG6, OTSG7 and ST8). The subroutines are called inside the CCGT and the results are printed in separate spreadsheets. Whenever the operating mode makes no use of any of the components, a value of zero for the parameters is given. All values are converted

back to degrees Celsius and bars for temperatures and pressures, respectively; and power values are displayed in MegaWatts.

4.5.1.5 Database and Graphical interface

The second main objective of the system was to provide a flexible and friendly interface between the internal code and the user. The advantages of choosing Excel® to develop the system were clear: direct access to spreadsheets, the possibility to design windows-like graphical tools and the instant creation of graphs and tables for results presentation.

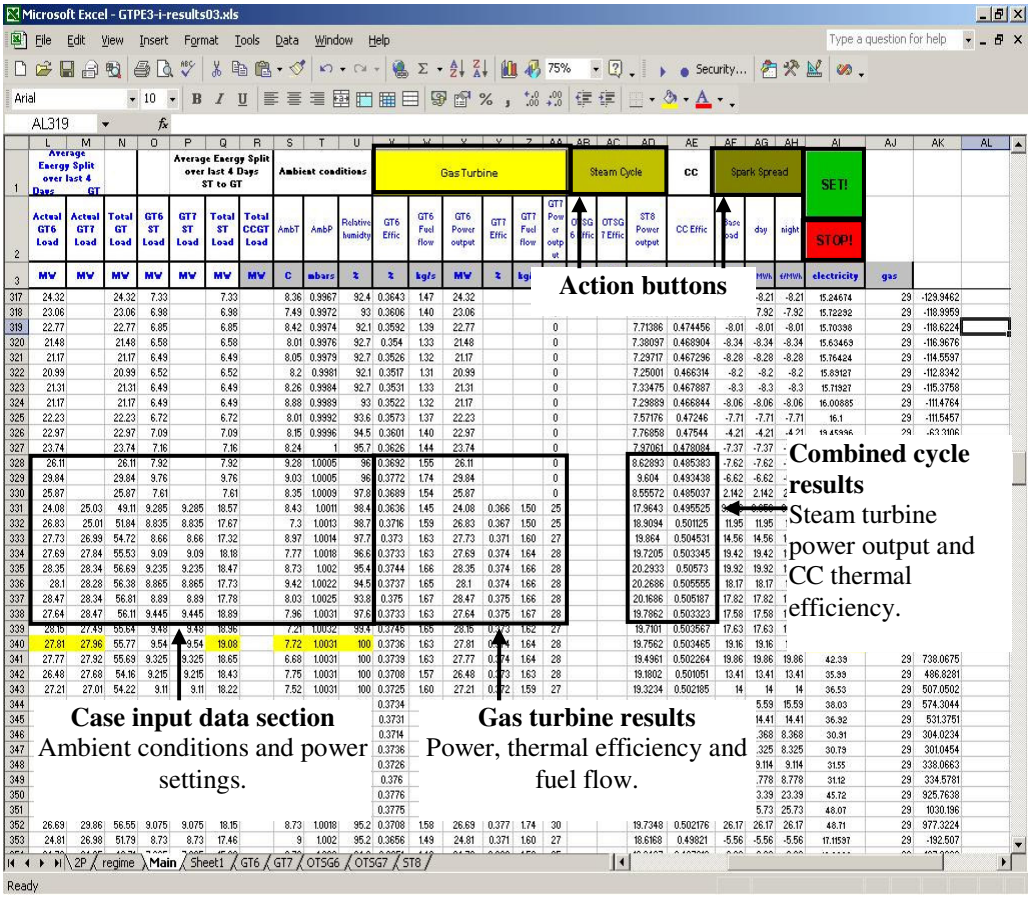

Figure 4-5 eCCGT "Main" database

The more adequate solution was to build the system around a single spreadsheet – named "Main" – that act as main database and point of entry to the user (see Figure 4-5). The spreadsheet contains the data required by the system's internal subroutines to conduct the performance simulation of the plant, extracted by dedicated I/O subroutines (see section 4.5.1.4.3). An additional benefit of the approach is the unlimited number of cases that can be created without the need to build external text files or declare large internal multidimensional arrays.

Once the database and internal subroutines were implemented, it was time to make a decision on which of the many parameters used by thermodynamic models needed to be

included in the "Main" spreadsheet. Certainly, the sets of parameters to be required by every case are the ambient conditions (temperature, pressure and relative humidity) and the power output demand. However, not all parameters such as degradation factors, isentropic efficiencies, etc. are expected to change during short term (day-to-day) or even medium term analyses. The inclusion of these types of parameters into the database would have saturated the spreadsheet visual space and reduce the observability on the results. Instead, it was decided to create windows-like user-forms to store the values of these parameters and make them available to the user and program (see Figure 4-6). A brief description each graphical user-form is found next:

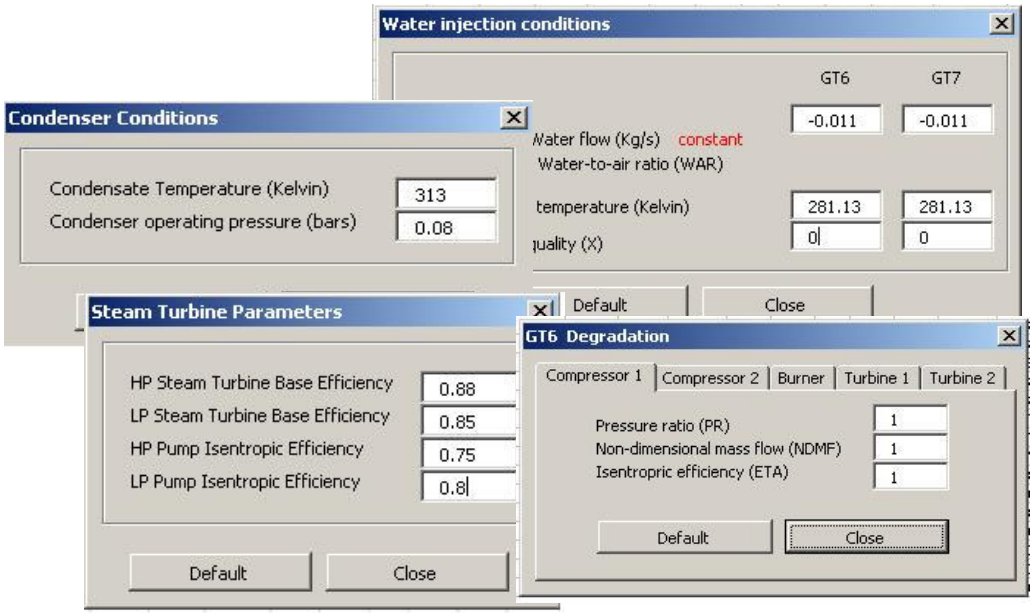

Figure 4-6 eCCGT graphical user interface

- *Gas turbine degradation.* The health parameters for all major components of the thermodynamic model are included in the form. The default value of one (1) signifies the clean condition of the component. Conversely, any reduction or increase of the parameters will simulate the degradation of the component performance. The safe range for the simulation of the degraded performance is [-3%, 3%] as convergence issues are experienced by the gas turbine engine model outside this closed range.

- *Water injection.* The conditions of water injection at the combustion chamber of the two engines can be accessed and modified in this form. As explained in Chapter 2, the use of a positive value for the variable *INJW* denotes a value in Kg/s, while a negative denotes the use of the water-to-air ratio (*WAR*).

- *Steam turbine parameters.* The form allows the modification of the isentropic efficiencies of the HP and LP turbine sections and pumps. This feature of the system would help in any adaptation of the steam turbine performance, or, the simulation of deteriorated conditions.

- *Condenser operating conditions*. As mentioned in section 4.5.1.1, the decision to not include a separate thermo-hydraulic model of the condenser demanded a provision to define the values for the condensate exit temperature and operating pressure.

All graphical user-forms are displayed by pressing the different action buttons embedded in the "main" spreadsheet (see Figure 4-5). The *Gas Cycle* button shows the gas turbine degradation and water injection forms, while the *Steam Cycle* displays the steam turbine and condenser forms.

To start the analysis the user must press the green *SET* button. A small window asking for the start and end row numbers of the cases to be analysed will appear. Finally, the GO button is pressed to launch simulation.

The results of the plant's overall performance simulation are printed into the main database while detailed results for each component are sent to separate spreadsheets (GT6, GT7, OTSG6, OTSG7 and ST8). A series of existing graphs plotting the most important technical and economic parameters of the plant's performance will be automatically updated, reducing the post-processing of data to a minimum.

4.5.2 Data collection system (DCS)

The data collection system has been developed in collaboration with MEA's O&M department. The first attempts to retrieve the information from the power plant control system for the gas turbine engines (GT6 and GT7) were done by hand. Obviously, this was a time-consuming task that only provided few data sets every month. The process involved the utilization of the actual control room computers to extract every variable by hand to then record the value on a hard copy form. This hard copy included the parameters requested from Cranfield University and others chosen by MEA engineers.

The main objective of the system second generation was to automate the extraction process. As a result MEA acquired the ICONICS software capable of remotely retrieving data from the plant's control system. ICONICS allows the user to have access to the plant's control system database through a web based connection. The data can be imported into an Excel® spreadsheet be populated with the control system's variables tags before executing the program. The same old gas turbine data form was populated with ICONICS tags reducing the collection time from 30 to less than 5 minutes. The remaining disadvantage of the system was the manual operation of the software. The reported 5 minutes were mostly consumed before and after the engineer executed the program every time more data was needed.

A third generation of the data collection system was designed to overcome disadvantage of the previous phase. The main modification was the development of Excel-VBA based macros that will automatically run the process at predefined time steps over the chosen period. Having improved the functionality of the system, the focus changed to increase data reliability and accuracy:

- Steady state conditions must be met at the time of the collection
- At least one reading should be obtained for every half-hour time block during the whole day
- The data must reflect the performance of the entire combined cycle.
- The data must be automatically sent to Cranfield University by email

A simple statistical analysis to calculate the standard deviation of the different parameters under the expected steady-state operating conditions has been carried out. The program could then automatically determine if the data was collected during a transient or steady state conditions, and shift the collection to one time step forward. Unfortunately, a few complications have been encountered during the implementation of this strategy holding the development of the full automated system for few months.

4.6 CCGT Performance simulation

In this section the results of the combined cycle performance simulation under different ambient and operating conditions are presented. A special attention is given to performance parameters such as: exhaust temperature and mass flow, thermal efficiency and steam turbine production. In some cases extra parameters are included to help explaining a particular behaviour.

4.6.1 Effect of ambient conditions on CCGT performance

The ambient conditions have a significant effect on the performance of any thermal engine or cycle. All thermal cycles used in the generation of power such as Brayton, Rankine, Diesel, Carnot, etc. are in some way limited by the ambient operating conditions. This section presents the results of the simulation of the CCGT performance under different ambient temperature, relative humidity and pressure conditions, assuming a constant gas turbine engine power output.

4.6.1.1 Ambient temperature

This subsection describes the effect of ambient temperature on CCGT thermal efficiency with special attention to the gas turbine engine performance. An ambient pressure of 1 bar and relative humidity of 60% were assumed. The simulation does not take into account the increase in electrical losses incurred by the secondary equipment as a function of ambient temperature. Therefore, the results would differ from reality as consumption at the cooling towers, pumps and other auxiliary equipment increases with ambient temperature.

First, the effect of ambient temperature on the gas turbine engine performance is described. An increase in ambient temperature produces a drop in air density that hampers the performance of the compressor: a drop in pumping capacity and pressure ratio are expected. A shift in operating point drives the compressor to work at a lower isentropic efficiency thus increasing the compressor discharge temperature. For a constant GT power output, the fuel consumption must rise to account for the loss in pressure ratio. This increase in fuel flow is marginally reduced by the increase in

compressor discharge temperature. The previous scenario generates a rise in the exhaust gases temperature and a drop in mass flow.

Figure 4-7 and Figure 4-8 show the simulation results for different ambient temperatures as a percentage change from baseline at 0 °C.

The thermal efficiency simulation results present a growing rate for temperatures below 15 °C before reaching a plateau, slowly residing at temperatures above 30 °C. This behaviour is contradictory to the expected performance. The thermal efficiency of thermal cycles increases as ambient temperature or sink temperature decreases. A closer look to the results reveals the cause of this inconsistency. While the GT model produced correct results over the testing range, the steam turbine show an increase in power output for higher ambient temperatures.

A review of the steam cycle performance computational tools – including the initial conditions defined to generate the empiric correlations – is recommended.

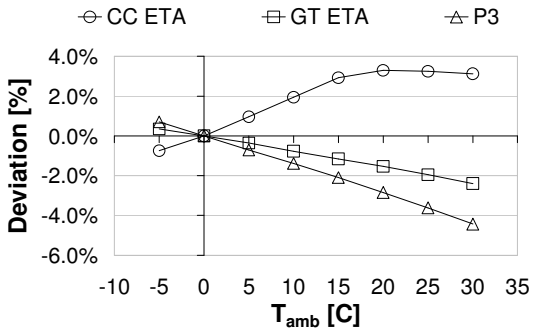

Figure 4-7 Effect of ambient temperature on CCGT performance (1)

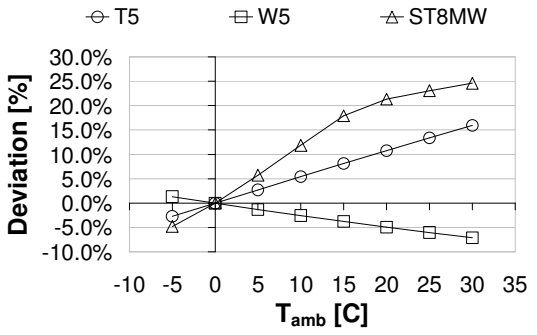

Figure 4-8 Effect of ambient temperature on CCGT performance (2)

In practice, the gas turbine engine's inlet plenum temperature will never reach a temperature below 7°C as the anti icing system is automatically turn on by the control system of the plant to prevent the formation of ice at the GT inlet and first compressor blades surfaces that could lead to the physical deterioration of the compressor.

4.6.1.2 Relative Humidity

A sensitivity analysis on different performance parameters as a function of relative humidity at different ambient temperatures is found next. A constant ambient pressure of 1 bar is considered. The injection of water at the combustor is set to 0.011 WAR. All results are given in percentage variation to 60% relative humidity conditions.

The effect of the relative humidity on the CCGT performance becomes more prominent at high ambient temperatures as the amount of water vapour in the air is larger. As explained in Chapter 2, moist air is a mixture of water vapour and dry air that presents a small change in molecular weight and specific heat (or enthalpy) relative to dry air. The change in properties modifies the full non-dimensional parameters in the gas turbine

engine components' characteristic causing the compressor to shift its operating point to accommodate the change in mass flow. As a consequence, the presence of water vapour in air reduces the compressor discharge temperature and pressure. Nonetheless, this variation in the compressor performance does not affect the exhaust conditions. Figure 4-9 and Figure 4-10 show a very small variation in W_5 and T_5 that can be considered as negligible for the bottoming cycle performance.

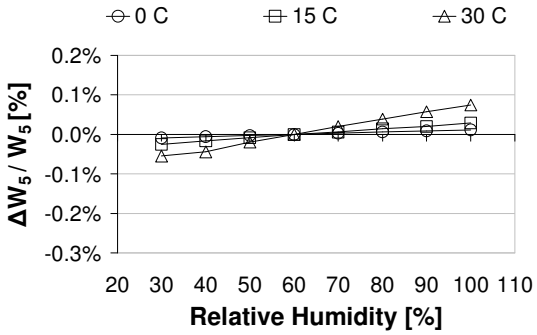

Figure 4-9 Exhaust gases mass flow (W_5)

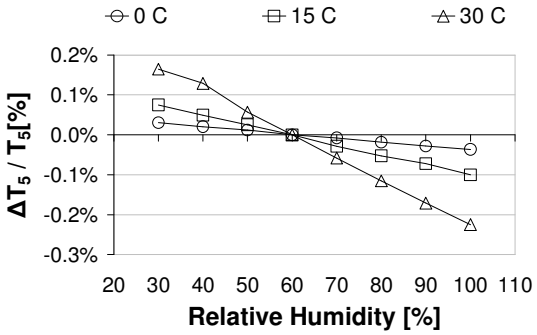

Figure 4-10 Exhaust gases temperature (T_5)

Figure 4-11 and Figure 4-12 show the deviation in thermal efficiency for the combined cycle and gas turbine, respectively. It is clear there is no perceptible difference between graphs, thus, the entire effect of humidity on the GT performance is passed onto the CCGT. The results confirm the conclusion reached above regarding the effect of humidity on the steam cycle performance. A reduction of around 0.4% in CCGT's thermal efficiency is expected when relative humidity increases from 60% to 100%.

In practice, the inlet filtering systems at the intake of the gas turbines would trap the water vapour reducing relative humidity inside the engine. On the other hand, the pressure drop across the filters would increase.

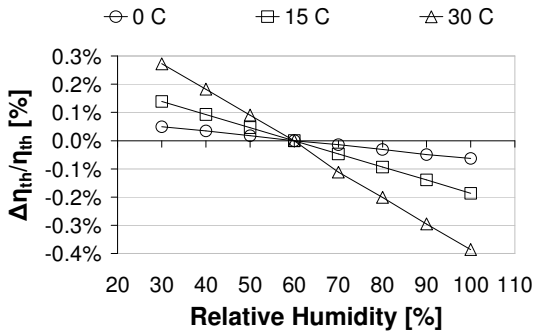

Figure 4-11 CCGT thermal efficiency [η_{th}]

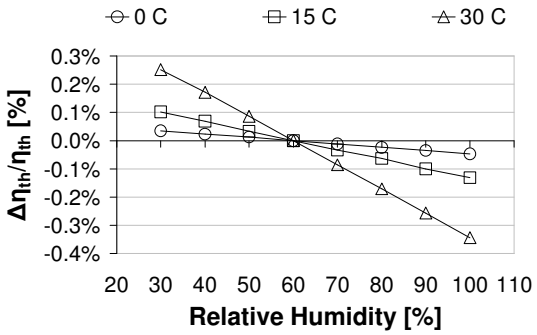

Figure 4-12 GT thermal efficiency [η_{th}]

4.6.1.3 Ambient pressure

A study of the effect ambient pressure has on the CCGT performance is presented in this subsection. A constant ambient temperature of 15°C and relative humidity of 60%

were considered. The gas turbine engine operates in the wet combustion cycle mode. No intake or filter losses were considered. All results are given in percentage variation with respect to 1 bar ambient pressure.

The performance of the gas turbine engine is benefited by an increase in ambient pressure. Figure 4-14 shows the simulation results for P_3 and T_3. Although the real pressure ratio (P_3/P_{amb}) decreases, the compressor discharge pressure rises. The compressor discharge temperature drops as a consequence of the reduced pressure ratio. Whereas the inlet mass flow increases as the air density drops. Finally, the GT engine experiences an improvement in thermal efficiency as less fuel is burned.

The exhaust gases present lower temperatures (T_5) and higher mass flows (W_5) as a result of the correction in the GT performance. Nevertheless, the magnitude of the variation in T_5 and W_5 is very small reducing the absolute effect on the CCGT performance. An increase in ambient pressure from 1 bar to 1.015 bars result in a drop in the overall plant's thermal efficiency of 0.16%.

The performance of the gas turbine and combined cycle will have an opposite behaviour for a reduction in ambient pressure. The simulation results suggest that a larger pressure drop at the inlet of the GT, represented as a lower ambient pressure, could benefit the plant's performance.

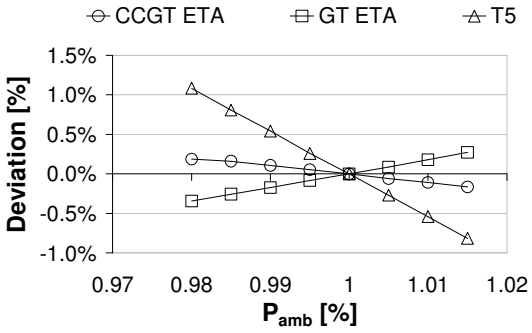

Figure 4-13 Effect of ambient pressure on CCGT performance (1)

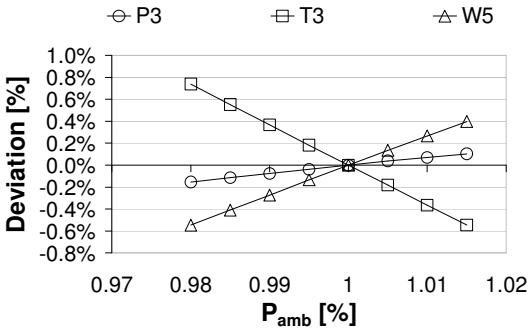

Figure 4-14 Effect on ambient pressure on CCGT performance (2)

4.6.2 Effect of GT power settings on CCGT performance

This section presents the CCGT performance simulation results for different gas turbine power settings. Ambient operating conditions of 15 °C, 1 bar and 60 % relative humidity are considered. The gas turbine engine is operated in the wet combustion mode, that is, with the injection of water at the combustion chamber. The simulation of the gas turbine engine performance includes the effect of variable geometry at the front section of the compressor. The VSV schedule is a function of the GT power settings only. The results are presented as the percentage deviation from 31 MW conditions.

The operation of the gas turbine engine at off-design conditions has a detrimental effect on its performance. The thermal efficiency of the engine decreases at low power settings as the internal components operate outside their maximum efficiency point. The air

mass flow drops as the engine's power output requirements can be met with a fraction of the nominal value at lower operating temperatures. The use of variable geometry alleviates part of the performance loss as it changes the flow's angle of incidence on the blades increasing the compressor or turbines isentropic efficiencies.

Figure 4-15 shows the effect of part load operation on the exhaust gases conditions. The exhaust gases temperature T_5 falls nearly 8% while the mass flow experiences a drop of nearly 24% at power settings close to 18MW. Clearly, this scenario has a great effect on the amount of energy contained in the exhaust gases that eventually could be transformed into addition shaft power at the steam turbine.

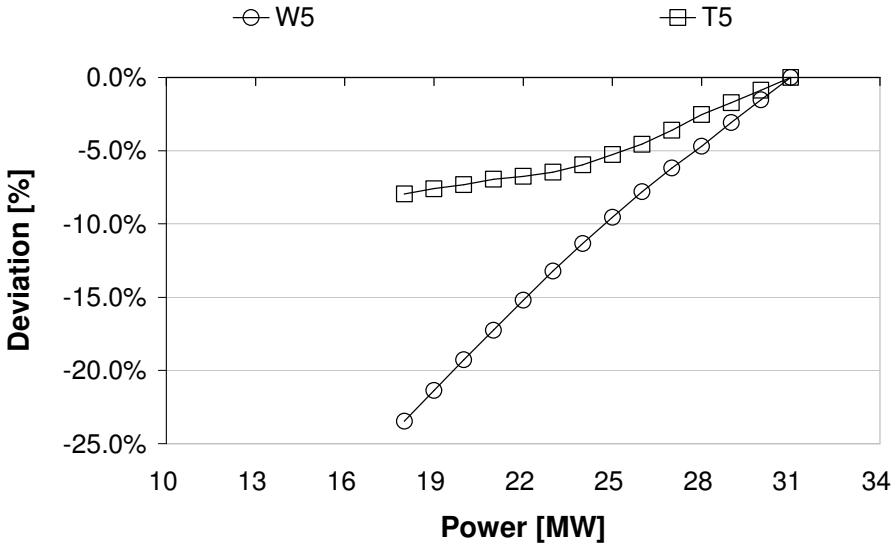

Figure 4-15 Exhaust gases temperature (T_5) and mass flow (W_5)

In fact, the change in the exhaust gases conditions over the gas turbine engine power range directly affects the off-design performance of the steam cycle. The steam turbine and steam generator must adapt their operating points to maintain a safe operation and extract as much energy as possible from the reduced energy content on the exhaust gases.

The steam turbine uses the sliding pressure control logic to set the operating pressures at the steam generator. The pressures are a function of the exhaust gases temperature and mass flow. The live steam temperatures are often set using a pinch point value close to 15°, although in some cases, for safety and reliability reasons, the temperature is limited to a specific maximum value depending on the materials characteristics. Figure 4-16 shows the variation in the steam cycle's operating pressure and steam mass flows over the GT's operating range.

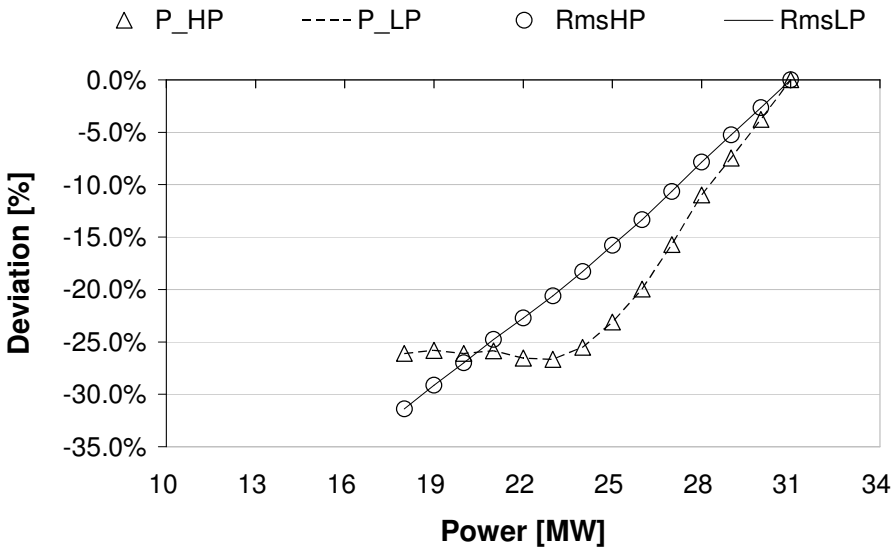

Figure 4-16 OTSG operating pressures and feedwater mass flows

The actual operation of a steam generator similar to MEA's double pressure OTSG subordinates the low pressure circuit LP to the conditions of the high pressure HP. In fact, the control logic makes use of empiric correlations to define the feedwater mass flow ratio between the HP and LP circuits to calculate the initial operating conditions of the boiler. A similar approach was used during the design of the steam generator model.

In practice, during the initial ramp up of the steam turbine, the throttle pressure is maintained constant until the energy conditions in the cycle are appropriate to generate steam of higher quality. The results shown in Figure 4-16 show a variable throttling pressure that needs to be corrected. A revision of the empiric correlations used and/or the implementation of an additional control algorithm for the throttle pressure is adviced.

In the case of the operating pressures, a fixed ratio between the HP and LP circuits was implemented. As a result, the variation of both HP and LP pressures and feedwater (steam) mass flows – relative to the full load operating conditions – is exactly the same.

The HP and LP steam generation falls to nearly 68% of the full load conditions at power settings close to 18 MW. On the other hand, the operating pressures of the steam cycle drop to 72% of the full load conditions, presenting a plateau around 24 MW that can be explained by the reduction in the exhaust gases temperature falling rate at the same power.

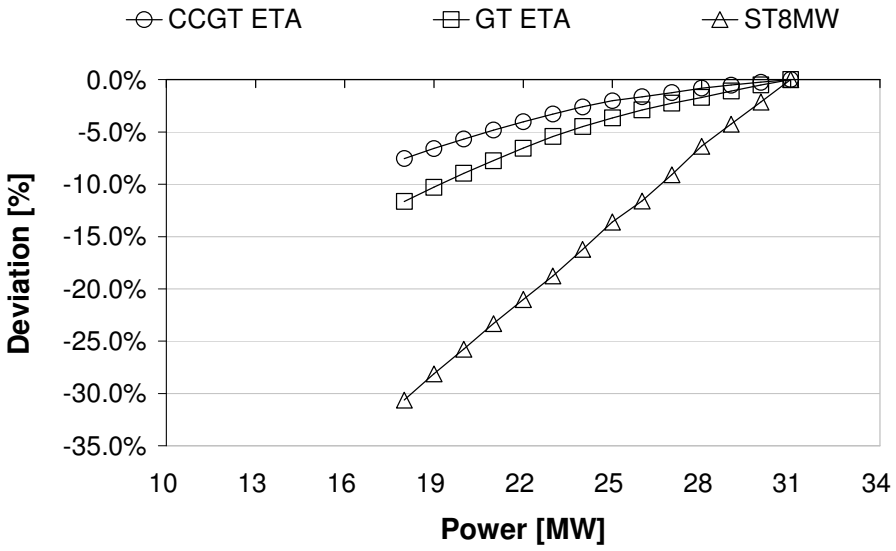

Figure 4-17 CCGT performance main parameters

Figure 4-17 summarises the change in the combined cycle performance as affected by part load operation of the gas turbine engine. As expected, the gas turbine engine's thermal efficiency falls in nearly 12% from full load conditions at 18 MW. Driven by the decline in available energy in the exhaust gases, the production of power at the steam turbine presents a fall of nearly 32% at the lower end of the power range. In this case, the falling rate of the steam production is higher to that of the gas turbine engine's thermal efficiency.

In the end, the combined cycle's thermal efficiency does fall with lower GT load factors, however, the continuous, though diminished, steam turbine production compensates for the loss in GT's thermal efficiency. Only a 7.5% drop in thermal efficiency from nominal conditions is experienced by the entire plant at 18 MW.

4.6.3 Effect of GT performance degradation on the CCGT performance

Two of the more common health deterioration cases are analysed: compressor front stages and high pressure turbine performance degradation. The simulation modifies the scaling factors of the component characteristics to account for a loss in mass flow, isentropic efficiency, pressure ratio, etc. Ambient conditions of 1 bar, 15 °C and 60% relative humidity are considered. The performance simulation of the gas turbine engine includes the effect of the injection of water in the combustion chamber.

4.6.3.1 Compressor

The deposition of solid particles, oils, minerals, etc. on the compressor blades – often referred to as *fouling* – causes a drop in the compressor performance. This change in operating conditions of the compressor will affect the entire gas turbine performance,

and eventually, the combined cycle performance. Figure 4-18 shows the results of the combined cycle performance simulation assuming various levels of compressor performance degradation.

The reduction in area and the loss in the blades' performance manifested as lower compressor isentropic efficiency and pressure ratio generate a drop in the compressor's pumping capacity. The compressor discharge temperature rises as the isentropic efficiency drops; and an increment in fuel consumption is required to maintain a constant power output, pushing the exhaust gases temperature up. Ultimately, the thermal efficiency of the gas turbine engine decreases.

The steam turbine production is also affected by the degradation in compressor performance. The rise in T_5 is not enough to outweigh the effect of the falling exhaust gases mass flow, hence, the steam production should decline. An overestimation of the steam mass flow generation overcompensates the fall in cycle's thermal efficiency.

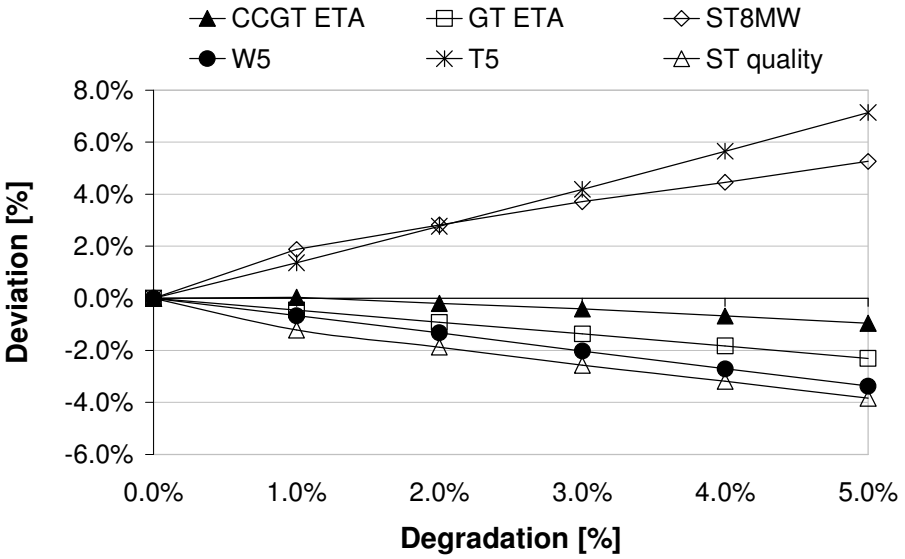

Figure 4-18 Effect of Compressor 1 degradation on CCGT performance

4.6.3.2 High Pressure Turbine (HPT)

The physical deterioration of the high pressure turbine is a common scenario caused by high operating temperatures that induce failure modes such as hot corrosion. The results of the HPT degraded performance simulation are displayed in Figure 4-19. Only two cases (1 and 2% degradation) are reported. The unusual exhaust gases conditions produced by the GT model created convergency problems at the boiler thermodynamic model.

The mass flow compatibility between the HPT and the compressor will force the later to change its operating point to accommodate a reduction in turbine flow and isentropic efficiency. By doing so, the pressure ratio across the compressor will drop, and, with it, the inlet air mass flow. Since the engine is operated using the power output as handle,

an additional amount of fuel is burned to compensate for the HPT performance degradation. Consequently, the thermal efficiency of the engines decreases while the exhaust gases temperature, T_5, increases.

Similarly with the compressor, the steam generator model overestimates the steam production that shifts up the combined cycle's thermal efficiency. In reality, the drop in exhaust mass flow will outweight the increase in T_5 therefore reducing the steam generation. A revision of the empiric correlations used in modelling the steam generator is recommended; adding the exhaust mass flow as a variable would correct the results.

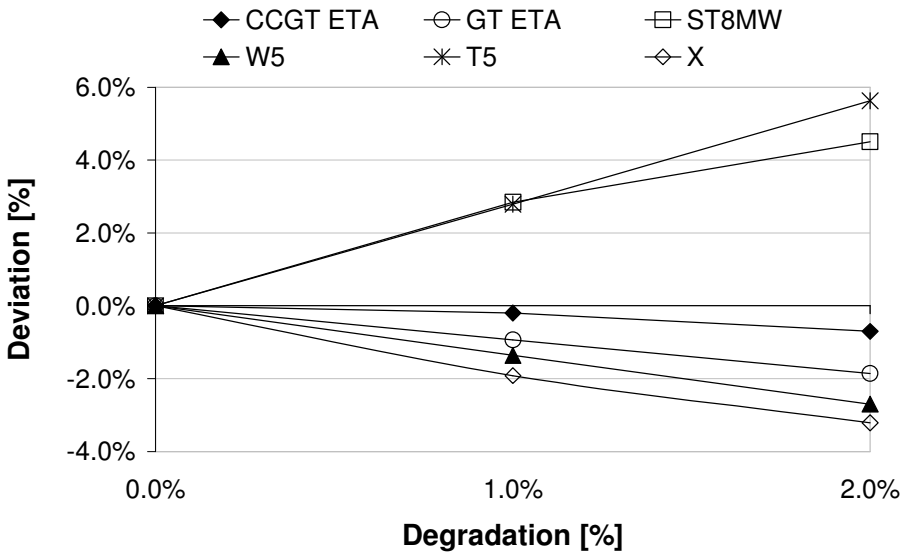

Figure 4-19 Effect of HPT performance on CCGT performance

In the end, the combined cycle's thermal efficiency decreases regardless the extra power generated at the steam turbine. Since the results of the previous case present similar values of combined cycle thermal efficiencies for a degradation of 2%, a continuation of the current case study will eventually show a reduction of around 1% in plant's thermal efficiency for a degradation of 5%.

4.6.4 Effect of the wet combustion GT operating mode on the CCGT performance

This section analyses the effect water injection in the gas turbine combustor has on the CCGT performance. As mentioned in Chapter 2, the main objective of the injection of water at the combustion chamber is the reduction of the atmospheric emissions of the engine, particularly of oxides of nitrogen (NOx) that tend to increase with flame temperatures. The additional flow of water in the combustion chamber quenches the flame temperature as water absorbs energy to reach a superheated steam state at the exit of the combustor, thus, reducing the formation of NOx. Unfortunately, this practice has a major negative effect on the gas turbine performance decreasing the thermal efficiency of the engine regardless the increase in the power output result of the change in the working fluid properties and turbine mass flow.

Clearly, the overall plant's thermal efficiency will decline as the exhaust gases temperature – one of the most important parameters in the production of additional power at the steam cycle – decreases with the injection of water at the GT combustor. Figure 4-20 and Figure 4-21 present the results of a sensitivity analysis of the plant's performance to different values of water-to-air ratio (*WAR*), assuming the nominal operating conditions of the gas turbine to be *WAR*=0.011. The simulation was done using the gas turbine power output as handle.

When the injection of water is eliminated completely, that is *WAR* equals zero, the plant's performance sees an increase of nearly 4% consequence of an improvement in steam production of 6% and the recovering of 2% points in thermal efficiency by gas turbine engine. This is influenced by the increase in exhaust gases temperature (T_5) of 3% despite the reduction of around 1% in exhaust gases mass flow (W_5).

The increase in steam quality at the end of the steam turbine LP section can be explained by the reduction in operating pressure result of the sliding pressure empiric correlations used for the performance simulation, a function of exhaust temperature only.

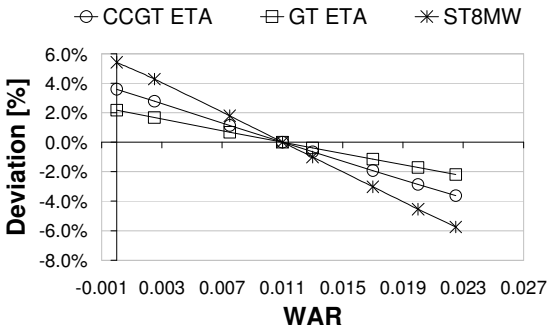

Figure 4-20 Effect of water injection on CCGT performance (1)

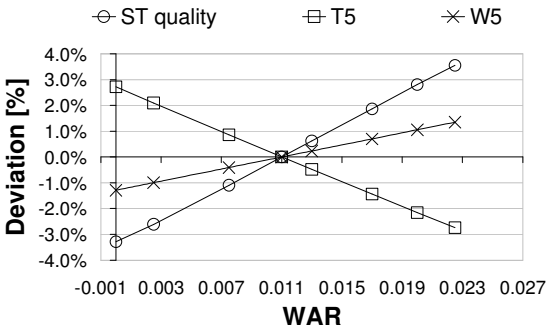

Figure 4-21 Effect of water injection on CCGT performance (2)

From a technical point of view only, there is a real case for an operator of a power station with similar specifications to those of MEA's Pulrose Plant to switch-off the emission abatement system in order to reduce the production costs by cutting the fuel consumption. However, this strategy can not be implemented without considering the environmental restrictions and regulations under which the plant operates.

4.6.5 Effect of condenser operating pressure on CCGT performance

An important parameter in the steam cycle is the condenser operating pressure. The Rankine cycle considers the expansion of the steam to a pressure below atmosphere conditions as a mean to increase the pressure ratio across the turbine last stages, the power production, and, ultimately, the thermal efficiency of the steam turbine. A secondary negative effect is the degradation of the steam quality end point as the expansion lines finishes further into the saturation bell of the T-s water diagram. An increase in the liquid phase of the steam has a negative impact on the performance of

the turbine last stages, thus, hampering the energy extraction. However, this negative effect is outweighed by the increase in available energy.

From a practical point of view, the use of negative operating pressures at the condenser increases the power consumption from cooling towers and vacuum pumps reducing the overall thermal efficiency of the plant. The water/steam mixture has to be cooled down to the corresponding saturation temperature to achieve a negative pressure in the condenser. Hence, ambient temperature and pressures become limiting factors of the condenser operating conditions. Another limiting factor is the physical deterioration of the heat transfer elements of a cooling tower as deposition of mineral particles on the transfer surfaces reduces the heat extraction from the water/steam mixture.

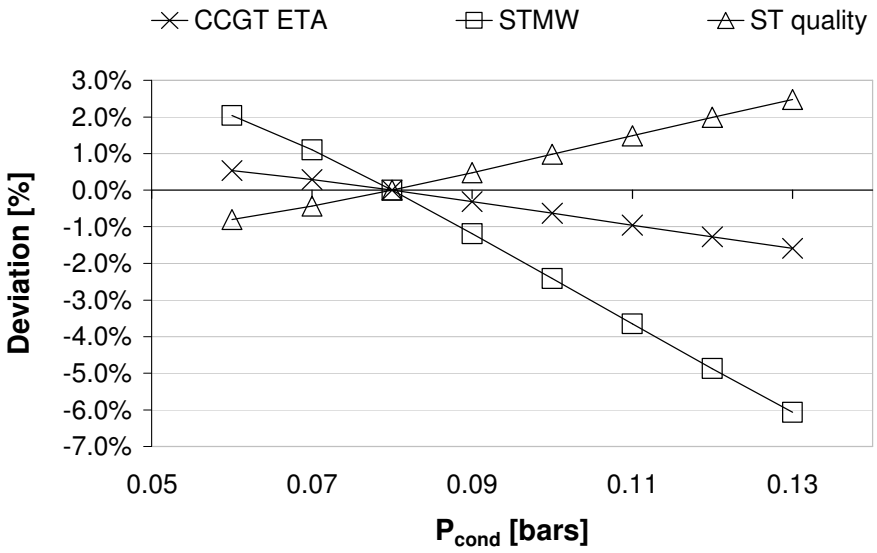

Figure 4-22 Effect of condenser pressure on CCGT performance

Figure 4-22 presents the effect of the condenser pressure variation on four cycle parameters: CC thermal efficiency (CCGT ETA), GT thermal efficiency (GT ETA), steam quality (ST quality) and pumps work consumption (PUMPMW). The results do not include electrical losses from auxiliary equipment (cooling towers and vacuum pumps). As mentioned earlier, an increase in the condenser operating pressure will reduce the power production at the steam turbine, and, consequently, the overall combined cycle thermal efficiency. For example, a change in condenser pressure from 0.080 bars to 0.110 bars produce a drop in the combined cycle thermal efficiency of 1% as the steam production declines nearly 4%. As expected, the quality of the steam increases with the condenser operating pressure.

4.7 CCGT Operations simulation

The previous section described the effect different parameters have on the performance of a CCGT power station with similar specifications to MEA's Pulrose Plant. These variables included the ambient conditions (temperature, pressure and relative humidity), operating modes and degradation. The analyses quantified the deviation in the main

cycle's performance parameters caused by changes in a single variable while all other factors were kept constant.

In reality, the performance of a power station is affected by the simultaneous change of more than one parameter making it difficult for any individual to correctly assess the plant's performance. The objective of this section is to evaluate the system's capability to simulate a multivariable performance analysis of a CCGT power station. Special attention is given to the main performance parameters such as fuel flow consumption, thermal efficiency and power output.

4.7.1 Field data

The data was automatically collected from the control digital system of the plant every 30 minutes using the *Data Collection System* (DCS) described in section 4.5.2. Some of the data points were not recorded during steady state conditions as the latest data reliability and accuracy capabilities of the DCS are yet to be implemented. The economic parameters such as the electricity and gas spot prices were obtained from NETA's website and MEA's trading support system.

4.7.2 Ambient conditions

A cold day during the winter of 2007 was chosen for the analysis. The energy and electricity markets are strongly correlated to the seasons of the year. In the UK, the prices of electricity and gas are higher during winter time when the demand rises while low prices are seen during warm days. In other parts of the world, the summer prices can reach the winter levels due to the massive air conditioning installed capacity. Figure 4-23 to Figure 4-25 show the three more important ambient parameters: temperature, pressure and relative humidity for the day under analysis.

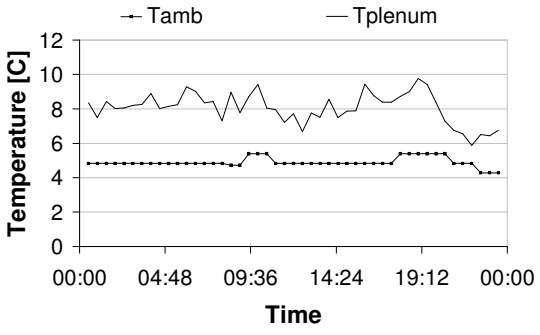

Figure 4-23 Ambient (T_{amb}) and GT Inlet Plenum (T_{plenum}) Temperatures

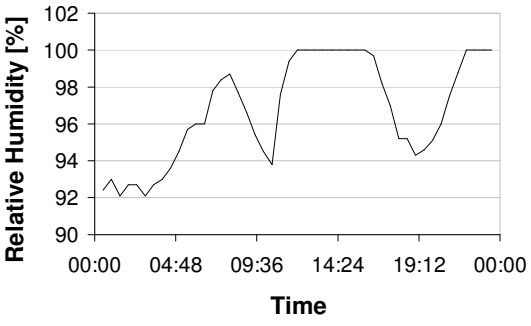

Figure 4-24 Relative humidity

High relative humidity and low ambient temperatures are an undesirable combination for the operation of a gas turbine engine as the ice formation on the inlet and first compressor stages surfaces is highly probable. Pieces of ice break apart from the main formation damaging the blades downstream. To prevent the ice formation, some engines are fitted with an anti icing system that makes use of warm air from the engine enclosure to increase the temperature of the air above the ice formation limits.

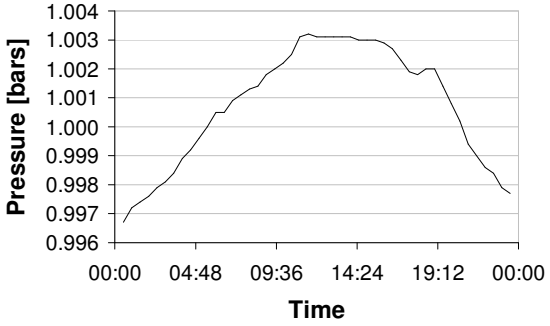

Figure 4-25 Ambient pressure

The particular ambient conditions of the day under analysis activated the anti incing system increasing the air temperature from ambient conditions (T_{amb}) up to the reported value for the inlet plenum temperature (T_{plenum}) as shown in Figure 4-23.

4.7.3 Generation regime

Figure 4-26 presents the generation regime of the plant for a cold day of winter 2007 over half hour time blocks. The production of each of the main cycle's components as well as the total generation is depicted as a percentage of the actual load over the maximum load of the day. It can be observed that during off-peak conditions (23:00 hrs to 06:00 hrs) gas turbine engine #6 (GT6) is generating around 75% of the load whilst the steam turbine (ST8) accounts for the remaining 25%. Around 06:00 hrs the gas turbine engine #7 (GT7) starts production with the same operating levels of the GT6 and its respective OTSG generates more steam for the stem turbine. The scenario is maintained throughout the day to meet the maximum demand after which the GT7 is gradually taking off-line and with it part of the ST8 production. At the end of the day the GT6 and ST8 are back generating the power to the plant's demand.

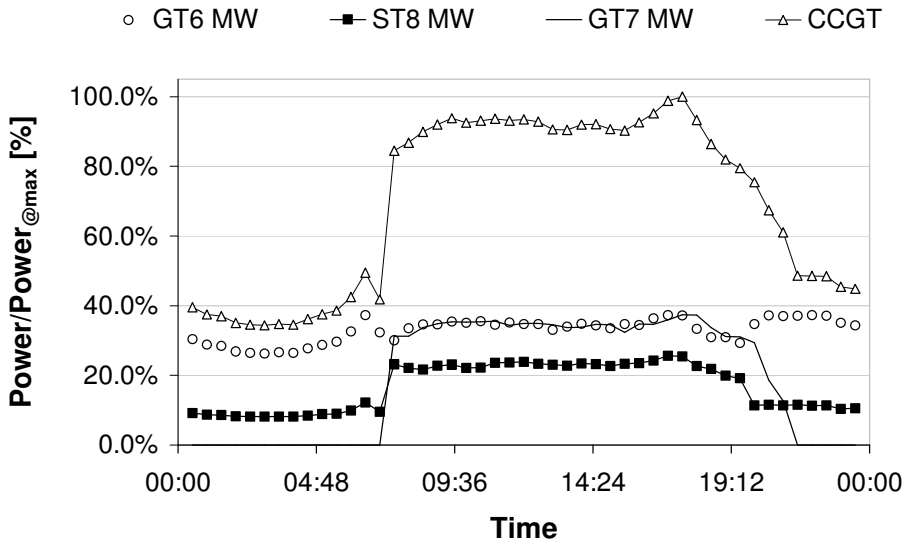

Figure 4-26 CCGT generation regime

It is expected that the plant maintains a fairly constant thermal efficiency throughout the day as the operator is choosing to use the combined cycle mode at all times, even though the demand could be met during some parts of the day by the gas turbine engines alone. From a practical point of view, the continuous operation of the steam cycle avoids the long start-up leading times of the OTSG and ST8.

4.7.4 Operations simulation

The results presented in this section demonstrated the robustness of the eCCGT system (see section 4.5.1) to carry out multivariable performance simulation analyses. Special attention is given to the main cycle's performance parameters i.e. fuel consumption, thermal efficiency and power output, as these variables are key for the economic assessment of the plant's operations covered in Chapter 6.

Figure 4-27 and Figure 4-28 present the percentage deviation between the simulated and real fuel consumption for GT6 and GT7, respectively. A very positive scenario is observed for GT6 with errors within a 2% band and an average of 0.68% across the generation regime. However, highly variable error values were obtained for GT7 even though the power settings of the engine remain fairly constant during its operation and close to GT6 engine (see Figure 4-26). The only plausible explanation for the simulation errors above the median (1.2%) is the data points were recorded during or close to the transient operation of the engine. In fact, some of these data points coincide with the start-up and a brief ramping down periods presented by GT7.

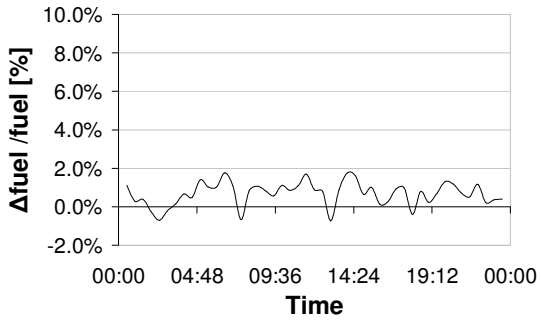

Figure 4-27 GT6 fuel flow (*f*)

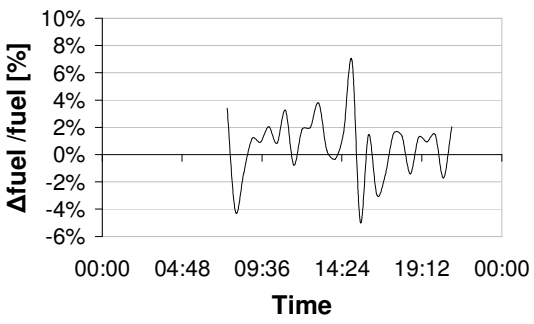

Figure 4-28 GT7 fuel flow (*f*)

Although the results of performance simulation for the gas turbine engines show an acceptable match between simulated and real values for fuel consumption, other parameters such as the exhaust gases temperature and mass flow present large errors (as described in Chapter 2). This situation originates a less acceptable performance simulation results for the steam generator and turbine.

Figure 4-29 shows the percentage deviation between the actual and the real steam turbine (ST8) power output. An error of nearly 10% is reported for the simulation points between 0:00 to 7:00 hrs, while an encouraging 2% error is found from 10:30 to 24:00 hrs, with only a couple of cases presenting high error magnitudes around 20:00 hrs. It is during the periods presenting the largest errors in ST8 production that the power

settings of GT6 are the lowest. At which the error in the GT off-design performance simulation becomes larger.

Despite the overestimation of the steam cycle performance, Figure 4-30 presents an encouraging scenario for the CCGT overall performance simulation. The results have an error average of only 0.63% and a median of 0.2%. Combining the results of the total power output and the fuel consumption a reasonable estimation of the plant's overall thermal efficiency could then be made for later use in the economic analysis of the plant.

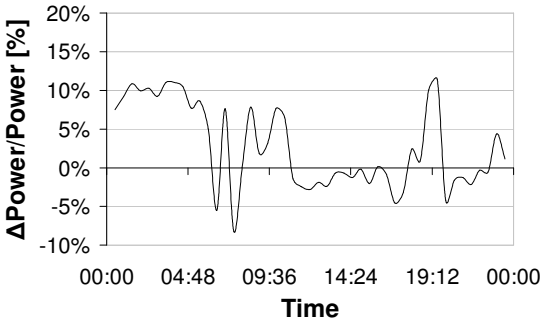

Figure 4-29 Steam turbine power output

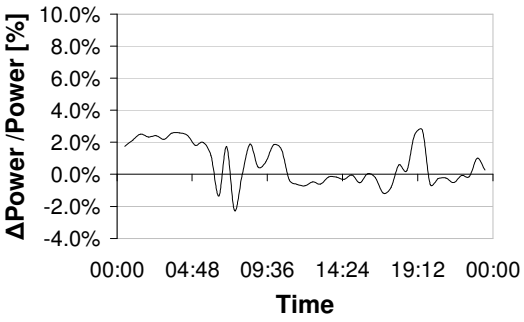

Figure 4-30 Combined Cycle power output

4.8 Summary

The chapter described the integration of the performance simulation programs for the GT, OTSG and ST into a single platform for the simulation of CCGT performance. Since the concepts and theory of the Brayton-Rankine combined cycle are well known, only a brief literature review on the most representative publications and books was made. The theoretical background was also shortened as the main challenge was the successful computational integration of the software and development of the required functional characteristics.

The integrated program was developed using Visual Basic for Applications (VBA) compiler inside Microsoft Excel®. This proved to be the best solution as VBA provides excellent connectivity between external programs and Excel®, and ready-made tools to create a practical graphical user interface.

A series of sensitivity analysis on the CCGT performance were carried out emphasizing the importance the Brayton cycle has on the combined cycle performance. The impact of ambient conditions, water injection at the combustor of the GT and the performance degradation of GT components (compressor and turbine) were covered.

Finally, a multivariable performance analysis of the operations of a power plant was successfully completed. The results show the accurate estimation on the fuel consumption and total power output that can be used for the operations optimisation and risk management analysis addressed in Chapter 6.

SECTION II

PLANT DIAGNOSTICS

Chapter 5 Gas Turbine Engine Performance Diagnostics

5.1 Introduction

The following chapter introduces the concept of gas turbine diagnostics focusing on the Gas Path Analysis (*GPA*) technique, and makes an assessment of the computational tool for engine diagnostics developed at Cranfield University, PTYHIA, using simulated degraded performance data.

The diagnostics techniques allow the operator to identify early engine component performance degradation that can be associated with physical deterioration of the parts. Additionally, it allows the operator to create a more accurate and detail maintenance schedule to minimise shut down time, maintenance costs, spare parts costs, increase reliability and availability.

The impact of the eventual implementation of an engine diagnostic system in Manx Electricity Authority's (*MEA*) operations will allow them to accurately quantify the operating and maintenance (*O&M*) costs associated with the two LM2500+ gas turbine engines part of its Pulrose Power Plant. The system will facilitate the implementation of Condition Based Maintenance (*CBM*) strategies based on the diagnostic system outputs and the accurate estimation of fuel consumption for economic purposes.

Section 5.3 presents a brief literature review on the main gas turbine engine diagnostics techniques including the traditional and, the more advanced, performance based techniques. Then a more detailed description of the theory behind the method used is found in section 5.4.

A description of the computational tool developed at Cranfield University that facilitates the application of Gas Path Analysis technique is found in section 5.5. Finally, section 5.6 presents the results of an assessment of the tool using simulated degraded performance, and states some guidelines for the effectively use of the tool with MEA's LM2500+ engines.

5.2 Nomenclature

$\bar{z}$	Engine dependent parameter vector
$\bar{x}$	Fault signature or Component parameter vector
$\bar{y}$	Ambient and operating condition parameter vector
$\bar{v}$	Noise vector
$\tilde{\bar{x}}$	Calculated fault signature
a	Conditions at baseline performance
A	Clean performance at point *a*
A_1	Degraded performance at point *a*
ANN	Artificial Neural Network
b	Conditions at degraded performance

B	Clean performance at point *b*
B	Burner
B_1	Degraded performance at point *b*
C1	Front section of compressor
C2	Rear section of compressor
CBM	Condition Based Maintenance
CFC	Component Fault Case
DOCGPA	Discrete Off-design Case Gas Path Analysis
F	Fuel flow
FCM	Fault Coefficient Matrix
GA	Genetic Algorithm
GPA	Gas Path Analysis
GUI	Graphical User Interface
H	Influence Coefficient Matrix
h( )	Vector valued function
HOT	High Order Terms
ICM	Influence Coefficient Matrix
K	Number of fault sensors, Kelvin degrees
K_1	Number of simultaneous sensors excluded
kW	Kilo Watts
L	Total number of SFCs
M	Number of measurements
MEA	Manx Electricity Authority
MW	Mega Watts
N	Number of engine health or independent parameters
n	Iteration index number
N	Gas generator rotational speed
N_1	Number of engine health or independent parameters left in every SFC
NDMF	Non-Dimensional Mass Flow
NN	Neural Network
O&M	Operations and Maintenance
P	Total number of sensors
P25	Compressor bleed-off pressure
P3	Compressor discharge pressure
P48	Power turbine inlet pressure
SFC	Sensor Fault Case
T1	Gas generator turbine
T2	Power turbine
T3	Compressor discharge temperature
T48	Power turbine inlet temperature
T5	Exhaust gas temperature
W	Number of simultaneous degraded components
x	Component independent parameter
z	Engine dependent parameter

Greek letters

σ	Convergence criterion
η	Isentropic efficiency
Γ	Non-Dimensional Mass Flow
β	Difference between measured and predicted performance deviations
Δ	Vector differential
ζ	Prediction error
α	Relaxation factor
δ	Differential operator

Subscripts

0	Initial conditions, initial operation point, clean conditions
i	Index
m	Index
y	Ambient and operating conditions

Superscripts

#	Pseudo-inverse matrix
-1	Inverse matrix
T	Transpose matrix

5.3 Literature review

The engine performance degradation is a major concern during the operation of any gas-turbine engine in different fields. The purpose of engine diagnostics or monitoring is to lead to actions taken on the basis of judgments made from directly measured or inferentially calculated information [124]. There are two major types of techniques: the traditional techniques (vibration, oil analysis, debris monitoring, visual inspection, boroscope inspection, etc) and the thermodynamic performance-based techniques.

In reality the implementation of a complete diagnostics and monitoring system needs from a large set of technologies to provide a reliable diagnostic [125-129]. The two techniques have a complementary rather than competitive relationship since the strengths of ones compensate for the weaknesses of others. The traditional techniques are mostly destined to assess the physical-mechanical condition of internal engine components such as bearings, rotors, disks, etc. On the other hand, the performance-based techniques analyse the overall performance of major engine components such as compressor, turbines and combustors. The next sections provide a description of the more common traditional and performance-based techniques.

5.3.1 Traditional techniques

The number of techniques used in the traditional diagnostics and monitoring is large and increasing as new technologies are being introduced in the field. Mature methods such as oil analysis, borescope inspection, parameter trending and vibration analysis are

being complemented by advanced optic technologies, thermal imaging, combustion flame imaging, acoustic analysis, among others.

The base of all monitoring and diagnostics technologies is the improvement and development of new and clever instrumentation and control systems, from the sensor transducer programs initiated by engine manufacturers [130] and incipient data systems for aircraft and industrial engines [131] to state-of-the-art sensor systems part of the most advanced military aircrafts [132, 133]. Few of the more common and mature monitoring techniques are described next:

The oil analysis technique consists in a qualitative or quantitative analysis of the debris contained in the oil used to lubricate and/or cool different components inside an engine [134]. The technique is particularly targeted to assess the condition of bearings, shafts, and gear boxes, among others [135, 136]. A sample of oil is extracted from the engine to conduct an analysis that aims to determine the extent of wear in the components as a function of the amount of debris found in the oil [137]. Initially, the quantitative analysis was performed off-line at specialized laboratories that made the technique a complex and time consuming process. However, the introduction of quantitative on-line debris monitoring systems reduced the complexity of the practice and increased the accuracy for advanced warnings [136, 138].

Another traditional diagnostic technique is the vibration monitoring. Focused specifically on the dynamic components i.e. rotor, blades, bearings, disks, gears, etc. can determine if there is any imbalance or misalignment within the engine components or elements. The method can detect any fault presented in an early stage as well as a fully developed problem leading to catastrophic failure [139, 140]. The traditional approach measures rotor blade vibration using tip-timing via non-contact probes in the engine casing [141]. A more advanced non-invasive method uses microphone arrays to obtain the vibration acoustic signature of the component before conducting the diagnostic analysis.

Optical instrumentation is commonly used to obtain information on positioning, clearances and misalignments of dynamic components, for example, the laser-powered optical proximity probe developed by Pratt & Whitney for clearances measurements of rotating to stationary components [142, 143]. New technologies are being developed to assess the state of thermal barrier coatings and the integrity of the component using particular wavelengths of light i.e. luminescence spectroscopy, laser backscatter, optical coherence tomography, thermal imaging and semi-infrared backscatter [144].

On the other hand, the visual inspection of the engine components provides an early identification of abnormal conditions prior to detection, and it involves the direct assessment of images by the diagnostic engineer [145, 146]. In the 1970s, borescope colour photography was introduced into the marine gas turbine condition monitoring systems with satisfactory results [147]. The implementation of new technologies such as the fibre optic sensors facilitated the recording of image, wavelength spectrum and flicker frequencies from inside

an operating gas turbine combustor. This signature is analysed using image processing software to identify certain engine conditions or malfunctions [148, 149].

5.3.2 Thermodynamic performance-based techniques

5.3.2.1 Gas Path Analysis

The Gas Path Analysis (GPA) is a technique that allows the user to know the overall engine performance through the usage of a mathematical model which relates the measurable parameters of a real engine i.e. temperatures, pressures, speeds, fuel flow, and power output with the fundamental component characteristics i.e. efficiencies, mass flow capacities, and nozzle areas [124]. This method only considers thermodynamic properties of the gas path components and it does not provide any extra information about the physical or mechanical behaviour of the compressor blades, combustor liners, turbine nozzle, etc. The previous statement supports the fact that the traditional diagnostic techniques will not disappear from the gas turbine industry since they provide valuable complementary information on the engine integral condition.

The objective of the GPA technique is to provide enough information about the engine performance and then to compare it against the design performance to identify any possible component fault that originated that shift in performance [150]. It is clear that GPA method –and any other diagnostic technique- finds its justification in the O&M management while it allows the administration to take an educated decision on the maintenance expenses that claim a large proportion of the running or operating costs of a gas-turbine-engine-owner in the aero [151] or industrial sectors.

In 1967, Urban [152] introduced the GPA concept that was implemented by major engine manufacturers (Doel [153], Volponi [154], Barwell [155]), and other authors such as [156-161]. Later implementations of the technique [162-165] present results in tune with past work. A review on the technique was first carried out by Smetana [166] and extensively covered in Li [167] performance-based diagnostics review.

The GPA technique – in its most basic form – considers the simplification of the system by the exclusion of any sensor noise and bias and any deviation in operating and ambient conditions from baseline. Further simplification on the system is done through the elimination of the high-order-terms in a Taylor-series expansion at the vicinity of the solution [168]. The result is a set of linear equations where an influence coefficient matrix (*ICM*) provides the proportionality effect from the deviation in the component fundamental characteristics on the engine performance. Henceforth, the change in component parameters can be obtained from the inversion of the *ICM* into the fault coefficient matrix (*FCM*). A detailed analysis is found in section 5.4.1. The main two advantages of this approach are method simplicity and speed. On the other hand, the method presents three major drawbacks: a) imperative data validation, b) solution inaccuracies, and, the most important c) the smearing effect.

As mentioned before, the data used in the diagnostic must come from fault-and-noise-free sensors and uncorrelated measurements from right locations. The solution inaccuracies can be reduce only if the effect of the ambient and operating conditions is eliminated, but a permanent error will be found due to the linearistaion of the system. The smearing negative effect is intrinsic to the original idea since the aerothermodyamic relationships between component fundamental characteristics and engine performance parameters are not limited to one-to-one associations.

The introduction of optimal estimation techniques such as weighted-least-squares and Kalman filters were aimed to improve the results from linear GPA. The weighted least squares objective was to reduce the inaccuracy caused by sensor error [153, 154, 169, 170, 171]. The method uses historical statistical data describing the probabilistic distribution of sensor measurements in order to filter current performance state, therefore, it was mostly used by engine manufacturers or operators of large fleets with access to such data. Although the method shows an improvement relative to the basic gas path analysis, it can not effectively handle large magnitude faults and, in some cases, it increases the smearing effect on the results demanding a careful assessment from the analyst [170].

Another optimal estimation technique implemented is the Kalmar Filter method. The concept reduces the dependency from historical data and estimates the current state from the next previous time steps and the current measurement. The technique effectively reduces the effect of sensor error [155, 162, 163, 172, 173]. To improve the accuracy of the diagnosis, an extended version of the Kalman filter that linearizes the non-linear function around the current estimates using the Jacobian matrix of the system was implemented [174-176].

5.3.2.2 Non-linear methods

The non-linear methods consist in the use of accurate thermodynamic engine models to simulate the performance of the engine under clean and degraded conditions to optimise a predefined objective function. A comparison between the linear GPA and non-linear methods were conducted reporting significant inaccuracies of linear GPA when large magnitude faults were analysed [177, 178].

5.3.2.2.1 Non-linear GPA

Probably one of the most straight forward non-linear methods is the one developed by Escher and Singh [160]. It presented a non-linear technique based on the consecutive application of the linear-GPA solver powered by the Newton-Raphson optimisation method. The method solves the accuracy issues of the linear GPA but remains vulnerable sensor error and operating and ambient conditions bias.

Li [179] developed an integrated gas turbine sensor and engine component diagnostic system that aims to isolate fault sensors, correct the data from any deviation in operating or ambient conditions and reduce the smearing effect. The concept of GPA-index provide a standardize measure of the fitness of the diagnosed to real conditions similar to that presented in [180]. The GPA-index is used to compare a series of combinatorial

component fault cases (*CFC*) and sensor fault cases (*SFC*) to isolate the fault component and sensor respectively. A similar implementation of non-linear GPA for sensor validation was also found in [159].

5.3.2.2.2 Multiple operating points method

One way to reduce the smearing negative effect is ensuring the number of measured performance parameters must be greater than or at least equal to the number of component parameters, also called measurements redundancy. However, this requirement is sometimes difficult to meet by practical and/or economic restrictions. To overcome this limitation, Stamatis *et al* [180] introduced the concept of the Discrete Operating Conditions Gas Path Analysis (DOCGPA), followed by other authors such as [181-184]. Using a linear performance diagnostic model at different operating points a more reliable and accurate solution can be found when a limited number of measurements is available. This technique is efficient when operating points are far apart in the engine envelope, although inefficiencies for closely spaced operating points were observed by Gulati [183]. To overcome this problem, and include the effects of measurement noise, Grondstedt [181] proposed the use of non-linear performance model and genetic algorithms based optimisation techniques (least-squares).

5.3.2.2.3 Adaptive technique

Stamatis et.al. [185] introduced the adaptive performance simulation concept that suggests the use of specific scaling factors to represent changes in engine performance. Hence, the modifications factors are the ratio of parameter values of reference performance maps to the values of the actual maps [167]. To reduce the everlasting smearing effect an optimal measurement identification technique and a health index to were introduced by Stamatis et al [186], and later implemented in [187]. Later implementation of the technique for performance simulation and diagnostics purposes is found in [188, 189, 184] uses a combinatorial approach to the multiple operating point technique based on the adaptive performance simulation method.

5.3.2.2.4 Bayesian belief networks

The Bayesian belief networks provide *a posteriori* statistical knowledge about the state of a system using previous knowledge on the system and a progressive learning structure. It can process real and simulated data to create a probability function of different component degradation cases therefore capturing the full non-linear nature of the system. Palmer [190] designed a diagnostics system that integrated test cell measurements, GPA results, operational data and performance-model simulated values to define the learning parameters of the network. Consumi and d'Agostino [191] make also use of a statistical inference tool applied to a maximum likelihood estimate method where a gaussian *a priori* probability density function is initially assumed for the unknown parameters [167]. Latest implementation of the technique is found in [192-194]. Yavuz [195] uses this technique to build a diagnostics and predictions systems using only oil related variables with satisfactory results.

5.3.2.2.5 Neural networks

The gas turbine engine field is not strange to artificial neural networks (ANN) activity. They are applied to a number of topics within the field of gas turbines: engine component diagnostics [196-201], sensor diagnostics [202, 203], performance modelling [204, 206], control systems [207], stress analysis [208-210], among others.

A neural network is a parallel distributed processor made up of simple processing units, which has a natural propensity for storing experimental knowledge and making it available for use [211]. ANNs provide an alternative to traditional or GPA diagnostics techniques for the reason that ANNs keep the non-linearity of the system, successfully handles noise measurements [212, 201] and can serve as an optimisation tool for an engine monitoring system [205, 213]. The ANNs are an excellent technique while they allow the solution of complex systems without the difficulty of solving analytical models. The disadvantages shown are data intensiveness, need an iterative design to find the optimum structure and ANN types to be used, and the most important; they present limited generalization [214]. A comparison between ANN-based and Kalman Filters conducted by Volponi [173] showed Kalman Filters have a slightly advantage on accuracy over the ANN.

The types of ANN used are feed forward back propagation [197, 203, 215, 216], probabilistic [202, 192, 217], Kohonen [218], among the more popular. Li [167] presents a review on the most popular types of ANN used gas turbines diagnostics research.

5.3.2.2.6 Genetic algorithms

The genetic algorithms (GA) are a searching and optimisation technique that can be used for highly irregular solution surfaces with several local maximum/minimum. The solution is obtained when an objective function – a measure of the difference between predicted and measured values – achieves its minimum value [167]. The algorithm uses three basic operations selection, crossover and mutation to approximate a solution [219]. Assuming a multivariable system, the selection operation picks the solutions (contained in strings) with the best results for the next generation. The crossover operation allows part of the solution strings to be exchanged between each other. Finally, the mutation gives fresh information in the mature solutions to account for any lost information in previous generations.

In the gas turbine engine diagnostics field, the GA can deliver an accurate solution keeping the non-linearity of the system and cope with noise and sensor bias [219, 220]. The main reason why GAs became so popular at optimisation tasks is that they have the capacity to locate the global optimum in a multimodal landscape [221], under these particular circumstances, any other optimisation technique such as hill-climbing or calculus-based methods will not reach the global optimum [220]. When coupled with a multiple operating-point adaptation (MOPA) method [180] the GA can increase the accuracy of the diagnosis exercise when a reduced or limited set of measurements is used [181, 183]. The implementation of GA into transient [222] and off-design performance adaptation [223] applications had achieved satisfactory results.

The technique presents some shortcomings in the extended times for convergence that increases proportionally to the number of simultaneous fault components considered. The method can face a competing-fault-class condition when more than one fault class are identified due to the proximity of the fitness values, prior knowledge of the system is essential to overcome this last issue as well as a proper choice of fitness function [220].

5.3.2.2.7 Fuzzy logic

Another advanced computational technique used in the gas turbine engine diagnostics field is the fuzzy logic. The fuzzy logic is a method to formalise the human capability of imprecise reasoning that allows the individual to judge under uncertainty [224]. It can be understood as a non-linear input-output mapping of a vector of features into a scalar result [225]. The mapping of the inputs is done following four steps: fuzzification (creation of the membership functions), application of the rules, an inference engine that aggregates the consequences across the rules, and a defuzzifier [226].

The method has been implemented by authors as a stand-alone technique [225-228] or combined with genetic algorithms, neural networks, among others. The results suggest that it is possible to obtain reliable diagnostics predictions for cases with very few parameters and many gaps in the data [226].

5.4 Theoretical method

5.4.1 Linear GPA

Gas Path Analysis (GPA) allows the user to determine the overall engine performance through the usage of a mathematical model which relates the measurable parameters of a real engine i.e. temperatures, pressures, speeds, fuel flow, and thrust with the fundamental component characteristics i.e. efficiencies, mass flow capacities, and nozzle areas [124]. The relationship between the component characteristics, the ambient and operating conditions and the effect of noise signals is:

$$\vec{z} = h(\vec{x}, \vec{y}) + \vec{v} \qquad 5\text{-}1$$

Where $\vec{z}$ is the engine dependent vector, $\vec{x}$ is the component parameter vector, $\vec{y}$ is the ambient and operating condition parameter vector, $\vec{v}$ is the noise vector and $h(\ )$ is a vector valued function. To simplify the system we eliminate the noise vector $\vec{v}$. For changes in the vicinity of $\vec{z}$ we can expand equation into a Taylor series for any given operating point denoted by subscript "0" we have:

$$\vec{z} = \vec{z}_0 + \left.\frac{\delta h(\vec{x}, \vec{y})}{\delta \vec{x}}\right|_0 (\vec{x} - \vec{x}_0) + \vec{z}_0 + \left.\frac{\delta h(\vec{x}, \vec{y})}{\delta \vec{y}}\right|_0 (\vec{y} - \vec{y}_0) + HOT \qquad 5\text{-}2$$

If the high order terms (*HOT*) are neglected the linear simultaneous equation system can be written as:

$$\Delta\vec{z} = H \cdot \Delta\vec{x} + H' \cdot \Delta\vec{y} \qquad 5\text{-}3$$

Further simplification of the linear system can be achieved if no deviation from the standard ambient and operating conditions is considered, $\Delta\vec{y} = 0$, leading to:

$$\Delta\vec{z} = H \cdot \Delta\vec{x} \qquad 5\text{-}4$$

The matrix *H* is constructed by the application of a controlled perturbation to the system in form of a component fault. A small perturbation is implanted on every element of $\vec{x}$ and the effect on $\vec{z}$ is recorded in *H*. The matrix provides the proportionality constant for the linear system. Hence, to solve for vector $\vec{x}$, the inversion of the influence coefficient matrix (*ICM*), H, into the fault coefficient matrix (*FCM*), H^{-1}, is required:

$$\Delta\vec{x} = H^{-1} \cdot \Delta\vec{z} \qquad 5\text{-}5$$

When the number of measurements, *M*, is larger than the number of engine health parameters, *N*, that is *M>N,* the linear system is under-determined and can not be solved using the regular inverse matrix calculations. Instead, the pseudo-inverse matrix concept is applied through the following definition:

$$H^{\#} = H^{T}\left(HH^{T}\right)^{-1} \qquad 5\text{-}6$$

On the other hand, when *N>M* the system is over-determined. In such case the pseudo-inverse definition is modified to

$$H^{\#} = \left(H^{T}H\right)^{-1}H^{T} \qquad 5\text{-}7$$

Finally, equation 5-4 is solved,

$$\Delta\vec{x} = H^{\#} \cdot \Delta\vec{z} \qquad 5\text{-}8$$

This method is idealistically simple and provides quick solution to gas turbine engine diagnostics. It also has the advantages of fault isolation, quantifications and multiple fault diagnostics [167]. In order to warrantee an acceptable degree of certainty on the diagnosis results, some considerations must be made [150]:

- The fault components that exist must be among those being sought. This point responds to the fact that GPA can only provide information on any component's condition if the data collected come from a thermodynamic-state inside or near the component being sought. This is more notorious with the two or three spool engines that require a large set of instruments as they hold several components within. For example, the method will not detect a fouled low-pressure compressor out of data coming from the high-pressure turbine.
- The measurements taken must be meaningful related to the problems sought and detectably respond to changes therein. The Thermodynamic Laws involved in the concept of the gas turbine engine directly influence the success of the diagnostics effort. If the dependent parameter being monitored does not have any thermal

relation with the fault component or does not show any sensitivity to changes in the independent parameters from that specific component, the method will not provide accurate results.

The main disadvantage of the linear GPA technique is intrinsic to the method. In reality, the effect of a single degraded component will generate a deviation in the performance that is reflected on various independent parameters. This phenomenon is called the smearing effect, and it is more evident when analysing complex engines i.e. multispool. One way of reducing the impact of the smearing effect is to have a larger number of engine measurements, *M*, than component parameters, *N*, also called measurement redundancy. However, technical or economic reasons may impose a restriction on the number of sensors available.

Another source of error in the prediction of the *FCM* using the linear-GPA technique comes from the mathematical simplifications done to the thermodynamic system. The elimination of the high-order-terms to facilitate the solution of the simultaneous equations generates an error that in some cases can be the same magnitude of the performance deviation caused by the degradation.

To attempt the correction of these two main sources of error, two complementary methods are used: the non-linear GPA developed Escher and Singh [160] and the GPA-index technique introduced by Li [178].

5.4.2 Non-Linear GPA

The aim of the non-linear GPA is to minimize the error between the real and the calculated change in the independent parameter vector caused by the linearisation of the multivariable function (equation 5-1). The method consists of an iterative approximation to the non-linear solution by the means of the linear-GPA technique powered by the Newton-Raphson numerical method. Figure 5-1 illustrates this process. The convergence of the process is declared when the error between the exact solution and the predicted solution equals a predefined small value, σ. The prediction error for each measurable performance parameter is described by next equation,

$$\zeta_i = \frac{z_{i,predicted} - z_{i,measured}}{z_{i,measured}} x100\% \qquad 5\text{-}9$$

where ζ_i is the prediction error for the i_{th} performance parameter. The method's main advantage is the fast solution to a system that represents the intrinsic relationship between the engine performance and the aero-thermodynamic parameters.

The mathematical compromises taken impose several requirements that must be fulfilled if a satisfactory solution is being sought. The data acquisition process has to:

(i) Clean the measurements from noise and bias, and

(ii) Eliminate any performance shift caused by an ambient and operation condition deviation from the baseline.

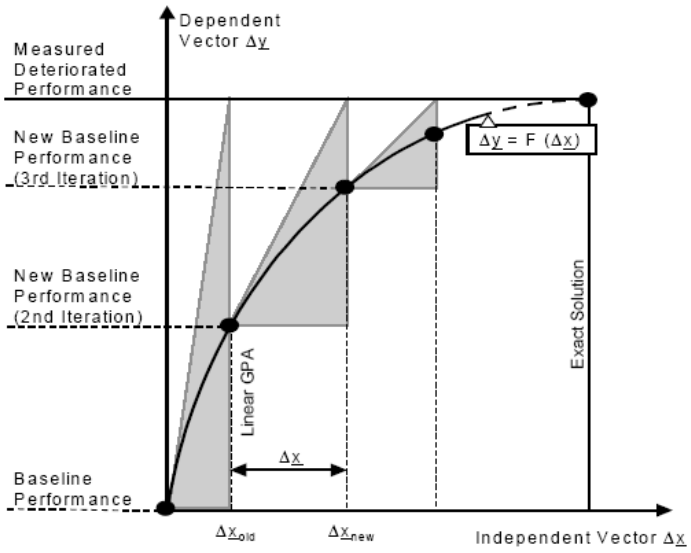

Figure 5-1 Simplified illustration of the non-linear GPA [160]

5.4.3 GPA index

The GPA Index concept was introduced by Li [178] to effectively identify the most probable components to be degraded in an engine using its fault signature (performance parameters). The concept helps reducing the smearing effect, therefore, increasing the reliability of the performance-based diagnostics system. It is defined as follows:

$$GPAIndex = \frac{1}{1+\beta} \tag{5-10}$$

with β calculated as follows

$$\beta = \sum_{i=1}^{N} \left| \frac{\Delta z_i}{z_0} - \frac{\Delta z_{0,i}}{z_0} \right| \tag{5-11}$$

where Δz_i is the predicted deviation for the *ith* parameter, $\Delta z_{0,i}$ is difference from the baseline value for the *ith* parameter and z_0 is the parameter's baseline value. If the set is correct, β is small and the GPA index value approaches to 1. On the other hand, if the predefined set is different from the actual set of degraded components the error is large and the GPA index takes values near to 0 (zero). GPA-index values above 0.8 are considered as conclusive evidence of fault or component degradation. Although some discretion from the analyst may still be required when more than one case present high values or fall short of 0.8 but is clearly differentiated from the rest. The complete process followed to calculate the GPA index is shown in Figure 5-2.

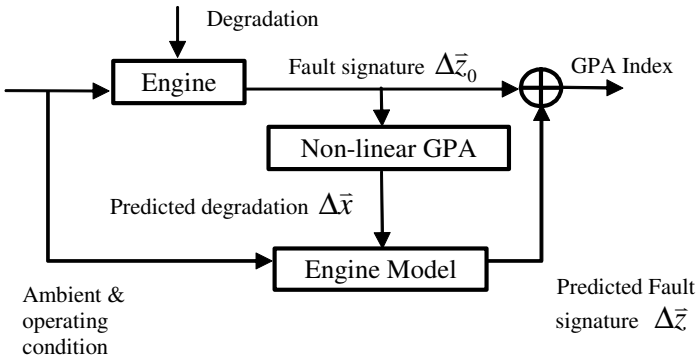

Figure 5-2 Calculation of GPA-index [179]

A predicted degradation vector $\Delta\vec{x}$ for an arbitrary set of parameters from potential degraded components using the engine's ambient & operating conditions is fed into the engine performance simulation model to generate the predicted fault signature $\Delta\vec{z}$. The operation of any engine under specific ambient & operating conditions in the presence of unknown levels of degradation on one or multiple engine components will generate a deviation from the clean performance of the engine called the fault signature $\Delta\vec{z}_0$. The difference between the measured deviation and the predicted deviation will define the GPA index for that particular case.

Ultimately, the GPA-index has to be understood as a standardised and more reliable way of representing the accuracy of the GPA-based diagnostics through *a posteriori* check of the calculated degradation $\Delta\vec{x}$ using a thermodynamic engine model. Nevertheless, the method still relies on the GPA technique to locate and estimate the magnitude of the degradation in the engine. Therefore, it remains vulnerable to the smearing effect.

5.4.4 Component Fault Cases

A solution to the smearing effect predicament is the integration of GPA-index with the engine component fault cases (*CFC*) concept [184, 219]. The *CFC* technique involves the creation of a large domain of combinatorial degraded-component cases, including those where the smearing effect is larger, that will produce a series of individual GPA-indexes. By increasing the number of cases, the incidence of the correct degraded component(s) in the *CFC*s producing GPA-indexes closer to 1 increase. In other words, the degraded component will be present in most of the cases with a GPA-index close to unity. Whereas the components affected by the smearing effect will not show the same repeatability or GPA-index magnitudes.

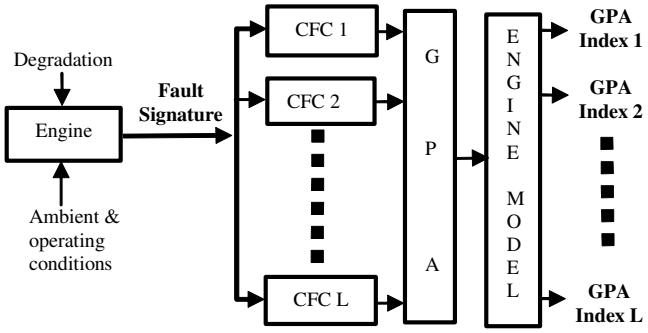

Figure 5-3 Component fault case method diagram flow [179]

The total number of *CFC*s is defines by the maximum number of simultaneous degraded engine components, *W,* defined by the user and the total number of engine components. For example, assuming an engine with 6 components and *W*=2, to number of component fault cases is equal to 21. In order to take advantage of any measurement redundancy, *N*>*M*, it is important to restrict the number of simultaneous degraded components to a small number.

5.4.5 Sensor fault detection

The performance-based diagnostics techniques depend on accurate sensors made them vulnerable to any faults present on the instrumentation. The diagnostic techniques described in the previous sections are unable to carry out a successful diagnosis of a degraded engine with fault input data.

The lack of a statistically-significant performance database from MEA's engines prevented the implementation of a sensor fault detection system such as the ones described by Doel [153] and Provost [229]. Similarly, the code complexity and the time consuming training process – to be performed for every type of engine – of a neural network (NN) based system for sensor fault detection did not favoured its use. As a result, the sensor fault case (*SFC*) method, introduced in [179], was favoured.

The *SFC* technique is a diagnostics tool that uses GPA-index to find fault sensors in a predefined set. The sub sets including degraded or faulty sensor(s) will generate an incorrect predicted fault signature, consequently a poor GPA-index value. On the other hand, when the right sensor(s) fault are excluded from the diagnostics analysis, the predicted fault signature $\Delta\vec{z}$ will be closer to the original fault signature $\Delta\vec{z}_0$ leading to GPA-index values close to 1. It is assumed from the total number of sensors *P*, there will be *K* total number of fault sensors, therefore the total number of *SFC*s will be defined by

$$L = \frac{P!}{K_1!\cdot(P-K_1)!} \qquad K_1<K \tag{5-12}$$

where K_1 is the number of simultaneous sensors excluded and must be less than K. Finally, a comparison between all *SFC*s is done to identify the most likely sensor(s) to be degraded. The *SFC*s presenting the highest GPA-indexes are chosen are the most likely sensors to produce fault measurements.

GPA shortcomings to deliver reliable diagnostics results with limited measurements impose a natural restriction to the *SFC* method. Assuming N_1 is the number of engine health parameters left in every *SFC*, the following relation must be met at all times or the result of the sensor fault detection process will not be reliable,

$$P - K_1 > N_1 \qquad 5\text{-}13$$

So far, the magnitude of the sensor fault is considered to be within a certain threshold close to the correct value. If the sensor bias is too large, the method will fail to converge during the GPA-index analysis. An additional filter is implemented to identify such extraordinary cases and declare a sensor failure at the start of the sensor diagnostics analysis.

5.4.6 Data validation

The data validation capability allows *PYTHIA* to process real and simulated engine performance data before conducting any diagnostic analysis. As mentioned in section 5.4.1, all diagnostics systems using the GPA technique demand the correction of the engine performance measurement deviation caused by instrumentation noise & bias and ambient & operating conditions. To comply with the previous statement different authors using GPA have adopted different techniques using statistical distributions of sensor error and noise [153, 154, 169-171]. The lack of any statistically significant sensor error or noise data from MEA's engines favoured the development and implementation of the performance-based approach described in this section.

The instrumentation noise error is reduced using simple mathematical algorithms while the presence of a sensor bias (fault) is detected using the sensor diagnostics technique described above. The correction technique for the ambient and operating conditions has two steps: a) preliminary correction of the data assuming no degradation, and b) *a posteriori* correction using the first predicted degradation vector.

The clean (baseline) and degraded data files are loaded using the data acquisition module in *PYTHIA*. The program shows the clean data and degraded data side to side for direct and quick analysis.

5.4.6.1 Noise and bias

The noise reduction tool has two options: the rolling average and the exponential averaging implemented in [230, 231]. The rolling average technique is the result of the summation of m number of data points divided the same number of samples.

$$\bar{z}_i = \frac{1}{m}\sum_{1}^{m} z_{i-m} \qquad 5\text{-}14$$

The ten point exponential average makes use of the following equation to compute the value of each measurement.

$$\bar{z}_i = 0.85 \cdot \bar{z}_{i-1} + 0.15 \cdot z_i \qquad 5\text{-}15$$

In theory, the correction has to account for any sensor bias present. One method to remove noise and bias sensor from the raw data is using statistical information of the sensors for clean and degraded conditions. To generate such database a large fleet of similar engines is needed. Instead the implementation of the performance-based method described in section 5.4.5 in PYTHIA was favoured.

5.4.6.2 Ambient and operating conditions

5.4.6.2.1 Initial correction

The diagnostic process accuracy relies on the ability to estimate the deviation in performance between the clean or baseline and the actual condition. From another perspective, the likelihood of recording field data at the same ambient and operating conditions than the baseline is very low therefore a correction to be actual performance is done.

The correction method assumes that *a* is the condition where the baseline is set and *b* the condition where degraded engine performance is measured. It is also assumed that $\Delta z_{i,a}$ is the performance deviation at point *a* and $\Delta z_{i,b}$ is for point *b*. The measurement correction from *b* to *a* is $\Delta z_{i,AB}$ for the clean engine and $\Delta z_{i,A1B1}$ for the degraded engine. From Figure 5-4 it can be seen that

$$\Delta z_{i,a} + \Delta z_{i,AB} = \Delta z_{i,b} + \Delta z_{i,A1B1} \qquad 5\text{-}16$$

Therefore, the actual performance deviation at condition *a* is

$$\Delta z_{i,a} = \Delta z_{i,b} + (\Delta z_{i,A1B1} - \Delta z_{i,AB}) \qquad 5\text{-}17$$

The engine thermodynamic model can be used to simulate the clean engine performance at points *A* and *B* using the ambient and operating baseline *a* and actual *b* conditions. Together with the actual degraded performance at point *B1* under the actual conditions *b*, the following can be known,

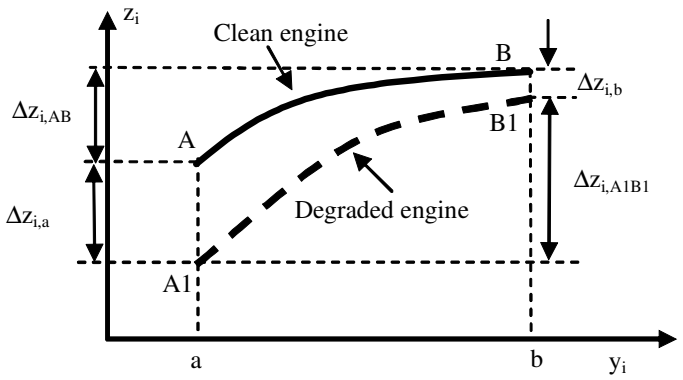

Figure 5-4 Measurement correction against ambient and operating conditions [178]

$$\Delta z_{i,AB} = z_{i,B} - z_{i,A}$$
$$\Delta z_{i,b} = z_{i,B} - z_{i,B1} \qquad \text{5-18}$$

The calculation of $\Delta z_{i,b}$ will include the residual error from the noise correction to $z_{i,B1}$. Finally, the only factor to be known is $\Delta z_{i,A1B1}$. Unfortunately, there is no way to approximate it because the degradation magnitude and location are unknown. A first diagnostic analysis must be carried out before having a first estimation.

5.4.6.2.2 A posteriori correction

The second step in the ambient and operating conditions correction method considers an iterative approach in order to remove or reduce the effect from the factor $\Delta z_{i,A1B1}$ as shown in Figure 5-5.

An initial correction for the ambient and operating conditions $\Delta\vec{y}$ at *n=0* is done using the engine model to calculate the performance deviation with clean engine $\Delta\tilde{\vec{x}} = 0$ conditions $\Delta\vec{z}_{y,0}$. The corrected performance deviation $\Delta\vec{z} - \Delta\vec{z}_{y,0}$ is used in the diagnostics analysis. The Sensor Fault Case (*SFC*) method identifies any instrumentation bias to complement the correction described in the previous sub section. The Component Fault Case (*CFC*) method will produce an estimated first degradation vector $\Delta\tilde{\vec{x}}_0$.

The vector $\Delta\tilde{\vec{x}}_0$ is reinserted into the engine model to calculate the performance deviation from points *A1* to *B1* on a degraded engine $\Delta z_{i,A1B1}$ and complete the estimation of the performance deviation from clean to degraded conditions at baseline *a*. The process is repeated until the difference between two consecutive values for the degradation vector tends to a predefined limit value,

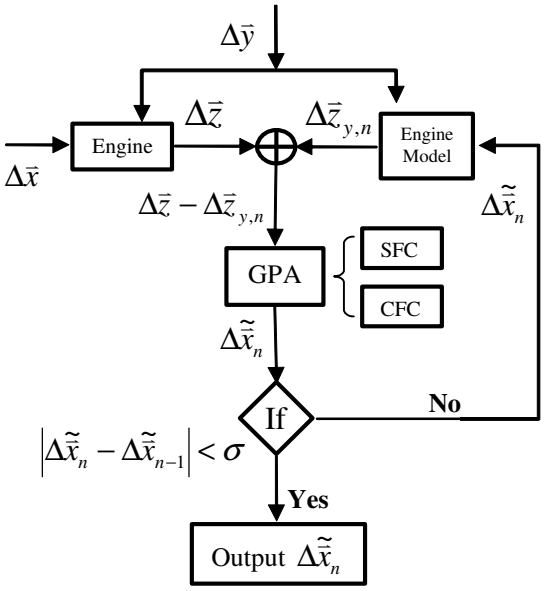

Figure 5-5 A-posteriori correction of ambient and operating conditions with degradation [178]

$$\left|\Delta\tilde{\tilde{x}}_n - \Delta\tilde{\tilde{x}}_{n-1}\right| < \sigma \qquad 5\text{-}19$$

where σ is the convergence criterion and n is the iteration number. An under-relaxation factor α is used during the iterations to enhance the convergence and the updated prediction of engine degradation [178].

$$\Delta\tilde{x}_{i,n} = \Delta\tilde{x}_{i.n-1} + \alpha \cdot \left(\Delta\tilde{x}_{i.n} - \Delta\tilde{x}_{i,n-1}\right) \qquad 5\text{-}20$$

where a recommended value for α is between 0.3 to 0.7.

5.4.7 Measurement selection

The measurement setting module allows the user to define an initial set of measurements to be used in the diagnostics analysis. This capability enables the user to conduct a preliminary analysis on a large number of sets without having to install the sensors on the engine. The final measurement set has to consider the following aspects to comply with GPA demands as well as some practical considerations [229]:

a) *Operating conditions.* The temperature and pressure operating conditions of a sensor may restrict the actual installation of the sensor.
b) *Existing vs. New Sensors*. Almost all types of gas turbine engines come with a fixed and original set of measurements used for control purposes. The analyst should try to accommodate the final set to those already existing. Otherwise, implementation costs of the diagnostic system will rise.

c) *Number of sensors*. In theory, the more sensors available the best results obtained from GPA-based diagnostics system (every time they comply with points *d* and *e*). Measurement redundancy reduces the negative impact of the smearing effect on the results, and therefore, it is desirable situation by any diagnostics engineer. However practical and/or economic restrictions (diagnostics system implementation budget) will determine the final number of sensors.
d) *Sensitivity of sensors*. The measurements taken must be meaningful related to the problems sought and detectably respond to changes therein.
e) *Correlation*. In theory, measurements used for diagnostics purposes must not be correlated to each other

5.5 Computational tool

5.5.1 PYTHIA

PYTHIA is a computational program developed at Cranfield University. The program has two main modules: performance simulation and performance diagnostics.

The performance simulation module allows the simulation of design and off-design performance cases. The module is a graphical user interface (*GUI*) for Turbomatch, therefore, all the capabilities mentioned in Chapter 2 are available in *PYTHIA*'s performance simulation module. The results are given in the traditional Turbomatch's output text file or through a spreadsheet that formats and organizes the results by simulation case. Further description of this module is outside the scope of this section.

The performance diagnostics module is the more extensive module in *PYTHIA*. The main objective of the module, as its name suggests it, the identification of faulty engine components and sensors and the quantification of that degradation. It also includes a design and off-design point adaptation module [223, 232] to increase Turbomatch's performance simulation capability accuracy. The main five features used for the work described in this chapter are: engine component diagnostics, sensor diagnostics, measurement simulation and data acquisition.

5.5.2 Degradation implantation

The Diagnosis Degradation Setting module allows the implantation of degradation on different engine components to generate the simulated degraded performance. The module demands the activation of a degradation box and to select the component to be degraded. *PYTHIA* allows only degradation on the main components such as compressors, turbines and burner. A negative or positive value for the *efficiency* and *mass flow capacity,* are required for compressors and turbines, while burners need only the *efficiency* value.

5.5.3 Measurement simulation

PYTHIA can generate sets of simulated measurements for clean or degraded engines at different ambient and operating conditions. Sensor noise and bias can be added to the simulated data to emulate a real scenario that allow to test the different tools implemented such as noise correction, ambient and operating conditions correction and sensor diagnostics.

5.5.4 Data acquisition

In the Data Acquisition module the data is corrected for any instrumentation noise and deviation in ambient and operating conditions from baseline. The user must choose the type of correction for the ambient and operating conditions, before loading the clean and degraded data onto the screen. Once the correction is finished, two single points from the clean and degraded performance are chosen for further analysis.

5.5.5 Fault quantification

In the Fault quantification module the final set of measurements to be used in the diagnosis and the potential faulty components to-be-searched are chosen. After the data is corrected for instrumentation noise and ambient & operating conditions inside the data acquisition module, the fault signature Δz from the initial set of measurements is calculated. At this stage, the user selects the set of measurements to be used in the diagnosis by evaluating the sensitivity of each measurement. In order to apply the *CFC* method is necessary to define the number of total components to-be-searched. The selected components and the number of simultaneous degraded components will give the total number of *CFC*s to be processed.

5.5.6 Sensor diagnostics

The Sensor Fault Detection module is based on the *SFC* method. The user has to define the number of simultaneous degraded sensors and choose the searching component set from the number of component chosen in the Fault quantification module. The option to obtain the linear and non-linear solution to the problem is available for the user. The results of the diagnostic including the GPA-index value for every *SFC* are displayed on the screen.

5.5.7 Engine component diagnostics

In the Engine component diagnostics module the number of simultaneous degraded components that define the total number of *CFC* is defined. The user has the option to decide if a linear or non-linear approximation is to be performed. Results for every *CFC* including GPA-index and the predicted degradation are displayed on the screen. In the case a sensor fault was detected by the *SFC* module, the user has to unselect the sensor from the set of dependent parameters inside the Fault quantification module before attempting any engine component diagnostic analysis, or else, an inaccurate prediction will be obtained.

5.6 LM2500+ Performance Diagnostics

This section presents a detailed analysis of the diagnostics techniques described in earlier sections using simulated performance data. Different ambient and operating conditions and implanted degradation scenarios are defined to establish the guidelines for the successful usage of the tool.

5.6.1 Measurement set

Only the set of available measurements from MEA's LM2500+ control system has been considered for the analysis as listed in Table 5.1. In theory, the degree of success of GPA, consequently of *SFC*, relies on the selection of an appropriate set of uncorrelated measurements that provide high levels of observability. In practice, cost and operating limits (temperature) issues restricts the number of available measurements.

Table 5.1 Available measurement set in MEA's LM2500+ engine

Label	Description
T3	Compressor discharge temperature
P3	Compressor discharge pressure
T48	Power turbine inlet temperature
P48	Power turbine inlet pressure
F	Fuel Flow
N	Gas generator shaft speed
T5	Exhaust gas temperature
P25	9^{th} stage bleed air pressure

5.6.2 Sensor diagnostics with simulated data

The objective of this section is to evaluate the sensor diagnostics method described in section 5.4.5. As mentioned earlier, the *SFC* method relies on GPA method strengths and weaknesses, therefore, it is important to assess the tool in order to identify the conditions needed to have a satisfactory diagnostic of sensor fault for MEA's LM2500+ engines. The analysis has various phases that assess the method using simulated data with different quantitative (sensor noise and bias magnitude, component degradation magnitude, etc) and qualitative (ambient and operating conditions, location of the implanted sensor fault and component) characteristics.

5.6.2.1 Searching component set

The *SFC* method undertakes an exhaustive search of the fault by comparing the actual fault signature vector with a series of simulated vectors. To create these simulated signature vectors a number of components more likely to present both sensor and component degradations is selected. The set of components has a quantitative effect on the results, therefore, a preliminary study to identify the more effective set was carried out. It is important to mention that only the main components of the engine can be selected (compressors, burner or turbines).

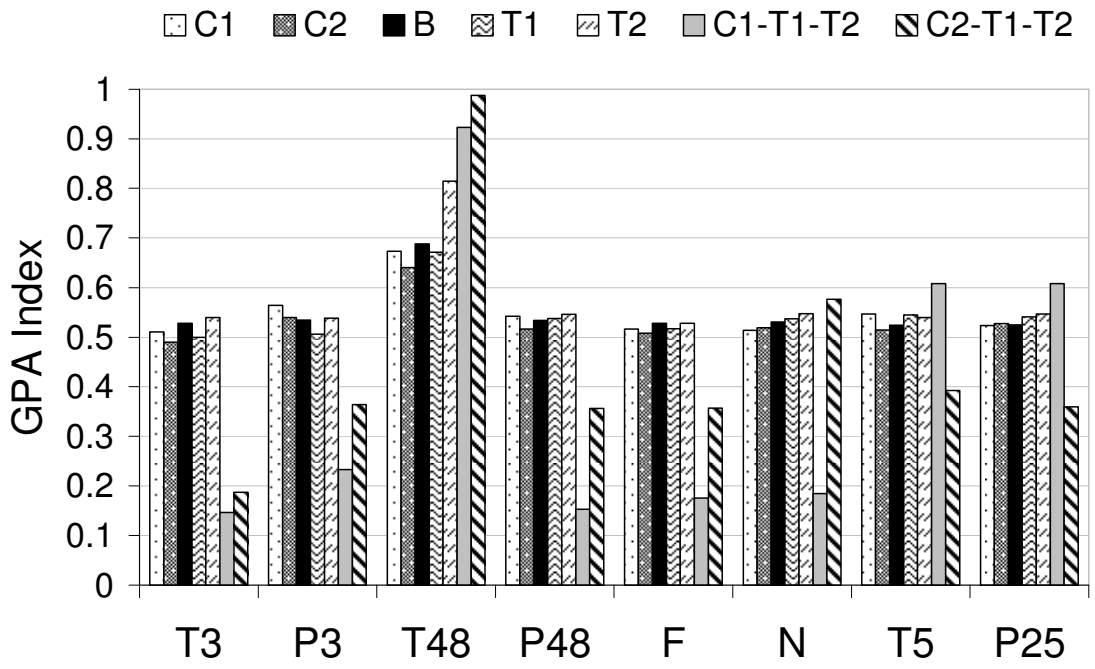

Figure 5-6 Comparison between searching component sets for sensor diagnostics

To conduct a qualitative comparison between the single component set and the multiple component set approaches, a fault (bias) of 4% in T48 sensor was implanted. Figure 5-6 shows the results of the comparison between five single-component and two triple-component sets.

Clearly the C1-T1-T2 and C2-T2-T3 components sets provide satisfactory results showing GPA-index values of 0.922 and 0.988 for T48, respectively. On the other hand, it is only T2 single-component set that provide a favourable conclusion. The rest of the single-component sets present a degree of ambiguity that would require further analysis. The only disadvantage of the multiple-component set approach is the increase in convergence time, however, this can be overturned with state-of-the-art computing hardware. The C1-T1-T2 and C2-T1-T2 component sets are studied in more detail in the following sections to choose the more efficient of the two.

5.6.2.2 Data validation for sensor diagnostics

The data validation capabilities of *PYTHIA* are tested in this section using the C2-T1-T2 component set. Three different cases are considered: a) No correction, b) Correction without degradation (see section 5.4.6.2.1), and c) Correction with degradation (see section 5.4.6.2.2). The noise reduction rolling average technique (see section 5.4.6.1) is used for all three cases.

The assumptions made included the implantation of a fault of 4% in sensor T48 and noise levels of 1% of the simulated measurement mean value. An analysis of the real data recorded from the control system at MEA's power plant show average noise levels

below this threshold, therefore, it is considered to be a good benchmark. The deviation in ambient temperature was set to + 9.3 K and 2MW deviation in power output.

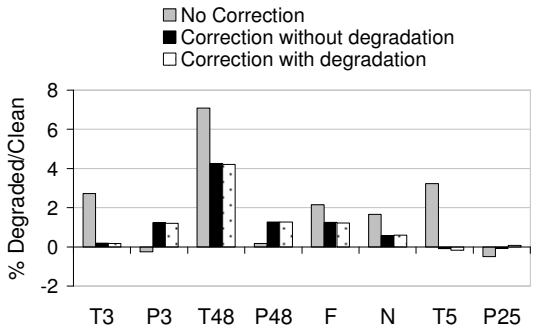

Figure 5-7 % difference between degraded and clean performance

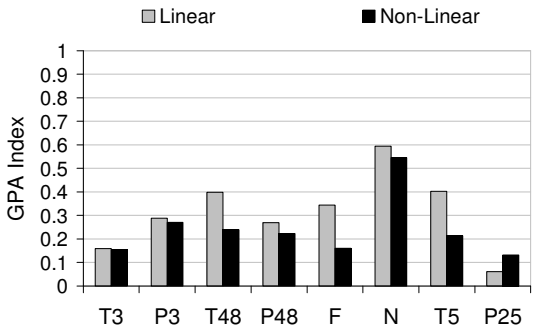

Figure 5-8 Sensor diagnostics results with no correction

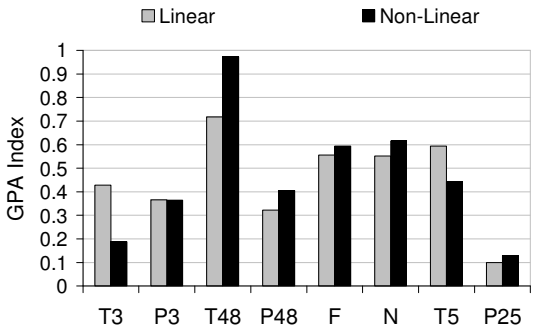

Figure 5-9 Sensor diagnostics results with initial correction

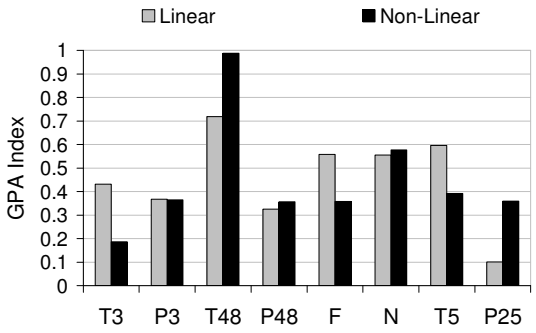

Figure 5-10 Sensor diagnostics results with *a-posteriori* correction

The noise levels were reduced using the rolling average filter technique described in section 5.4.6.1. Figure 5-7 shows the deviation between the degraded and clean performance (fault signatures) for three cases where the data validation for ambient and operating conditions of *PYTHIA* were tested. The three cases are No correction, initial correction and full (*a posteriori*) correction. It can be observed there is a considerable difference between the two corrected and no correction cases, particularly in parameters such as T3, T48 and T5. The engine stations temperatures are affected by shift in ambient temperature from the baseline conditions.

The results of the sensor diagnostic for each case are shown in Figure 5-8 to Figure 5-10. Clearly, the accuracy of the analysis in the case where no correction was made is poor. The isolated sensor is N (speed) with a maximum GPA-index of 0.6 that can not be considered as conclusive. On the other hand, the corrected cases show extraordinary accuracy as detecting the actual sensor fault by conferring it GPA-index values of 0.988 and 0.9731 for the initial correction and *a-posteriori* correction cases, respectively.

The results of the analysis suggested all subsequent analysis to include the correction for noise, and ambient and operating conditions. Such conclusion can also be transferred to diagnostics exercise using real data.

5.6.2.3 Sensitivity analyses

5.6.2.3.1 Case Study 1

Although the previous two sections proved the ability of the *SFC* method to detect a sensor fault in present of changes in ambient and operating conditions and data noise, it is important to find the safe operation of the *SFC* method. By knowing this information a procedure to extract information from MEA'S engines when conducting a sensor and component diagnostic can be created.

The performance of the engine was simulated using *PYTHIA* measurement simulation module. The magnitude of the data noise was set to 1% of the simulated measurement mean value. Based on the fact ambient temperature has a greater effect on the engine performance than ambient pressure, it was decided to only modify the former in + 9.3 °K over the baseline value. An initial increase of 2MW over baseline conditions was considered.

The fault diagnostics module is expected to work with real data that may include measurements from degraded engine components (compressor, burner or turbine) therefore it was decided to implant a small degradation to simulate those conditions. A likely reduction of -1% in isentropic efficiency and -1% in capacity at the front section of the compressor were considered.

The analyses evaluate the accuracy of the two C1-T1-T2 and C2-T1-T2 sets to detect an implanted sensor fault of 4% on T48. The data is validated using the full correction capabilities of *PYTHIA*. The noise is reduced using the rolling average method, and the *a posteriori* correction is made for all cases. Four different cases were tested:

A. Sensor bias + Degradation
B. Noise + Sensor bias + Degradation
C. Amb&Ops + Sensor bias + Degradation
D. Amb&Ops + Noise + Sensor bias + Degradation

The cases' complexity increases from A to D. The first only test the *SFC* method under the simplest conditions without the presence of any deviation from baseline conditions or noise. In contrast, Case D brings all possible perturbations into play: ambient and operating conditions and noise.

Figure 5-11 and Figure 5-12 show the results for the Non-linear *SFC* method applied to all four cases for set C1-T1-T2 and C2-T1-T2, respectively. In both cases, the method was successful in isolating the faulty sensor (T48) in cases B and C but failed to give conclusive information for cases A and D. It has been mentioned that GPA-index values above 0.8 are considered as conclusive evidence of fault or component degradation. Although some discretion from the analyst may still be required when more than one case present high values or fall short of 0.8 but is clearly differentiated from the rest.

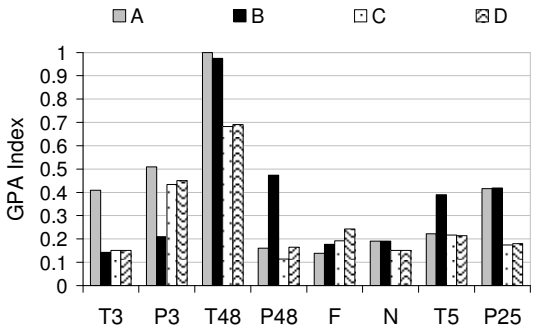

Figure 5-11 Sensor diagnostics results using component set C1+T1+T2

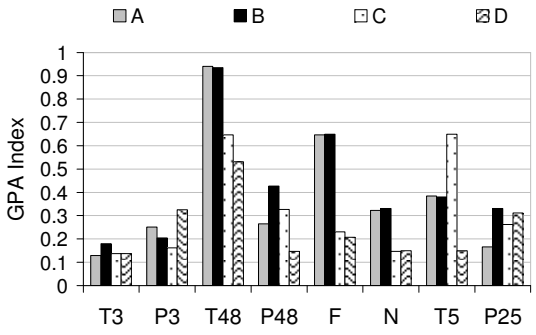

Figure 5-12 Sensor diagnostics results using component set C2+T1+T2

Two major conclusions can be drawn from this first analysis. Noise alone has no impact on the sensor diagnostics as there is no significant difference between the GPA-index values obtained in *Case A* and *B*. In other words, the noise reduction technique used is effective. Secondly, the ambient and operating conditions perturbation has a great effect on the ability of the method to isolate the appropriate sensor fault.

So far there is not a clear advantage from any of the two searching component sets, therefore, the following studies will continue presenting results for both.

5.6.2.3.2 Case Study 2

This second study has the intention of knowing if the magnitude of the sensor bias could improve the results from Case D using either searching component set. The hypothesis was that the sensor bias magnitude was being covered by the performance change resulting from the implanted degradation or noise levels. Hence, increasing the magnitude of the bias the *SFC* method would identify the fault.

The sensor fault was set to 8% on T48 whilst noise and, ambient and operating conditions remain unchanged. The results show that the magnitude of the sensor fault has no major effect on the method's ability to isolate the sensor fault. While the results from component set C1+T1+T2 show similar values to those from the previous section, the set C2+T1+T2 has a poor performance.

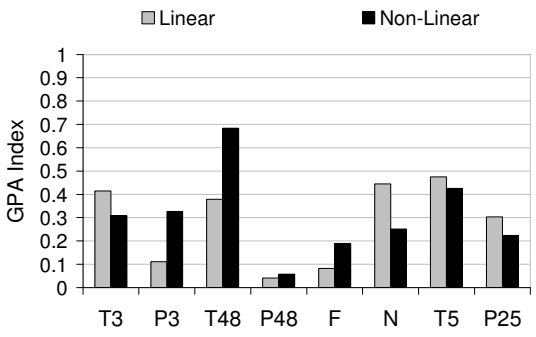

Figure 5-13 Sensor diagnostics results using set C1+T1+T2 for sensor bias of 8%

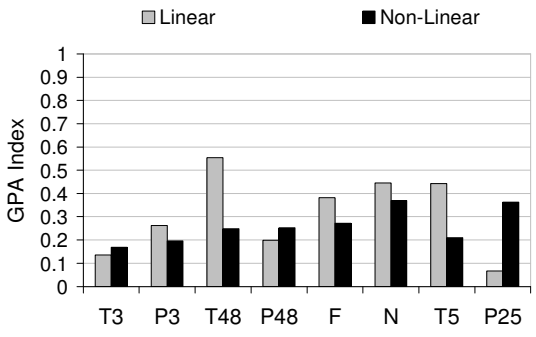

Figure 5-14 Sensor diagnostics results using set C2+T1+T2 for sensor bias of 8%

5.6.2.3.3 Case Study 3

The results from the previous two studies indicate the ambient and operating conditions deviations are solely responsible for the inability of the method to isolate a sensor fault. The objective of this third case study was to determine which of the ambient (temperature) or operating (power output) conditions had a greater effect on the diagnostic results. The analyses were carried out using the two known searching component sets.

Figure 5-15 and Figure 5-17 show the results for the case considering only a deviation in power output for sets C1+T1+T2 and C2+T1+T2 respectively. The method continued failing to provide conclusive evidence trying to isolate the implanted T48 sensor fault. In the case of component set C2+T1+T2, the results for the linear-*SFC* method present larger GPA-index values than those reported by the Non-linear *SFC* method. This could be explained by some convergence problems of the engine model. On the other hand, the C1+T1+T2 set present two sensors with very similar GPA-index values around 0.7 from which no answer can be drawn.

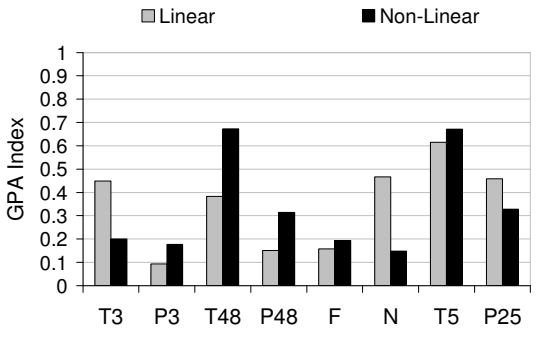

Figure 5-15 Sensor diagnostics results using set C1+T1+T2 for power deviation of 2MW only

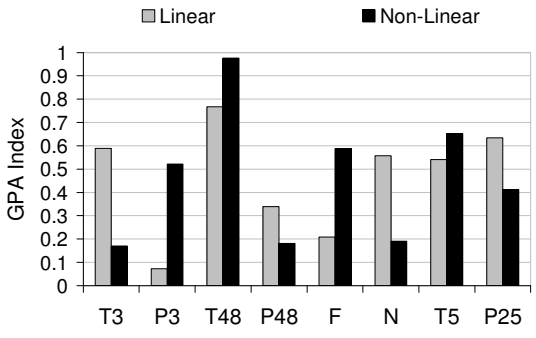

Figure 5-16 Sensor diagnostics results using set C1+T1+T2 for ambient temperature deviation of 9.3 degrees only

On the contrary, the ambient temperature deviation case presented an optimal performance (Figure 5-16 and Figure 5-18). Both sets, C1+T1+T2 and C2+T1+T3, present very similar results with GPA values of 0.76 for the linear-*SFC* method and 0.98 for the non-linear option.

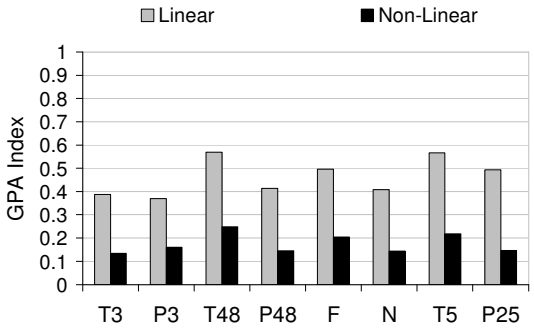

Figure 5-17 Sensor diagnostics results using set C2+T1+T2 for power deviation of 2MW only

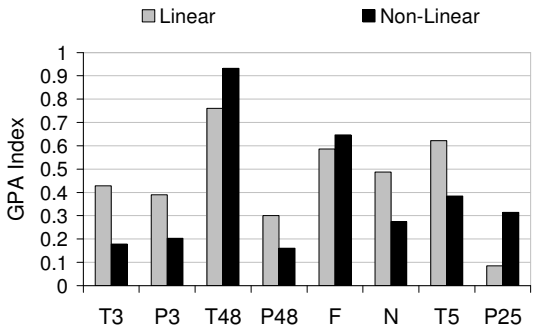

Figure 5-18 Sensor diagnostics results using set C2+T1+T2 for ambient temperature deviation of 9.3 degrees only

5.6.2.3.4 Case Study 4

Once the power output deviation from baseline conditions was identified as the main responsible for the method's inconsistency, it became necessary to establish a safe operability range of the *SFC* method in order to warrantee accurate diagnostics. The power deviation was set to 1MW and 500kW from baseline conditions maintaining all other assumptions unchanged. Again, the analysis was carried out using C1+T1+T2 and C2+T1+T2 component sets. Until this point the performance of the two components sets have been similar, hence there was not enough information to back a crucial choice. However, the results obtained in this case study began to shape the future decision.

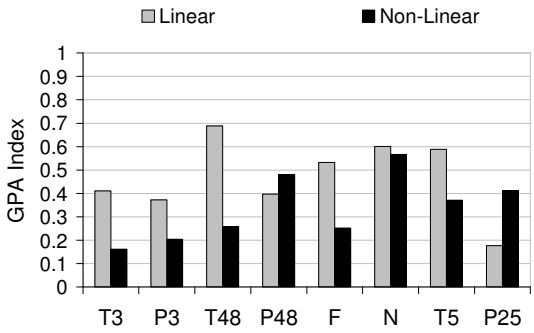

Figure 5-19 Sensor diagnostics results using set C2+T1+T2 for power deviation of 1MW

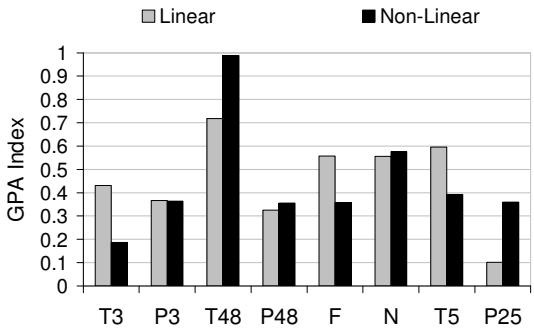

Figure 5-20 Sensor diagnostics results using set C2+T1+T2 for power deviation of 500kW

C2+T1+T2: Figure 5-19 shows no improvement in the 1MW case from the initial power deviation of 2MW. The linear method produces a non conclusive scenario with GPA-index of 0.6882 for T48 and two more sensors showing values close to 0.60. However, the non-linear *SFC* method completely misses the prediction even reporting

GPA-index values lower than those obtained with the linear method. Again, this could be the result of convergence issues.

On the positive side, the case with 500kW deviation from baseline conditions (see Figure 5-20) delivers exceptional results. Good prospects are observed with the linear method that are confirmed when the non-linear option is used. A conclusive scenario is reached with the non-linear *SFC* method showing GPA-index value of 0.988 for T48.

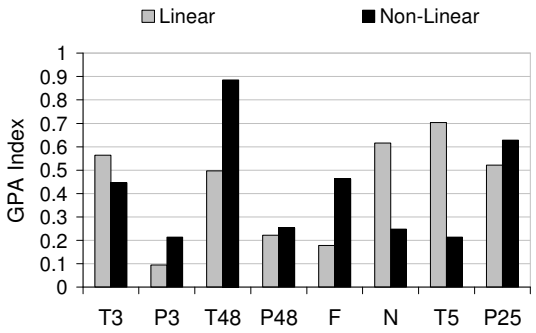

Figure 5-21 Sensor diagnostics results using set C1+T1+T2 for power deviation of 1MW

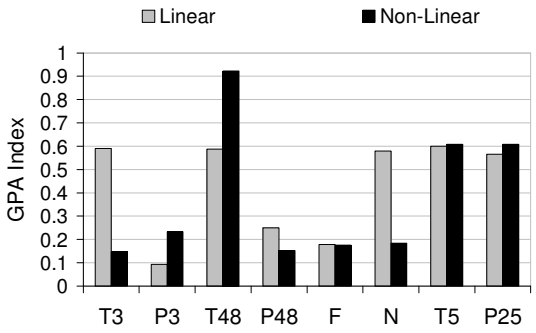

Figure 5-22 Sensor diagnostics results using set C1+T1+T2 for power deviation of 500kW

C1+T1+T2: Figure 5-21 and Figure 5-22 show results for cases 1MW and 500kW respectively. Contrary to the results obtained with the C2+T1+T2 set, the non-linear *SFC* method shows conclusive GPA-index values of 0.8849 for the power settings 1MW case. In the same way, a convincing result of 0.9229 for the 500kW power output deviation case is found.

This means using the C1+T1+T2 set will allow the analyst to use data recorded up to 1MW off the baseline conditions – even when the C2+T1+T2 set fails to provide conclusive results – with the certainty the *SFC* method will deliver an accurate diagnostic.

5.6.2.3.5 Case Study 5

The final case study tests the *SFC* method's ability to locate the sensor fault when implanted in different sections of the engine. The implanted component degradation was also relocated to find out the sensor diagnostic sensitivity to this variable. The following four degradation combinations were considered for the study:

A. Sensor fault with 4% bias on T48 and degradation (-1% η, -1%Γ) on front section of compressor (C1).
B. Sensor fault with 4% bias on T48 and degradation (-1% η, -1%Γ) on gas generator turbine (T1).
C. Sensor fault with 4% bias on T3 and degradation (-1% η, -1%Γ) on front section of compressor (C1).
D. Sensor fault with 4% bias on T3 and degradation (-1% η, -1%Γ) on gas generator turbine (T1).

All cases assume a deviation of + 9.3°K in ambient temperature and noise level of 1% the mean value of measurement. A deviation in power output deviation of 500kW from baseline was used.

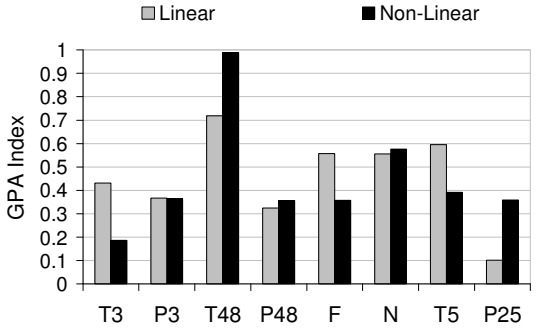

Figure 5-23 Sensor diagnostics results using set C2+T1+T2 for implanted sensor bias on T48 and degradation on C1

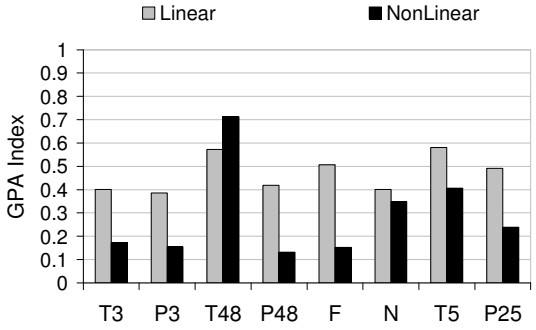

Figure 5-24 Sensor diagnostics results using set C2+T1+T2 for implanted sensor bias on T48 and degradation on T1

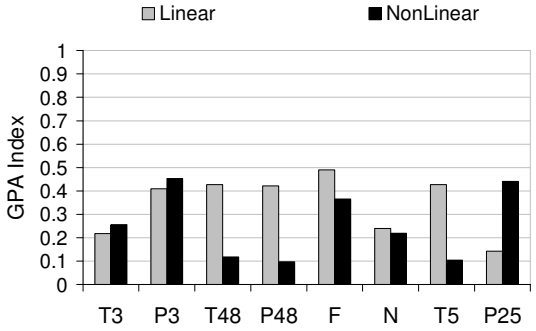

Figure 5-25 Sensor diagnostics results using set C2+T1+T2 for implanted sensor bias on T3 and degradation on C1

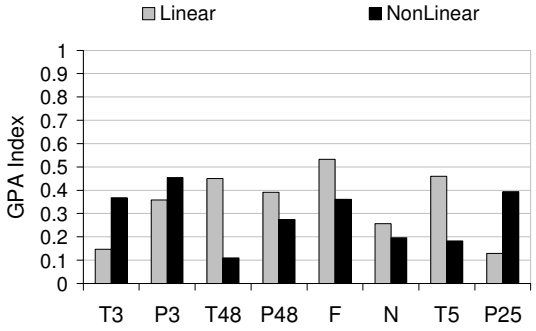

Figure 5-26 Sensor diagnostics results using set C2+T1+T2 for implanted sensor bias on T3 and degradation on T1

The results of the analyses using the C2+T1+T2 component set were not entirely satisfactory. The results show the method is partially able to isolate a fault on T48 but completely fails when the sensor fault is located on T3 irrespective of the location of the implanted degradation. The non-linear *SFC* method produces a GPA-index value of 0.988 for the T48-C1 (Figure 5-23) combination while it is only able to deliver a value of 0.712 for the T48-T1 combination (Figure 5-24). The later can not be considered as conclusive although the fairly low magnitude of GPA-index for other sensors confers the T48 sensor result more credibility.

A poor performance to isolate the sensor faults implanted on T3 when using the C2+T1+T2 component set was obtained (see Figure 5-25 and Figure 5-26). The linear solution for the two T3-C1 and T3-T1 combinations delivers poor GPA-index values of around 0.4 for practically all sensors. Following the same behaviour, the non-linear *SFC* method is unable to reach an accurate solution for any of the two combinations.

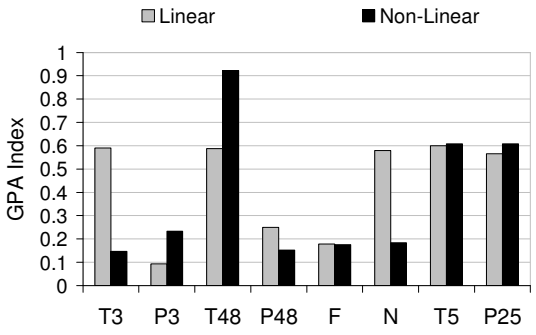

Figure 5-27 Sensor diagnostics results using set C1+T1+T2 for implanted sensor bias on T48 and degradation on C1

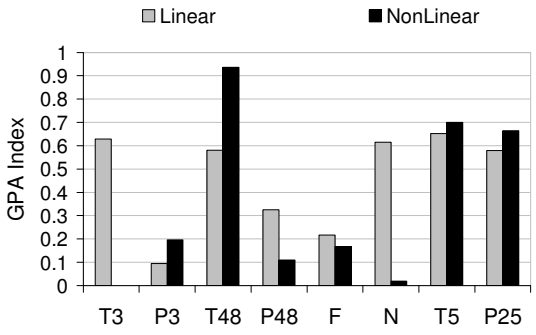

Figure 5-28 Sensor diagnostics results using set C1+T1+T2 for implanted sensor bias on T48 and degradation on T1

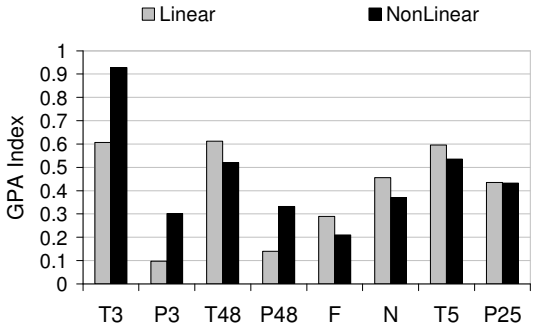

Figure 5-29 Sensor diagnostics results using set C1+T1+T2 for implanted sensor bias on T3 and degradation on C1

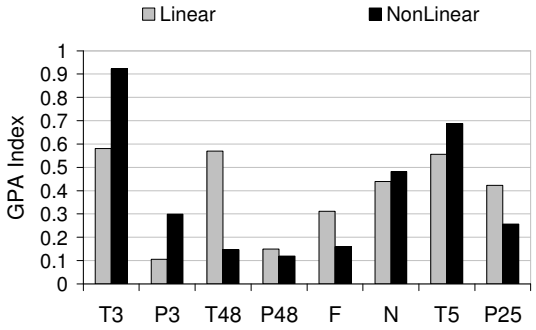

Figure 5-30 Sensor diagnostics results using set C1+T1+T2 for sensor bias on T3 and degradation on T1

On the other hand, the solution delivered the *SFC* method using the C1+T1+T2 component set is very encouraging (refer to Figure 5-27 to Figure 5-30). The method delivers excellent results for all degradation combinations with GPA-index values above 0.9 using the non-linear method. The use of C1 instead of C2 in the searching component set allows the *SFC* method to detect the implanted sensor fault in T3 since the performance of C1 is not described by T3 sensor. The lesson learned was that the *SFC* method will be have problems to detect sensor faults that describe the performance of an engine component used as part of the searching component set.

5.6.3 Engine Component diagnostics with simulated data

The section reports the findings of a series of sensitivity analyses aiming to create a best practice procedure for future engine component diagnostics activities on MEA's LM2500+ engines.

Since GPA is the engine of the *SFC* and the *CFC* methods, the results and conclusions reached on the previous section hold for the component diagnostic exercise. Based on the findings from section 5.6.2, the data validation techniques for noise reduction and correction of the ambient and power deviations from baseline are used for all analyses.

During these analyses no sensor fault was implanted as it reduces the chances of constructing the influence coefficient matrix with measurement redundancy.

The analysis makes use of the same limited set of measurements listed in section 5.6.1 to obtain valuable insights of the methods' performance under real conditions. In the case of the searching component sets, all components – C1, C2, B, T1 and T2 – are selected as potentially degraded components. The main difference between the *SFC* and *CFC* methods, regarding the searching component sets, is that the *SFC*'s searching set is used to isolate through an elimination process the sensor fault even if the isolated sensor does not describe the performance of any of the chosen components. On the other hand, the *CFC* will only allocate a deterioration value to one (or more) of the chosen components. From a practical point of view, a fundamental condition of a component diagnostic analysis is the lack of certainty on the location of the deteriorated component(s), thus, it is expected that every component is considered as potentially degraded.

5.6.3.1 Sensitivity analyses

5.6.3.1.1 Case study 1

This study evaluates the performance of the engine component diagnostics method using simulated degraded performance measurements that delivered positive results in the sensor fault detection analyses. The aim is to find if the conditions demanded from the data (real or simulated) by the *SFC* method could be extended to the *CFC* method. The characteristics of the simulated degraded performance measurements were -1%η and -1%Γ implanted degradation on the compressor front section (C1) and ambient temperature and power output conditions deviations of + 9.3°K and 500kW, respectively. Finally, a noise signal of 1% was added to the simulated measurements and no sensor fault was implanted.

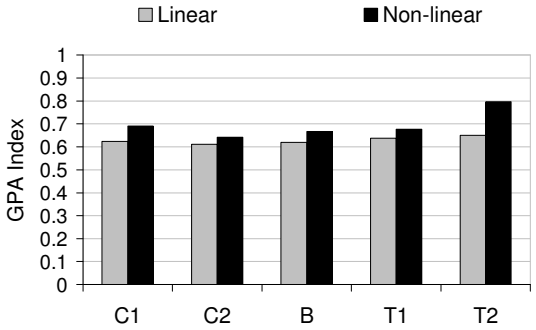

Figure 5-31 Linear and non-linear GPA index component diagnostics results

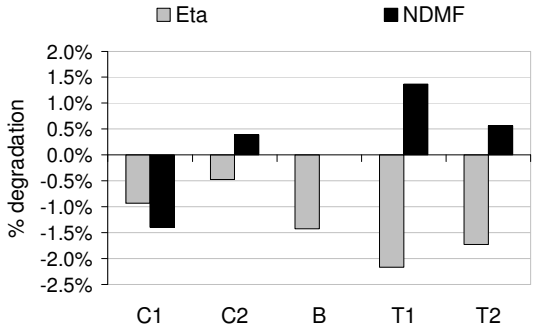

Figure 5-32 Non-linear predicted degradation

Unfortunately, the *CFC* method was not able to isolate and quantify the implanted component degradation (see Figure 5-31) from the simulated data. A GPA-index value of 0.6232 was conferred to C1 by the linear method with similar results for the rest of the components. In the case of the non-linear *CFC*, the GPA-index value increases to

0.6904 but it is T2 that obtains an index of 0.7967. As explained in the introduction for this section, the failure of the *CFC* method – contrasted with the success from *SFC* method to isolate the right sensor fault from similar simulated performance data – relies on the internal workings of both methods. While the *SFC* method uses GPA component diagnostics results to cross out the healthy sensors, the *CFC* method depends on the results from GPA to isolate the deteriorated component.

5.6.3.1.2 Case study 2

The inaccurate diagnostic results from the previous study forced to take one step back to assess the effect of each of the perturbations considered for the simulation of the degraded performance data. The implanted component degradation magnitude and location (-1%η and -1%Γ on C1) was kept unchanged and no sensor fault was implanted. Three cases were analysed:

I) noise signal of 1% only
II) power output deviation of 500kW only
III) ambient temperature deviation of 9.3 degrees only

As expected, the deviation in power output from baseline conditions has a negative effect on the ability of *CFC* method to produce an accurate and conclusive solution. Figure 5-34 shows the results for case II with power deviation as the only perturbation apart from the implanted component degradation on C1. The non-linear *CFC* method delivers an inconclusive GPA-index value of 0.6834 for C1 while the highest value is conferred to T2. It could be inferred that it is because the performance of the power turbine (T2) is highly dependant on the auxiliary power demanded from the engine that any deviation from baseline conditions create a performance perturbation that is miss read as deterioration on T2 by the *CFC* method. The tool estimated a degradation of -1.288% η and -1.511% Γ on C1, which is not entirely inaccurate, but, it is only because the degradation is known beforehand that such a statement can be made.

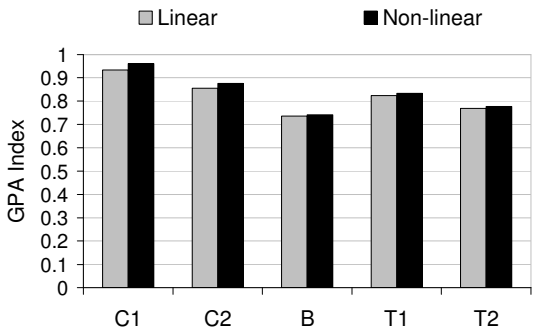

Figure 5-33 GPA index component diagnostics results for Case I

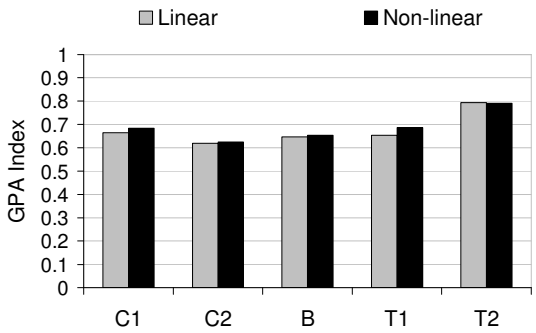

Figure 5-34 GPA index component diagnostics results for Case II

On the other hand, the noise and ambient deviation cases present optimistic preliminary scenarios, which could be improved with a more exhaust analysis considering up to two

degraded engine components. Figure 5-33 reports the findings for case I (noise signal + degradation).

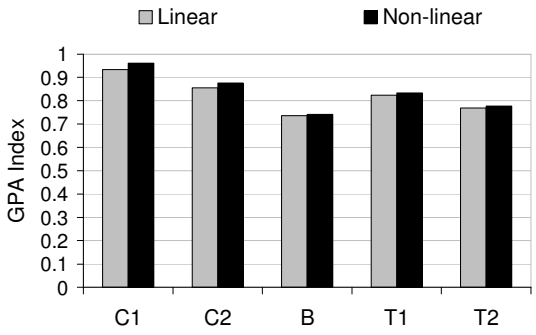

Figure 5-35 GPA index component diagnostics results for Case III

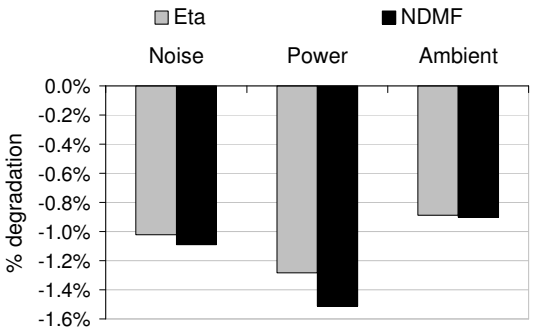

Figure 5-36 Non-linear predicted degradation on C1 for all cases

The estimated values of GPA-index of 0.9615 for C1 and degradation of -1.022% η and -1.09% Γ on C1 gave the certainty that noise signals – of the magnitude considered for this analysis – have no effect on the *CFC* method diagnostics potential.

In the case of the ambient temperature deviation (Figure 5-34), the *CFC* method approximated a degradation of -0.888% η and -0.9015% Γ on C1 with a strong GPA-index value of 0.9522.

The results from this case study, complemented with the knowledge obtained in the sensor diagnostics section, suggests that *PYTHIA*'s data validation tool, particularly the correction of data from power output deviation from baseline conditions is not as efficient as expected.

5.6.3.1.3 Case Study 3

The objective of the case study 3 was to determine if the magnitude of the component degradation could improve the results of *CFC* method from case study 1. The hypothesis was that an increase in the implanted degradation would outweigh the negative effect of the power output deviation. The simulated degraded performance included: noise signal of 1% the mean value of the measurement, ambient temperature deviation of 9.3°K, a deviation in power settings of 500kW, and no implanted sensor fault. Two scenarios were set for the analysis:

I. Implanted degradation of -2% η and -2% Γ on C1
II. Implanted degradation of -3% η and -3% Γ on C1

No sign of improvement in the diagnostic came from results of *scenario I* as observed in Figure 5-37 and Figure 5-38. Although the *CFC* method estimated a degradation of -2.347% η and -2.742 Γ on C1 the results can not be considered as definite as C1 presents an unconvincing GPA-index of 0.6325 that is exceeded by a value of 0.6535 conferred to T2. In conclusion, the results present the same behaviour than Case Study 1.

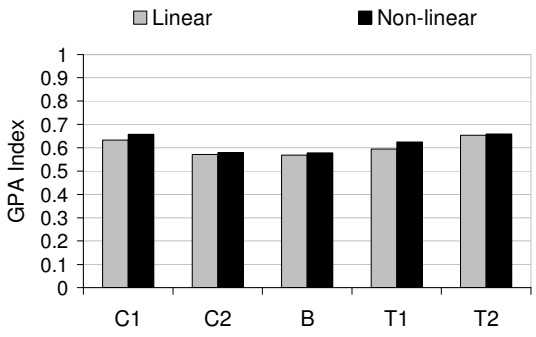

Figure 5-37 GPA index component diagnostics results for Case I

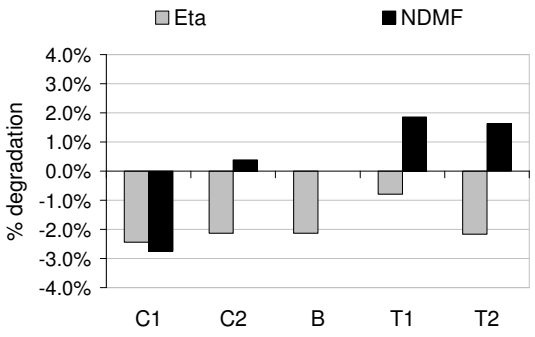

Figure 5-38 Non-linear predicted degradation for Case I

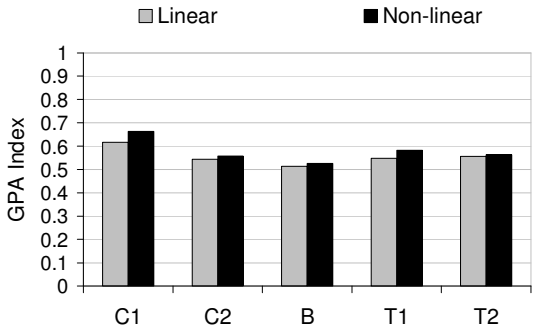

Figure 5-39 GPA index component diagnostics results for Case II

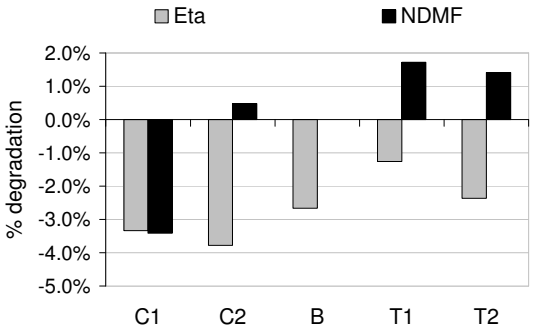

Figure 5-40 Non-linear predicted degradation for Case II

Even though the solution for *scenario II* was not decisive either, the unfavourable behaviour observed in the first analysis was reverted as the highest GPA-index value was conferred to C1 (0.6644). Such results also granted some credibility to the estimated degradation results that reported values on C1 of -3.337% η and -3.415% Γ.

It can be concluded that the magnitude of the performance degradation is not a dominant variable when assessing the ability of *CFC* method to detect the deterioration of any engine component from data recorded at power settings different to baseline conditions.

5.6.3.1.4 Case Study 4

The purpose of Case Study 4 is to assess the accuracy of the *CFC* method to isolate and quantify different components deterioration from data recorded under the favourable conditions derived from the past three case studies. The simulated degraded performance used in this analysis present noise levels of up to 1% the mean value of the measurements, a deviation in ambient temperature of 9.3°K, but it do not include any power output deviations from baseline conditions or sensor fault. A performance deterioration of -1% η and -1% Γ was applied to components C1, C2, T1 and T2 to create four different component degradation cases:

I. Implanted degradation of -1% η and -1% Γ on C1
II. Implanted degradation of -1% η and -1% Γ on C2
III. Implanted degradation of -1% η and -1% Γ on T1
IV. Implanted degradation of -1% η and -1% Γ on T2

So far, all case studies had only considered a single degraded component scenario that produces five component fault cases (*CFC*), one for each component: C1, C2, B, T1 and T2. In order to achieve results with a higher level of confidence the number of simultaneous degraded components must be increase to two (at least), giving a number of fifteen (15) *CFC*s listed in Table 5.2.

Usually, the *CFC*s compound-cases including the component presenting the higher GPA-index in the first single *CFC*s will show a high GPA-index, although a small (or sometimes large) discrepancy between this cases may be found. Assuming the component degradation is unknown to us, a discriminatory process must follow the *CFC* method results in order to identify the component reporting similar values of deterioration throughout the *CFC*s and if those results are backed up by a distinctive GPA-index among the rest of the *CFC*s. An average of the five GPA-index and estimated degradations are calculated.

In the case any of the *CFC*s do not reach convergence, frequently noticed when estimated degradation values of 6% (an artificial limit inside *PYTHIA* code) are reported, it is removed before the final analysis is carried out as explained beforehand. Next, the results of the analyses on four of the engine components are presented in condensed form using the averages values for GPA-indexes and degradations.

Table 5.2 Component Fault Cases

No.	*CFC*	No.	*CFC*
1	C1	9	C1+T2
2	C2	10	C2+B
3	B	11	C2+T1
4	T1	12	C2+T2
5	T2	13	B+T1
6	C1+C2	14	B+T2
7	C1+B	15	T1+T2
8	C1+T1		

Figure 5-41 to Figure 5-44 depict the results for the cases where the degradation was implanted on C1 and C2. The first particularity about the solutions presented is the narrow gap between the GPA-indexes of the component with the implanted degradation and the rest of components. In *Case I*, the averaged non-linear predicted solution for C1 is 0.9671 closely followed by C2 with 0.8978. Section 5.4.3 discussed the fact any diagnostic case, regardless for sensor or engine component analysis, presenting GPA-index values above 0.8 could be considered as a conclusive or significant case. However, the picture presented in this case challenges that same guideline, not because of failure to reach the minimum required mark but for the fact ALL components

surpassed it. C*ase II* results present the same behaviour where the rear section of the compressor (C2) is associated with a GPA-index of 0.977 while C1 obtains a value of 0.8785. This situation may be caused the limited set of available measurements that reduce the ability of GPA as mentioned in section 5.4.1.

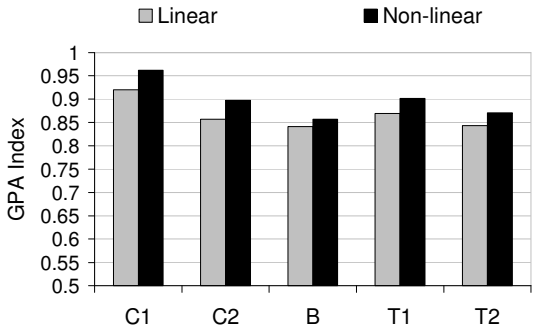

Figure 5-41 GPA Index component diagnostics results for Case I

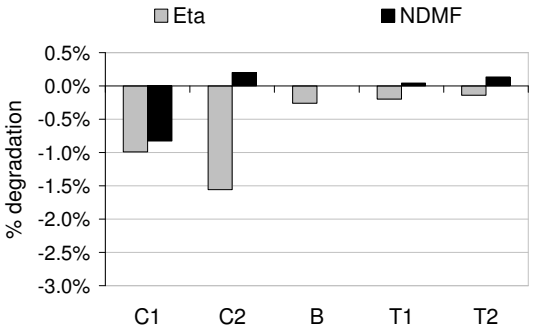

Figure 5-42 Non-linear predicted degradation for Case I

The magnitude of the predicted degradation for both cases is within a respectable range from the exact value of the implanted degradation. In *Case I*, the *CFC* method produces an exact approximation of the degradation of isentropic efficiency at the same time that underestimates the loss of capacity in nearly 20% (-0.99% η and -0.827% Γ). It is worth notice there is a risk of considering the degradation on C2 (-1.55% η) an authentic prediction since it is supported by a rather high GPA-index. It is only after looking into the results of every *CFC* calculated that the prediction is discarded on the grounds of inconsistency. The magnitude of the estimation is different for every *CFC* (-1.5%, -0.36%, -1.44%, -2.5% and -2% η), and it was the combination of low and high values that produced a credible averaged figure. In contrast, the deterioration estimates for C1 kept a fairly constant value throughout the *CFC*s.

The solution for *Case II* presents an overestimation of isentropic efficiency degradation of 50% contrasted by an exact estimation of capacity loss (-1.614%η and -1.06% Γ).

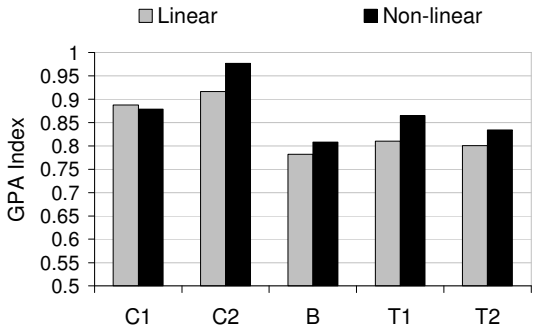

Figure 5-43 GPA Index component diagnostics results for Case II

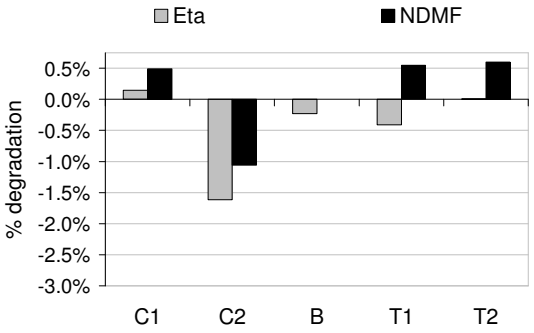

Figure 5-44 Non-linear predicted degradation for Case II

Case III presents a more favourable scenario that facilitates the interpretation of the results (see Figure 5-45 and Figure 5-46). A GPA-index of 0.9438 and a prediction of -1.185% η and -0.859% are correctly conferred to T1. In this case, the difference between T1 and the component with the second best GPA-index value (C1) is more noticeable. In *Case IV* results show even a more accurate prediction of the degradation on the correct component T2 with values of -1.023% η and -0.987 Γ supported by a dominant GPA-index value of 0.98 (Figure 5-47 and Figure 5-48). It is worth mention the accuracy of the diagnostic is result of the number of measurements at the hot end of the engine that successfully describe the performance of the power turbine, which improve the functioning of the *CFC* method.

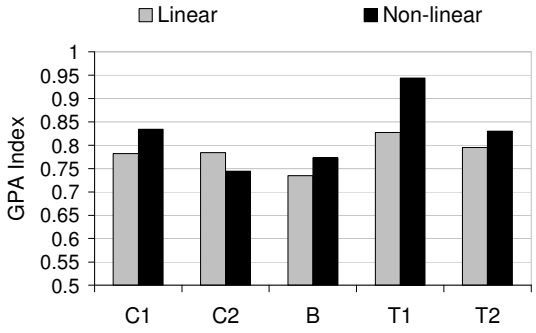

Figure 5-45 GPA index component diagnostics results for Case III

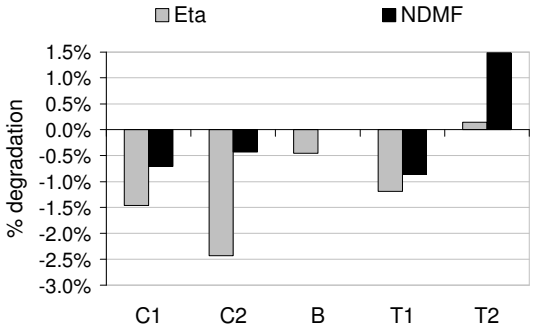

Figure 5-46 Non-linear predicted degradation for Case III

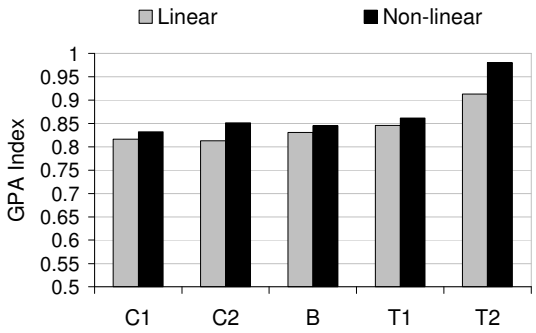

Figure 5-47 GPA index component diagnostics results for Case IV

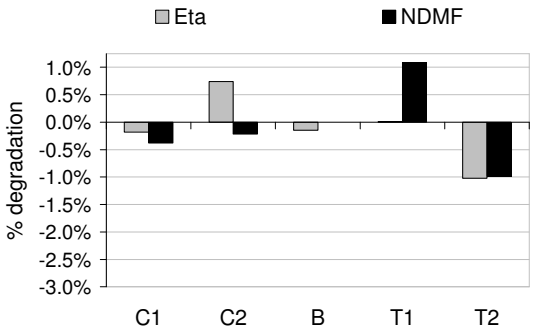

Figure 5-48 Non-linear predicted degradation for Case IV

The following conclusions can be drawn on the *CFC* method ability to isolate and quantify previously known single component degradation. Errors in the magnitude of the predicted degradation are expected for all but the power turbine component. The prediction could only be improved if a more complete set of measurements is available for diagnostic. Finally, as mentioned by Doel [170], it is a task of the analyst to discern between useful and worthless information before providing a final recommendation as there is not such as an infallible diagnostic technique.

5.6.4 Guidelines

A set of guidelines based on the observations and conclusions reach during the assessment of the *SFC* and *CFC* diagnostic methods are presented here. The intention of this section is to facilitate the application of the diagnostic tools described in this chapter to future analysts. The guidelines are found next:

Data noise:

- Noise signals of up to 1% the mean value of a measurement do not affect the result of the diagnostic method.
- The noise reduction technique implemented in *PYTHIA* provides a good filtering capability as proven in section 5.6.2.3.1 and section 5.6.3.1.2.

Power settings:

- The deviation in performance caused by power settings different to the baseline conditions can not be effectively corrected using the data validation techniques implemented in *PYTHIA*.
- The sensor fault diagnostics module delivers acceptable results with data presenting deviations up to 1MW from baseline conditions (section 5.6.2.3.4).
- The engine component diagnostics method fails to provide satisfactory results when a deviation in power settings in present in the analysed data (refer to section 5.6.3.1.2).
- Hence, field data can not be recorded at power settings other than those similar to the baseline performance or the accuracy of the method is dramatically reduced.

Ambient conditions:

- The deviation in ambient conditions i.e. temperature and pressure from baseline performance have a limited effect on the diagnostic results as reported in section 5.6.2.3.3 and section 5.6.3.1.2.
- The initial correction of performance deviation provides a good filtering tool for performance deviations caused by ambient conditions.
- Hence, field data can be recorded at ambient temperature and pressure different to that of the baseline performance.

Sensor fault diagnostics:

- An effective set of searching components C1+T1+T2 that has the potential to isolate fault sensors in the cold and hot sections of the engine was discovered (refer to section 5.6.2.3.4).

Engine component diagnostic:

- The accuracy of the component diagnostic method is limited by the number of measurements available. Degradations on the hot section of the engine are more likely to be correctly isolated and quantified than those on the cold section (see section 5.6.3.1.4).
- The need of a highly accurate off-design engine performance simulation tool is vital for the correct assessment of the engine's health.

5.7 Summary

This chapter presented an introductory review of different gas turbine engine performance diagnostics techniques including the traditional techniques such as oil, vibration and acoustics, optical and visual analyses, and more advanced performance-based techniques including gas path analysis (GPA), neural networks, genetic algorithms, fuzzy logic among others.

A more detailed description of the GPA technique concept and its advantages and weaknesses was carried out. The mathematical background behind the method was revised and extended into the non-linear solution of the system using a method introduced in Escher and Singh [160]. The importance of data validation techniques for the successful implementation of GPA was highlighted and some available methods discussed.

PYTHIA, a computational tool for engine performance simulation and diagnostics developed at Cranfield University was reviewed. The most important modules within the tool were briefly described.

A complete analysis of the sensor and engine component diagnostics modules applied to MEA's LM2500+ engines was carried out. A progressive assessment of the required conditions to increase the methods' accuracy and reliability including ambient and operating deviations from baseline conditions, data noise, sensor bias location and magnitude and implanted degradation magnitude and location was made. Finally, a set of guidelines for the recollection of data and interpretation of results was found.

SECTION III

PLANT MANAGEMENT

Chapter 6 CCGT Operations Optimisation and Risk Management

6.1 Introduction

In commodity-like electricity markets, such as that in the UK, power generation companies trade their production through the System Operator into the wholesale markets. Sellers and buyers in the market must define their trading position before the gate closure (half hour ahead of the delivery time). The gate closure period allows a system operator, such as National Grid in the UK, to go through a complex network balancing process and to settle any imbalance contracts just before time when supply and demand must meet.

The process to resolve any imbalances can be pushed from either the supply or demand sides. Nevertheless, any correction to a company's reported position involves a financial penalty. The optimisation of the operation processes of a power generation company will aim to reduce any variability in the production levels and to avoid any penalties derived from reduced reliability and availability values.

The commodity-like electricity markets carry the volatility of the other energy markets (oil and gas) into play. All participants in the market, either buyers or market makers, should implement a sensible risk management strategy (or strategies) to hedge their operations against the different types of risk.

This chapter conducts an economic assessment of the operations of a CCGT power plant similar to MEA's Pulrose plant and suggests appropriate optimisation strategies to increase the profitability of the business (see section 6.6). Additionally, a list of short and long term risk management strategies are proposed to protect the business from market and operating volatility (see section 6.7).

A brief description of the concepts of the wholesale markets structure, spark spread, risk sources and risk management instruments and services is found in section 6.4. The further development of the CCGT performance simulation program described in Chapter 4 to estimate the economic performance of the plant using the spark spread concept is described in section 6.5.

6.2 Nomenclature

BM	Balance Mechanism
BSC	Balance and Settlement Code
C	Costs, Cable losses
CCGT	Combined Cycle Gas Turbine
E	Electricity Price
F	Forward or future price
FPN	Final Physical Notifications
G	Gas Price
HPT	High Pressure Turbine

HR	Heat Rate
HSPT	High Speed Power Turbine
I	Gas Interconnector
I/O	Input and Output
IPP	Independent Power Producer
K	Strike price
M	Maintenance costs
MEA	Manx Electricity Authority
MMBtu	Million-BTU
MWh	MegaWatt-Hour
NETA	New Electricity Trading Agreement for England and Wales
O&M	Operations and Maintenance
OTC	Over-the-counter
P	Price
p	Pence
S	Transco costs
S	Electricity Spot price
SBP	System Buying Price
SSP	System Selling Price
T&D	Transmission and Distribution
T	Expiration time
th	Therm
UKPX	UK Power Exchange
VBA	Visual Basic for Applications

Greek letters

η_{th}	Thermal efficiency

Subscripts

e	Electricity
g	Gas
H	Heat rate
T	Expiration time

6.3 Literature review

The use of thermo-economic models to assess the performance of different generation technologies has become a usual practice in the power industry. A large number of publications are devoted to the preliminary-design optimisation of entire power plants [5, 233, 234] or single components [235-237]. In most cases, the technical performance results are used to simulate the operating cash flows of the plant and to subsequently evaluate the financial performance of the project. Traverso and Massardo [233] conducts a comparative analysis a number of generation technologies looking for the best technical specifications to improve the internal rate of return in hypothetical power generation projects. Valdes [236] conducts a parametric optimisation of a steam generator using genetic algorithms to evaluate its effect on the overall combined cycle plant economic performance. Most of the before mentioned work is done to serve the origination end of power generation projects rather than the operators.

Research oriented to the demand side of the power generation technology is also abundant. Although, the main ideas have a more practical approach: how to start-up and shut-down an engine the most efficient way to reduce emissions [238] or how to assess the economic impact of the part load operation of a small generation unit in a hotel [239]. This may sound "ordinary" but it would demand more advanced technical simulation capabilities than those used for research work destined for the origination side. Commercial software such as GateCycle [5] Thermoflow [6], EtaPro [7], among others have the power to deliver the needed information to both ends of the market.

A more common research topic is the optimisation of the generation schedule also called load factor management. Research work in this area normally fall into two categories: the computer-based system using advanced optimisation algorithms such as genetic algorithms, fuzzy logic, neural networks, or, the knowledge-based approach that uses the operator experience to create a scenario database [240-242]. Ultimately, decisions inside power generation companies, more frequently in medium and small companies like MEA, are taken by humans. Practitioners in the power industry use the spark spread concept as an effective and fast way to assess the economic viability of the plant.

6.4 Theoretical background

6.4.1.1 Operating in commodity-type electricity markets

The UK wholesale market was design to facilitate the trading between generators, supplier, traders and customers. NETA wholesale market has four main stages: the forwards and futures markets, the short-term power exchanges, a Balancing Mechanism and a new imbalance settlement process [243].

6.4.1.1.1 Forwards and futures markets

The forwards and futures market is a dedicated space for trading contracts between parties. The ranges of these contracts vary from 1 or more years ahead to 24 hours ahead of real time. Contracts can be places using remote means i.e. telephone or internet, and through power traders or brokers.

The forwards and futures market takes advantage from the price transparency provided by the spot markets. The intention of this market is to reduce volatility by providing the system operator the data for to forecast of the load and to plan future supply strategies. Many kinds of derivatives are traded in this market: simple weather derivatives or more advanced contracts.

6.4.1.1.2 Power exchanges

The UK power exchange (UKPX) offers physical electricity contracts for trading on its 24x7 electronic platform. The spot market is used for balancing and trading purposes and consists of half-hourly contracts of electricity as well as discrete standardised block

made up of the individual half hours. All spot contracts traded on the Eurolight platform are automatically cleared and notified [244].

6.4.1.1.3 Balancing mechanism

The Balancing Mechanism (BM) exists to ensure that supply and demand can be continuously matched in real time by the system operator. The BM operates from gate closure through to real time. The gate closure is set to one hour before real time. The system operator needs to be able to assess the physical position of market participants as the market moves towards the balancing stage to ensure that security of supply is maintained. All market participants must inform National Grid Co of their net physical flows both in the forward and futures contract markets and power exchanges.

The final physical notifications (FPN) provide a baseline for bids and offers to the BM from generators and from the demand side. The system operator purchases offers to increase generation or decrease demand and/or bids to decrease generation or increase demand, and other balancing services (ancillary services) to balance the system.

6.4.1.1.4 Imbalance settlement

After real time, the settlement system agent, Elexon, compares the contractual position of each market participant with actual metered output and demand. Any contracts taking place in the BM are settled through the Balancing and Settlement Code (BSC) process. If a generator delivered more electricity than stated on its FPN, it is said to be "long" on its position; conversely, it would be "short" when it fails to deliver the notified output at gate closure. In the first case, the generator will receive the System Selling Price (SSP) for the excess; in the second instance they will pay the System Buying Price (SBP) for the deficit. These prices, SSP and SBP, are defined to inflict a penalty on the generator or supplier without the discipline to meet their contracts in time and volume.

6.4.1.2 Operations assessment using the spark spread concept

The power plant operators in the industry use a modification of the financial spark spread concept to assess the economic viability of their operations under the existing economic and technical conditions at any point in time.

Spark spread is defined as a cross-commodity option paying out the difference between the electricity price and the cost of the fuel multiplied by the industry average heat rate. The financial industry defines the spark spread [245] using the operating heat rate (HR)of the plant in MMBtu/MWh, the electricity price in £/MWh (P_e) and gas price in £/MMBtu (P_g) in a basic expression as follows:

$$Payoff = \max\left(P_e - HR \cdot P_g, 0\right) \qquad 6\text{-}1$$

Some practitioners in the power industry replace the heat rate with the thermal efficiency, η_{th}, a more accessible parameter calculated during the operation of the plant. In addition, two more coefficients representing different operating marginal costs are introduced [246]. C_e represents the costs incurred by the company in maintenance, T&D

and electricity trading to and from the network. On the other hand, C_g, correspond to the costs related to the transport and trade of gas

$$Payoff = \max\left(\left[P_e - C_e \right] - \left[\frac{P_g + C_g}{\eta_{th}} \right], 0 \right) \qquad 6\text{-}2$$

The spark spread can then be equated to the operating margin of the plant. A positive spark spread means there is an economic incentive to generate electricity from fuel bought at price P_g and selling it to the system at price P_e. On the other hand, a negative spark spread would indicate there is no profit to be made from the operation of the plant for the existing market conditions [247, 248]. Therefore, it will make more sense to sell the gas back into the system. The concept provide useful insights of the particular power generation assets to potential investors, therefore, it can be used as an effective way to value power generation assets [249-251].

It is important to highlight that the non-linearity of the generation assets have a direct impact on the O&M costs. The start up, shut down, ramping up/down, engine degradation, and ambient atmospheric conditions have an effect on the marginal operating costs, hence, the nominally reported spark spread value may differ from the actual value. High resolution generation optimisation models are needed to more accurately approximate the true spark spread on an asset.

In the case of the Manx Electricity Authority (MEA), a negative spark spread would send an economic signal to import power through an interconnector cable to the UK while a positive spread would indicate that it would profitable to generate directly from the CCGT and export the surplus to the UK, provided the bilateral contracts are in place.

As mentioned earlier, the formula for the spark spread used by practitioners in the power generation industry considers extra operating costs variables that give the spark spread a more robust structure. The following is a list of these costs, followed by the actual expression used:

1. Actual electricity (export) price in £/MWh (E)
2. Cable losses and charges in % (C)
3. Actual gas price (import) in p/th (G)
4. Transco's variable costs between NBP and Moffat in p/th (S)
5. Gas Interconnector commodity charge in p/th (I)
6. CCGT variable maintenance costs in £/MWh (M)
7. Thermal efficiency (η_{th})
8. Gas price "swing" factor in p/th (P)

Hence,

$$\Pr ofit / Loss = \left[E - C - M \right] - \left[\frac{\left(G + S + I + P \right) \cdot 0.3412}{\eta_{th}} \right] \qquad 6\text{-}3$$

- **Gas price swing factor (P)**

The gas contracts are normally quoted with a 'swing' factor, which allows for a variable amount of gas to be taken within defined limits. A 110/90 swing factor will allow for a minimum take of 90% of the nominal volume, and a 110% for the maximum take. A 110/90 can also be defined as a 22% swing factor (1.22 = 110/90). It is obvious a premium is charged for 'swing'.

- **Gas Interconnector commodity charge (I)**

The interconnector commodity charge is the additional cost for the transport of gas to the Isle of Man. A foreign exchange risk can be present if the payment is made in a foreign currency. However, exchange rate risk can be fixed by hedging risk in the foreign exchange market.

- **Thermal efficiency (ηth)**

The thermal efficiency value used in the power industry is 49%. Nevertheless, this parameter is very sensitive to the atmospheric and operating conditions, and can be down to 39% when the plant is run in an open Brayton cycle.

6.4.1.3 Electricity markets risk sources

6.4.1.3.1 Market risk

The liberalization of the electricity markets during the last decade brought big changes to the industry. The paradigm of buying and selling electricity from the vertically integrated companies in a regulated market with captive consumers changed to a more commodity-like trading of the electricity at different forwards and futures markets and spot power exchanges where the physical and financial domains meet [252].

The deregulation of the electricity industry had the intention to expose the industry to the market forces. Competition would drive the energy prices down, add transparency to the market, increase the demand side responsiveness and encourage the investment in new technology. In the case of investment in generation capacity – the more capital intensive sector of the industry – the abolition of the regulated rate of return price caps would transfer the capital risks from the consumers to the shareholders. In theory the liberalisation of the electricity markets was the right move to foster economic growth by allowing the energy intensive firms to increase their competitiveness in the global market. These economic benefits would reach the end consumers introducing a choice of the supplier companies [253].

In reality, poor design and deficient implementation brought negative even catastrophic consequences for the country or region [254], UK [255] and California [256] markets respectively. From these mistakes, the formula for a successful liberalisation of the electricity markets was learned (handle with care!).

In order to have a successful story in the liberalisation of an electricity market the following points should be addressed: a) a healthy capacity margin must exist at the time of the liberalisation, b) the power exchanges must deliver price transparency to the

participants, and c) the bulk of the electricity has to be traded at the futures and forwards markets.

If all these requirements are met, the price volatility will remain at bay, there will be no capacity shortages, transmission congestion can be controlled to a safe level avoiding market power abuse in the isolated regions, the future and forward markets will blossom. At the end it is important to recognize that volatility and risk are intrinsic characteristics of a liberalised market, as confirmed by any other commodity and energy markets.

6.4.1.3.2 Financial risk

The market reforms have partially shifted the investment risk from the consumers to the producers. Ideally, shareholders bear all the investment risk and consumers bear the price risk. In reality, market imperfections such as lack of demand reaction, abuse of locational market power, and political resistance to high prices, have made the regulators to introduce price caps and capacity payments. These extra regulatory measures allocate risks between consumers and producers by limiting price volatility for consumers and assuring investment cost recovery for generators.

6.4.1.3.3 Operating risk

The procurement of the production inputs (fuel, spare parts, sensors, etc), a vital element within the operations of a company, defines the operating costs, therefore, the electricity tariffs. From all the inputs, fuel is the most important as it accounts for a substantial percentage of what the end user pays. Unfortunately, the characteristics of the fuel markets, commodity type markets, make it a volatile product with direct impact on the production costs.

6.4.1.4 Risk management instruments and services

Risk management is probably the most common activity related to the trading industry. It responds to the development of competitive markets with healthy power exchanges and futures and forwards markets that brought an end to the regulated markets with their fixed prices and long-term contracts. The volatile character of electricity and the complicated systems and their operation have contributed to the emergence of the power marketers' products and services.

This section introduces some of the financial and physical instruments used in risk management and hedging by marketers. The information suits to organized exchanges and over-the-counter (OTC) markets. In the US, most of the futures and options on futures contracts are traded at exchanges. The diversity of contracts at OTC markets include forwards, swaps, plain vanilla options, and exotic options like spark spread options.

6.4.1.4.1 Risk management services

The electricity industry reform has contributed to the proliferation of electricity trading companies that operate in the newly formed wholesale and retail markets [257, 258]. In regulated electricity markets with long-term contracts with fixed prices and captive consumers there is not any need for trading and risk management services. These services are only justifiable in liberalized markets where prices are mostly determined by market forces i.e. supply and demand, expectations of future supply and demand, and regional or temporal price variations. The most important factor driving the demand for trading and risk management services, however, is price volatility [257].

The risk management services in the electricity market are relatively new, but they are leveraged by the large experience from the older energy and capital markets that developed the financial tools and techniques to get the job done [259, 260]. Some of the financial/physical instruments used in the electricity markets are the electricity forwards, electricity futures, electricity swaps and plain and exotic electricity options. Forward contracts are the most popular instruments since they provide a fixed price framework similar to the conditions in the regulated markets, which can be easily managed by market players. Whereas the more advanced options contracts are being used to hedge output and price volatilities and to value assets and infrastructure [261].

The products and services offered by the marketers to their clients are designed to fit specific needs ranging from asset management to business performance. Some customized services are designed to address a particular concern, to cover a menacing risk exposure, or to finance a complicated transaction. Other services deliver vital information that otherwise will be unreachable or would signify higher costs. Transaction management and liquidity are also available to their clients with anonymity, when it is desired. A more detailed description of these services is found next:

> The *facilities management services* aim to improve the utilisation, maintenance, and operation of the assets, plants, infrastructure, and personnel. These services are usually offered in a bundle with traditional trading advice and management. The savings from the improved operations are usually shared among the two parties in equal shares or, when the marketer absorbs the development costs, the marketer obtains a high percentage.
>
> The *total energy services and solutions* look to reduce overall energy costs by a careful selection of input fuels (natural gas, diesel, etc) and end-use energy (electricity, heating, steam, etc) that increase the thermal efficiency of the asset, plants, etc. The risk level associated with these products is limited.
>
> The traders provide the popular *risk management services* that provide price stability and risk hedging to their clients. Usually, lack of knowledge and/or limited resources at the companies forces them to rely on the marketers to develop their risk management strategy. The following section provides a description of the most common instruments used with this purposes.
>
> *Tolling contracts* are similar to a common electricity supply contract signed between a buyer i.e. power marketer, and an owner of a power plant but with

notable differences. For a upfront premium paid to the plant owner gives to the buyer the right to either operate and control the scheduling the power plant with the ISO or simple take the output electricity during pre-specified time period subject to certain constraints [247].

The demand for *structured or customized services* has risen as more sophisticated clients look for new solutions to their needs. They require extensive effort to negotiate and consummate, and could easily include a group of clients across industries.

6.4.1.4.2 Electricity forwards

Electricity forwards contracts represent the obligation to buy or sell a fixed amount of electricity at a pre-specified contract price, known as the forward price, at certain time in the future, called expiration time. The payoff of a forward with a forward price F at a future T is

$$Payoff = (S_T - F) \qquad 6\text{-}4$$

where S_T is the electricity spot price at time T. The particularity of electricity forwards is that the underlying asset, in this case the electricity, and its price are not fixed-in-time and constant. The underlying asset price change in the power exchange during the delivery time. The S_T is calculated using the average of the spot prices at expiration time T.

Independent power producers (IPPs) are the natural sellers (short position) and the suppliers and retail companies are the buyers (long position). Some of the forwards contracts are only financial contracts, which are settled through financial payments. The forwards contracts are the primary instruments used in electricity price risk management.

6.4.1.4.3 Electricity futures

Futures contracts are similar to the forward contracts in the payoff structure. The contracts are highly structured in specifications, transaction requirements and settlement procedures. Another characteristic of the futures contracts is that the volume traded is significantly smaller than that in the forwards contracts.

Futures contracts have some advantages over forwards contracts. They can only be traded on organized exchanges reducing the risk of any counterpart default. Futures provide market transparency and lower transactions costs as they can only be settled with a financial payment as they are considered to be a derivative instrument of the power spot market. Unfortunately, they present some rigidity in the specifications and volumes allowed.

6.4.1.4.4 Electricity swaps

Electricity swaps are financial contracts that enable their holders to pay a fixed price for the underlying electricity, regardless any price volatility, over the contracted time period. The opposite is also possible when selling the electricity. They are referenced to a variable spot price at either the generator's or consumer's location. Electricity swaps can be viewed as a strip of forwards contracts with multiple expiration times and the same forwards price.

Electricity locational basis swaps are also commonly used to fix the price of the electricity at a geographic location that is different from the delivery point of a futures contract. These contracts are useful to hedge the price difference of spot prices at two different locations.

6.4.1.4.5 Electricity options

It was not until the liberalisation of the UK, US and Nordic markets that options contracts started to be widely used. The emergence of the wholesale markets during the 1990s and the dispersion of the option concept and risk management techniques have created a varied range of options. They are not only based on the underlying price anymore but also other attributes like volume, delivery location and timing, quality, and fuel type.

Plain call and put options

Electricity call and put options offer their purchases the right, but not the obligation, to buy or sell a fixed amount of underlying electricity at a pre-specified strike price by the option expiration date. The payoff of an electricity call option with K strike price at maturity time T is

$$Payoff = \max(S_T - K, 0) \qquad 6\text{-}5$$

where S_T is the electricity spot price at time T. The underlying asset can be either an exchange-traded electricity futures or physical electricity. The options are popular as an effective tool to merchant power plants and power marketers for hedging price risk because generation capacities can be catalogued as real options.

Spark spread options

Spark spread are cross-commodity options paying out the difference between the electricity price and the cost of the fuel and other variable operating costs multiplied by a given generation plant's heat rate. The amount of fuel required to generate a unit of electricity is linked to the plant's thermal efficiency. The heat rate, the inverse quantity of the thermal efficiency, hence is defined as the ratio between the heat input and the power output.

The holder of a European spark spread call option written on fuel G at a fixed or strike heat rate K_H has the right, but not the obligation, to pay at the option's maturity K_H time the fuel price at maturity time T and receive the price of one unit of electricity [249]. Thus the payoff at maturity time T is

$$Payoff = \max(S_T - K_H \cdot G_T, 0) \qquad 6\text{-}6$$

where S_T and G_T are the electricity and fuel prices at time T, respectively. The spark spread options are an effective tool when hedging the price risk of the output electricity.

From the operational point of view this quantity is of interest as it reflects the operating margin of the plant. A simple interpretation would suggests that when the spark spread is positive it is profitable to generate electricity using fuel at the current prices and dispatching it into the system, while a negative spark spread would indicate a loss [248]. Even if the start up and ramping costs are not included in the calculations, the signals given by this instrument present useful insights into the economic reliability of power generation capacity. This information on the hands of potential investors can be then used as an effective way to value power generation facilities [247, 250].

6.5 Computational tool

This section described the general characteristics of a new module of the eCCGT program developed to carry out the economic performance calculations of the plant. As part of the eCCGT system it was programmed using Visual Basic for Applications (VBA) compiler. This module was designed to maintain an effective connectivity with existing subroutines and user forms.

The *spark spread* module contains the subroutine of the same name where the calculations for the baseline, day and night spark spread are made. The *spark spread* subroutine can be accessed in two ways: a) as part of the main *Control* logic, or b) as a stand alone subroutine. In either way, two subroutines are responsible of the input and output (I/O) of the data to and from the subroutine: *LoadSS (or LoadSSVariable*) and *PrintSS*. The I/O subroutines are found in the *PrintResults* module.

Figure 6-1 depicts the improved flow chart for the *Control* subroutine. The spark spread calculations are performed for every case study after the program completes the estimation of the technical performance of the plant. The *LoadSS* subroutine retrieves all values used from the spark spread user-form (see Figure 6-2) except the thermal efficiency of the plant which is extracted from the *Main* spreadsheet. Once the spark spread subroutine ends, the *PrintSS* subroutine put the results onto the *Main* spreadsheet.

In the case the *sparkspread* subroutine is called from the user-form with the same name (see Figure 6-3), the user has the option to choose between constant and variable values of electricity and gas prices for each case study. While the “constant” option follows the same routine explained before, the “variable” option extracts the electricity and gas prices and thermal efficiency from the *Main* spreadsheet.

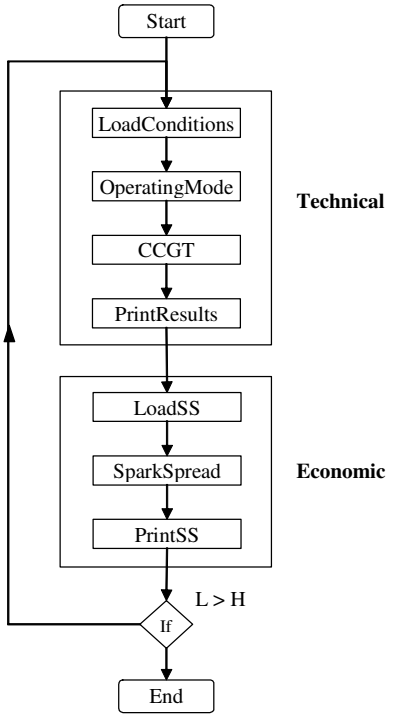

Figure 6-1 Improved Control subroutine flow chart

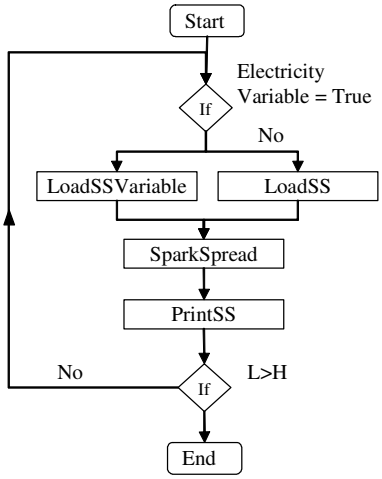

Figure 6-2 Spark spread stand alone action flow chart

Following the same design philosophy used for the technical modules of the eCCGT program, the *spark spread* user form was developed to avoid the saturation of the *Main* spreadsheet with columns input and output data.

The form is displayed with the action button of the same name. It allows the user to modify the value of every parameters from equation 6-3, and in the case of the electricity and gas prices, an option button indicates if the spark spread calculations will use constant or variable values for each of the case studies. Once the analysis conditions are defined by the user, the *Calculate* button launches a small window where the numbers of cases are type in by the user.

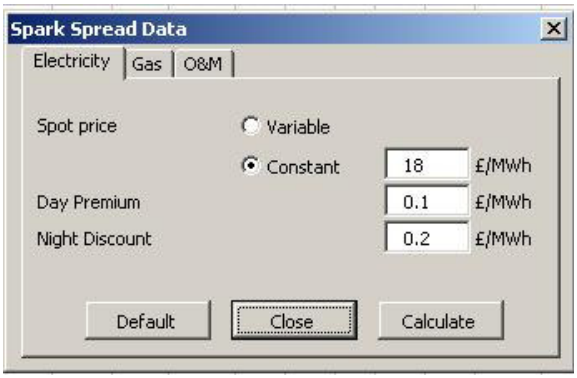

Figure 6-3 Spark Spread user form

6.6 Operations optimisation

This section presents the successful implementation of the CCGT performance simulation tool (see Chapter 5) in the optimisation of the operations of a CCGT power station similar to MEA's Pulrose Plant. Additionally, the potential economic benefit of an advanced gas turbine engine diagnostic system such as Pythia is demonstrated.

The baseline economic performance of the plant is estimated for a cold day of winter 2007 is established. Three optimisation strategies are developed based on the simulation results obtained from the performance simulation program eCCGT.

6.6.1 Baseline performance

The baseline economic performance of the power station is calculated using the results from the technical simulation of the plant presented in Chapter 4. The spark spread is estimated using a variable price for the electricity. Obviously, this assumption can only be made if the economic analysis is retrospective in nature. For future based analysis, a detailed forecast of the power market main variables is required. The development or implementation of any forecasting tools is out of the scope of this project but it can be an excellent opportunity to develop the system capabilities further.

The electricity and gas prices used for the simulation are shown in Figure 6-4 and Figure 6-5, respectively. The electricity price is the System Sell Price (SSP) in £/MWh for the UK power market for that particular day. The price follows the normal trend of peak and off-peak prices. The low demand of electricity during night time (off-peak) increases the available supply pushing the price down close to an operating cost average of the entire system. After 06:00 hrs the demand starts to rise and with it the price for electricity, reaching a value around 40 £/MWh around 9:00 hrs. The maximum of the day normally comes between 18:00 and 20:00 hrs that coincides with the end of a normal working week day. After the peak, the price gradually falls to values experienced during the night.

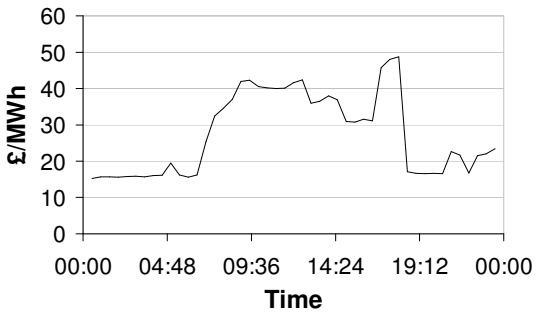

Figure 6-4 System Selling Price (SSB)

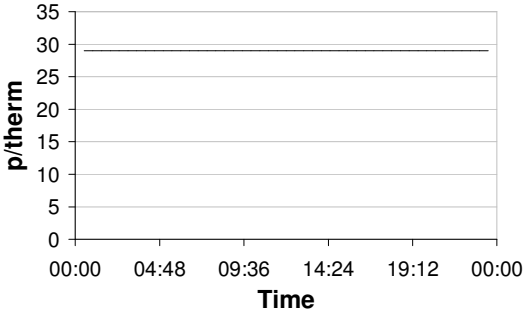

Figure 6-5 Gas price

In the case of the gas, a fixed price of 29 p/therm was used. It is extremely rare to see a change in gas price for immediate delivery. A variation in price could be experienced if gas is bought at the spot market during a dynamic week. When gas is bought through a

series of forward or futures contracts the price can remain constant over a number of weeks and even months.

The eCCGT program retrieves the value for the thermal efficiency and electricity price for each of the 48 half-hour time blocks to construct the profit/loss daily schedule. The results are presented as ratio of the actual profit (or loss) to the total operating profit of the day (see Figure 6-6).

Inevitably, the generation of electricity during the off-peak period translates into a loss. There is not a single block during the off-peak period where the plant can at least break even. The spark spread definition would advice to shut down the power plant during the off-peak time, however, technical and even political circumstances can affect the decision to generate at a loss. On the other hand, the rise in electricity price during the peak time turns the fate of the plant around delivering a healthy profit margin.

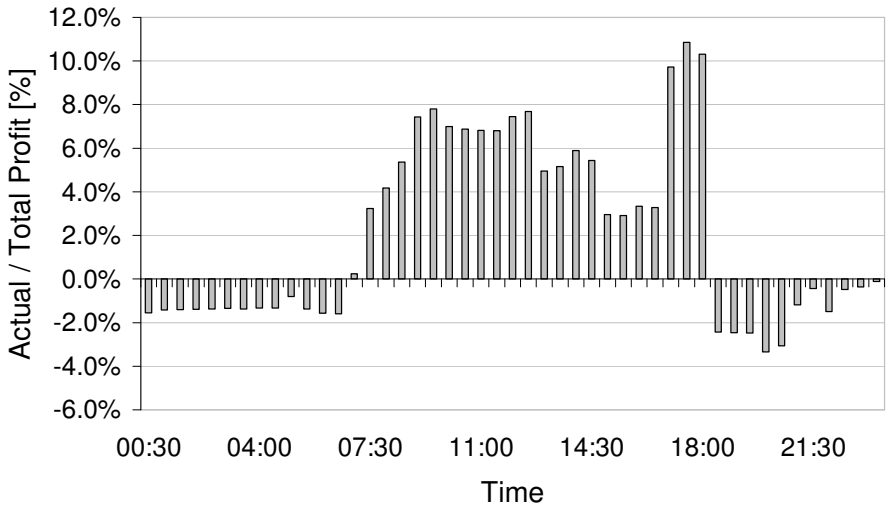

Figure 6-6 Baseline economic performance for a cold day winter 2007

6.6.2 Optimisation strategy 1: Emissions abatement system

The aim of this section is to present a real opportunity to increase the profitability of the plant through a simple change in the technical operation of the plant.

The emissions abatement system used with MEA's LM2500+ engines increases the fuel consumption, therefore, reducing the operating margin of the plant. Since MEA operates within the flexible environmental regulations of the Isle of Man, there is a possibility to switch off the emissions abatement system during days or months when the power markets present a thin spark spread.

Figure 6-7 shows the difference in profit/loss daily schedule between the baseline and the outcome of following this strategy. The total savings derived are approximately

£1100/day or £33000/month under the particular ambient, operating and market conditions.

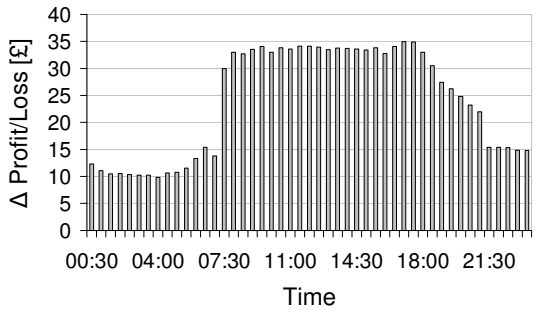

Figure 6-7 Saving/Loss from optimisation strategy 1

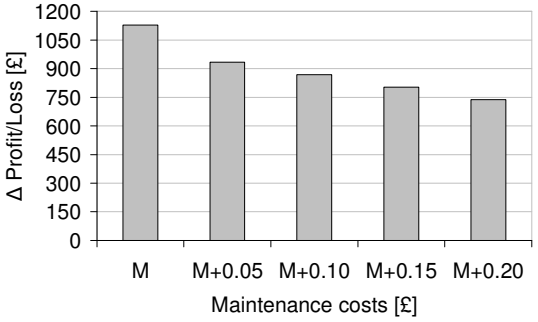

Figure 6-8 Variation in saving/loss for an increase in maintenance costs (M)

It is worth notice, the operation of the gas turbine engine without the injection of water at the combustor increases the temperatures at the hot section of the engine. Higher temperatures reduce the life of the components increasing the maintenance costs per unit generated. Ultimately, this reduction in operating life of the engines can affect the reliability and availability of the plant.

When an increase in maintenance costs of the plant (*M*) is considered as secondary effect of the "polluting" strategy the net savings will drop (see Figure 6-8). For example, an increase in *M* of £0.20 per unit generated will reduced the initial benefit to only £750/day, a drop of 31% in expected savings. Hence it is important to pay attention to the bottom line of the operations as the "polluting" strategy could end in red numbers.

6.6.3 Optimisation strategy 2: Performance diagnostics system

The objective of this section is to prove the potential benefit of the implementation of an advanced diagnostic system into the operations of a CCGT power station. The effect of the engine degradation on the profitability of the plant should justify the development of a system such as Pythia (see Chapter 5) as a mean to optimise the operations of the plant.

Aware of the innacurate results obtained in section 4.6.3 the cases presented here are those which show a clearer negative effect of the compressor and hot section degradation on the cycle's performance and, consequently, the profitability of the plant.

6.6.3.1 Compressor

This section analyses the effect of the compressor degradation on the profitability of a CCGT power station. It is important to mention the simulation makes no provision for the loss in useful life of the parts at the hot end of the engine. Such conditions will eventually degrade the turbines of the engine increasing the maintenance costs considerably.

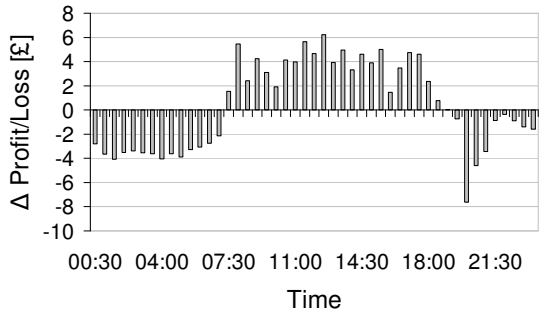

Figure 6-9 Compressor degradation 5% effect on the profit/loss

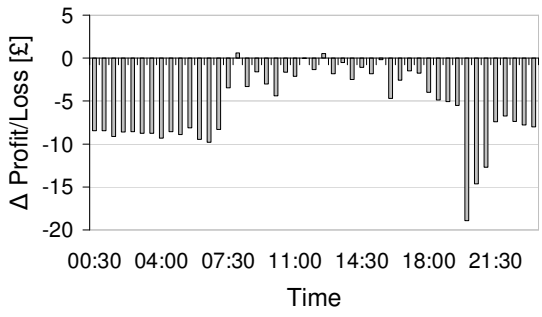

Figure 6-10 Compressor degradation 7% effect on the profit/loss

Even with the overestimation of steam production, the cases report a net loss of 60£/day and 260£/day for the 5% and 7% degradation, respectively.

The most common solutions to compressor degradation is compressor washing. There are two main categories: on-line and off-line techniques, each with their own advantages and disadvtanges. The on-line washing technique allows the operator to recuperate part of the lost efficiency whilst maintaining the production, thus, reducing the economic losses. However, this process only is able to recuperate a limited percentage of the total performance loss. Another shortcoming of the technique is the negative effect of the injected washing fluids on the combustor and hot end.

The off-line washing technique is able to recuperate most of the compressor lost efficiency since it involves a more throughly cleaning process. Obviously, the technique demands the plant to be shutdown therefore it brings an extra cost to the operation. The washing has to be performed when there is certainty the positive effect of the procedure will offset the loss in revenue. Its execution during planned outages is the common practice.

Neither the off-line nor on-line washing techniques will restore the compressor performance to its initial health condition. There is an irreversible percentage of engine's efficiency. Such losses are related to blade erosion, corrosion, seals wear out, rotor misalignment, etc.

The use of advanced diagnostics technologies can provide enough information to support any corrective or preventing decision from the operator, increasing the life of the equipment.

6.6.3.2 Turbines

The analysis considers two degradation scenarios: 2% degradation on the high pressure turbine (HPT) and 2% degradation on the high speed power turbine (HSPT). Figure 6-11 and Figure 6-12 present the results for the HPT and HSPT, respectively.

The net loss for the HPT degradation case is £63/day. On the other hand, a more considerable loss of £353/day or £10590/month comes from the operation of the plant with 2% degradation on the high speed power turbine. A significant difference is observed between the two cases in the profit/loss daily schedule of the plant. In the HPT case, the degradation reduces the profit made during the peak time and increases the loss during the off-peak periods. However, the degradation of the HSPT causes a completely inverse scenario from the baseline performance. It is during the peak time that the plant is loosing the most. This behaviour can be explained from the fact the degradation of the HSPT performance has a direct impact on the power output from the gas turbine, therefore, the higher the power output demanded from the engine the higher the losses.

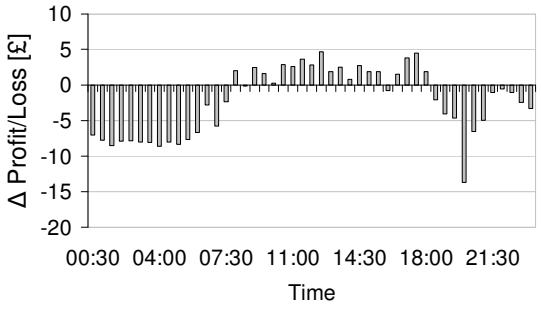

Figure 6-11 HPT degradation 2% effect on profit/loss schedule

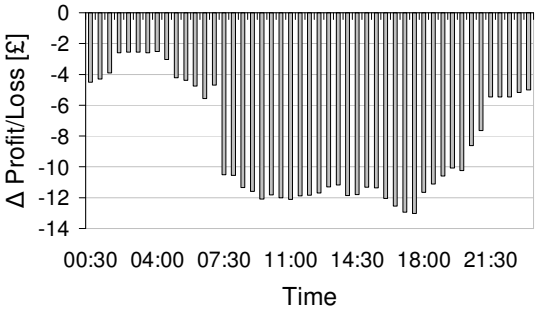

Figure 6-12 HSPT degradation 2% effect on profit/loss schedule

It is clear that no concession can be made when any component at the hot end of the engine presents a decrease in performance. Any deterioration would immediately develop into a loss. The use of an advanced diagnostics program can deliver the right information at the early stages of the degradation reducing the operating risk of the plant.

6.6.4 Optimisation strategy 3: Gas swing factor

The third optimisation strategy is intended to capitalise on the ability of the CCGT performance simulation program to estimate the total fuel consumption of the plant by reducing the gas swing factor. It is assumed the gas swing premium remains constant.

As explained in section 6.4.1.2, the gas swing factor is the product of the gas swing capacity band (in percentage) and the swing premium. The less certainty about the gas consumption of the plant the larger the swing factor has to be to avoid any penalties or excessive payments for same day delivery in the spot market (if available). The proposed strategy is looking to optimise the existing hedging strategy rather than defining a new method.

Figure 6-13 shows the fuel consumption as a ratio of actual to total fuel consumption for each time block. The accuracy of the estimation has an average error of only 0.68% as indicated in Chapter 5.

If the eCCGT program is used to forecast the fuel consumption of the plant the swing capacity band can be reduced, as a result the profitability of the plant grows (see Figure 6-14). Net savings of £281/day or £8430/month can be obtained by reducing the swing capacity band in 25%. On the contrary, a drop of £297/day in the plant's profitability is expected for an increase of 25% in the swing capacity band.

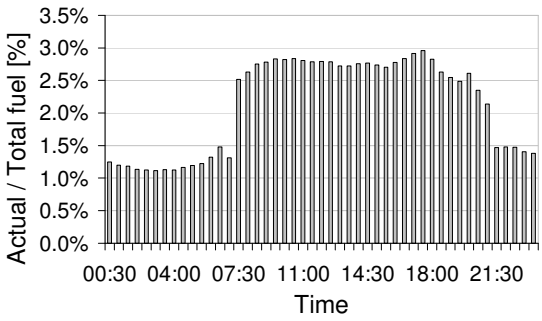

Figure 6-13 Fuel consumption schedule

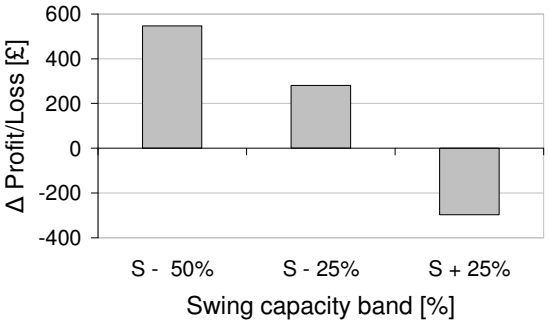

Figure 6-14 Net saving/loss from change in swing capacity band

6.7 Risk Management

The main objective of this section is to define a series of risk management strategies to hedge the operations of a CCGT power station similar to MEA's Pulrose Plant. The identification of the main economic and technical risk variables is made through a sensitivity analysis. Four hedging strategies are described: exposed operations, load factor maximisation, gas futures and gas options on futures.

6.7.1 Market vs. operating risk

The market or operating variables with the largest influence on the profitability of a power plant are the risk variables. The development of a risk management strategy aims to contain their influence on the operations of the power generation asset. In some cases the risk variables are solely driven by market forces i.e. electricity and gas, although, others are directly linked to the technical operation of the plant i.e. maintenance costs, thermal efficiency, transmission losses.

A sensitivity analysis on the plant profitability is conducted to quantify the impact of the variability of the different economic and technical parameters from the spark spread formula. The results are presented in two groups: the economic parameters and operating parameters. The economic parameters include the gas and electricity prices and the trading costs. On the other hand, the technical parameters are: the thermal efficiency of the plant (otherwise called heat rate), maintenance costs and transmission costs. Other parameters used in the spark spread calculations, either economic or technical fail to register useful variations, thus, their effect is neglected. Figure 6-15 and Figure 6-16 show the results of the sensitivity analysis for the economic and technical group, respectively, as the net profit/loss relative to the baseline performance.

The results of the economic sensitivity analysis reaffirm the major influence of electricity and gas market prices on the profitability of the plant. Both parameters outweigh the small impact of the trading costs (swing premium and swing capacity band) which are one order of magnitude below the two big variables. However, the net effect of the two variables on the operating profit is opposite. While the profitability of the price is directly proportional to the electricity price, it is inversely proportional to the gas price. In other words, with a rise in electricity market prices the operating profits of the plant will grow. Conversely, with an increase in gas market prices the profitability will drop.

For an increase in the electricity market prices of around 10% the operating profit of the plant will increase in £4000/day. On the contrary, a fall in electricity price of 10% will reduce the profitability of the plant in £4000/day, a considerable portion of the baseline profit in both cases. The concerning factor is that a variation of 10% in either way is a not so rare scenario, in fact, it is common. For example, the change in the day-ahead delivery electricity spot price from one day to the next is around 3% in late September 2007 [262].

In the case of the gas, the scenario is as dramatic as with the electricity prices. A drop in operating profit of £3700/day will come if the gas market prices increase in 14%. A similar amount of £3700/day is made if the gas market prices fall in 14%. Again, a change of this magnitude is not unusual in the gas spot market. A change of 7.13% for one day to the next is seen for the day-ahead delivery market in late September 2007 [262].

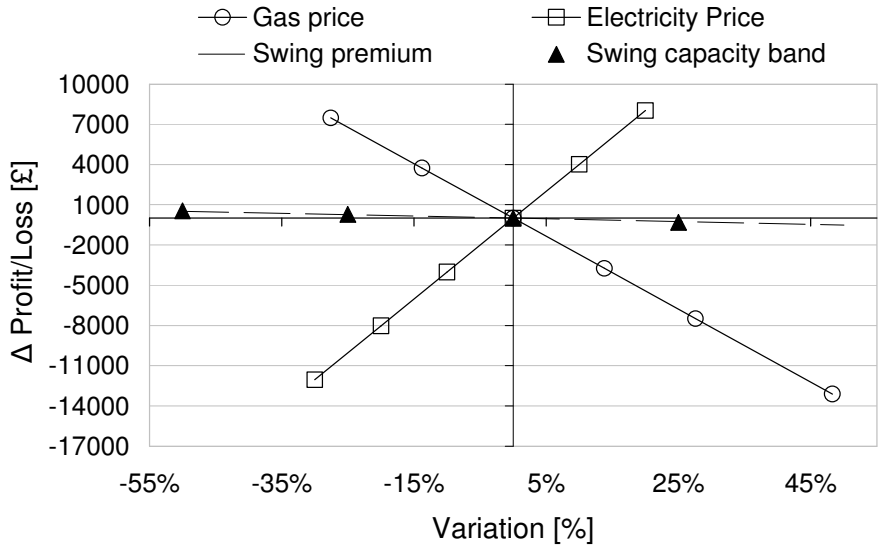

Figure 6-15 Economic sensitivity analysis

The outcome of the technical sensitivity analysis singled out the thermal efficiency as the most important variable of the group. First, the thermal efficiency is a function of the load factor of the plant. The more time the plant is operating at its full capacity the higher the thermal efficiency. Second, the thermal efficiency defines the amount of gas consumed by the plant. A reduction in thermal efficiency increases the gas consumption

of the plant, consequently, based on the results from the economic analysis, the operating profit drops, and vice versa.

The thermal efficiency has a non-linear behaviour clearly displayed in Figure 6-16. For a drop of 10% in thermal efficiency, the operating profit of the plant falls in £3150/day, whilst a reduction in 30% carries a loss of £12100/day.

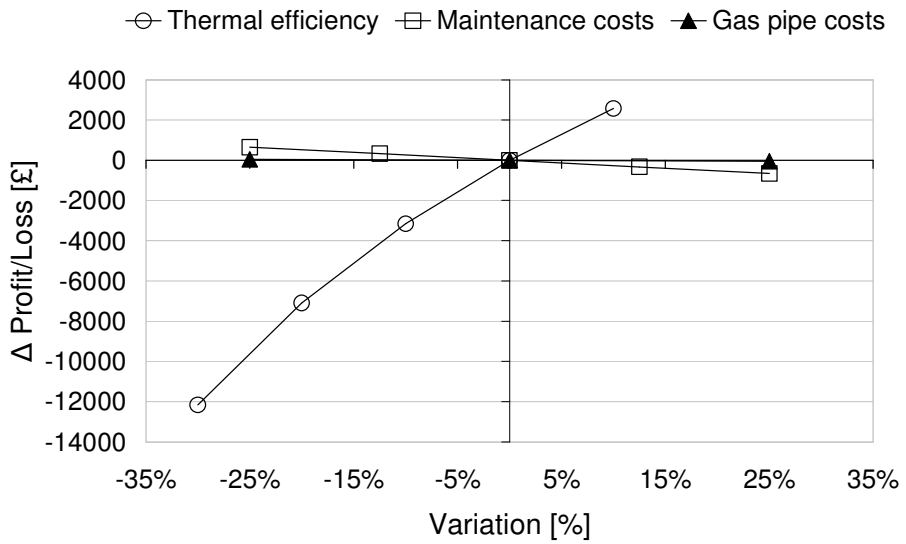

Figure 6-16 Technical sensitivity analysis

Although the rest of the economic and technical parameters are discarded as a major source of risk, they can play an important role in the operating profit. The reduction of each of these secondary costs will have a positive effect on the profitability of the plant as shown in the previous section. Once the three main risk variables have been identified some hedging strategies are proposed.

6.7.2 Risk management strategies

The proposed risk management strategies aim to hedge the operations of the power generator while preserving the "real option" attribute of the power plant. The asset operator has the "option" to generate electricity or not from the gas bought in advance. If the electricity price in the UK market is below the production costs of the plant, the asset operator would have the option to sell the gas and buy the electricity. Four strategies are described: exposed operations, load factor maximisation, gas futures and gas options on futures.

6.7.2.1 Strategy 0: Exposed operations

The risk management strategy any operator can follow is *impassiveness*. The operations will be totally exposed to the high volatility of the gas and electricity markets at a time when the short and long term scenarios of the energy markets look bleak. The security of energy issues around the world prompt to act now.

Assuming the cost structure of the operations similar to the one described with help of the spark spread definition used by practitioners at MEA (see section 6.4.1.2), the only risk management initiative in place is the fuel swing factor. This strategy is limited to protect the operations of the plant against any variation in the daily fuel consumption from the contracted values.

This type of hedging instrument is set in place when the fuel consumption of the power plant can not be forecasted with certainty. This situation is more common during the infancy of a power station when the number of disruptive events is higher. Once the availability and reliability values of the plant have settle down to normal values the fuel swing factor could be removed. Section 6.6.4 presented an optimisation of this risk management strategy by the simulation of the fuel consumption using the eCCGT program.

6.7.2.2 Strategy 1: Load factor maximisation

The strategy 1 aims to reduce the negative effect of the variation in the thermal efficiency by maximising the production of the plant. As mentioned before, the thermal efficiency is a function of the load factor of the plant. The objective is to maximise and fix the load factor of a power station that otherwise operates in part load conditions.

Figure 6-17 presents the concept of the load factor maximisation strategy. The ideal scenario will allow the operator to sell the total production capacity surplus to a third party. However, any positive variation in the local demand at time of delivery would leave the local operator with no means of supplying the excess demand as the full production surplus is tied up to the contract with the third party. A more conservative approach is the implementation of a safety capacity band to absorb any variation between actual and forecasted local demand (see Figure 6-18).

The performance of the plant under the improved generation schedule can be simulated using the eCCGT program. An accurate estimation of the fuel consumption can be used to secure the supply of gas needed to meet the production surplus and local demand.

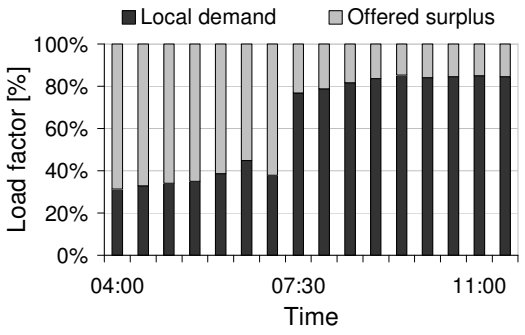

Figure 6-17 Ideal load factor maximisation strategy concept

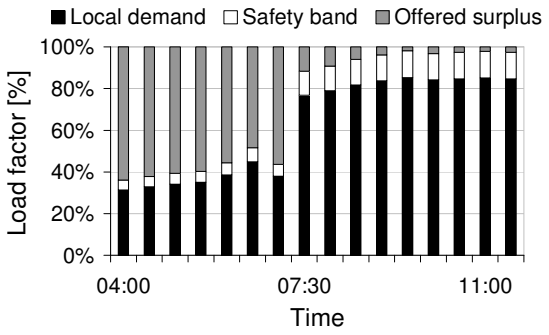

Figure 6-18 Load maximisation strategy including safety capacity band

6.7.2.3 Strategy 2: Gas futures

Futures contracts on gas or power are common risk management instruments in the power industry. The futures contracts enable the buyer to fix their fuel operating costs over a predefined number of days, weeks, months or even years.

Figure 6-19 shows the variation in the October 2007 futures contract from mid August to late September in Euros/MWh. In a liquid futures market the bid price close to the expiration date of the contract is a very strong indicative of the expected spot market price on day of expiration. Someone who bought a futures contract back in 14/08/2007 has saved around 3 Euro/MWh compared to the price on 25/09/2007. On the other hand, the buyer of a gas futures contract on 21/09/2007 has lost 1 Euro/MWh in four days.

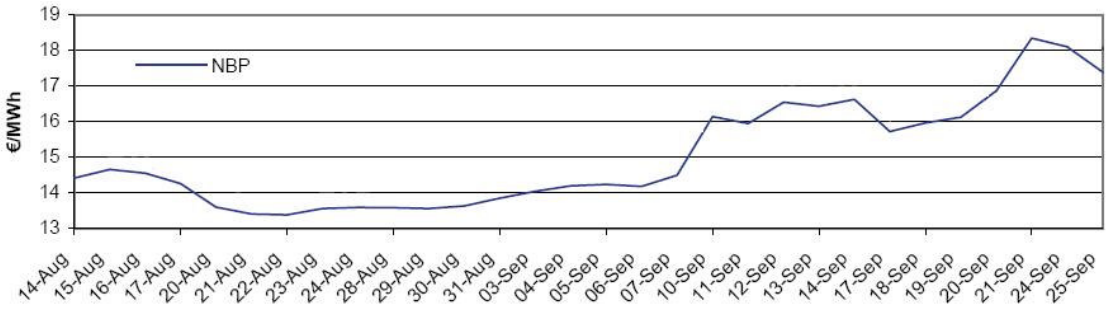

Figure 6-19 Month + 1 Price assessments - October 2007 [263]

Clearly, the ability to accurately estimate the demand of the plant for October 2007 back in mid August could signify excellent savings with respect of the price on 25/09/2007. Another option is to hedge only a percentage of the future production and buy the remaining at the spot market.

As mentioned in section 6.4.1.4.3, the futures contracts present some rigidity in the specifications and traded volumes allowed. The minimum volume per contract in the major OTC gas futures markets is 25000 therms. However, a contract for a lower volume could be obtained from a brokerage firm for an extra charge.

6.7.2.4 Strategy 3: Option on gas futures

Instead of buying gas in the futures market at the current prices, the operator can choose to “wait and see” before acting. This strategy can be realised buying a Call Option on a futures contract. The call option will give the holder the right but not the obligation to buy gas futures at a predefined price on the expiration day of the contract.

The following hypothetical scenario can illustrate the benefit of the use of options. The high volatility of the gas market during the last months had prompted the operator of a generation asset to hedge his operations for next year. Instead of buying a futures contract at the current high prices he decides to wait for a down trend in the market and get the gas at a discounted price.

A Call Option would hedge the operations for the down side of risk. If the gas futures prices have a sudden increase during the following months the option would allow him to pay for the gas future at a hedged price. Figure 6-20 shows the payoff of a Call option with strike price of 45 p/therm and premium of 2.2 p/therm.

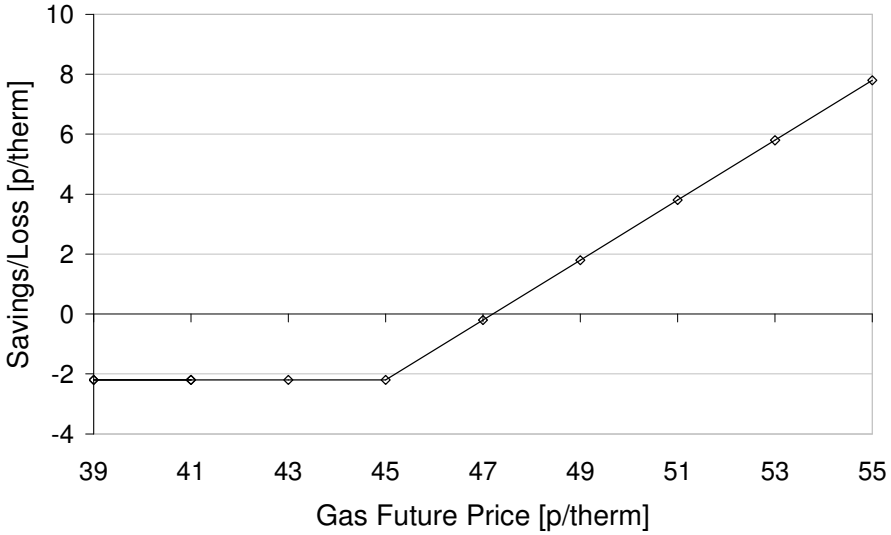

Figure 6-20 Call option payoff

If the price of the gas futures contract does not go beyond the 47.2 p/therm during the following months the operator would have lost all or part of the option premium as he would be better off buying the contract at the current price. On the other hand, if the price reaches 49 p/therm the operator would have saved around 1.8 p/therm as he will be entitled to buy the gas at only 45 p/therm plus the option premium of 2.2 p/therm. The savings become more substantial as the price of the futures rises. For a final price of 55 p/therm, net savings of 7.8 p/therm could be made.

This type of strategy is sought by companies with low positive cash flows or financial instability that could not resist the full extent of the gas price volatility. The use of this instrument does not make the use of advanced forecasting tools compulsory as the main objective is to set a “pain threshold” for the company.

6.8 Summary

This chapter presented a series of operations optimisation and risk management strategies for a power plant similar to MEA’s Pulrose Plant. A brief introduction to the liberalised electricity markets, spark spread and risk management was made.

The implementation of the spark spread concept into the CCGT performance simulation program described in Chapter 5 was successfully made.

A quantification of the economic benefit created through the implementation of the proposed operations optimisation strategies was made. The strategies were supported

with technical and economic results from the eCCGT program. The potential benefit of the implementation of a gas turbine performance diagnostics system was reaffirmed.

A series of risk management strategies were defined. The identification of the economic and technical risk variables was made. The strategies proposed were: the load factor maximisation, exposed operations, fuel futures and fuel options. The general implications and considerations for the execution of the strategies were explained.

Chapter 7 General conclusions and Recommendations

7.1 General conclusions

This thesis presented a novel application of advanced performance simulation and diagnostics computational programs for the generation of operations optimisation and risk management strategies for a CCGT power station similar to MEA's Pulrose plant.

The main program eCCGT was integrated from existing and new individual performance simulation codes of the main components of a CCGT power station. The specifications of MEA's LM2500+ engines demanded the modification of Turbomatch code for performance simulation. A new model for a once-through steam generator (OTSG) was created. The Steamomatch model developed by Zewbek was implemented for the performance simulation of the steam turbine. The eCCGT system was integrated in a user friendly and flexible environment into Microsoft Excel® with excellent comments from MEA during the presentation of the tool.

The assessment of an existing gas turbine engine performance diagnostics system called Pythia was also conducted. The objective was to identify the best practice for the usage of the system under the data and sensor restricted scenario presented by MEA's LM2500+ engines.

An economic module was implemented into the eCCGT program to simulate the profitability of the plant. The module was based on the practitioners' approach to the spark spread concept. An economic evaluation of the operations of a CCGT power station was successfully completed. Applicable optimisation strategies were presented with corresponding economic impact on the plant. Finally, a number of risk management strategies aimed to protect the operations of a power generator from the main risk variables were introduced.

> *The general contribution to knowledge of this project is the confirmation that the use of technological advanced tools such eCCGT and Pythia can positively affect the way an operator manages a power generation asset through the implementation of virtually proven optimisation and risk management strategies.*

A detailed account of all different technical and economic contributions made by the author is found next. The first section describes the characteristics of the new eCCGT program and the development of all its parts.

- As mentioned before, the specifications of MEA's LM2500+ demanded the implementation of new capabilities into Turbomatch code. This features included the simulation of: ambient humidity, water injection at the combustor, multifuel performance and the correction of the engine components' characteristics for the change in working fluid. Modification of the input and output files to account for the new capabilities was also included. All new

capabilities were validated through an intensive simulation of different ambient and operating conditions. In the case of the thermodynamic properties subroutine, the results showed excellent match against Walsh and Fletcher [12] and McBride's Chemical Equilibrium with Applications (CEA) [45] results assuming a complete combustion

- The adaptation of the thermodynamic model of the LM2500+ developed in Turbomatch was made. The adaptation used real data extracted from the control system of MEA. The design point adaptation presented excellent results with a total error of 0.2%. On the other hand, the off-design adaptation showed variable deviation from the field data. Attempting to correct the off-design simulation error a VSV scheduling function dependent of power output was implemented with acceptable results. The final error levels for the off-design simulation are within 3% at points far from design operating conditions.

- A new thermodynamic model for the simulation of the OTSG was created. The main contribution of the model was the introduction of a theoretical-practical approach that uses the heat transfer fundamentals together with empiric correlations derived from field data recorded at MEA. The code calculates the thermohydraulic performance of the boiler using the energy balance theory and the heat transfer fundamentals. The adaptation of the model to the single and double pressure operating conditions showed acceptable errors levels within a 7% band. However, some inconsistencies were found during its used as part of the combined cycle model that suggests improvements in the empiric correlations are needed.

- The three main thermodynamic models of the main components of a CCGT power station were integrated in the eCCGT program. The functional requirements of the system favoured the use of the Visual Basic for Applications (VBA) compiler in Microsoft Excel ®. This decision allowed to develop a dedicated graphical user interface (GUI) coupled with the powerful capabilities of Excel® spreadsheets. The system allows the user to simulate any number of cases under almost any ambient and operating conditions.

- A module for the simulation of the economic performance of the plant was implemented into the eCCGT program. This module is based on the concept of spark spread. The program allows the user to create an endless number of case studies on the effect all economic and technical variables used in the spark spread definition have on the profitability of the plant. The analysis uses the results from the technical performance simulation.

Once the techno-economic tools were developed, an assessment of the performance simulation and diagnostics capabilities of eCCGT and Pythia, respectively, was done. A summary of the results is found next:

- A simulation of the performance of a CCGT power station similar to MEA's Pulrose plant was made. The reported figures of the sensitivity analysis on the

CCGT performance simulation are in line with the general thermodynamic behaviour described in the open literature. The ambient temperature was identified as the most influential geographical/physical dependent parameter. The predominant role of the gas turbine engine in the combined cycle was reaffirmed. A revision of the empiric correlations used in the performance modelling of the steam generator is adviced.

- An assessment of the generation schedule of the plant for a cold day of winter 2007 was done. Variable ambient and operating conditions for each of the 48 time block forming the daily operations were evaluated. The results for the key parameters such as fuel flow, thermal efficiency and power output showed accuracy values within 2% average error.

- The assessment of an existing gas turbine performance diagnostics system under the restrictive sensor and data conditions found on a power station similar to MEA's Pulrose plant was performed. The analysis consisted on the systematic evaluation of the different capabilities of the system. Different values of data noise, sensor bias, ambient and operating conditions were added to the performance simulation of specific component degradation cases. A final set of guidelines to increase the rate of success in the use of the diagnostics system was generated. The guidelines define the exact safe range of operating and ambient conditions at which the data extraction from the control system of the power plant should be done.

The real value of the eCCGT program in the simulation of the economic performance of a CCGT power plant was discovered during the evaluation of different operations optimisation and risk management strategies.

- A retrospective analysis of the profitability of the plant was performed using the results from the technical simulation and real electricity and gas prices values. A baseline profit/loss schedule of the plant was calculated from the results of the technical simulation of the generation schedule. The reported values for each of the 48 time blocks forming the daily operations showed an unavoidable loss during the off-peak market period of the day offset by the profit made during the peak hours, resulting in an overall positive cash flow for the day.

- A number of optimisation strategies aiming to improve the economic performance of the plant were proposed and evaluated. These strategies were supported by an accurate simulation of the modified generation schedule using the CCGT performance simulation program. Savings of 12% of the baseline profitability of the plant were estimated when the emission abatement system of the plant is switched off. The reported values for the plant's economic performance generated by different levels of performance deterioration in the gas turbine engine reaffirmed the importance of the gas turbine engine performance diagnostics system as a mean of early detection. From all cases, the degradation of the power turbine was identified as more negative parameter whereas a performance deterioration of 2% can bring a loss equal to 4.3% of the

baseline profitability of the plant. A brief assessment of the effect reducing the gas swing factor in the production cost structure was made.

- Finally, the appropriate risk management strategies aiming to protect the operations of a CCGT power plant from the main sources of market and operating risk were defined. A sensitivity analysis on the profitability of the plant for a variation in all economic and technical parameters defined in the spark spread concept derived from power industry practitioners was conducted. The electricity price, gas price and thermal efficiency were identified as the more dominant variables in the economic performance of the plant. An important requirement for the proposed hedging strategies was to maintain the "real option" characteristic of the generation asset. The implementation of a physical hedge to the load factor of the plant was identified as the first step into the road for an integral hedging strategy. The use of gas futures and options on gas futures was outlined. Hypothetical scenarios to exemplify the benefit of the two risk management instruments were generated. The accurate estimation of the fuel consumption of the plant for the period to be hedged was identified as one of the most important aspects for a successful implementation of the strategies. Clearly, the performance simulation and diagnostics capabilities of the CCGT computational programs coupled with advanced demand forecasting techniques could deliver the appropriate conditions to protect the operations of the a power plant similar to MEA's CCGT Pulrose plant.

7.2 Recommendations

7.2.1 GT performance simulation

- The energy balance model for the water injection at the combustor can be improved by the implementation of the full energetic balance considering the change in chemical and state enthalpies for all the constituents of the mixture. These modifications will increase the accuracy of the results in 1 or 2%.
- The thermodynamic properties estimation subroutine can be improved by assuming incomplete combustion process at the combustor. The set of polynomials used for the calculation of the properties allow the fast and easy implementation of this capability. Preliminary comparisons between the improved Turbomatch and CEA program was done. The results showed error levels below 0.5% for all types of fuels available in Turbomatch.
- A big discrepancy between the field data and the simulation at the hot end of the engine was found during the design point adaptation. A field and statistical analysis of the measurements of the hot end could provide some information on the behaviour.
- The implementation of a bleed-off schedule as a function of the speed could be implemented to improve the results of the simulation.
- The generation of a new compressor map from field data would increase the simulation results at off-design conditions.
- The VSV schedule implemented in the eCCGT program was function of the power settings only. A more efficient approach would create a new VSV schedule using the gas generator speed as dependent variable. In order to implement this change, the new

TM subroutine inside Excel®, or if preferred, a new "wrapper" subroutine in FORTRAN must be created.

7.2.2 . GT performance diagnostics

- The level of dependency of the different capabilities of the program on the gas turbine performance model should be reduced.
- The improvement of the module responsible for the elimination of the performance deviation caused by a shift in the operating conditions from the baseline is vital. This variable was identified as the more critical for the restrictive scenario found at MEA. The use of specialised neural networks and statistic algorithms in the development of a second generation of data correction and filtering could be an option.

7.2.3 OTSG performance simulation

- As mentioned before a revision of the empiric correlations used to avoid any over or incorrect estimation of the combined cycle's performance is required.
- The implementation of a two variable empiric correlation for the estimation of the operating pressures of the steam cycle should allow the simulation of the whole combined cycle under unusual ambient and operating conditions. The new correlation should include both the exhaust temperature and mass flow. The current function delivers wrong pressure values when there is a change in exhaust mass flow without the corresponding drop in temperature. These scenarios are experienced during high ambient temperatures and the gas turbine engine degradation.
- There is scope for the improvement of the single pressure system operating mode. A preliminary analysis on the implementation of a particular empiric correlation of the stack temperature for the single pressure operating system was done. The new empiric correlation would have produced more accurate results for the steam mass flow and stack temperature. The stand alone evaluation of the boiler code delivered positive results but its integration into eCCGT as a dynamic link library (DLL) failed.
- The calculation of the double phase heat transfer coefficient should be improved. The nucleating and convective boiling heat transfer coefficient models were not fully implemented into the model. An average of the nucleating boiling was made for the length of the estimated evaporator section. It is important to implement an internal loop to evaluate the quality of the steam at different points and define the appropriate heat transfer coefficient.
- The implementation of a closed loop between Turbomatch and the OTSG models to simulate the effect of the pressure drop across the steam generator on the performance of the gas turbine engine could deliver better results. In order to achieve this objective, the pressure drop model in the steam generator needs to be check and improved.
- The model needs to simulate the transient performance of the boiler. The simulation of the transient performance of the steam generator would allow the user to generate more complex generation schedules looking to optimise the operations of the plant. Obviously, the transient performance would include time as the predominant variable in the thermo hydraulic model.
- The first steps into the creation of a second generation OTSG performance simulation model were taken. The new code uses a modularised structure that can

simulate the performance of the boiler as a sum of the total number of rows and to calculate the specific, more accurate conditions at the end of each row. The continuation of this work is greatly encouraged.

7.2.4 CCGT performance simulation

- The implementation of a condenser model would improve the results of the whole CCGT. A more desirable model would involve the thermo hydraulic analysis of the heat exchanger, although, a more simple thermodynamic analysis could provide acceptable values.
- The future implementation of empiric correlations to calculate the losses as a function of load factor and ambient conditions would increase the accuracy of the simulation. These losses may include all secondary equipment for all the main components of the plant.
- A closed loop between the gas turbine engine backpressure and the pressure drop across the steam generator could help the gas turbine simulation results for the exhaust conditions. It is necessary to create an iterative process to feed the calculated pressure drop from the OTSG model back into the Turbomatch simulation. The turbine entry temperature (TET) can then be modified to achieve the power output.
- The future implementation of time dependant deterioration curves could offer a more realistic scenario when simulating the performance of the plant over larger periods. The implementation of more complex degradation schedules could simulate the different cycles of on and off-line washing.

7.2.5 Operations optimisation and Risk management

- There is scope for the development and implementation of an advanced optimisation technique in the eCCGT program. Having a defined generation schedule with 48 or more time blocks, the optimisation module would select the right operating mode over the whole day to maximise the thermal efficiency of the plant. The start-up times for the boiler and steam turbine should be included as part of a more complete control subroutine to avoid unrealisable solutions.
- The implementation of a forecasting tool, internal or external to eCCGT, would provide an all rounded tool for the operations optimisation and risk management of the plant. The main focus of this tool would be to try to forecast the demand on the island, however, a great contribution would be done if the gas and/or electricity prices could be estimated.
- It is paramount that an Activity Based Costing system is implemented at Manx Electricity Authority. A more exact estimation of the maintenance costs would improve the accuracy of the performance degradation results. The ultimate goal is to implement a Condition Based Maintenance strategy.

References

1. Manx Electricity Authority. Business Plan 2005. 6. 2005. Douglas, Isle of Man Government.

2. Departement of Trade & Industry. 3 Year Strategic Plan: April 2001-March 2005. 2001. Douglas, Isle of Man Government.

3. Manx Electricity Authority. Anual Report 2000-2001. 2001. Isle of Man, MEA.

4. GE - Aero Energy. LM2500+ Marine Gas Turbine [Web Page]. Accessed 2007 Jul 30. Available at: http://www.gepower.com/prod_serv/products/aero_turbines/en/downloads/lm2500plus.pdf.

5. General Electric. GateCycle Software [Web Page]. Accessed 2007 Jul 30. Available at: http://www.gepower.com/prod_serv/products/oc/en/opt_diagsw/gatecycle.htm.

6. ThermoFlow Inc. Knowledge=Power [Web Page]. Accessed 2007 Jul 30. Available at: http://www.thermoflow.com/.

7. General Physics. EtaPro [Web Page]. Accessed 2007 Jul 30. Available at: http://www.etapro.com/.

8. Gas Turbo Inc. Gasturb 10 [Web Page]. Accessed 2007 Jul 30. Available at: http://www.gasturb.de/Products/GasTurb/gasturb.html.

9. Macmillan W. L. Development of a Modular Type Computer Program for the Calculation of Gas Turbine Off Design Performance. Ph.D. Thesis ed. Cranfield University; 1974 Sep.

10. Gu Y G, Palmer J R. A mathematical model for computing the effects of air humidity, fuel composition and gas dissociation on gas turbine performance and its application. ASME Paper No. 86-GT-114. 1985.

11. Bird J, Grabe W. Humidity effects on gas turbine performance. Int Gas Turb & Aero Cong and Expo; Orlando, Florida. USA: ASME; 1991.

12. Walsh and Fletcher. Gas Turbine performance. Oxford, UK: Blackwell Science Ltd; 1998.

13. Roumeliotis I, Mathioudakis K. Moisture condensation effect on turbine performance tests. ASME Turbo Expo; Vienna, Austria. USA: ASME.

14. Yan J, Ji X Jonsson M. Thermodynamic property models for the simulation of advanced wet cycles. ASME Turbo Expo; Georgia, USA. USA: ASME; 2003.

15. Ritchey I, Fisher E H Agnew G D. Water spray cooling of gas turbine cycles.

IMechE. 2000; 214(Part A):203-211.

16. Mathiodakis K, Tsalavoutas T. Uncertainty reduction in gas turbine performance diagnostics by account for humidity effects. Eng for Gas Turbine Power. 2002; 124(Oct):801-808.

17. Jonsson Maria, Yan J. Humidified gas turbines - a review of proposed and implemented cycles. Energy. 2005; 30:1013-1078.

18. GE - Aero Energy . LM6000 SPRINT Gas generator set [Web Page]. Accessed 2007 Jul 30. Available at: http://www.gepower.com/prod_serv/products/aero_turbines/en/downloads/lm6000_sprint.pdf.

19. Johnke T, Mast M. Power Boosters - technologies to enhance gas turbine power output on demand [Web Page]. Accessed 2007 Jul 30. Available at: www.siemenswestinghouse.com/download/pool/mast_engl_3.pdf.

20. Anon. Water injection can add 50% to gas turbine power. Gas Turbine World. 1987; 17(3):34-36.

21. Meacock A J, White A J (Hopkinson Laboratory). The effect of water injection on multi-spool gas turbine behaviour. ASME Turbo Expo; Vienna, Austria. USA: ASME; 2004.

22. Horlock J H. Compressor performance with water injection. ASME Turbo Expo; New Orleans, USA. ASME Paper 2001-GT-0343, 2001

23. Hartel C, Pfeiffer P. Model analysis of high-fogging effects on the work of compression, Anon. ASME Turbo Expo; Atlanta. USA: ASME; 2003.

24. Meher-Homji C B, Mee T R III. Inlet fogging of gas turbine engines: Part A - Theory, psychometrics and fog generation. ASME Turbo Expo; Munich, Germany. USA: ASME; 2000.

25. Meher-Homji C B, Mee T R III. Inlet fogging of gas turbine engines: Part B: practical considerations, control and O&M aspects. ASME Turbo Expo; Munich, Germany. USA: ASME; 2000.

26. Arar Malath (General Electric). Gas turbine corrected parameter control -humidity correction - sensors evaluation and selection. ASME Turbo Expo; The Netherlands. USA: ASME.

27. Shaw, H. The effects of water, pressure, and equivalence ratio on nitric oxide production in gas turbines. ASME J Eng. Power. 1974; 96 :240-246.

28. Koch H. Investigations and measures for the reduction of gas turbine emissions. Sulzer Technical Review. 1974; 56(2):61-67.

29. Lefebvre, A. H. The role of Fuel preparation in low emission combustion. ASME

J. Eng. Gas Turbines Power. 1995; 117:617-654.

30. Kreitmeier, F. Frutschi H. U. and Vogel M. Economic Evaluation of methods for reducing NOx emission of gas turbines and combined cycle plants. ABB Review. 1992; 1/92:29-36.

31. Hauhe W E, et. al. User experience - operating a 300 MW base load cogeneration plant with high water injection rates to control NOx emissions. ASME ; Toronto, Canada. USA: ASME; 1989.

32. Robinson Thomas. Water injected LM1600 installation and operating experience. ASME; The Netherlands. USA: ASME; 1994.

33. Urbach H B, et. al. Water injection into navy gas-turbine combustors to reduce NOx emissions. IGTI Conference; Sweden. USA: IGTI; 1998.

34. Cowell, L (Solar Turbine Incorporated). Ten years of DLE industrial gas turbine operating experience. ASME Turbo Expo; The Netherlands. USA: ASME; 2002.

35. Dobbeling K (Alstom Power). 25 Years of BBC/ABB/Alstom lean premix combustion technologies. ASME Turbo Expo USA: ASME; 2005.

36. Mathioudakis K. Analysis of the effects of water injection on the performance of a gas turbine. Journal of Engineering for Gas Turbines and Power. 2002; 124:489-495.

37. Mathioudakis K . Evaluation of steam and water injection effects on gas turbine operation using explicit analytical relations. IMechE J Power and Energy. 2002; 216(Part A):419-431.

38. Cardu, M. Baica M. Gas turbine with total water injection in the combustion chamber. Energy Conversion and Management. 2002; 43:2395-2404.

39. Fraize W E. Effect of steam injection on the performance of gas turbine power cycles. ASME Turbo ExpoUSA: ASME; 1978.

40. Cheng D Y (Cheng Power Systems). The chronological development of the Cheng cycle steam injected gas turbine during the past 25 years. ASME Turbo Expo; The Netherlands. USA: ASME; 2002.

41. Boyle, Robert J. Effect of steam addition on cycle performance of simple and recuperated gas turbines. NASA Technical Paper . 1979; 1440 :51.

42. Wang F.J., Chiou J. S. Integration of steam injection and inlet air cooling for a gas turbine generation system. Energy Conversion and Management. 2004; 45:15-26.

43. Wang F.J., Chiou J. S . Performance improvement for a simple cycle gas turbine GENSET-a retrofitting example. Applied Thermal Engineering. 2002; 22:1105-1115.

44. Maunsbach K. et al. Integration of advanced gas turbines in pulp and paper mills for increased power generation. International Gas Turbine and Aeroderivative Congress and Exhibition. US: ASME; 2001; 123, 734-740.

45. McBride B.J., Gordon S. Computer Program for Calculation of Complex Chemical Equilibrium Compositions and Applications-II Users Manual and Program Description. NASA Reference Publication - 1311. USA: NASA; 1996.

46. Jones R, Trout A Wear J (NASA). Combustion gas properties of various fuels of interest to gas turbine engineers. Joint Power generation ; Toronto, Canada. USA: ASME; 1984.

47. Guha A. An efficient generic method for calculating the properties of combustion products. IMechE. 2001; 215(3):375-387.

48. Cengel Y, Boles M. Thermodynamics. USA: McGraw-Hill; 2002.

49. Strehlow R. Combustion Fundamentals. New York, USA: McGraw-Hill; 1984.

50. Molnar M, Marek J. Simplified two-time step method for calculating combustion and emission rates of jet-A and methane fuel with and without water injection. 43rd AIAA Aerospace Sciences Meeting and Exhibit; Reno. USA: AIAA; 2005.

51. Moore M J . NOx emission control in gas turbine for combined cycle gas turbine plant. IMechE. 1996; 211(Part A):43-52.

52. van Wylen G, et al. Fundamental of classical thermodynamics. New York, USA: John Wiley; 1994.

53. Rabinovich V A, Beketov C G. Moist gases thermodynamic properties. Begell House; 1995.

54. Walk K Jr. Advanced thermodynamics for engineers. New York, USA: Mc-Graw-Hill; 1995.

55. Buker D, Span R Wagner W. Thermodynamic property models for moist air and combustion gases. Journal of Engineering for Gas Turbines and Power. 2003; 125:374-384.

56. Ji X, Lu X Yan J. Survey of experimental data and assessment of calculation methods of properties for the air-water mixture. Applied Thermal Engineering. 2002; 23:2213'2228.

57. Li Y G, Singh R (Cranfield University). An advanced gas turbine path diagnostics system - PYTHIA. XVII International Symposium on Air Breathing Engines; Munich, Germany. ISABE; 2005.

58. Wilcock R C, Young J B Horlock J H. The effect of turbine blade cooling on the cycle efficiency of gas turbine power cycles. J Eng Gas Turbine and Power. 2005 Jan; 127:109-120.

59. Li Y G, Pilidis P Newby M. An adaptation approach for gas turbine design point performance simulation. ASME Turbo Expo; Reno-Tahoe, Nevada. USA: ASME; 2005.

60. Lo Gatto E, Li Y G Pilidis P. Gas turbine off-design performance adaptation using a genetic algorithm. ASME Turbo Expo; Barcelona, Spain. USA: ASME; 2006.

61. Saravanamuttoo H. I. H. Gas Turbine Theory. USA: Prentice Hall; 2001.

62. Moliere M, Pommel F (General Electric). Alternative fuels in gas turbine applications: A simple method for assessing the influence of fuel on performances. ASME Turbo Expo; Munich, Germany. USA: ASME; 2000.

63. Dechamps, P. J. and Galopin, J.-F. Once-through heat recovery steam generators working with sub- and supercritical steam conditions for combined cycles. Proceedings of the 1997 International Gas Turbine & Aeroengine Congress & Exposition; Orlando, FL. USA: ASME; 1997; c199710p.

64. Bethune III, J. L. Use of the computer for dynamic analysis of a power plants performance. 17th Int ISA Power Instrum Symp; Boston, Mass. ISA; 1974: 17-26.

65. Leithner, R. Comparison of Once-through Forced Flow Boilers, Once-through Forced Flow Boilers with Full Capacity Circulation, and Natural Circulation Boilers. VGB-Kraftwerkstechnik. 1983; 63(7):553-568.

66. Jarkovsky, J.; Fessl, J., and Medulova, V. Steam generator dynamic mathematical modelling and its using for adaptive control systems testing. Power Systems Modelling and Control Applications - Selected Papers from the IFAC Symposium; Brussels, Belg. Publ by Pergamon Press Inc; 1989: 167-174.

67. Bruens, N. W. S. PWR plant and steam generators dynamics. Afdeling der Werktuigbouwkunde (Report) WTHD ed.. Delft, Holland: Technische Hogeschool Delft; 1981; 128.

68. Abdalla, M. A. Four-region, moving-boundary model of a once-through, helical-coil steam generator. Annals of Nuclear Energy. 1994; 21(9):541-562.

69. Lee D H. Studies of heat transfer and pressure drop relevant to sub- critical once-through evaporators. SodiumCooled Fast Reactor Engineering (Proc Paper). 1970.

70. Sanathanan, C. K.; Sandberg, A. A.; Clark, F. H. ; Burke, O. W., and Stone, R. S. Dynamic modelling of a large once-through steam generator. 17th Int ISA Power Instum Symp (Technical Paper); 1972: 321-330.

71. Bogorinski, Peter. DYNOT-3 - A simulation code for sodium-heted once-through steam generators. 10th IMACS World Congress on System Simulation and Scientific Computation. Montreal, Can. Int Assoc for Mathematics & Computers in Simulation; 1982: 147-149.

72. Kim, K.; Gabler, M. J., and Carlson, R. D. Once-through testing of the CRBRP prototype steam generator. Papers Presented at the ASME Winter Annual Meeting.; Boston, MA, USA. USA: ASME; 1987, p. 7.

73. Duffy, T. E. and Schneider, P. H. Advanced combined-cycles from 8 MW to 23 MWAnon. Proceedings of the 55th Annual Meeting of the American Power Conference. Part 1 (of 2); Chicago, IL, USA. Publ by Illinois Inst of Technology; 1993: 1733-1741.

74. IST. Once through steam generator multi-pressure operational manual. Innovative Steam Technology2002: p. 55.

75. Anon. Thermal-hydraulic analysis of once-through steam generators. EPRI NP: Electric Power Research Institute (Report); 1980; 1431. pp. var paging.

76. Ngoma, G. D.; Sadiki, A., and Wamkeue, R. Efficient approach in modelling and simulation of dual pressure once-through heat recovery steam generatorSmedley K.M. Proceedings of the Seventh IASTED International Multi-Conference - Power and Energy Systems; Palm Springs, CA. USA: IASTED; 2003: 218-223.

77. Chan, K.; Ariffin, A. E.; Chew, Y. C.; Lin, C., and Ye, H. Validated combined-cycle power plant model for system and station performance studies. 2004 International Conference on Power System Technology, POWERCON: IEEE; 2004: 1991-1997.

78. Lausterer, G. K.; Franke, J., and Eitelberg, E. Mathematical modelling of a steam generator. 6th Digital Comput Appl to Process Control, Proc of the IFAC/IFIP Conf; Duesseldorf, W Ger. IFAC by Pergamon Press; 1980: 411-417.

79. Dumont M.N., Heyen G. Mathematical modelling and design of an advanced once-through heat recovery steam generator. Computer and Chemical Engineering. 2004; 28:651-660.

80. Green, C. H.; Lis, J., and Hitchcock, J. A. Modelling of AGR boiler thermal performance. J Nuclear Energy. 1985; 24(6):367-380.

81. Aleksandrov, V. V. and Rassokhin, G. N. Predicting the dynamic instability of once-through sodium-water steam generators. J Thermal Engineering (English Translation of Teploenergetika). 1985; 32(11):634-637.

82. Katayama, T.; Ohki, T.; Inoue, T., and Nakayama, S. New approach to optimal control of supercritical once-through steam generator. Proceedings of the Ninth Triennial World Congress of IFAC 1985; Budapest, Hung. IFAC; 1985.

83. Johnson, L. E. Fouling in nuclear once-through steam generators. Papers Presented at the ASME Winter Annual Meeting.USA: ASME; 1987 p.5

84. Hassan, Yassin A. Assessment of boiling heat transfer correlations for once-through steam generators. J Nuclear Technology. 1988; 81(3):446-449.

85. Ju Huaiming; Zhang Youjie; Huang Zhiyong; Liu Zhiyong; Li Jun, and Yu Yu. Experimental and operational verification of the HTR-10 Once-through steam generator (SG). J of Nuclear Science and Technology. 2000; 41(7):p. 765-770.

86. Rakopoulos C.D.; El-Shirbini A.A., and Murgatroyd W. Theoretical investigation of the dynamics of two-phase flow in vapor generators and comparison with experimental results. Conf Institution of Mechanical Engineers; Istanbul, Turk. Hemisphere Publ Corp (NATO Adv Study Inst Book); 1979: 1077-1104.

87. Matsuoka, Takeshi; Nariai, Hideki, and Kobayashi, Michiyuki. Study on the flow instability in a once-through steam generator for integrated type marine water reactor (Part 3: Analysis of steady state performance). Papers of Ship Research Institute. 1985; 22(1):13-42.

88. Glebov, V. P.; Klevtsov, I. A.; Kyaar, Kh. A.; Lausmaa, T. M.; Moskvichev, V. F., and Eskin, N. B. Investigation of a once-through steam generating tube under conditions of DNB of the second kind . J Thermal Engineering (English Translation of Teploenergetika). 1987; 34(12):673-677.

89. Fan, P.; Qiu, S.-Z., and Jia, D.-N. An investigation of flow characteristics and critical heat flux in vertical upward round tube. J Nuclear Science and Techniques. 2006; 17(3):170-176.

90. Incropera F., De Witt D. Fundamental of heat and mass transfer. USA: John Wiley & Sons Inc ; 1996.

91. Somerscales E F C. Fouling of heat transfer surfaces - A historical review. J Heat Transfer Engineering. 1990; 11(1):11-36.

92. Gnielinski V. VDI heat atlas. Dusseldorf, Germany: VDI-Verlag; 1993.

93. Sieder and Tate. Ind. Eng. Chem. 1936; 28:1429.

94. Kattan N, Thome J. R Favrat D. Flow boiling in horizontal tubes Part 3: Development of a new heat transfer model based on flow patterns. Journal of Heat Transfer. 1998; 120(1):156-165.

95. Cooper, M. G. Heat transfer rates in saturated pool boiling - A wide-ranging examination using reduced properties. Advanced in Heat Transfer. 1984; 16:157-239.

96. Dittus E.J., Boelter L. M. K. Publications on Engineering. University California, Berkeley. 1930; 2:443.

97. Steiner, D. VDI heat atlas. Dusseldorf, Germany: VDI-Verlag, HBB ; 1993.

98. Lockhart R.W, Martinelli R. C. Proposed correlation for isothermal two-phase two-component flow in pipes. Chem.Eng.Progr. 1949; 91:434-442.

99. Shah R.K., Sekulic D. Fundamentals of Heat exchanger design. 4th ed. Hoboken,

USA: John Wiley & Sons; 2003.

100. Gaddis E.S., Gnielinski. Pressure drop in cross flow across tube bundles. Inte. Chem.Eng. 1994; 25:1-15.

101. Martin H. The generalized Léveque equation and its practical use for the prediction of heat and mass transfer rates from pressure drop. Chem. Eng. Sci. 2002; 57:3217-3223.

102. McBride B.J., Gordon S. Computer Program for Calculation of Complex Chemical Equilibrium Compositions and Applications-II Users Manual and Program Description. NASA Reference Publication - 1311. USA: NASA; 1996.

103. Dechamps P.J. Fonctions programmables pour l'Evaluation des propriétés thermodynamique des fluidesBelgium: University of Lič ge (Report); 1992.

104. Ganapathy V (ABCO Industries). Heat-recovery steam generators: Understand the basics. J Chemical Engineering. 1996; August 199632-45.

105. Boyce, M. P. Handbook for cogeneration and combined cycle power plants. New York : ASME Press; 2002.

106. Zwebek, A. I. Combined cycle performance deterioration analysis [Thesis (Ph.D.)]. UK: Cranfield University, School of Engineering; 2002.

107. Desideri, Umberto and Fibbi, Andrea. Simplified approach to off-design performance evaluation of combined cycle powerplant's with single-pressure steam cycles. Proceedings of the 7th Congress & Exposition on Gas Turbines in Cogeneration and Utility Industrial and Independent Power Generation; Bournemouth, Engl. USA: Publ by ASME; 1993: 199-207.

108. Seyedan, B.; Dhar, P. L.; Gaur, R. R., and Bindra, G. S. Computer simulation of a combined cycle power plant. Heat Recovery Systems & CHP . 1995; 15(7):619-630.

109. Hannett, L. N. and Feltes, J. W. Testing and model validation for combined-cycle power plants. 2001 IEEE Power Engineering Society Winter Meeting; Columbus, OH. 2001: 664-670.

110. Zhu, Y. and Frey, H. C. Simplified performance model of gas turbine combined cycle systems. Journal of Energy Engineering . 2007; 133(2):82-90.

111. Zwebek, A. I. and Pilidis, P. Degradation effects on combined cycle power plant performance -part III: Gas and steam turbine component degradation effects. Journal of Engineering for Gas Turbines and Power. 2004; 126(2):306-315.

112. Ramaprabhu, V. and Roy, R. P. A computational model of a combined cycle power generation unit. Journal of Energy Resources Technology. 2004; 126(3):231-240.

113. Sarabchi, K. and Polley, G. T. Thermodynamical optimization of a combined cycle plant performance. Proceedings of the International Gas Turbine and Aeroengine Congress and Exposition; Hague, Neth. Publ by ASME; 1994: 1-10.

114. Erbes, M. R. and Gay, R. R. Gate/cycle predictions of the off-design performance of combined-cycle power plants. Simulation of Thermal Energy Systems: Presented at the Winter Annual Meeting of the ASME; San Francisco, CA, USA. USA: Publ by ASME; 1989: 43-41.

115. Shirakawa, M. Development of a thermal power plant simulation tool based on object orientation. Journal of Power and Energy. 2006; 220(6):569-579.

116. Griffin, Patrick R.; Elmasri, Maher; Chen, Gwo-Tung; Kamppila, Stephen, and Basile, Frank. Power plant simulation software for optimizing thermodynamic and financial plant operation. Proceedings of the 1996 International Gas Turbine and Aeroengine Congress & Exhibition; Birmingham, UK. ASME; 1996.

117. Knight, R.; Obana, M.; von Wowern, C.; Mitakakis, A.; Perz, E.; Assadi, M.; Moller, B. F.; Sen, P.; Potts, I.; Traverso, A., and Torbidoni, L. GTPOM: Thermo-economic optimization of whole gas turbine plant. Applied Thermal Engineering. 2006; 128(3):535-542.

118. Chan, K.; Ariffin, A. E.; Chew, Y. C.; Lin, C., and Ye, H. Validated combined-cycle power plant model for system and station performance studies. International Conference on Power System Technology, POWERCON, 2004: 1991-1997.

119. Horlock, J. H. Combined power plants : including combined cycle gas turbine (CCGT) plants . Oxford: : Pergamon Press; 1992.

120. Deschamps, P. J. Part load operation of combined cycles plants with and without supplementary firing. ASME Cogen-Turbo 94; Portland, USA. Liege, Belgium: ASME; 1994.

121. Kehlhofer, R. Combined-cycle gas and steam turbine power plants . Tulsa, Oklahoma : : PennWell; 1999.

122. Sae-Lim, Jirasak. Combined cycle gas turbine performance & simulation and trading management [MsC Thesis]. UK: Cranfield University; 2006.

123. Cotton, K. C. Evaluating and improving steam turbine performance. USA: Cotton Fact; 1998.

124. Urban L.A. Gas path analysis applied to turbine engine condition monitoring. 1972(AIAA-72-1082).

125. Hamilton, Keith R. and Chopin, Matthew H. Diagnostic engine monitoring for military aircraft. Proc Annu Reliab Maintainability Symp. 1975. Washington, DC, USA; 1975.

126. Tichbon, A. W. Engine condition monitoring civil requirements - A british airways view . Proceedings of the 14th Symposium Aircraft Integrated Monitoring Systems.; Friedrichshafen, W Ger. DFVLR; 1988: 9-26.

127. Walker, John and Summerfield, Alan. Marine gas turbines - Engine Health monitoring - New approaches. ASME Gas Turbine Conference and Exhibition.; Anaheim, CA, USA. ASME; 19876 pPapers Presented at the ASME Gas Turbine Conference and Exhibition.

128. Roemer, M. J.; Orsagh, R. F.; Kacprzynski, G. J. ; Scheid, J.; Friend, R., and Sotomayer, W. Advanced Gas Turbine Engine Test Cell Troubleshooting and Diagnostics. Proceedings of the 48th International Instrumentation Symposium; San Diego, CA. USA: ASME; 2002: 287-300.

129. Ziebarth H K and Chang J D . Aircraft gas turbine condition analysis instrumentation. Its use for the status diagnosis of naval turbine engines. ASME Paper. 1971; 12 p.

130. Erickson B E . Some control and accesory condiderations for gas turbine engines. An engine manufacturer's viewpoint. SAE. 1969; (Paper 690724).

131. Passalacqua, J. R. TRENDS - An automatic gas turbine diagnostic system. ASME Paper. 1975; (75 -GT-82).

132. Novis, A. and Powrie, H. PHM sensor implementation in the real world - A status report. 2006 IEEE Aerospace Conference; Big Sky, MT. IEEE; 2006.

133. Behbahani, A. R. Need for robust sensors for inherently fail-safe gas turbine engine controls, monitoring, and prognostics. 52nd International Instrumentation Symposium 2006; Cleveland, OH. 2006: 200-211.

134. White, J. V. Reliability of filtration equipment in diesel and gas turbine systems. Diesels, Gas Turbines, and Their Systems - The Need for Reliability.London, Engl: Mechanical Engineering Publ Ltd; 1985: 53-57. Diesels, Gas Turbines, and Their Systems - The Need for Reliability.

135. Gutenev, B. S.; Vilenkin, A. V.; Gorodetskii, V. N., and Bezsonov, A. N. Evaluation of life rolling-contact bearings using synthetic oils. Chemistry and Technology. 1978; 14(3-4):292-293.

136. Taubert, T. Full-flow debris monitoring in gas turbine engines.1981.

137. Scott, D.; McCullagh, P. J., and Campbell, G. W. Condition monitoring of gas turbines - An exploratory investigation of ferrographic trend analysis. Wear. 1978; 49(2):373-389.

138. Howard, P. L. The application of quantitative debris monitoring technology to industrial gas turbine monitoring. Pineridge Press. 1987.

139. Mironov, A. G. and Doroshko, S. M. Use of vibration spectrum characteristics for aircraft gas turbine engine flow path diagnostics. Soviet Aeronautics (English Translation of Izvestiya VUZ, Aviatsionnaya Tekhnika). 1986; 29(2):51-55.

140. Clifton, D. A.; Bannister, P. R., and Tarassenko, L. A framework for novelty detection in jet engine vibration data. Key Engineering Materials. 2007; 347305-310.

141. Anderson, J. M.; Bailie, S. T., and Ng, W. F. Acoustic monitoring of axial compressor rotor blade vibrations. 12th AIAA/CEAS Aeroacoustics Conference; Cambridge, MA. AIAA; 2006: 2204-2220.

142. Hardy, H. D. Use of laser-powered optical proximity probe in advanced turbofan engine development. Symp on Instrum for Airbreathing Propul, Nav Postgrad Sch; Monterey, CA, USA. 1974: 317-323.

143. Wenyi, W. Disk crack detection and diagnosis for gas turbine engines. 2006 IEEE Aerospace Conference; Big Sky, MT. 2006.

144. Ellingson, W. A.; Visher, R. J.; Lipanovich, R. S., and Deemer, C. M. Optical NDT techniques for ceramic thermal barrier coatings. Material Evaluation. 2006; 64(1):45-51.

145. Hunter R C. Engine failure prediction techniques, AIRCR ENG JOURNAL, 1975; 47(3 , ISSUE 853).

146. Simms, W. H. Boroscoping of gas turbine engines for condition monitoring. Sawyers Gas Turbine Int. 1976; 17(6):32-33.

147. Ridler, William J. Borescope color photography: A new engineering technology for marine gas turbine condition monitoring. Turbomach Symp, 4th, Proc; Texas, USA. Tex A&M Univ; 1975: 95-101.

148. Morey, W. W. and Angello, L. C. Diagnostics from imaging inside gas turbine combustors. Optical Techniques for Industrial Inspection.; Quebec City, Can. SPIE; 1986: 306-313. Optical Techniques for Industrial Inspection.

149. Savage, K. P.; Winkleman, B. C.; Beitel, G. R.; Plemmons, D. H.; Catalane, D. R., and Hiers III, R. S. Imaging probes for gas turbine engines. AIAA/ASME/SAE/ASEE 42nd Joint Propulsion Conference; Sacramento, CA. AIAA; 2006: 11-16.

150. Urban, L. A. Parameter selection for multiple fault diagnostics of gas turbine engines . J Eng Power Trans ASME. 1975; 97 Ser A(2):225-230.

151. Krok M.J. and Ashby M.J. Condition-based, diagnostic gas path reasoning for gas turbine engines. Proceedings of the 2002 IEEE International. UK: IEEE; 2002: 227-234.

152. Urban L A. Gas Turbine Engine Parameter Interrelationships. Windor Locks, Ct, USA: HSD UTC; 1967.

153. Doel, D. L. TEMPER - a gas-path analysis tool for commercial jet engines. J Eng Gas Turbines and Power. 1994; 116(1):82-89.

154. Volponi A J. Gas path analysis: An approach to engine diagnostics. Proceedings of the 35th Meeting of the Mechanical Failures Prevention Group.; Gaitherburg, MD, USA. Cambridge Univ Press; 1983: 298-313. Time-Dependent Failure Mechanisms and Assessment Methodologies.

155. Barwell M J. COMPASS -Ground based engine monitoring program for general applications. Aerospace Technology conference and exposition; Long Beach, California. 1987.

156. Ebstein, Alan R. Gas turbine module performance analysis 1977; (SAE Prepr, 770992):13 p.

157. Danielsson, Sven-Goeran. Gas path analysis applied to pre and post overhaul testing of JT9D turbofan engine1977; (SAE Prepr, 770993):22 p.

158. Grewal M.S. Gas turbine engine performance deterioration modellind and analysis. PhD ed. Cranfield: Cranfield University; 1988.

159. Escher P. Gas turbine data validation using gas path analysis. Proceedings of ASME Turbo Expo 2002; Amsterdam, The Neatherlands. USA : ASME; 2002; c2002.

160. Escher P C and Singh R. An object-oriented diagnostics computer program suitable for industrial gas turbines. 21st (CIMAC) International congress of combustion engines; Switzerland. 1995.

161. Simani S, Fantuzzi C. Diagnosis techniques for sensor faults of industrial processes. IEEE Transanctions on Control Systems Technology. 2000; 8(5):848-855.

162. Kong, C.; Ki, J., and Kim, T. Optimal Measurement Parameter Selection of Turboprop Engine Using GPA Approach. Int J Turbo and Jet Engines. 2003; 20(2):171-182.

163. Vodopianov, V. E. Probabilistic gas path analysis for gas turbine engines and its application. 2004 ASME Turbo Expo; Vienna. USA : ASME; 2004: 563-571.

164. Zwebek, A. I. and Pilidis, P. Application of GPA to combined cycle gas turbine plants. 2004 ASME Turbo Expo; Vienna. USA: ASME; 2004: 225-232.

165. Della Gatta, S. and Adami, P. Fault detection and identification by gas path analysis approach in heavy duty gas turbine. 2006 ASME 51st Turbo Expo; Barcelona. USA: ASME; 2006: 581-592.

166. Smetana, Frederick O. Turbojet engine gas path analysis - A review . AGARD Conf Proceedings; Liege, Belg. 1974: 13 p.

167. Li Y G. Performance-analysis-based gas turbine diagnostics: a review. Journal of Engineering Power and Energy. 2002; 216(Part A):363-377.

168. Donaghy, M J. Gas Path Analysis - Fault diagnosis using DETEM. MsC ed. School of Engineering: Cranfield University; 1991.

169. Urban, Louis A. Gas path analysis of commercial aircraft engines . Proceedings of the 11th Symposium on Aircraft Integrated Data Systems; Cologne, West Germany. DFVLR; 1982: 323-357.

170. Doel D.L. Interpretation of weighted-least-squares gas path analysis results. Journal of Engineering for Gas Turbines and Power . 2003; 125:624-633.

171. Gronstedt, T. Least squares based transient nonlinear gas path analysis. ASME Turbo Expo 2005; Reno-Tahoe, NV. USA: ASME; 2005: 705-714. - Gas Turbie Technology: Focus for the Future.

172. Luppold R H; Roman j R; Gallops G W, and Kerr L J. Estimating in-flight engine performance variations using Kalman filter concepts1989; (AIAA-89-2584).

173. Volponi A.J., Depold H. The use of kalman filter and neural network methodologies in gas turbine performance diagnostics: A comparative study. ASME Turbo Expo; Munich, Germany. USA: ASME; 2000.

174. Provost M J. COMPASS: A generalised ground-based monitoring system. Engine conditions monitoring - Technology and Experience. 1988

175. Cordoba, O. Gas path analysis study for overhaul engines. ASME Turbo Expo 2005; Reno-Tahoe, NV. 2005: 497-505. - Gas Turbie Technology: Focus for the Future.

176. Dewallef, P. and Leonard, O. On-line performance monitoring and engine diagnostic using robust Kalman filtering techniques. 2003 ASME Turbo Expo; Atlanta, GA. USA: ASME; 2003: 395-403.

177. Kamboukos P, Mathioudakis K. Comparision of linear and non-linear gas turbine performance diagnostics. Proceedings of ASME Turbo Expo 2003; Atlanta, USA. USA: ASME; 2003; c2003.

178. Li, Y. G. Gas turbine diagnosis using a fault isolation enhanced GPA. 2004 ASME Turbo Expo; Vienna. USA: ASME; 2004: 361-369.

179. Li Y G, Singh R (Cranfield University). An advanced gas turbine path diagnostics system - PYTHIA. XVII International Simposium on Air Breathing Engines; Munich, Germany. ISABE; 2005.

180. Stamatis A, Mathioudakis K Berios G and Papailiou K. Jet engine fault detection with discrete operating points gas path analysis. Journal of Propulsion and Power. 1991; Vol.7(No.6).

181. Gronstedt T U J (Chalmers University of Technology). Identifiability in multi-point gas turbine parameter estimation problems. Proceedings of ASME Turbo EXPO 2002; The Neatherlands. ASME; 2002; c2002.

182. Kobayashi T and Simon D. A hybrid neural-genetic algorithm technique for aircraft engine performance diagnostics. 37th AIAA/ASME/SAE/ASEE Joint Propulsion Conference and Exhibit; Salt Lake City, Utah. USA; 2001.

183. Gulati A, Zedda M Singh R. Gas turbine engine and sensor multiple-point analysis using optimisation techniques. In: AIAA/SAE/ASME/ASEE 36th Joint Propulsion Conference and Exhibit; 2000.

184. Aretakis N, Mathioudakis K. Non-linear engine component fault diagnosis from a limited number of measurements using a combinatorial approach. Proceedings of ASME Turbo Expo 2002; Amsterdam, The Neatherlands. USA : ASME; 2002; c2002.

185. Stamatis A; Mathioudakis K, and Papailiou K D. Adaptive simulation of gas turbine performance. J Eng Gas Turbine and Power. 1990; Aprill 1990(112):168-175.

186. Stamatis A; Mathioudakis K, and Papailiou K. Optimal measurement and health index selection for gas turbine performance status and fault diagnosis. J Eng Gas Turbine and Power. 1992; ASME(114):209-216.

187. Santa I. Diagnostics of gas turbine engines based on thermodynamic parameters. 6th Mini Conference on Vehicle System Dynamics, Identification and Anomalies; Budapest. 1998.

188. Visser, W. P. J.; Kogenhop, O., and Oostveen, M. A generic approach for gas turbine adaptive modeling. 2004 ASME Turbo Expo; Vienna. USA : ASME; 2004: 201-208.

189. Wu H; Xiao H, and Jiang J J. Adaptive simulation of turbfan engine component performance. J Propulsion Technology. 2005; 26(5):430-433.

190. Palmer, Carl A. Combining Bayesian belief networks with gas path analysis for test cell diagnostics and overhaul. Proceedings of the 1998 International Gas Turbine & Aeroengine Congress & Exhibition; Stockholm, Sweden. USA: ASME; 1998.

191. Consumi M and d'Agostino L. Monitoring and fault diagnosis of a turbjet by Bayesian inference. 13th ISABE Conference; Chattanooga, Tennessee. USA; 1997.

192. Romesis, G. and Mathioudakis, K. Setting up of a probabilistic neural network for sensor fault detection including operation with component faults, 2003, J Eng Gas Turbines and Power; 125(3):634-641.

193. Bednarski, M. Example of learning Bayesian networks from simulation data, 2005; Computer Assisted Mechanics and Engineering Services, 12(2-3):103-110.

194. Gorla, R. S. R. Probabilistic analysis of gas turbine field performance, 2006; International Journal of Turbo and Jet engines, 23(3):183-190.

195. Yavuz, M. C.; Sahin, F.; Arnavut, Z., and Uluyol, O. Generating and exploiting Bayesian networks for fault diagnosis in airplane enginesAtlanta, GA; 2006; : 250-255. 2006 IEEE International Conference on Granular Computing.

196. Patel, V. C.; Kadirkamanathan, V., and Thompson, H. A. Novel self-learning fault detection system for gas turbine engines. Proceedings of the 1996 UKACC International Conference on Control. Part 1 (of 2); Exeter, UK. IEE; 1996: 867-872.

197. Torella, G. and Lombardo, G. Neural networks for the diagnostics of gas turbine engines. Proceedings of the 1996 ASME Turbo Asia Conference; Jakarta, Indonesia. USA: ASME; 1996: 1-11.

198. Kanelopoulos, K.; Stamatis, A., and Mathioudakis, K. Incorporating neural networks into gas turbine performance diagnostics. Proceedings of the 1997 International Gas Turbine & Aeroengine Congress & Exposition; Orlando, FL, USA. USA: ASME; 1997.

199. Eklund, N. H. and Goebel, K. F. Using neural networks and the rank permutation transformation to detect abnormal conditions in aircraft engines. 2005 IEEE Mid-Summer Workshop on Soft Computing in Industrial Applications; Espoo, Findland. IEEE; 2005: 1-5. SMCia/05 - .

200. Ghoreyshi, M. and Singh, R. Using Neural Network for diagnostics of an industrial gas turbine. 2004 ASME Turbo Expo; Vienna, Austria . USA: ASME; 2004: 625-634.

201. Bettocchi, R.; Spina, P. R.; Pinelli, M., and Venturini, M. Artificial intelligence for the diagnostics of gas turbines. Part I: Neural network approach. ASME Turbo Expo 2005 ; Reno-Tahoe, NV. USA: ASME; 2005: 9-18. - Gas Turbie Technology: Focus for the Future.

202. Mathioudakis, K. and Romessis, C. Probabilistic neural networks for validation of on-board jet engine data. Proceedings of the Institution of Mechanical Engineers, Part G: Journal of Aerospace Engineering. 2004; 218(1):59-72.

203. Xiradakis, N. and Li, Y. G. Gas turbine and sensor fault diagnosis with nested artificial neural networks. 2004 ASME Turbo Expo; Vienna, Austria. 2004: 351-359.

204. Caguiat, D.; Scharschan, J.; Zipkin, D., and Nicolo, J. Applied neural network for navy marine gas turbine stall algorithm development. 2006 IEEE Aerospace Conference; Big Sky, MT. USA: IEEE; 2006.

205. Dodd, N. and Martin, J. Using neural networks to optimise gas turbine aero engines. Computing and Control Engineering Journal. 1997; 8(3):129-135.

206. Patnaik, S. N.; Guptill, J. D.; Hopkins, D. A., and Lavelle, T. M. Optimization for aircraft engines with regression and neural-network analysis approximators. J Propulsion and Power. 2001; 17(1):85-92.

207. Nabney, I. T. and Cressy, D. C. Neural network control of a gas turbine. Neural Computing and Applications. 1996; 4(4):198-208.

208. El-Shafei, A.; Hassan, T. A. F.; Soliman, A. K.; Zeyada, Y., and Rieger, N. Neural Network and Fuzzy Logic diagnostics of 1X Faults in Rotating Machinery. ASME Turbo Expo 2005; Reno-Tahoe, NV. USA: ASME; 2005: 851-860. - Gas Turbie Technology: Focus for the Future.

209. Parthasarathy, G.; Menon, S.; Richardson, K.; Jameel, A.; McNamee, D.; Desper, T.; Gorelik, M., and Hickenbottom, C. Neural network models for usage based remaining life computation. 2006 ASME 51st Turbo Expo; Barcelona, Spain. USA: ASME; 2006: 995-1002.

210. Widrich, M.; Sinha, A.; Suarez, E., and Cassenti, B. Applications of neural networks to the real-time prediction of metal temperatures in gas turbine engine components. 2006 ASME 51st Turbo Expo; Barcelona, Spain. USA: ASME; 2006: 561-569.

211. Haykin, Simon. Neural networks: a comprehensive foundation. Upper Saddle River, NJ: Prentice Hall; 1999.

212. Ogaji S, Singh R. Advanced engine diagnostics using artificial neural networks. Proceedings of the 2002 IEEE International Conference on Artificial Intelligence Systems (ICAIS'-02): IEEE; 2002.

213. Mcneely, M. New remote engine health monitoring service available. Diesel Progress North American Edition. 2007; 73(5):74-75.

214. Jaw L C. Neural networks for model-based prognostics. IEEE Aerospace Applications Conference Proceedings. 1999; v 3:21-28.

215. Kong, C.-d.; Ki, J.-y.; Kang, M.-c., and Kho, S.-h. Intelligent performance diagnostics of a gas turbine engine using user-friendly interface neural networks. Aircraft Engineering and Aerospace Technology. 2004; 76(4):391-397.

216. Zedda M and Singh R. Fault diagnosis of a turbofan engine using neural networks: A quantitative approach. 1998; AIAA-98-3602.

217. Patel, V. C.; Kadirkamanathan, V.; Kulikov, G. G.; Arkov, V. Y., and Breikin, T. V. Gas turbine engine condition monitoring using statistical and neural network methods . IEE Colloquium (Digest). 1996; (260):X-XI.

218. Tian, Z.-G.; Meng, X.-Y., and Dong, Z.-D. Kohonen neural network-based gas turbine fault diagnosis. Reneng Dongli Gongcheng/ J Eng Thermal Energy and Power. 2005; 20(6):562-564.

219. Zedda M and Singh R. Gas turbine engine and sensor fault diagnosis using optimisation techniques. 35th AIAA/SAE/ASME/ASEE; Los Angeles, CA. USA; 1999.

220. Sampath S, Singh R. Engine-fault diagnostics: an optimisation procedure. Applied Energy. 2002; 73:47-70.

221. Srinivas M, et. a. l. Adaptive probabilities of crossover and mutation in genetic algorithms. IEEE Transactions on Sytem, Man and Cybernetics. 1994; 24(4):656-667.

222. Sampath S, Li Y et. al. Fault diagnosis of a two spool turbo-fan engine using transient data: a genetic algorithm approach. Proceedings of ASME Trubo Expo 2003; Atlanta, Georgia. USA: ASME; 2003; c2003.

223. Lo Gatto E, Li Y G Pilidis P. Gas turbine off-design performance adaptation using a genetic algorithm. ASME Turbo Expo; Barcelona, Spain. USA: ASME; 2006.

224. Ross T J. Fuzzy logic with engineering applications. USA: MacGraw-Hill; 1995.

225. Ganguli R. Application of fuzzy logic for fault isolation of jet engines. 15th ISABE; Bangalore, India. USA: ISABE; 2001.

226. Gayme D; Menon S; Ball C; Mukavetz D, and Emmanuel N. Fautl diagnosis in gas turbine engines using fuzzy logic. IEEE Paper. 2003; 3756-3762.

227. Fuster P; Ligeza A, and Aguilar-Martin J. Abductive diagnostic procedure based on an AND/OR/NOT graph for expected behaviour: Application to a gas turbine. 10th International Congress and Exhibition on Condition Monitoring and Diagnostic Engineering Management; Espoo, Finland. COMADEM; 1997: 511-520.

228. Ogaji SOT; Marinai L; Sampath R/Singh R, and Prober S D (Cranfield University). Gas turbine fault diagnostics: a fuzzy logic approach. J Applied Energy. 2005; 8281-89.

229. Provost. The use of optimal estimation techniques in the analysis of gas turbines [PhD thesis]. Cranfield, UK: Cranfield University; 1995.

230. Depold HR and Gas F D. The application of expert systems and neural networks to gas turbine engine prognostics and diagnostics. J Eng Gas Turbines and Power. 1999; 121(ASME Paper 98-GT-101):607-612.

231. Ganguli, R. Jet Engine Gas-Path Measurement Filtering Using Center Weighted Idempotent Median Filters. J Power and Propulsion. 2003; 19(5):930-937.

232. Li Y G, Pilidis P Newby M. An adaptation approach for gas turbine design point performance simulation. ASME Turbo Expo; Reno-Tahoe, Nevada. USA: ASME; 2005.

233. Traverso, A. Massardo A. F. Thermoeconomic analysis of mixed gas-steam cycles. Applied Thermal Engineering. 2002; 22:1-21.

234. Knight, R.; Obana, M.; von Wowern, C.; Mitakakis, A.; Perz, E.; Assadi, M.; Mo?ller, B. F.; Sen, P.; Potts, I.; Traverso, A., and Torbidoni, L. GTPOM: Thermo-economic optimization of whole gas turbine plant. Applied Thermal Engineering. 2006; 128(3):535-542.

235. KaB, M.; Sabel, T.; Grei_l, O., and Risio, B. Optimisation of boiler operation through comparison of " identical" firing systems boiler simulations and field tests. VGB PowerTech . 2006; 86 (11):52-56; ISSN: 14353199 (ISSN).

236. Valdes M, Duran M. D. Thermoeconomic optimization of combined cycle gas turbine power plants using genetic algorithms. Applied Thermal Engineering. 2003; 23:2169-2182.

237. Vollmer, M.; Pedretti, C.; Ni, A., and Wirsum, M. Advanced bottoming cycle optimisation for large alstom CCPP. 2007 ASME Turbo Expo; Montreal, Que. 2007: 941-951. ISBN: 079184790X (ISBN); 9780791847909 (ISBN).

238. Matsumoto H. et.al. An expert system for startup optimization of combined cycle power plants under NOx emission regulation and machine life management. IEEE Transactions on Energy Conversion. 1996; 11(2):414-422.

239. Piacentino, A. and Cardona, F. On thermoeconomics of energy systems at variable load conditions: Integrated optimization of plant design and operation. Energy Conversion and Management . 2007; 48(8):2341-2355; ISSN: 01968904 (ISSN).

240. Markkula E. (Valmet Automation Inc, Tampere, Finl). Combined cycle power plant: control & optimization of operation. Sahko. 1989; v 62(n 6):28-33.

241. Reyes, A. A knowledge-based planning system for the daily operations in a power plant. ISA 2002 Technology Update Chicago, Il; 2002: 181-188. ISBN: 10540032 (ISSN).

242. Shiroumaru I, et. al. Integrated operation and management system for a 700MW combined cycle power plant. IEEE Transactions on Energy Conversion. 1992; 7(1):20-28.

243. Dettmer, R. Living with NETA. IEEE Review. 2005; July:32-36.

244. APXGroup. UKPX products and services [Web Page]. 2006; Accessed 2006 Sep. Available at: www.apx.com.

245. Ku, Anne. That exotic option called power. USA: 2002: 31-33.

246. Barnett, P. Spark Spread. Manx Electricity Authority2001: 9.

247. Deng, S. J. and et.al. Electricity derivatives and risk management. Energy. 2006; 31:940-953.

248. Poats, R. S. The spark spread as a measure of wholesale electricity's economic reliability. IEEE. 2002; 967-968.

249. Deng, S. and et al. Spark spred options and the valuation of electricity generation assets. IEEE Proceedings of the 32nd International Conference on System Sciences; Hawaii. USA: IEEE; 1999.

250. Hsu, M. Spark spread options are hot! The Electricity Journal. 1998; March:28-39.

251. Stephenson P and Paun M. Electricity market trading. Power Engineering Journal. 2001; December:277-288.

252. Tussing A.R. and Hatcher D.B. Prospects for an electricity futures market: Lessons from petroleum and natural gas. Resources Policy. 1994; 22:135-141.

253. Ramos-Real, F. J. Cost functions and the electric utility industry: A contribution to the dabate on deregulation. Energy Policy. 2005; 33:69-87.

254. Woo, C. K. Electricity market reform failures: UK, Norway, Alberta and California. Energy Policy. 2003; 31:1103-1115.

255. Yarrow, G. Capacity auctions in the UK energy sector. Utilities Policy. 2003; 11:9-20.

256. Woo, C. K. What went wrong in California's electricity markets? Energy . 2001; 26:747-758.

257. Weron, R. Energy price risk management. Physica . 2000; 285:127-134.

258. Sioshansi, F. The emergence of trading and risk management in liberaized electricity markets. Energy Policy. 2002; 30:449-459.

259. Mork, E. Emergence of financial markets for electricity: a European perspective. Energy Policy. 2001; 29:7-15.

260. Vehvilainen, I and et al. Managing electricity market price risk. European Journal of Operational Research. 2003; 145:136-147.

261. Woo, C. K. Cross hedging and forward-contract pricing of electricity. Energy Economics. 2001; 23:1-15.

262. Spectron Energy Services. SpectroMeter. Specton Market Summary. UK:

Spectron Energy Services Ltd; 2007; September 25 . 1 p.

263. HEREN Energy. European GasSpot Market . UK: HEREN Energy; 2007; September 25 . 17 p.